

Towards understanding fouling mechanisms in continuous crystallisation processes

A thesis presented for the degree of
Doctor of Philosophy
in the Faculty of Science
of the University of Strathclyde

by

Fraser Adam Mabbott

Strathclyde Institute of Pharmacy and Biomedical Sciences
August, 2017

Declaration of author's rights

This thesis is the result of the author's original research. It has been composed by the author and has not been previously submitted for examination which has led to the award of a degree.

The copyright of this thesis belongs to the author under the terms of the United Kingdom Copyright Acts as qualified by University of Strathclyde Regulation 3.50. Due acknowledgement must always be made of the use of any material contained in, or derived from, this thesis.

Signed:

Date:

Dedication

The work presented within this thesis is dedicated to my late brother, Graeme Ross Mabbott. Every day of my teenage years I aspired to be like my brother and he taught me how to live life. I'll have a cider or two once the viva is over.

Acknowledgements

Firstly I would like to express my thanks to my supervisor Professor Alastair Florence for the PhD opportunity in addition to the support and guidance throughout my studies. His encouragement when times got difficult are appreciated. Our deep discussions around the future of pharmacy were additionally entertaining and an interesting break from research.

A major thank you is necessary for Dr Cameron Brown as his patience and constant desire to help ultimately transformed my PhD studies and my experiences throughout as a researcher. Without his input I would have not completed my PhD and I am eternally grateful for his help. At the initial stages of my PhD, Dr Thomas McGlone was vital in transforming my mind-set from a community pharmacist to a researcher - I cannot thank him enough for this. A special mention goes to Dr Humera Siddique who has helped throughout my studies in addition to providing data which I have used within my thesis. I am also thankful of Vishal Raval, Dr Nadeem Javid and Dr Naomi Briggs who each helped throughout my research.

I would also like to express my gratitude towards the University of Strathclyde, CMAC and the The Engineering and Physical Sciences Research Council (EPSRC) for funding this research.

Finally, I would like to thank all my friends and family who have supported my research adventures over the last few years. The joy and laughter Aimee and Evan have provided as they have grown up over the last few years has been a vital escape from the mad world of research. Words cannot describe how appreciative I am of my parents, Elsbeth and Gordon, and their encouragement throughout my studies. Additionally, I am grateful to the bank of mum and dad and their frequent financial bailouts.

Abstract

Fouling involves the unwanted deposition and build-up of solid material on surfaces within a process. This problem is widely encountered in multiphase and solid phase processing in many industries including oil and gas, pharmaceutical and fine chemical manufacturing sectors. Although it is acknowledged to impact both batch and continuous processing methods it poses a particular challenge to the controlled operation of continuous crystallisation processes where extended operation under non-equilibrium conditions is required. Whilst the factors impacting on fouling have been proposed, there have been only a relatively limited number of studies into fouling mechanisms to date. With increased interest in deploying continuous crystallisation processes for pharmaceutical manufacturing, the motivation for this work was to develop an improved understanding of the influence of material properties and process conditions on fouling processes.

In this work, a number of studies were conducted in which key materials and process parameters were investigated. These have included different materials of construction (MOCs), process conditions (flow, supersaturation, temperature gradients (ΔT)) and crystallising solutions (solute and solvent). Primary fouling studies were conducted using a small scale batch crystallisation setup to explore the influence on MOCs, supersaturation and agitation rate upon both bulk crystal nucleation and surface fouling of paracetamol. The prominent fouling mechanism was found to be particle deposition which was influenced by supersaturation, agitation rate, different MOCs and exposure time.

Fouling is known to occur on heat exchange interfaces due to the localised supersaturation that can be generated e.g. in a plug flow continuous cooling crystalliser. A novel surface induced continuous crystallisation fouling assessment platform (C-FAP) was developed in conjunction with Cambridge Reactor Design (CRD). The C-FAP was evaluated as an assessment tool by exploring different MOCs and process conditions upon fouling and fouling mechanisms via in situ imaging and temperature measurement. The platform

was characterised and used to explore surface induction mechanisms in which initiation and growth was strongly influenced by different MOCs, with stainless steel showing a greater tendency than PTFE, in addition to the degree of supersaturation. The temperature difference across the MOC interface (ΔT_{MOC}) was demonstrated to influence nucleation and growth to varying extents.

An ideal scenario would be to be able to predict or rule out unfavourable combinations of solute, solvent and MOC properties early in process design to avoid late stage problems. A screen was carried out to assess the potential to develop a multivariate predictive model for fouling propensity and fouling behaviour. The models provide insight into the most influential parameters comprising MOC, solute, solvent and process descriptors to steer subsequent experiments. The importance of MOC properties and process conditions was highlighted for all models. A variety of assessment tools were demonstrated within this work in which recommendations for fouling evaluation were provided in addition to methods to further develop fouling understanding.

'Sometimes you can only find Heaven by slowly backing away from Hell'

Carrie Fisher

Contents

Declaration of author's rights	i
Dedication	ii
Acknowledgements	iii
Abstract	iv
Contents	vii
List of figures	xiii
List of tables	xxiii
List of abbreviations	xxvi
Nomenclature	xxviii
Greek letters	xxxii
Chapter 1. General introduction	1
1.1 Background	2
1.2 Continuous manufacturing of pharmaceuticals	6
1.3 Fundamentals of crystallisation	10
1.3.1 Introduction to crystallisation	10
1.3.2 Phase equilibria	11
1.3.3 Nucleation mechanisms	14
1.3.3.1 Homogeneous nucleation.....	15
1.3.3.2 Heterogeneous nucleation.....	18
1.3.3.3 Secondary nucleation.....	20
1.3.4 Crystal growth.....	21
1.3.5 Considerations associated with crystallisation processes	28
1.4 Fouling literature review.....	29
1.4.1 Fouling introduction	29
1.4.2 Previous fouling studies.....	32

1.4.2.1	Overview of fouling literature and measurements	32
1.4.2.2	Overview of fouling parameters	35
1.4.2.3	Factors impacting fouling.....	37
(a)	Materials of construction	37
(i)	Metallic MOCs	37
(ii)	Other MOCs	43
(b)	Process conditions.....	46
(i)	Hydrodynamics.....	46
(ii)	Temperature.....	47
(c)	Solution properties	49
1.4.2.4	Fouling mitigation	50
1.4.2.5	Fouling measurement methods	54
1.4.2.6	Modelling crystallisation fouling	56
1.4.2.7	Mechanisms related to crystallisation fouling	57
1.5	Motivation for research	60
Chapter 2. Aims and objectives		62
2.1	Aims.....	63
2.2	Objectives.....	64
Chapter 3. Materials and methods.....		65
3.1	Materials	66
3.2	Methods.....	69
3.2.1	MOC characterisation.....	69
3.2.1.1	Contact angle goniometry	69
(a)	Introduction	69
(b)	Methodology	71
3.2.1.2	Atomic force microscopy	73
(a)	Introduction	73
(b)	Methodology	74
3.2.1.3	Other methods.....	76
3.2.2	Statistical and computational approaches	76
3.2.2.1	PCA.....	76
3.2.2.2	DOE	77

3.2.2.3	CFD	80
3.2.3	Crystallisation fouling experiments	81
3.2.3.1	Small scale multiple batch crystallisation setup	81
3.2.3.2	Zebrafish platform	82
Chapter 4. MOC characterisation and evaluation for fouling studies		84
4.1	Selection of materials of construction (MOCs) and characterisation	85
4.1.1	Introduction to materials of construction	85
4.1.2	Materials to be explored	87
4.1.2.1	Stainless steel 316L	87
4.1.2.2	Hastelloy® C276	89
4.1.2.3	PTFE	89
4.1.2.4	PEEK.....	90
4.1.2.5	Borosilicate.....	91
4.1.2.6	Quartz	92
4.1.2.7	Silicon carbide	92
4.1.3	Descriptors from literature	93
4.1.3.1	Thermal conductivity	94
4.1.3.2	Specific heat capacity.....	94
4.1.3.3	Young's modulus.....	95
4.1.4	Descriptors required to be determined experimentally	96
4.1.4.1	Introduction.....	96
4.1.4.2	Materials and methods	96
(a)	Materials	96
(b)	Methods.....	97
4.1.4.3	Results and discussion.....	97
(a)	CAG and surface energy	97
(b)	AFM	100
(i)	AFM height micrographs	100
(ii)	Surface roughness measurement	104
4.2	Assessment of MOC diversity.....	107
4.2.1	Overview of material properties.....	107

4.2.2	Assessment of MOC diversity	109
4.3	Summary	111
Chapter 5. Investigating nucleation and fouling processes in a batch crystallisation of paracetamol in water		
112		
5.1	Introduction.....	113
5.2	Materials and methods	117
5.2.1	Materials.....	117
5.2.2	Methods.....	118
5.2.2.1	Basic crystallisation setup and investigatory method	118
5.2.2.2	Nucleation kinetics	120
5.2.2.3	Fouling behaviour.....	122
5.2.2.4	CFD analysis.....	125
5.3	Results and discussion.....	125
5.3.1.1	Nucleation kinetics	125
5.3.2	Fouling studies	135
5.3.2.1	General observations	135
5.3.2.2	DOE results.....	138
(a)	Total mass deposited.....	139
(b)	Area coverage.....	145
(c)	Model validation.....	150
5.4	Summary	151
Chapter 6. Development of a continuous flow assessment platform for fouling		
153		
6.1	Introduction.....	154
6.2	Proposed modifications	154
6.2.1	Flow cell design.....	155
6.2.2	Cold stream incorporation	158
6.2.3	Thermocouple addition.....	159
6.2.4	Additional modifications.....	161
6.3	Capabilities	162
6.4	Validation of C-FAP	164

(d) Model fitting with experimental fouling data	215
8.3 Results and discussion	216
8.3.1 Diversity of experimental study.....	216
8.3.2 Fouling measurements	218
8.3.3 Fouling behaviour screen	222
8.3.3.1 Model generation and evaluation	222
8.3.3.2 Validation of model.....	227
(a) Internal validation.....	228
(b) External validation.....	228
(c) Assessment of model's validation	228
8.3.4 Definitive fouling outcome model.....	232
8.4 Summary	234
Chapter 9. Conclusions and future work	236
9.1 Summary of thesis.....	237
9.2 Recommendations and future work	241
Chapter 10. References	247

List of figures

Figure 1.1: Proposed mechanisms for fouling adapted from Vendel and Rasmuson including proposed generic initiation processes.....	4
Figure 1.2: The function of solid interfaces impacting upon crystallisation related aspects and processes.....	5
Figure 1.3: Crystallisation system properties impacting upon fouling.....	5
Figure 1.4: High-level overview of stages in the pharmaceutical supply chain.....	7
Figure 1.5: Chemical structures of APIs present in Orkambi® [(a) lumacaftor and (b) ivacaftor)] and Prezista® [(c) darunavir]. Both medicines are continuously processed in their manufacture.....	10
Figure 1.6: Schematic highlighting the nucleation and growth of a crystal.....	11
Figure 1.7: A general solubility curve which highlights the key regions: stable, metastable and labile zones. The temperature difference between the equilibrium solubility curve (T_{sol}) and supersolubility curve (T_{nuc}) is known as the MSZW.....	14
Figure 1.8: Hierarchal types of nucleation.....	15
Figure 1.9: Contact angle schematic highlighting three different phases and associated interfacial energies.....	19
Figure 1.10: Schematic illustration highlighting the mechanisms of secondary nucleation.....	21
Figure 1.11: Atomic force microscopy (AFM) micrograph showing (a) a dislocation core from which (b) spiral growth of L-cystine occurs.....	22
Figure 1.12: Schematic highlighting the three different growth locations on crystal surface namely kinks, steps and terraces. In terms of energetics, kink locations are more favourable for growth followed by step locations. Growth upon terraces is the least favourable for attachment of growth units.....	23
Figure 1.13: Diffusion theory of crystal growth across adsorption and diffusion stagnant layers (two step concentration driving forces).....	25

Figure 1.14: Phenytoin packing arrangement highlighting anisotropic surface chemistries in particular (0,-1,-1,1) and (0,1,-1,1) faces (CCDC reference PHYDAN).....	27
Figure 1.15: (a) Crystallisation fouling present upon the internal surface of an operational COBC. (b) An image of a clean Fourier transform infrared spectroscopy (FTIR) probe with (c) resultant fouling upon all exposed surfaces after solution exposure as identified by Borissova et al.....	30
Figure 1.16: Image of L-glutamic acid fouling upon the internal heat transfer surface of a jacketed COBC in which COBC straight '11' had become fouled at the glass interfaces where heat transfer occurs.....	32
Figure 1.17: Typical fouling curve highlighting the induction period and fouling period in relation to heat transfer.....	34
Figure 1.18: Schematic highlighting deposition and removal of crystalline material on a fouled surface contributing to the fouling rate.....	35
Figure 1.19: Adapted figure from Geddert et al. highlighting contributing parameters to influence crystallisation and particle processes associated with fouling.....	36
Figure 1.20: Fouling resistance curves versus time for a range of metallic MOCs under identical process conditions highlighting the impact of different MOCs upon fouling induction time.....	39
Figure 1.21: Influence of surface treatments upon surface roughness and fouling induction time.....	41
Figure 1.22: Fouling resistance curves versus time for different surface roughness (Ra) values of stainless steel substrates.....	42
Figure 1.23: The impact of varying dispersive surface energy values of stainless steel/different PTFE-coated stainless steel substrates upon calcium sulphate deposition.....	43
Figure 1.24: The influence of flow velocity upon fouling resistance curves for calcium carbonate fouling.....	47
Figure 1.25: Nývlt and Veverka's plot illustrating critical time for scaling/fouling as a function of MSZW for various fouling molecules.....	49

Figure 1.26: Images of fouled surfaces under (a) silent conditions and (b) sonication. Fouling was more prominent under silent conditions.....	53
Figure 1.27: Adapted schematic figure highlighting initiation and growth mechanisms of crystallisation fouling involving fundamental crystallisation and particulate processes.....	58
Figure 1.28: Image of tabulated results from Vendel and Rasmuson’s research regarding collision initiation in which diverse fouling outcomes were identified for explored MOCs and solute molecules.....	59
Figure 1.29: Schematic of the relationship between nucleation processes, fouling and process conditions leading to process understanding.....	61
Figure 3.1: Schematic diagrams highlighting different wetting behaviours of water upon differing solid substrates.....	70
Figure 3.2: (a) CAG setup including software interface (b) close up view of goniometer stage, light source, camera and droplet source.....	72
Figure 3.3: Schematic of an AFM system and necessary components.....	74
Figure 3.4: (a) Bruker FastScan AFM setup (b) close up view.....	75
Figure 3.5: Examples of visual experimental design representations for full factorial and D-optimal design.....	78
Figure 3.6: (a) Internal contents of the incubator with the multi-position stir plate with 5 webcams to be positioned either side (b) Additionally for imaging purposes, a black background was used to enhance contrast allowing identification crystallisation events within an experimental vial.....	82
Figure 3.7: Library image of the Zebrafish platform.....	83
Figure 4.1: Different MOC types explored within this chapter including metals, polymers, glass-like materials and ceramics in addition to specific MOCs for each group.....	86
Figure 4.2: A commercially available COBC constructed from stainless steel 316L by Alconbury Weston Ltd.....	88
Figure 4.3: Repeating chemical monomer unit for PTFE.....	90

Figure 4.4: Repeating chemical monomer unit for PEEK.....	91
Figure 4.5: Protrix® SiC flow reactor produced by Chemtrix.....	93
Figure 4.6: Bar charts of average contact angle values (with standard deviations) for (a) water, (b) ethylene glycol and (c) diiodomethane.....	98-99
Figure 4.7: Total surface energy including polar (γ_s^{AB}) and non-polar (γ_s^{LW}) contributions for each unique MOC.....	100
Figure 4.8: AFM micrographs of (a) borosilicate and (b) quartz (scan area: 50 μm^2).....	101
Figure 4.9: AFM micrographs of stainless steel 316L (a) as received, (b) 280 grit mechanically polished and (c) electropolished (scan area: 50 μm^2).....	102
Figure 4.10: AFM micrographs of Hastelloy® C276 (a) as received, (b) 280 grit mechanically polished and (c) electropolished (scan area: 50 μm^2).....	103
Figure 4.11: AFM micrographs of (a) PTFE and (b) PEEK (scan area: 50 μm^2).....	104
Figure 4.12: AFM micrograph of SiC (scan area: 50 μm^2).....	104
Figure 4.13: Average Ra surface roughness values for (a) all unique MOCs explored and (b) glass related MOCs.....	106
Figure 4.14: Biplot containing MOC descriptors (black circles) and distribution of unique MOCs (coloured inverse triangles). Metallic MOCs and glass-like MOCs are both individually grouped whilst other MOCs are uniquely different.	110
Figure 5.1: Aspirin crystals (a) nucleated on the poly(4-acryloylmorpholine) surface whilst the absence of this polymer surface (b) resulted in bulk nucleation.....	115
Figure 5.2: Schematic summarising the aim of this experimental chapter. Various process parameters and different MOCs were to be explored and investigate their influence on both nucleation and fouling. Understanding the relationship between nucleation and fouling with respect to further mechanistic understanding was desired.....	117
Figure 5.3: Temperature-dependent solubility curve for PCM in water.....	118

Figure 5.4: Molecular chemical structure of PCM.....	118
Figure 5.5: An example batch crystallisation vial containing an inserted MOC coupon at a designated spatial configuration.....	119
Figure 5.6: Schematic representing an investigatory MOC coupon specifically highlighting the five planes on which fouling can occur.....	124
Figure 5.7: Example of merged images of fouled MOC coupons in addition to images after image analysis via MATLAB for (a) stainless steel and (b) PTFE.....	125
Figure 5.8: Percentage of experimental vials that nucleated within 8 hours for all explored conditions where n represents the total number of studied vials (n ranging from 10 to 30).....	127
Figure 5.9: Recorded images obtained of the nucleation point of PCM in water for supersaturation ratio 1.3 at an agitation rate of 350 rpm for stainless steel ((a) and (b)) and PTFE ((c) and (d)). Images (a) and (c) are the first image obtained once the prepared vials were added into the incubator with (b) and (d) the nucleation point from which the time difference (induction time) was obtained. The addition of PTFE into the investigatory vial resulted in bubble formation at its surface as observed in image (c). Once agitation begins the surface of PTFE becomes wetted.....	128
Figure 5.10: Boxplots for all investigated conditions. The data plotted highlights minimum and maximum values for dataset in addition to the median, 25% and 75% quartile values. Mean values are denoted by a filled circle icon. n represents the number of investigated vials.....	130
Figure 5.11: Nucleation rate calculated from average induction time values for investigated MOCs, supersaturation ratios and agitation rates of (a) 130 rpm, (b) 350 rpm and (c) 700 rpm.....	131-132
Figure 5.12: Schematic highlighting the relationship between nucleation and MOC fouling for the crystallising PCM in water solution.....	136
Figure 5.13: Images of stainless steel and PTFE at the nucleation point in a saturated solution of PCM in water ((a) and (c), respectively) showing	137

the different extents of fouling after 10 minutes at supersaturation 1.2 and 700 rpm. [Yellow dashed outline highlights the dominant location where fouling mainly occurs].....	
Figure 5.14: Shear rate distribution simulated upon exposed MOC coupon at agitation rates of (a) 130 rpm, (b) 350 rpm and (c) 700 rpm.....	138
Figure 5.15: Summary of fit plot for each fouling response model.....	139
Figure 5.16: Average total mass deposited upon MOC material coupons at 2.5 minute time intervals over 10 minutes for different agitation rates (130 rpm and 700 rpm) at supersaturation (a) 1.2 and (b) 1.4. Error bars represent standard deviation values and a non-weighted line of best fit was applied where Y intercept is not restricted and employed for all data. A near centre condition (supersaturation 1.3 and 350 rpm) was additionally investigated based upon experimental design as shown in image (c).....	142-143
Figure 5.17: 4D response contour plot for total mass deposited model (model expressions are detailed in Equation 5.5 and Equation 5.6).....	144
Figure 5.18: Average area coverage upon MOC material coupons at 2.5 minute time intervals over 10 minutes for different agitation rates (130 rpm and 700 rpm) at supersaturation (a) 1.2 and (b) 1.4. Error bars represent standard deviation values. A non-weighted line of best fit was applied where Y intercept is not restricted and employed for all data. A near centre condition (supersaturation 1.3 and 350 rpm) was additionally investigated as shown in image (c).....	147-148
Figure 5.19: 4D response contour plot for fouling area coverage model (model expressions are detailed in Equation 5.7 and Equation 5.8).....	149
Figure 6.1: Image of the C-FAP set-up comprising a number of modifications.....	155
Figure 6.2: Library image of conventional corrosion flow cell for Zebrafish including electrode positions and several ports.....	156
Figure 6.3: Schematic highlighting proposed alterations to conventional corrosion flow cell [not illustrated to scale].....	156

Figure 6.4: CFD diluted species distribution of (a) original flow cell design and (b) modified flow cell design.....	157
Figure 6.5: Final flow cell design based upon CFD results highlighting the modified entry and exit angles. Additional ports for Pt100 sensor which are detailed in 6.2.3 Thermocouple addition.....	158
Figure 6.6: Cold finger technique fouling assessment set up used by Nývlt and Veverka.....	159
Figure 6.7: Addition of Pt100 sensors to monitor the temperature of the solution and cold stream entering and exiting the bespoke flow cell.....	160
Figure 6.8: Imaging setup comprising a light source, commodity tripod and camera.....	161
Figure 6.9: Settling of PCM particles during the circulation of a PCM suspension via a peristaltic pump.....	163
Figure 6.10: Sequential images over a 12 hour period for (a) borosilicate and (b) C-276 as received at $\Delta T_{MOC} = 28.7^{\circ}\text{C}$	165
Figure 7.1: Selected examples of crystallisation processes and aspects contributing towards the logical design of a crystallisation process. However, fouling contributions are often neglected. Required details are process dependent therefore provided examples are not exhaustive.....	167
Figure 7.2: Continuous flow unit for fouling experiments utilised by Geddert and co-workers. The temperature difference (ΔT) across the flow cell can be calculated in addition to calculating fouling resistance values.....	169
Figure 7.3: Induction time measurements related to fouling including imaging and temperature measurements. For both measurements, induction times and growth kinetics can be determined.....	170
Figure 7.4: An example of PCM nucleation upon stainless steel where (a) the first indications of nucleation are difficult to detect with real time. The reliance on retrospectively serial imaging (b) where identifiable crystals were present was essential to determine accurate induction time	175

values. [Position of nuclei within the dashed blue oval].....	
Figure 7.5: Average induction time values (with standard deviation values) for all explored conditions for (a) stainless steel and (b) PTFE....	181
Figure 7.6: Average induction time values (with standard deviation values) for supersaturated PCM solutions associated with stainless steel and PTFE.....	182
Figure 7.7: Area coverage rate values for (a) undersaturated and (b) supersaturated PCM in water solutions under explored conditions.....	186
Figure 7.8: Example of images of PCM nucleation and subsequent growth upon (a) stainless steel and (b) PTFE.....	187
Figure 7.9: Image highlighting PCM crystals growing upon the stainless steel surface with bulk nucleation and growth occurring concurrently.....	188
Figure 7.10: Schematic of the Rattlesnake COBC in which fouling was identified within Module 2 and 3, respectively (green and red oval).....	190
Figure 7.11: Temperature and pump speed trends related to the continuous crystallisation of lactose monohydrate between Module 2 and Module 3 within the Rattlesnake platform.....	193
Figure 7.12: Temperature and pump speed trends associated between Module 2 and Module 3 of the Rattlesnake where fouling was identified i.e. 24 hours after initial operation (Figure 7.11).....	193
Figure 7.13: Temperature profiles of inlet and outlet hot solution and coolant thermocouples highlighting induction time and complete area fouling coverage (from imaging).....	195
Figure 7.14: (a) Example of a fouling resistance curve with respect to time based upon temperature trends of Figure 7.11 in which can be described as variable however an increasing trend is found between induction time (t_{ind}) and full MOC coverage. (b) Another example of a fouling resistance curve for the exact same conditions explored within image (a) highlighting lack of reproducibility and sensitivity.....	197

Figure 8.1: The proposed investigatory system parameters to be explored within the C-FAP to create predictive fouling models and establish the most influential parameters for each model.....	204
Figure 8.2: Molecular chemical structure of solutes used in this study comprising (a) PCM, (b) lovastatin (LOV), (c) aspirin (ASP), (d) adipic acid (AA) and (e) carbamazepine (CBZ).....	205
Figure 8.3: Molecular chemical structure of solvents used in this study including (a) water, (b) methyl isobutyl ketone (MIBK), (c) 1-propanol, (d) 1-butanol and (e) 2-propanol (IPA).....	206
Figure 8.4: Solubility curves for the solute/solvent pairs tested in this study comprising PCM in water (red curve), LOV in MIBK (black curve) [determined experimentally], ASP in 1-propanol (blue curve), AA in 1-butanol (green curve) and CBZ in IPA (violet curve).....	206
Figure 8.5: An example of a fouling area coverage against time after nucleation sigmoidal plot. The maximum gradient is denoted by the red line from which an area coverage rate can be determined.....	215
Figure 8.6: Two different model types to be generated within this chapter including specific fouling behaviour models and a definitive fouling outcome model.....	216
Figure 8.7: PCA scores plot for 1 st and 2 nd component generated for solute molecules to be investigated. External validation solute was located marginally out with the grouping yet within the Hotelling's ellipse [1 st component $R^2 = 0.577$, 2 nd component $R^2 = 0.285$, variance described = 86.2%].....	217
Figure 8.8: PCA scores plot for 1 st and 2 nd component generated for solvent molecules to be investigated. The external validation solute is located within the solvent grouping [1 st component $R^2 = 0.796$, 2 nd component $R^2 = 0.155$, variance described = 95.1%] (4-methyl-2-pentanone denotes MIBK and 2-propanol denotes IPA).....	217
Figure 8.9: Replicate of Figure 4.11 showing unique MOC diversity [1 st component $R^2 = 0.432$, 2 nd component $R^2 = 0.224$ variance described = 65.6%].....	218

Figure 8.10: Selected images highlighting the initial formation of crystalline material that was used for determining induction time values specifically (a) PCM [Exp 9], (b) LOV [Exp 8], (c) ASP [Exp 6] and (d) AA [Exp 7]. Red oval shows the location of nucleation initiation.....	220
Figure 8.11: Image of AA growth revealing the needle-like morphology and large number of growth locations.....	220
Figure 8.12: Series of images collected at several time point once experiments were initiated for (a) PCM in water [Exp 9], (b) LOVA in MIBK [Exp 16], (c) AA in 1-butanol [Exp 16] and ASP in 1-propanol [Exp 14]. Time values associated with each image specifies time point after experiment was initiated.....	221
Figure 8.13: Summary of fit plots for each fouling response model.....	223
Figure 8.14: Summary of fit plot for the definitive fouling outcome model.....	232
Figure 9.1: Significant fouling present upon the casing of an FBRM probe which had been introduced into a crystallising system.....	238
Figure 9.2: Summary of crystallisation fouling processes investigated within this thesis with explored factors identified to influence respective mechanisms.....	241
Figure 9.3: Schematic diagram highlighting the sequential approach for further fouling investigations.....	243
Figure 9.4: Establishing the relationship between fouling assessment methods to true results within a continuous crystallisation campaign.....	244
Figure 9.5: L-glutamic acid fouling encrustation along a COBC straight with flow direction left to right. Preferential fouling occurs upon the stainless steel thermocouple rather than the glass heat transfer surface whilst locations where the thermocouple is not present fouling on the vessel walls was dominant.....	245
Figure 9.6: Workflow for continuous seeded crystallisation in which fouling propensity and behaviour assessments occur within stage 5.....	246

List of tables

Table 1.1: Summary of measurements from literature utilised to describe fouling.....	55-56
Table 3.1: List of chemicals used in subsequent crystallisation fouling experiments detailing purity and source location (abbreviations for chemicals used herein are detailed within brackets).....	66
Table 3.2: Investigated MOCS including details on thickness, source location and dimensions each MOC is machined to for subsequent experimental chapters.....	68
Table 3.3: Probe solvents used to calculate surface energy values via CAG including liquid surface energy components.....	73
Table 3.4: Statistics employed by MODDE to describe generated models in addition to associated equations.....	79
Table 3.5: Accepted model statistics from literature.....	80
Table 4.1: Thermal conductivity values for each MOC from a variety of literature sources (References detailed within table).....	94
Table 4.2: Specific heat capacity values for each MOC from literature sources (References detailed within table).....	95
Table 4.3: Young's modulus values for each MOC from literature sources. (References detailed within table).....	95
Table 4.4: MOC characterisation quantitative dataset comprising experimental determined results (blue columns) and literature values (green columns).....	108
Table 5.1: PCM in water concentrations required to generate supersaturation ratios of 1.2, 1.3 and 1.4 for crystallisation experiments at 30°C.....	120
Table 5.2: Parameters explored for induction time experiments.....	121
Table 5.3: Experimental design for D-optimal DOE investigating supersaturation, agitation rate, exposure time after nucleation and MOCs.....	123

Table 5.4: Kruskal-Wallis test results highlighting p-values and assessment of parameter for significance.	134
Table 5.5: Table of simulated average shear rates within the bulk solution and at coupon surface.....	138
Table 5.6: Experimental and predicted fouling response results related to (a) stainless steel and (b) PTFE over the initial 10 minutes after bulk nucleation for supersaturation ratio 1.2 and agitation rate of 700 rpm....	150
Table 6.1: Capabilities and technical data of the adapted crystallisation fouling Zebrafish platform.....	163
Table 6.2: Potential investigations in which the C-FAP has the capacity to conduct.....	164
Table 7.1: Conditions explored including process parameters and MOC probed for C-FAP assessment.....	173-174
Table 7.2: Table of conditions explored within the Rattlesnake continuous crystalliser for lactose monohydrate in water.....	191
Table 8.1: Replicate of Table 4.4 highlighting all investigated MOCs including associated descriptors.....	207
Table 8.2: Different parameters to be explored to generate fouling models namely different MOCs, solutions, temperature differences across explored MOCs and solution flow rates.....	209
Table 8.3: Employed MOC, solute and solvent descriptors within the reduced combinatorial experimental design used to describe each parameter (with shorthand terms).....	211
Table 8.4: Experimental conditions selected by the reduced combinatorial experimental design including parameter descriptors for assessment in the C-FAP.....	212-213
Table 8.5: Fouling behaviour results for each experiment number as detailed in Table 8.3. Grey shaded rows indicate experiments where no fouling had occurred within the 24 hour timescale.....	219
Table 8.6: The top 10 greatest factors and factor interactions contributing towards each fouling response model. Effects	225

contributions for each generated model detailed within square brackets.....	
Table 8.7: Internal validation experiments including determined and predicted fouling measurements. Ranking order from smallest to largest value ranged from 1 to 5 within square brackets.....	230
Table 8.8: External validation experiments including determined and predicted fouling measurements. Rank order from smallest to largest value ranged from 1 to 5 within square brackets.....	231
Table 8.9: Top 10 factors and factor interactions contributing towards definitive fouling outcome. Effects contributions for each generated model within square brackets.....	233

List of abbreviations

AA	Adipic acid
AFM	Atomic force microscopy
ANN	Artificial neural network
API	Active pharmaceutical ingredient
ASP	Aspirin
C276	Hastelloy® C276
CAG	Contact angle goniometry
CBZ	Carbamazepine
C-FAP	Continuous flow fouling assessment platform
CFD	Computational fluid dynamics
CMP	Critical material properties
CNT	Classical nucleation theory
COBC	Continuous oscillatory baffled crystalliser
CPP	Critical process parameters
CQA	Critical quality attributes
DEM	Discrete element modeling
DOE	Design of Experiments
EMA	European Medicines Agency
EP	Electropolish
FBRM	Focused beam reflectance measurement
FDA	Food and Drug Administration
FEM	Finite element modelling
FEP	Fluorinated ethylene propylene
FTIR	Fourier transform infrared spectroscopy
HPMC	Hydroxypropyl methylcellulose
IPA	2-propanol
LGA	L-glutamic acid
LOV	Lovastatin
MHRA	Medicines and Healthcare Products Regulatory Agency
MIBK	Methyl isobutyl ketone

MLR	Multiple linear regression
MOC	Material of construction
MSZW	Metastable zone width
NIR	Near infrared
NME	New molecular entity
OBC	Oscillatory baffled crystalliser
PAT	Process analytical technology
PCA	Principal component analysis
PCM	Paracetamol
PEEK	Polyether ether ketone
PID	Proportional-integral-derivative algorithm
PLS	Partial least squares
PMMA	Poly(methyl methacrylate)
PRESS	Prediction residual sum of squares
PSD	Particle size distribution
PTFE	Polytetrafluoroethylene
PVDF	Polyvinylidene fluoride
QbD	Quality by Design
QCM	Quartz crystal microbalance
RT	Room temperature
SiC	Silicon carbide
SPM	Scanning probe microscopy
SS 316L, SS	Stainless steel 316L
UV	Ultraviolet
vdW	van der Waals

Nomenclature

$\frac{dm_f}{dt}$	Fouling rate (kg/m ² .s)
\dot{m}_d	Deposition rate (kg/m ² .s)
\dot{m}_r	Removal rate (kg/m ² .s)
$A_{CRYSTAL}$	Surface area of crystal (m ²)
A_{KIN}	Kinetic rate constant (#/s.m ³)
A_{MOC}	Area of MOC coupon exposed for fouling (m ²)
B_{Therm}	Thermodynamic rate constant
C_p	Specific heat capacity (kJ/kg.K)
C_{pCOL}	Specific heat values of cold fluid stream (kJ/kg.K)
C_{pSOL}	Specific heat values of hot solution stream (kJ/kg.K)
D_S	Diameter of stirrer (m)
M_{COL}	Mass flow rate of cold fluid stream (kg/s)
MOC_{PTFE}	MOC model term for PTFE
MOC_{SS}	MOC model term for stainless steel
M_{SOL}	Mass flow rate of hot solution (kg/s)
MS_{pe}	Mean square of the pure error
MS_{tot}	Total mean square of Y
N_s	Speed of the stirrer (rps)
P_O	Dimensionless power number of the agitator
R_G	Mass deposition rate (kg/m ² .s)
SS_{res}	Sum of squares of the residual, corrected for the mean

SS_{tot}	The total sum of squares of Y corrected for the mean
$T_{COL\ inlet}$	Temperature of the cold stream towards the rear of the MOC coupon (°C)
$T_{COL\ outlet}$	Temperature of the cold stream exiting from the rear of the MOC coupon (°C)
$T_{SOL\ inlet}$	Temperature of the solution entering the flow cell (°C)
$T_{SOL\ outlet}$	Temperature of the solution exiting the flow cell (°C)
T_{nuc}	Nucleation temperature (°C)
T_{sol}	Solubility temperature (°C)
V_L	Volume of liquid (m ³)
c^*	Equilibrium saturation concentration (kg/kg)
c_{Bulk}	Solute concentration within the bulk (kg/kg)
c_i	Solute concentration at interface (kg/kg)
k_G	Overall crystal growth coefficient (kg/m ² .s)
k_d	Mass transfer coefficient (kg/m ² .s)
k_m	Mass transfer coefficient (kg/m ² .s)
k_r	Integration rate coefficient (kg/m ² .s)
m_f	Final crystal mass (kg)
m_i	Initial crystal mass (kg)
p_{lof}	p-value for the lack-of-fit test
r_c	Critical nuclei radius (m)
t_g	Time to grow to a detectable size (s or min)
t_{ind}	Induction time (s or min)

t_n	Time to form stable nuclei (s or min)
t_r	Relaxation time (s or min)
n	Total number of investigated vials
\emptyset	MOC coupon diameter (mm)
AR	Agitation rate (rpm)
E	Young's modulus (GPa)
G	Linear growth rate (m/s)
J	Nucleation rate (#/s.m ³)
N	Number of individual crystals (#)
Q	Heat transfer rate (W)
R	Universal gas constant (8.314 J/mol.K)
Ra	Arithmetic average of the absolute values of a roughness profile (nm)
Re	Reynolds number
Rf	Fouling resistance (m ² .K/W)
Rz	Mean roughness depth (nm or μ m)
S	Supersaturation ratio
T	Temperature (K or °C)
U	Overall heat transfer coefficient (W/(m ² .K))
U_f	Overall heat transfer coefficient for fouled surface (W/(m ² .K))
U_o	Overall heat transfer coefficient for surface at initiation (W/(m ² .K))
V	Solution volume (m ³)

a	Standard activity of solution phase
a^*	Standard activity of crystalline phase
c	Solution concentration (kg/kg)
g	Order of growth process
k	Boltzmann constant (1.3805×10^{-23} J/K)
m	Solid mass deposited (kg)
r	Radius of the nuclei (m)
t	Time (s or min)
v	Molecular volume (m^3)
$\frac{P}{\bar{V}}$	Energy dissipation (W/m^3)

Greek letters

ΔT	Temperature difference ($^{\circ}\text{C}$ or K)
ΔT_{MOC}	Temperature difference across a MOC i.e. assumed to equal $T_{SOL\ inlet} - T_{COL\ inlet}$ ($^{\circ}\text{C}$ or K)
ΔT_{MSZW}	Temperature difference between T_{nuc} and T_{sol} ($^{\circ}\text{C}$ or K)
σ	Relative supersaturation
$\Delta\mu$	Difference in chemical potential (kJ/kmol)
μ_L	Chemical potential of solution phase (kJ/kmol)
μ_S	Chemical potential of solid phase (kJ/kmol)
μ_O	Standard potential (kJ/kmol)
ΔG	Overall free energy difference (kJ)

ΔG_v	Volume free energy difference (kJ)
ΔG_s	Surface free energy difference (kJ)
$\gamma_{Interfacial}$	Interfacial surface tension (mJ/m ²)
ΔG_{CRIT}	Critical overall free energy difference for critical nuclei size for homogeneous conditions (kJ)
$\Delta G'_{CRIT}$	Critical overall free energy difference for critical nuclei size for heterogeneous conditions (kJ)
Φ	Correction factor (or free energy ratio)
$\theta_{Nucleus}$	Contact angle of a crystalline nuclei (°)
$\theta_{Droplet}$	Contact angle of a liquid droplet (°)
γ_{sl}	Interfacial energy between foreign surface and liquid of interest (mJ/m ²)
γ_{cs}	Interfacial energies between crystalline nuclei and foreign surface (mJ/m ²)
γ_{cl}	Interfacial energies between crystalline phase and liquid of interest (mJ/m ²)
Δc	Crystal growth driving force (kg/kg)
α	Volume shape factor
ρ_{cryst}	Crystal density (kg/m ³)
ΔG_{het}	Overall free energy difference for heterogeneous conditions (kJ)
γ_{sv}, γ_s	Solid-vapour interfacial energy (mJ/m ²)
γ_{lv}	Liquid-vapour interfacial energy (mJ/m ²)
θ	Contact angle (°)

γ	Surface energy (mJ/m ²)
γ^{LW}	Dispersive surface energy component (mJ/m ²)
γ^{AB}	Polar surface energy component energy (mJ/m ²)
γ^+	Electron accepting contributions related to the polar surface energy component (mJ/m ²)
γ^-	Electron donating contributions related to the polar surface energy component (mJ/m ²)
γ_l	Surface energy of probe liquid (mJ/m ²)
λ	Thermal conductivity (W/(m.K))
ρ	Fluid density (kg/m ³)
ΔT_{LMTD}	Logarithmic mean temperature difference (°C)
ΔT_1	Temperature difference 1 i.e. $T_{SOL\ outlet} - T_{COL\ inlet}$ (°C)
ΔT_2	Temperature difference 2 i.e. $T_{SOL\ inlet} - T_{COL\ outlet}$ (°C)

Chapter 1. Introduction

1.1 Background

Crystallisation is a key unit operation in the manufacture of chemicals including pharmaceutical and fine chemical compounds.¹ It is essential that crystalline product obtained from a crystallisation process meets target product specifications typically including purity, particle size distribution (PSD), polymorphic form and morphology/crystal habit.² These attributes dictate the performance of the chemical product in subsequent processing and end product use. To obtain a crystalline product within specification, a high degree of system understanding involved within a crystallisation process is required. The pharmaceutical industry is increasingly implementing Quality-by-Design (QbD) approaches to ensure product quality.³ QbD seeks to assure consistent quality through fundamental understanding of the dependence of critical quality attributes (CQAs) on critical process parameters (CPPs) and critical material properties (CMPs).⁴⁻⁵

Crystallisation remains a complex multi-phase process involving various processes such as nucleation, growth, attrition, agglomeration and phase transitions.⁶ Fouling is another process to potentially occur during crystallisation. The unwanted or uncontrolled deposition of solute as a solid mass upon the internal surfaces within a vessel can have significant operation consequences yet remains a poorly characterised process. Fouling is defined as the unwanted deposition upon equipment surfaces.⁷ A number of terms are used within literature to describe fouling including encrustation and scaling⁸ however inconsistent terminology is prevalent within literature. Therefore, only the term fouling is used throughout this work. The accumulation of crystalline material above the solution/air interface can also be described as fouling.⁷ However, this specific interfacial phenomena was not a research interest within the present work.

Whilst a diverse array of research studies have been conducted to further understand the array of fundamental crystallisation processes listed above, the causes and mechanisms of fouling have received relatively limited attention. Although significant work has been conducted involving the fouling of heat

exchanger surfaces by inorganics⁹⁻¹¹, research regarding the fouling of small organic molecules such as pharmaceutical compounds within crystallising systems has not been extensively conducted with only a small number of studies reported in the literature.^{7,12-15}

Fouling can impact on the process economics, resources and energy utilisation of any process that it affects.¹⁶⁻¹⁷ Typically industrial processes are designed with the intention to avoid or limit fouling whilst obtaining the desired product at maximum yield.¹⁸ Given that crystallisations operate far from equilibrium under supersaturated conditions, a driving force for solute deposition is generated.¹⁹ Whilst the target is for solute molecules to grow into crystals within suspension, equipment surfaces exposed to the process fluid potentially provide a competing surface for adsorption and crystallisation processes to occur upon.

In the design of a crystallisation process, fundamental understanding of fouling mechanisms and their processes would contribute greatly towards process development i.e. to avoid conditions that promote fouling and develop strategies to mitigate surface fouling.²⁰⁻²¹ Generic fouling initiation mechanisms have been proposed by Vendel and Rasmuson¹² (Figure 1.1) which comprises both crystallisation and particulate processes. Once fouling has been initiated and a stable crystalline mass has formed, subsequent growth ensues with crystal material detachment a possibility. In addition to different mechanistic processes involved with fouling, a wide range of parameters notably material properties and process parameters can additionally influence fouling and associated mechanisms.^{9,17} However few further investigations have been conducted attempting to measure and define fundamental fouling mechanisms of organic compounds in crystallisation processes and establish the relationship between key physical, material or process parameters with the mechanism and extent of fouling that results.

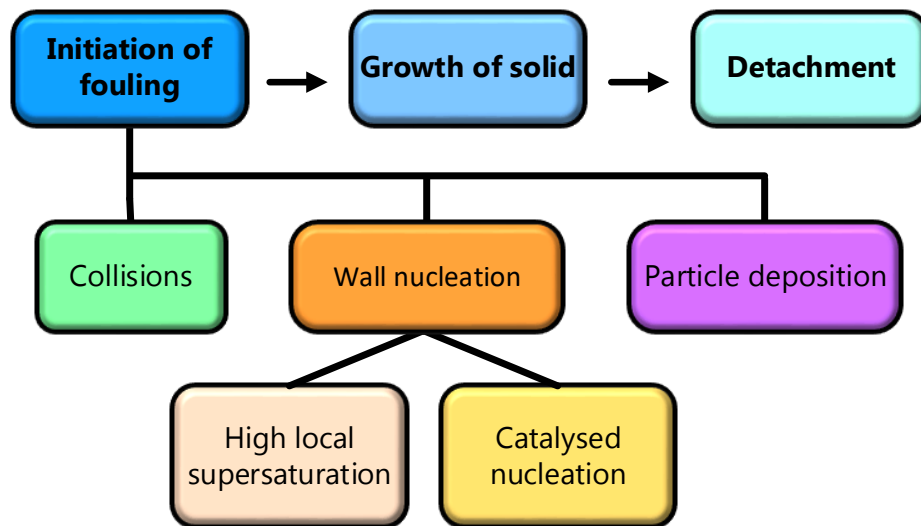


Figure 1.1: Proposed mechanisms for fouling adapted from Vendel and Rasmuson including proposed generic initiation processes.⁷

Solid interfaces have a distinct role in influencing numerous processes within a crystallising system as shown in Figure 1.2. One notable research field which has been probed within inorganic fouling studies is exploring fouling upon heat transfer surfaces manufactured from different materials of construction (MOC). There are a number of examples where differences in fouling have been identified between different investigatory MOCs under specified conditions²¹⁻²² (described in detail within (a) Materials of construction). Within conventional crystalliser platforms, whether operated as a batch or continuous crystalliser, a supersaturated crystallising solution is in contact with a variety of surfaces including vessel walls, impellers, baffles, transfer pipes and other crystalliser components with fouling potentially occurring upon any exposed MOC. Exploring the influence of different MOCs upon crystallisation fouling in addition to investigating process parameters and solution properties will enhance fundamental fouling understanding (Figure 1.3).

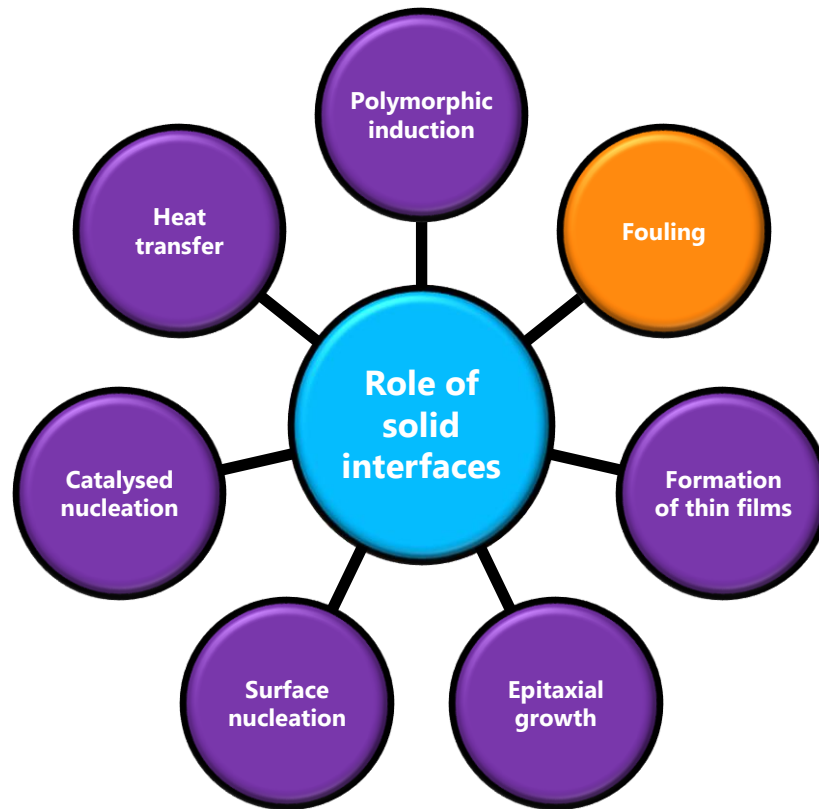


Figure 1.2: The function of solid interfaces impacting upon crystallisation related aspects and processes.^{7,23-25}

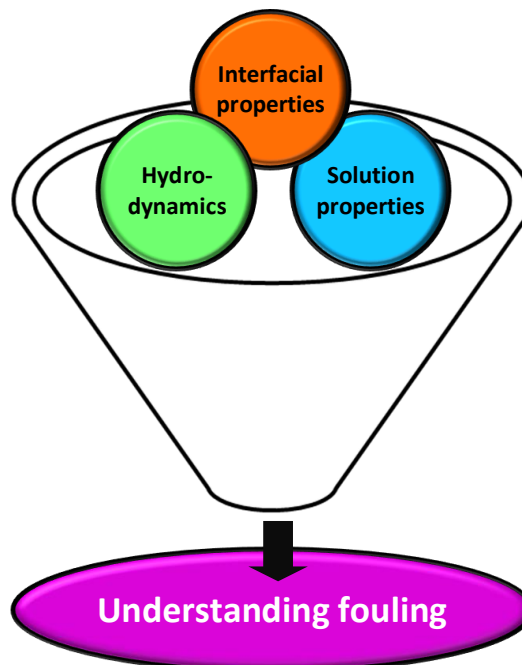


Figure 1.3: Crystallisation system properties impacting upon fouling.

There is considerable interest in the continuous manufacturing of pharmaceuticals in which the continuous crystallisation step is vital for end-to-end manufacture.²⁶⁻²⁷ A key interest herein is understanding crystallisation fouling mechanisms in continuous crystallisers, although any findings may be related to batch crystallisation processes. Mitigating or limiting fouling within a continuous crystalliser is highly desirable as these configurations are typically required to operate for extended periods of time to achieve the required product quantity. The goal is to provide an enhanced insight into fouling mechanisms from which continuous crystallisation campaigns can be conducted with little to no fouling present. Insight into fouling mechanisms will help direct future operational strategies to minimise fouling and the requirement for regular cleaning. Additionally, in the design of a continuous crystallisation process, understanding the influence of MOC properties, process parameters and solution properties of a specific crystallising system can inform useful compatibility relationships and specific parameter combinations that should be evaded e.g. roughened surface can promote surface induced fouling.²⁸ The notion of entering a new molecular entity (NME) into a continuous crystallisation process is traditionally challenging and is often associated with a trial and error approach. To address time, material and economic considerations, a systematic approach is desirable before arriving at a logical decision.²⁹ Assessing the fouling potential of a newly investigated system is therefore critical in the design of continuous crystallisation campaign. From a modelling perspective, exploiting the capability to predict fouling behaviour of an NME would considerably enhance process development decision making, leading to the creation of robust processes.

1.2 Continuous manufacturing of pharmaceuticals

The concept of continuous manufacturing is well established in other industries. It has been employed in a number of manufacturing sectors including oil and gas, chemicals, plastics and catalysis for decades.³⁰ However, historically the fine chemical and pharmaceutical industries have

operated primarily using batch methods.³¹ Pharmaceuticals have historically been high margin products for decades however, recently with drug patent expirations and the desire to reduce operating expenditure, there is a need to improve current manufacturing and process technologies to compensate.³²⁻³³ Consequently, continuous manufacturing of chemicals has received notable interest both from academia and pharmaceutical companies.^{32,34-36}

Manufacturing processes involved in the pharmaceutical industry are diverse and typically divided into two major stages namely primary and secondary processing (Figure 1.4). Primary processing involves the production of an active pharmaceutical ingredient (API) which includes chemical synthesis followed by work-up and crystallisation stages.²⁶ The product from the crystallisation stage is then isolated and dried to produce a dry, pure, free-flowing powder prior to secondary processing. Secondary processing comprises a variety of processes to formulate a medicine from a primary processed API with typical processes including powder blending, extrusion, granulation, tableting and encapsulation.^{31,37} Resultant formulations are packaged and transferred to storage and transfer facilities prior to distribution to pharmacies and patients. As a consequence of this make to stock approach, inventory levels can be considerable across the industry.³²

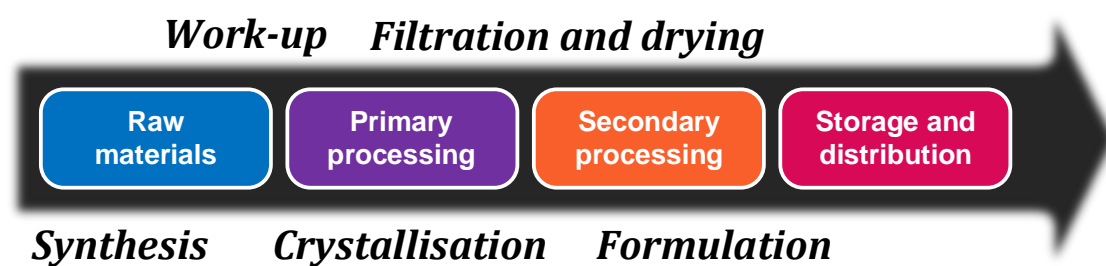


Figure 1.4: High-level overview of stages in the pharmaceutical supply chain.

The crystallisation stage in principle links the primary and secondary processing stages and is therefore a crucial manufacturing step. A crystallisation stage is designed to control the physical properties of an API. At

present, the processes involved in crystallisation remain poorly understood and still creates issues within an industrial manufacturing setting.³⁸

Batch pharmaceutical manufacturing has evolved to get medicines into regulated patient markets as rapidly as possible. Regulation is potentially restrictive and consequently limiting innovation within manufacturing technologies. Batch manufacturing processes have a number of associated problems including difficulties in process scale up, batch-to-batch variation and poor homogenous processing conditions. The consequence of these manufacturing issues may generate a product which may not meet quality specifications.^{1,32}

The concept of end-to-end continuous pharmaceutical manufacturing is attractive with a number of advantages in contrast to conventional manufacturing methods.³⁹⁻⁴⁰ Batch manufacturing operations tend to process large quantities of chemicals and solvents at any given time within one location. Continuous operations potentially allow hazardous or dangerous materials to be managed and processed in a safer and more efficient manner.²⁶ From an economic perspective, continuous manufacturing can potentially be a more attractive method of manufacturing with an associated reduction in energy expenditure and waste.³² The equipment footprint associated with continuous manufacturing can be considerably lower compared to batch equipment, reducing the capital costs associated with plants and providing more flexibility in deployment of assets.⁴¹ Research by Teoh et al. compared a chemical synthesis step via both continuous and batch operation in which the benefits of continuous processing were demonstrated. It was found continuous processes had greater than 66% less inventory at any point of time in addition to a significantly better volume reaction efficiency (10.8 kg/hour/m³ for batch process in contrast to 34 kg/hour/m³).⁴² Zhang and co-workers explored the use of continuous crystallisation in the manufacture of aliskiren hemifumarate in which the continuous crystallisation step generated crystal purity greater than 99% and a yield of 91.4%.⁴³ From a regulatory perspective, the concept of continuous manufacturing has been highlighted by the Food and Drug Administration (FDA) as a potential

approach to improve product quality³² and assure supply in which the FDA has recently encouraged and supported its implementation.⁴⁴

However, the adoption of novel processing technologies within the pharmaceutical industry presents a number of challenges. One of the major issues preventing the adoption of continuous manufacturing is altering the mind-set of key stakeholders and employees within existing organisations which have traditionally embraced batch manufacturing methods.³² The acceptance of continuous process submissions i.e. new market authorisations by regulatory agencies including Medicines and Healthcare Products Regulatory Agency (MHRA), European Medicines Agency (EMA) and FDA is also still required to demonstrate feasibility and regulatory acceptance. The previously highlighted agencies are highly regulated ultimately for safeguarding their associated patient populations. At present, existing pharmaceutical manufacturing facilities chiefly employ batch methods therefore the prospect of operating continuously would require considerable investment to reconfigure operations, workflows and up skill staff.^{1,32,45} However pharmaceutical companies are recognising continuous manufacturing advantages and conversion of batch-to-continuous manufacturing has already commenced. Selected pharmaceutical companies, namely Vertex and Janssen, have embraced continuous processing approaches in the manufacture of drugs such as Orkambi® and Prezista® (Figure 1.5) in which both have received FDA approval.⁴⁶

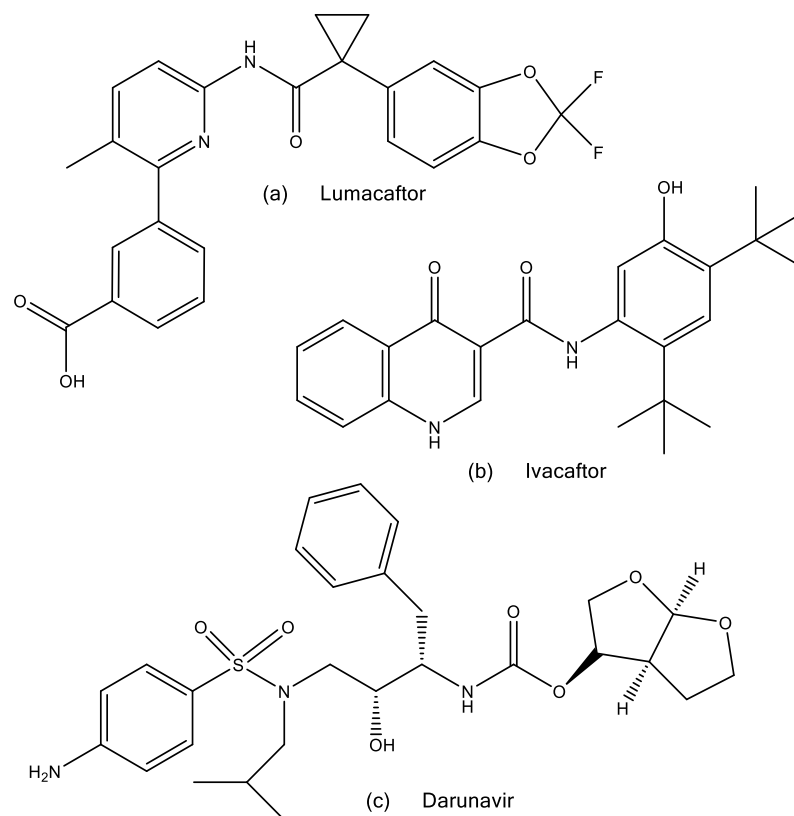


Figure 1.5: Chemical structures of APIs present in Orkambi® [(a) lumacaftor and (b) ivacaftor] and Prezista® [(c) darunavir]. Both medicines are continuously processed in their manufacture.

1.3 Fundamentals of crystallisation

1.3.1 Introduction to crystallisation

Crystallisation is a widely utilised purification and separation technique within the fine chemical and pharmaceutical manufacturing industries.⁶ Within the pharmaceutical sector, 90% of APIs are estimated to have a crystalline structure.⁴⁷ From a simplistic perspective, crystallisation involves a phase change from a solute in liquid or solution state to a crystalline solid. There a number of diverse crystallisation methods employed both in industry and academia comprising cooling, melting, evaporation and anti-solvent stages with, in particular instances, a combination of methods being utilised.^{6,48}

Crystallisation comprises two distinct phases namely nucleation and crystal growth.² Nucleation is a critical step in controlling the subsequent crystallisation process and involves the generation of crystal nuclei from a supersaturated solution.² Crystal growth encompasses the growth of the nuclei into an observable crystal (Figure 1.6). In order for crystallisation to occur a driving force, namely supersaturation, is essential.⁶

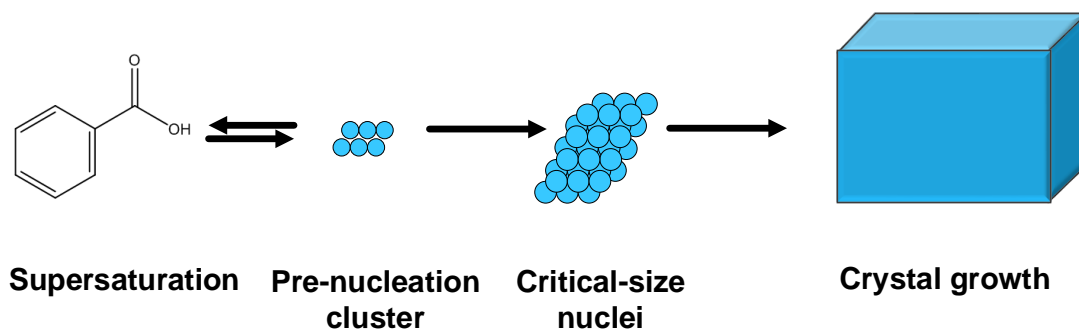


Figure 1.6: Schematic highlighting the nucleation and growth of a crystal.⁴⁹

1.3.2 Phase equilibria

When a solution is saturated, the chemical potential of the solution phase (μ_L) and the solid phase (μ_S) are equal. Therefore, the difference in chemical potential between the two phases ($\Delta\mu$) at equilibrium is zero.^{6,50}

$$\Delta\mu = \mu_L - \mu_S = 0 \quad (1.1)$$

A positive chemical potential difference ($\Delta\mu$ +ve) indicates that a solution is supersaturated whilst conversely a negative chemical potential difference ($\Delta\mu$ -ve) signifies an undersaturated solution.⁵⁰ The chemical potential of the solid phase (μ_S) and the solution phase (μ_L) can also be described in terms of standard potential (μ_o) and standard activity (a and a^*).

$$\mu_L = \mu_O + RT \ln a \quad (1.2)$$

$$\mu_S = \mu_O + RT \ln a^* \quad (1.3)$$

Furthermore Equation 1.2 and Equation 1.3 can be reconfigured as:

$$\frac{\Delta\mu}{RT} = \ln\left(\frac{a}{a^*}\right) = \ln S \quad (1.4)$$

Where

- $\Delta\mu$ = Chemical potential difference (kJ/kmol)
- R = Universal gas constant (8.314 kJ/kmol.K)
- T = Absolute temperature (K)
- a = Standard activity of solution phase
- a^* = Standard activity of crystalline phase
- S = Supersaturation

Where S is:

$$S = \exp(\Delta\mu/RT) \quad (1.5)$$

Supersaturation is typically expressed in two common ways namely supersaturation ratio (S) and relative supersaturation (σ). Supersaturation ratio is defined by:

$$S = \frac{c}{c^*} \quad (1.6)$$

Where c = actual solution concentration and c^* = equilibrium solution concentration. Relative supersaturation can be expressed as:

$$\sigma = \frac{c - c^*}{c^*} \quad (1.7)$$

An idealised solubility curve is illustrated in Figure 1.7. Typically the temperature – concentration phase diagram consists of three zones termed the stable, metastable and labile zones. The stable zone is located underneath the solubility curve in which a solution within this zone is termed as undersaturated and crystallisation cannot occur. Altering the solubility of a solution by methods such as cooling (Figure 1.7), anti-solvent addition or evaporation (Figure 1.7) will result in supersaturation generation. Within the metastable zone, crystallisation can occur however primary nucleation cannot occur spontaneously and requires some method of initiation. Further alteration of the composition of a solution will result in it entering into the labile zone and consequently spontaneous nucleation occur.⁶

For a typical cooling crystallisation, the difference in temperature between the point of solubility, T_{Sol} , and spontaneous nucleation, T_{Nuc} , as illustrated in Figure 1.7 is defined as the metastable zone width (MSZW), ΔT_{MSZW} :

$$\Delta T_{MSZW} = T_{Sol} - T_{Nuc} \quad (1.8)$$

MSZW can be measured by a number of techniques comprising imaging, turbidity measurement and focused beam reflectance measurement (FBRM).⁵¹⁻⁵² MSZW measurements can be employed to probe the influence of process parameters upon nucleation kinetics and ultimately enhance crystallisation system understanding and control. Influential parameters acknowledged to affect nucleation include temperature profile, solution history,

hydrodynamics, rate in which supersaturation is generated and notably the presence of different MOCs.^{6,53}

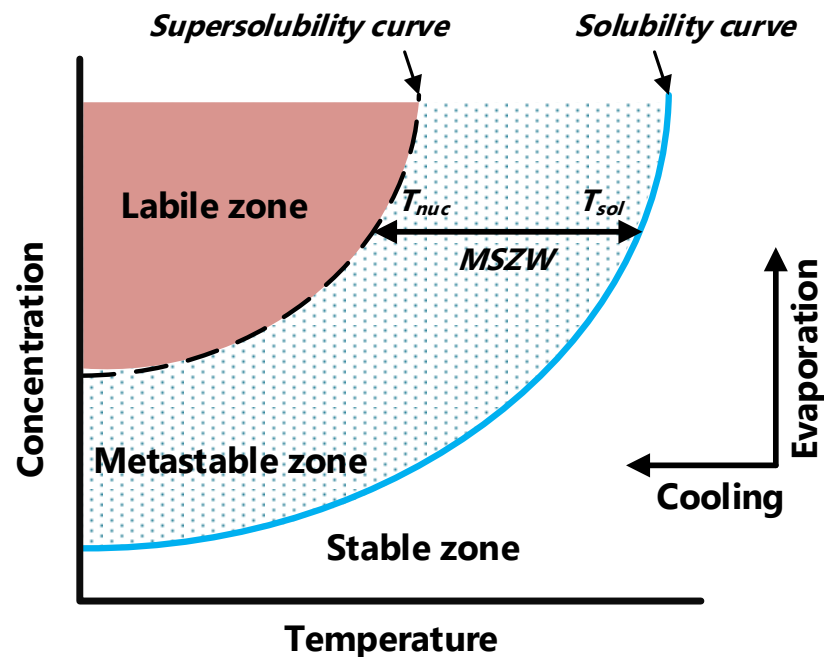


Figure 1.7: A general solubility curve which highlights the key regions: stable, metastable and labile zones. The temperature difference between the equilibrium solubility curve (T_{sol}) and supersolubility curve (T_{nuc}) is known as the MSZW.^{6,54}

1.3.3 Nucleation mechanisms

For crystallisation to occur, the generation of nuclei is an essential first step. Although poorly understood from first principles, there are a number of theories that can be used to describe experimental behaviour.^{49,55} At present nucleation studies are based upon empirical formulas and theories in which control is achieved by varying experimental parameters until the desired target outcome is met. Within an industrial setting, a view to simplify control is taken around nucleation using designs to avoid spontaneous nucleation and rely upon seeding strategies.⁵⁶

Nucleation is the kinetically controlled first stage of a crystallisation process in governing the initial formation of crystal embryos.^{49,57} An overview of

nucleation mechanisms is illustrated in Figure 1.8. The generation of crystal nuclei can form spontaneously (homogeneous nucleation) or be induced (heterogeneous nucleation and secondary nucleation). Nucleation is typically divided into two categories: Primary nucleation refers to the generation of nuclei whilst secondary nucleation requires the presence of crystalline material (termed seeds) to induce nucleation⁶. Primary nucleation can be further categorised into homogeneous nucleation and heterogeneous nucleation. Whilst homogeneous nucleation occurs spontaneously, heterogeneous nucleation requires the presence of an foreign surface to induce nucleation.²

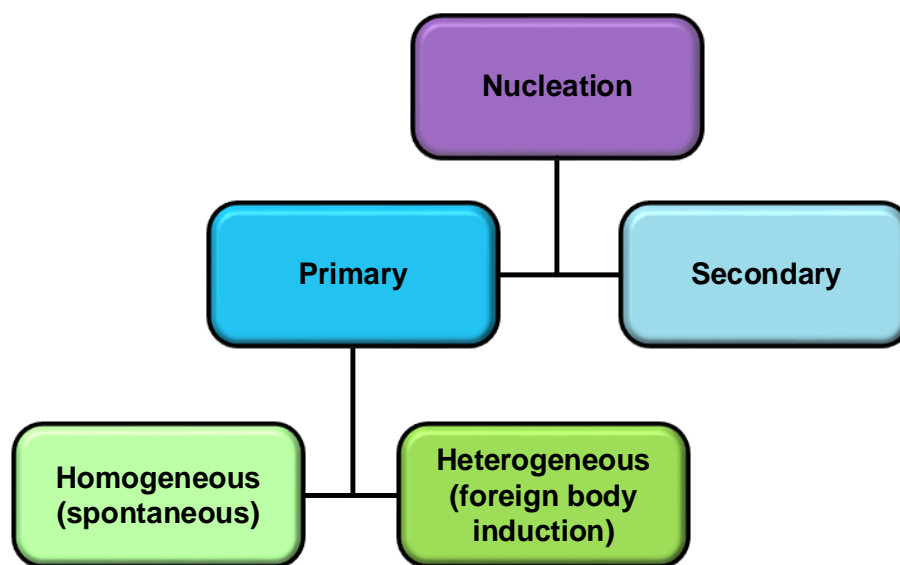


Figure 1.8: Hierarchical types of nucleation.²

1.3.3.1 Homogeneous nucleation

Crystallisation processes have been investigated extensively for decades. However, fundamental understanding of how a stable nucleus forms under homogenous conditions remains a challenge. It is considered that for nucleation to occur, an energy barrier must be overcome. Classical nucleation theory (CNT) dictates that the formation and dissolution of solute clusters is occurring simultaneously within a saturated solution. Within a supersaturated

solution, the movement of molecules is restricted in which the generation of solute clusters is favourable. The propensity of a formed solute cluster to become stable nuclei is dictated by the energy associated with its formation and growth. The overall energy difference (ΔG) between a solute particle and solute in solution can be termed as the summation of the surface excess free energy (ΔG_s) and the volume excess free energy (ΔG_v).^{6,50}

$$\Delta G = \Delta G_v + \Delta G_s \quad (1.9)$$

$$\Delta G_v = -\frac{4\pi r^3 \Delta \mu}{3v} \quad (1.10)$$

$$\Delta G_s = 4\pi r^2 \gamma_{Interfacial} \quad (1.11)$$

Where

r	=	Radius of the nuclei (m)
v	=	Molecular volume (m ³)
$\Delta \mu$	=	Difference in chemical potential (kJ/kmol)
$\gamma_{Interfacial}$	=	Interfacial surface energy (mJ/m ²)

The summation of ΔG_v and ΔG_s results in ΔG to pass through a maximum which relates to the critical free energy difference, ΔG_{crit} , and related nuclei radius, r_c , which is the minimum solute cluster size in order for it to remain a stable entity (Figure 1.6).

$$r_c = \frac{2\gamma v}{\Delta \mu} \quad (1.12)$$

The energy required for the formation of critical nucleus can be expressed as:

$$\Delta G_{crit} = \frac{16\pi\gamma^3}{3(\Delta G_v)^2} = \frac{4\pi\gamma r_c^2}{3} \quad (1.13)$$

The rate of nucleation, J , according to CNT can be expressed as an Arrhenius-type expression:⁶

$$J = A_{Kinetic} \exp(-\Delta G/(kT)) \quad (1.14)$$

Where

J = Number of nuclei formed per unit time per unit volume
(#/s.m³)

$A_{Kinetic}$ = Kinetic rate constant (#/s.m³)

k = Boltzmann constant (1.3805 x10⁻²³ J/K)

T = Temperature (K)

The dependence of nucleation rate upon supersaturation ratio can also be expressed as:

$$J = A_{Kinetic}(S) \exp\left(-\frac{B_{Therm}}{\ln^2 S}\right) \quad (1.15)$$

Where

B_{Therm} = Thermodynamic rate constant

Although CNT is traditionally utilised in the prediction of nucleation rates and to explain differences in observed rates, its validity when comparing to measured nucleation rates is debatable with large differences in associated values by potentially several orders of magnitude. CNT has a number of assumptions associated within its theory.⁴⁹ The first assumption is that nuclei are considered as spherical droplets. Secondly, it is presumed that the formation of nuclei is by single addition of solute monomers at a time and the nuclei formed has the same structure as the generated crystal. Another consideration concerning CNT is that the size of the nuclei is the only factor used to determine whether a formed nuclei is stable or unstable. Another theory has been proposed namely the two-step nucleation model.^{49,58} This proposed model relates to the formation of a dense liquid phase prior to nucleation which had been observed by a number of authors investigating protein crystallisation.⁵⁹⁻⁶⁰ It has been proposed that solute molecules rapidly merge into disordered clusters before transitioning into an ordered cluster structure or nuclei. However, fundamental understanding of this mechanism remains a challenge.

1.3.3.2 Heterogeneous nucleation

The notion of nucleation occurring under homogenous conditions is a rarity in practical circumstances which nucleation typically relies upon some method of induction.⁶ The presence of a foreign surface can provide this induction and can take a number of physical forms which include dust particles, internal vessel surface, impellers etc. Essentially any surface in contact with a crystallising solution can potentially induce nucleation in the presence of supersaturation. In heterogeneous nucleating conditions which are more prominent, the presence of a foreign surface can result in nucleation at lower ranges of supercooling in contrast to true homogenous nucleation. The overall free energy (ΔG) change associated with the generation of a critical nucleus under heterogeneous conditions ($\Delta G'_{crit}$) must be less than the resultant free energy change (ΔG_{crit}) related to homogenous nucleation.⁶

$$\Delta G'_{crit} = \Phi \Delta G_{crit} \quad (1.16)$$

Where the correction factor (or free energy ratio), Φ , can be determined from Equation 1.16⁶¹ which is calculated via the contact angle of a nuclei ($\theta_{Nucleus}$).

$$\Phi = \frac{(2 + \cos \theta_{Nucleus})(1 - \cos \theta_{Nucleus})^2}{4} \quad (1.17)$$

Figure 1.9 highlights the three segments of contact comprising two solid surfaces (namely substrate and crystalline solid nuclei) and a solution from which the contact angle can be determined.⁶

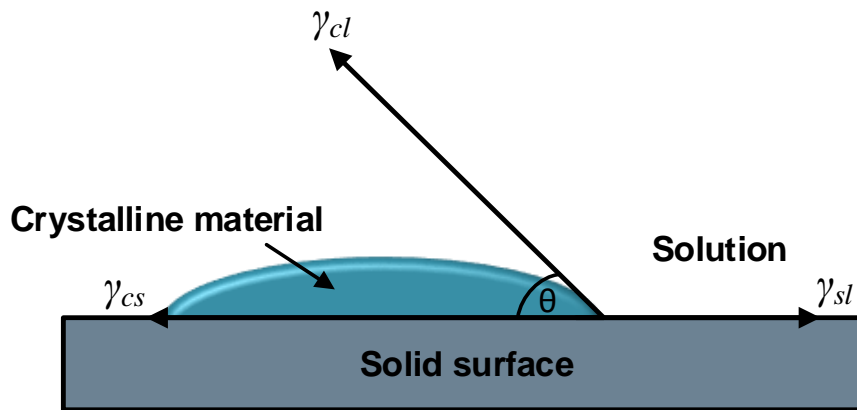


Figure 1.9: Contact angle schematic highlighting three different phases and associated interfacial energies.

The contact angle of the nucleus and associated surface energies are denoted by the expression:⁶

$$\gamma_{sl} = \gamma_{cs} + \gamma_{cl} \cos \theta_{Nucleus} \quad (1.18)$$

Where γ_{sl} , γ_{cl} and γ_{cs} correspond to the interfacial energies associated to foreign surface and liquid of interest, crystalline phase and liquid of interest and crystalline nuclei and foreign surface, respectively. The determined angle between the crystalline material and the foreign surface ($\theta_{Nucleus}$) relates to the interfacial energy contributions highlighted previously. When the angle is between 0° and 180° the overall free energy required for nucleation is less than that required for homogeneous nucleation hence favouring heterogeneous nucleation.⁶

1.3.3.3 Secondary nucleation

Secondary nucleation is the most prevalently occurring nucleation method within industrial crystallisation processes. Secondary nucleation occurs where parent crystals/seeds are added into a solution. The presence of parent crystals results in inducing new nuclei generation mainly through contact methods (Figure 1.10).⁶² Crystals can be subjected to hydrodynamic conditions within a crystalliser resulting in potential damage. Crystals can collide with a number of physical surfaces including vessel walls, impeller, baffles and each other. This can result in crystals breaking into smaller fragments/crystals and nuclei within the bulk solution. Additionally hydrodynamic shear forces have the potential to generate secondary nuclei from exposed crystal surfaces (Figure 1.10).⁵⁰ One distinct advantage of secondary nucleation in a crystallisation includes directing nucleation of desired polymorphic form. However, potential issues with secondary nucleation comprise the generation of crystal fines which results in a crystalline product with a wide PSD.^{6,50}

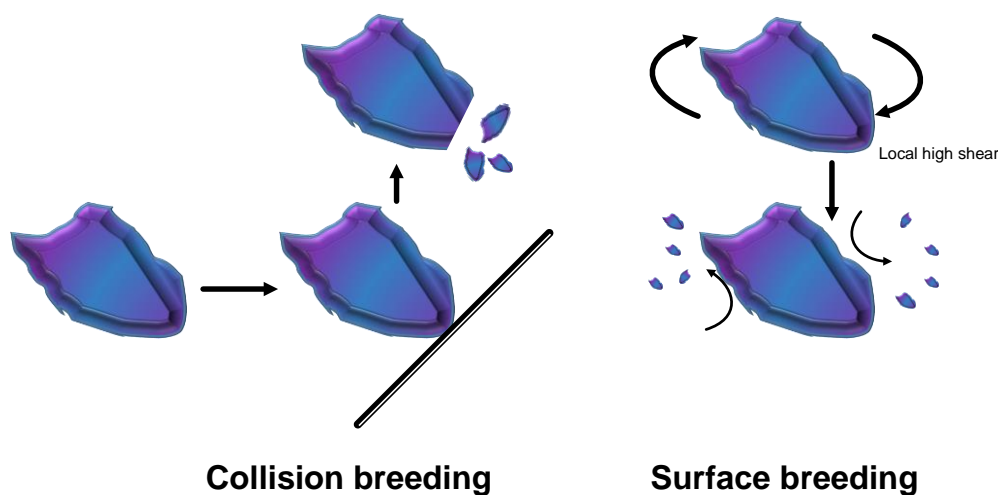


Figure 1.10: Schematic illustration highlighting the mechanisms of secondary nucleation.⁶²

1.3.4 Crystal growth

Following the generation of nuclei, these stable entities grow into larger crystalline particles via crystal growth in the presence of supersaturation. There are a number of factors relevant to crystal growth from which growth theories have been proposed including surface energy, molecular adsorption and diffusion.⁶ Crystal growth is generally considered to consist of two stages where primarily solute molecules within the bulk solution diffuse to and adsorb onto the crystal face followed by adsorbed molecules integrating into the crystal lattice structure with both stages occurring under different concentrations. Surface defects and the presence of impurities can also impact crystal growth although these effects are hard to predict.⁶³

Crystal growth theories involving surface energy assume crystals grow and form a shape to minimise surface area. The surface energy theory has a number of considerable limitations in which important crystallisation parameters such as supersaturation and solution movement cannot be explained in terms of crystal growth. Evidence regarding this theory is limited therefore it is generally not utilised to describe crystal growth.⁶ Simple considerations such as this are not sufficient on its own to describe growth.

The adsorption layer theory was suggested by Volmer.⁶¹ It is considered that solute molecules reach the surface of a crystal and become loosely adsorbed. However, these molecules are free to move across the crystal surface (surface diffusion) whilst having a dynamic equilibrium between the bulk solution and the adsorbed solute layer. The adsorbed solute molecules will attach into the lattice structure where the attractive forces are greatest and will occur in a step-wise fashion until a whole new plane crystal face is achieved. After a new plane crystal face has been formed, for growth to continue, a new crystallisation centre must form. It is proposed solute growth units form a monolayer island nucleus with further solute growth units adding to this feature in order to complete the next plane. From a mechanistic perspective it is widely accepted that crystals do not grow in a perfect layer by layer manner as described by Volmer's model. It is considered most crystals contain dislocations (Figure 1.11) on their surface which results in the generation of steps or kinks which can act as potential sites for solute growth units to incorporate⁶ as illustrated in Figure 1.12.

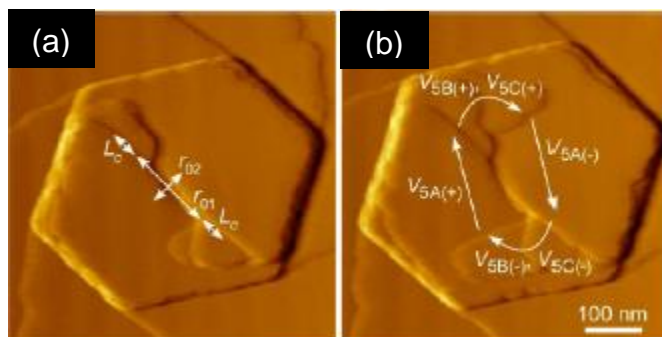


Figure 1.11: Atomic force microscopy (AFM) micrograph showing (a) a dislocation core from which (b) spiral growth of L-cystine occurs.⁶⁴

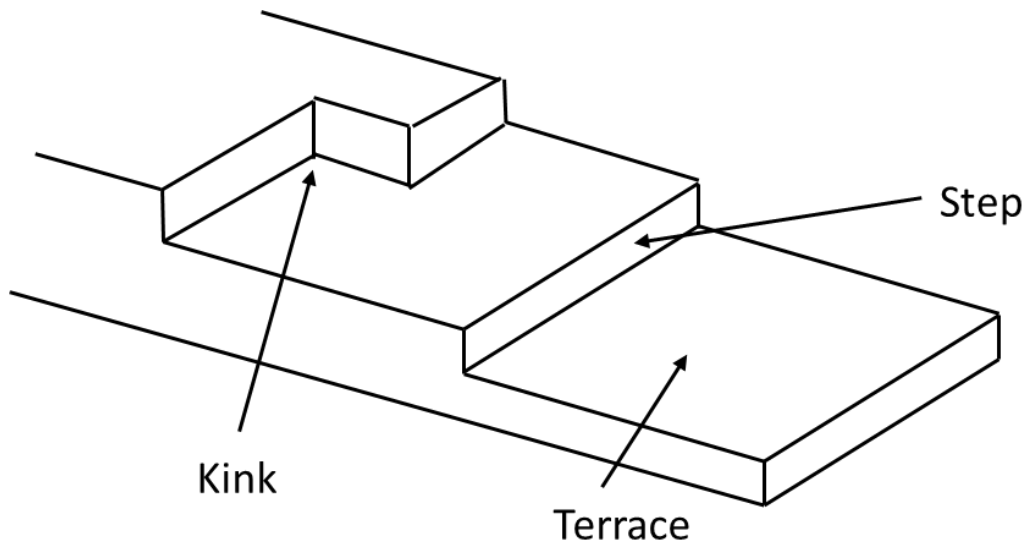


Figure 1.12: Schematic highlighting the three different growth locations on crystal surface namely kinks, steps and terraces. In terms of energetics, kink locations are more favourable for growth followed by step locations. Growth upon terraces is the least favourable for attachment of growth units.⁶

The diffusion theory associated with crystal growth was proposed by Noyes and Whitney⁶⁵ and is grounded on the difference between the concentration at a solid crystal face and concentration of the bulk solution to drive crystal growth. Also, it is assumed that crystallisation is the reverse of dissolution.⁶⁶ The crystal growth rate is governed by the concentration difference between the crystal surface and the bulk solution is defined as:

$$\frac{dm}{dt} = k_m A_{crystal} (c_{Bulk} - c^*) \quad (1.19)$$

Where

- m = Solid mass deposited (kg)
- t = Time duration in which deposition occurs (s)
- k_m = Mass transfer coefficient (kg/(m².s))
- $A_{crystal}$ = Surface area of crystal (m²)

c_{Bulk} = Solute concentration within the bulk (kg/kg)

c^* = Equilibrium saturation concentration (kg/kg)

The diffusion theory was then further developed by Berthoud⁶⁷ and Valetton⁶⁸ in which it was proposed that two steps were involved in crystal growth (Figure 1.13) i.e. diffusion of solute molecules to the surface of a crystal followed by the integration of molecules in the crystalline structure via a first order reaction. It is generally accepted that the diffusion step is related linearly to the concentration difference. Similar to other crystal growth theories, the diffusion theory has limitations however crystal growth rates have been measured by employing this theory.⁶

$$\frac{dm}{dt} = k_d A_{Crystal} (c_{Bulk} - c_i) \quad (1.20)$$

$$\frac{dm}{dt} = k_r A_{Crystal} (c_i - c^*) \quad (1.21)$$

Where

k_d = Mass transfer coefficient (kg/(m².s))

k_r = Integration rate coefficient (kg/(m².s))

c_i = Solute concentration at interface (kg/kg)

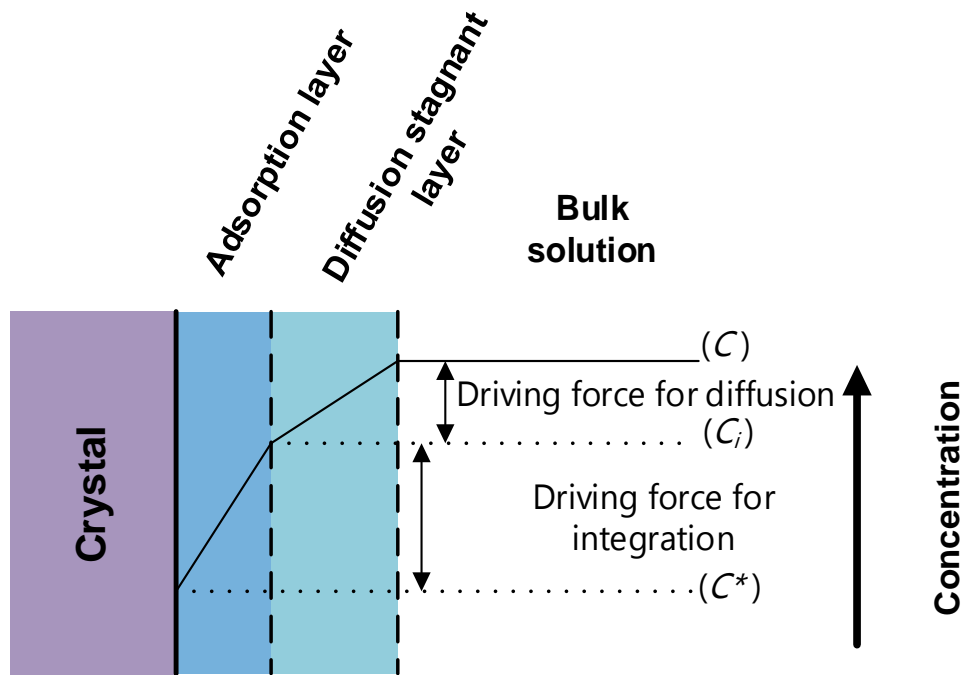


Figure 1.13: Diffusion theory of crystal growth across adsorption and diffusion stagnant layers (two step concentration driving forces).⁶

In reality measurement of solute concentration at the interface is incredibly difficult therefore c_i is replaced by an overall concentration driving force $(c - c^*)$.

$$\frac{dm}{dt} = k_G A_{crystal} (c - c^*)^g \quad (1.22)$$

Where

k_G = Overall crystal growth coefficient (kg/(m².s))

g = Order of growth process

Equation 1.22 can be rearranged into:

$$R_G = \frac{1}{A} \frac{dm}{dt} = k_G \Delta c^g \quad (1.23)$$

Where

R_G = Mass deposition rate (kg/(m².s))

Δc = Crystal growth driving force [$c_{Bulk} - c^*$] (kg/kg)

Crystal growth is crystal face specific with different growth rates associated with different crystal faces. An example of different crystal face chemistries of phenytoin are shown in Figure 1.14 which ultimately dictate subsequent crystal growth. Crystal morphology is dependent upon associated crystal face growth rates in which the slowest growing face having the largest influence of crystal morphology.^{66,69} Imaging techniques have been employed to measure crystal growth rates including optical microscopy⁷⁰ and atomic force microscopy (AFM).⁷¹ Miyazaki and co-workers employed AFM to investigate the elongation growth rate of nifedipine in the presence and absence of selected polymers⁷² highlighting the sensitivity of this approach.

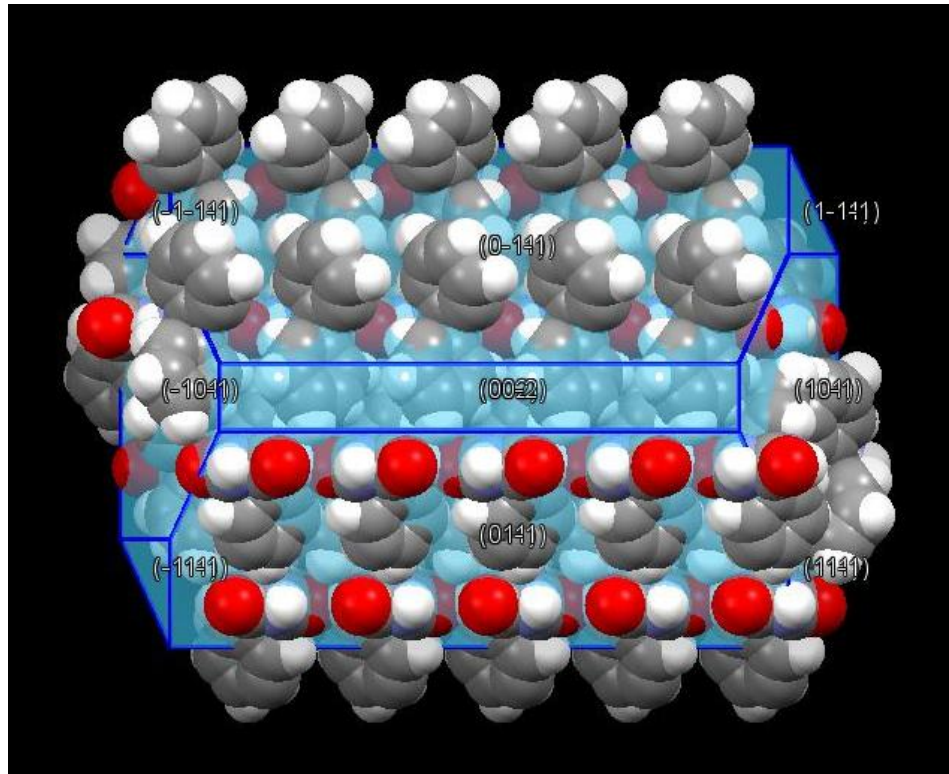


Figure 1.14: Phenytoin packing arrangement highlighting anisotropic surface chemistries in particular (0,-1,-1,1) and (0,1,-1,1) faces (CCDC reference PHYDAN).⁷³

From a fundamental approach, studying single crystal growth can be used to obtain individual crystal face growth rates. Regarding crystalliser design, crystal growth rates are typically expressed in terms of mass produced per unit time per unit area of crystal surface rather than individual face growth rates. The overall linear growth rate, G (m/s), can be expressed as:⁶

$$G = \frac{m_i^{\frac{1}{3}} - m_f^{\frac{1}{3}}}{(\alpha \rho_{cryst} N)^{\frac{1}{3}} t} \quad (1.24)$$

Where

m_i = Initial crystal mass (kg)

m_f = Final crystal mass (kg)

α	=	Volume shape factor
ρ_{cryst}	=	Crystal density (kg/m ³)
N	=	Number of individual crystals
t	=	Time (s)

1.3.5 Considerations associated with crystallisation processes

Crystallisation processes and their basic design are often difficult due to the complexity of multiphase processes. However, for a given crystallisation process the generated crystalline product, as described previously, must meet specified regulatory requirements in which product quality is governed by CQA.²⁶ In relation to pharmaceuticals, the most critical attribute for a crystalline product is chemical purity as this is vital in terms of patient safety upon administration.⁷⁴ Other important specified properties relate to physical phase purity i.e. polymorphic form and also particle properties including morphology and PSD.⁷⁵ Polymorphic form and PSD can influence the performance of a drug formulation via altering bioavailability and consequently clinical outcome.⁷⁶ The crystallisation step in pharmaceutical manufacturing is commonly followed by further downstream processes. The physicochemical properties of generated crystalline product can have a considerable influence upon downstream processes e.g. needle crystal morphology potentially causing filtration issues. Therefore, it is vital that satisfactory understanding of a given crystallisation process is achieved to have confidence in developing a robust process.

A number of issues can arise during a crystallisation campaign that can ultimately impact a crystalline product in addition to process productivity. Crystalline particles generated from a crystallisation process can potentially be affected by encountered environments. Attrition can arise with crystals colliding with solid surfaces present within a crystalliser or by crystal-crystal collisions. Attrition results in the generation of fines that alter PSD and also

decrease crystal quality due to fragmentation.^{6,50} Additionally, crystalline particles generated from a crystallisation process have the potential to physically interact through processes such as aggregation or agglomeration which can be an undesirable outcome.⁷⁷ A common problem which arises frequently with crystallisation in continuous flow is the formation of blockages which can halt a successful crystallisation campaign. As a result, equipment is typically designed to prevent blockages from occurring.⁷⁸⁻⁷⁹ The accumulation of crystalline deposits can limit the operational efficiency of process equipment by decreasing heat transfer and mass transfer. Therefore, fouling during a crystallisation campaign should be avoided.

1.4 Fouling literature review

1.4.1 Fouling introduction

Fouling is defined as the unwanted deposition of crystalline material upon a surface¹⁷ and, within both batch and continuous crystallisation processes, is considered as a significant detriment to quality and control.⁸⁰ The consequences of fouling is variable and dependent upon what stage the fouling deposit has developed to, from a minor reduction in heat transfer to catastrophic unstable crystalliser operation. Typically, the fouled layer consists of solute molecules from the crystallising system. Therefore, a reduction in product crystal yield is anticipated when fouling has occurred.⁷ Fouling of surfaces utilised for heat transfer such as vessel walls can result in a reduction in heat transfer due to the crystalline layer's insulating properties. This results in altered thermal conditions within a crystalliser with reduced product quality in addition to increased energy consumption to compensate for the reduction in heat transfer efficiency.¹⁷ Fouling within pipe-line structures such as the continuous oscillatory baffled crystalliser (COBC), as illustrated in Figure 1.15 (a), results in cross-sectional narrowing and, in extreme cases, complete structure blockage which can create dangerous pressure build-ups.⁶ Fouled deposits are unstable and are liable to detach under shear stress.⁸¹ Large

detached fouled masses are capable of damaging equipment including agitators or pumps in addition to blocking inlet and outlet openings.⁶ Probes and sensors in contact with a crystallising system can potentially foul⁷, as illustrated in Figure 1.15 (b) and (c), where fouling can affect the reliability of process information being gathered.⁸²⁻⁸³ For a given continuous crystallisation process, it is generally anticipated that fouling will eventually occur at some stage during its operation. Dependent upon the extent of fouling, a fouled crystalliser will be required to be shut-down and cleaned which is costly in terms of time and resources. Both the physical consequences and economic challenges of fouling make it an phenomena which should be prevented or limited as much as possible⁸⁴ to allow extended crystalliser operation.

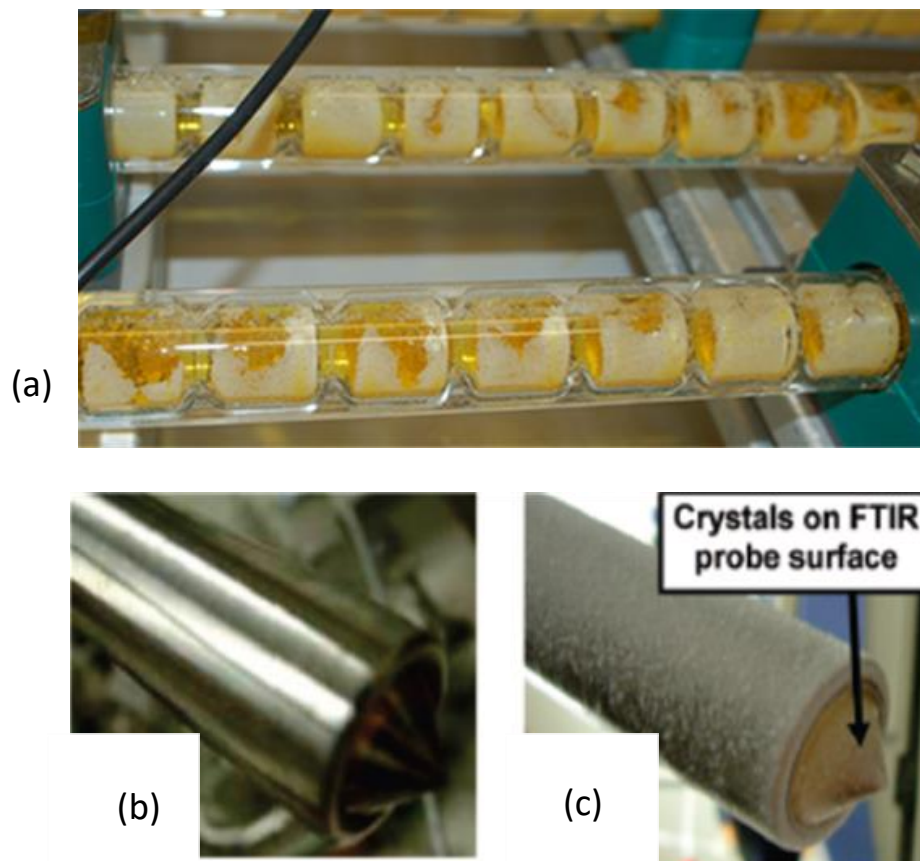


Figure 1.15: (a) Crystallisation fouling present upon the internal surface of an operational COBC. (b) An image of a clean Fourier transform infrared spectroscopy (FTIR) probe with (c) resultant fouling upon all exposed surfaces after solution exposure as identified by Borissova et al.⁸³

From a crystallisation perspective, fouling can potentially occur on any surface in contact with a supersaturated solution. The most prominent cause for fouling to occur in a crystalliser is the generation of local high supersaturation such as cooling jackets, as observed in Figure 1.16, where a large temperature difference (ΔT) exists between the cooled surface and the bulk solution. This is a particular issue in cooling crystallisation processes where a solid surface is employed for indirect heating/cooling. The actual local supersaturation at the surface is uncertain and is also dependent upon the hydrodynamics conditions within a crystalliser.⁶ Local supersaturation can also be caused by vapour-liquor interfaces (as highlighted in 1.1 Background; this phenomena will not be investigated), inadequate agitation and flow stream interactions which are principally related to reactive or anti-solvent crystallisation techniques. Brown and co-workers experienced fouling in the anti-solvent continuous crystallisation of salicylic acid which subsequently limited the operational capacity of the crystalliser.⁸⁵ Fouling can be considered as a crystallisation process albeit an unwanted process as it is influenced by supersaturation. Therefore, relationships associated with nucleation, growth and agglomeration processes can potentially be related to fouling. Duncan and Phillips⁸⁶ and Shock⁸⁷ determined a connection between the MSZW of a crystallising solution and its potential to foul. It was determined that the supersaturation range in which fouling was unlikely to occur is the same as the MSZW for nucleation within the bulk. Ritter found that increasing supersaturation resulted in a decrease in fouling induction time highlighting the importance of supersaturation on fouling.⁸⁸

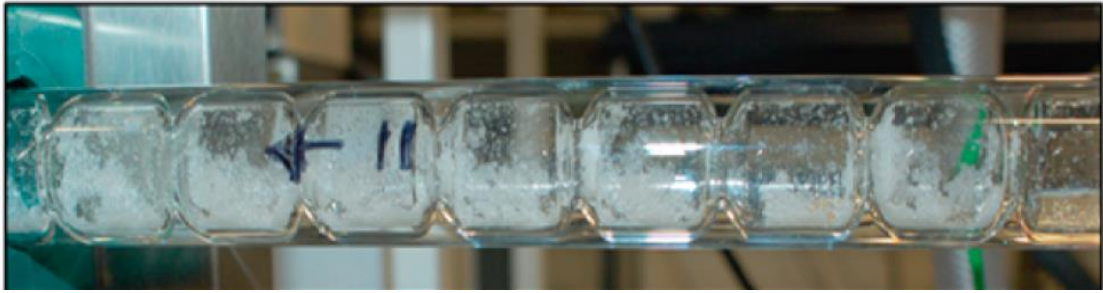


Figure 1.16: Image of L-glutamic acid fouling upon the internal heat transfer surface of a jacketed COBC¹⁸ in which COBC straight '11' had become fouled at the glass interfaces where heat transfer occurs.

Fouling can still ensue even when great effort has been dedicated to controlling supersaturation. Molecular level relationships comprising interactions with solute and solvent molecules and a surface can potentially result in fouling to occur e.g. hydrogen bonding and van der Waals (vdW) forces. In order to comprehend these interactions, the solute and solvent molecular properties such as hydrophobicity, polarity and 3D-structure must be taken into account in addition to the inherent properties of the material substrate the fouled surface is constructed from.⁸⁹

1.4.2 Previous fouling studies

1.4.2.1 Overview of fouling literature and measurements

Fouling research comprises a variety of diverse fouling types such as corrosion fouling, microbiological fouling and reaction fouling. However, the basis of this literature review focuses upon reports relevant to crystallisation fouling. Extensive studies have been focused on heat exchanger fouling by inorganic compounds in which outcomes and learnings can be related to organic compounds such as pharmaceuticals. The bulk of the present literature review focuses on findings from heat exchanger fouling research. However, a small number of crystallisation fouling studies involving organic systems have also been highlighted.

Within heat exchanger fouling, the fouling process is progressive and consists of two distinct stages namely an induction period and a fouling period (Figure 1.17).⁸⁹ Within the induction period, initial crystals are formed and grow upon the surface in which notably these deposits have a negligible effect upon the overall heat transfer coefficient (U). Notably initial crystals deposited upon the surface can potentially enhance heat transfer due to increased surface roughness and enhanced turbulence.⁹⁰ However, as more crystals form/grow and reach a critical value the fouling process progresses into the fouling period where heat transfer is impacted. Within the fouling period the crystalline deposits further grow and develop into a more compact, crystalline layer. As the fouling layer progresses, the heat transfer efficiency between the crystallising system and the fouled surface decreases. Within heat exchanger fouling studies, the impact of fouling on heat transfer is utilised to measure fouling quantitatively termed fouling resistance (R_f) which is defined as:

$$R_f = \frac{1}{U_f} - \frac{1}{U_o} \quad (1.25)$$

Where U_f and U_o are the overall heat transfer coefficients when the surface is fouled and clean, respectively. Fouling resistance is determined at a given frequency which provides several details regarding fouling. Once fouling begins to impact heat transfer, a fouling induction time can be determined which is distinctly different to tradition crystallisation induction time definition (detailed further in Chapter 7 Fouling assessments in novel flow platform). Also, a rate expression can be deduced from the gradient of the fouling slope in terms of heat transfer in addition to evaluating the extent of fouling based upon the magnitude of difference between the fouling resistance values at the induction time and fouling resistance as fouling continues towards reaching a plateau.

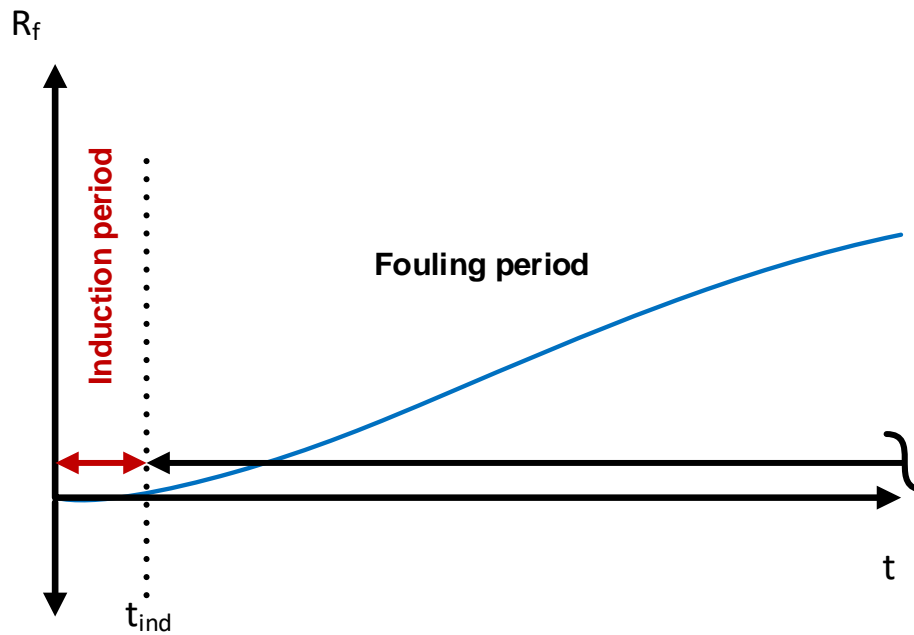


Figure 1.17: Typical fouling curve highlighting the induction period and fouling period in relation to heat transfer.

The fouling period consists of two simultaneously competing processes namely deposition and removal (Figure 1.18). A generic fouling rate ($\frac{dm_f}{dt}$) comprised of deposition rate (m_d) and removal rate (m_r) can be described in terms of mass deposition rate and fouling resistance.^{17,91}

$$\frac{dm_f}{dt} = m_d - m_r = R_f \quad (1.26)$$

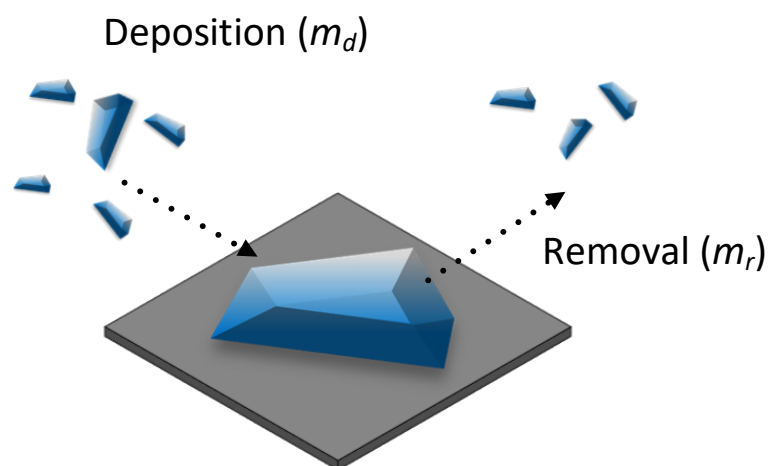


Figure 1.18: Schematic highlighting deposition and removal of crystalline material on a fouled surface contributing to the fouling rate.

It is considered that the deposition process associated with fouling is a function of nucleation rate. The removal process is strongly dictated by the relativities of shear stress due to the hydrodynamics and the strength of adhesive forces between the fouled mass and surface. Additionally, deposition typically occurs from a moving solution which exerts shear stress at a given surface. Therefore, the fouling material must have sufficient adhesive and/or cohesive interactions associated with generated particles and the fouling surface which supersedes associated shear removal forces.⁸⁹

1.4.2.2 Overview of fouling parameters

For a given fouling system it is beneficial to distinguish between process and interface conditions (Figure 1.19) both of which are a function of the crystalline fouling layer.⁹² Process conditions which are acknowledged to impact fouling include the crystallising system (solvent and solute properties), supersaturation, pH, flow velocity and hydrodynamic regime and the introduction of additives. Interface conditions which can influence fouling behaviour comprises surface temperature, surface energy and contributing components, surface roughness, surface topography, number of nucleation

sites, surface type and also the aging of the encrusted layer. It should be noted that the previous two lists are by no means exhaustive.

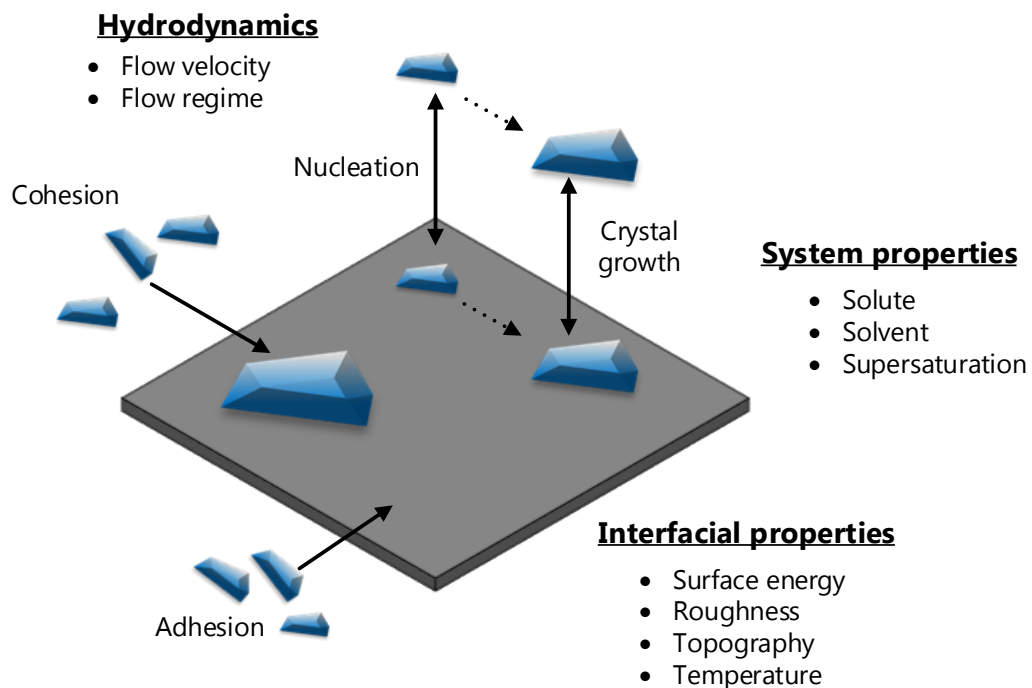


Figure 1.19: Adapted figure from Geddert et al. highlighting contributing parameters to influence crystallisation and particle processes associated with fouling.⁹²

The properties of the surfaces in contact with a crystallising solution are important in impacting fouling in addition to influencing the crystallisation process. Interfacial properties including surface roughness, wettability and surface energy possessed by a surface are the important in influencing adhesion processes.⁹³

Surface roughness is acknowledged to impact nucleation processes and also the adhesion of particles.^{22,93-95} The roughening of a surface alters its wettability in addition to altering nucleus contact angle ($\theta_{Nucleus}$). The rate of primary heterogeneous nucleation, J , (nuclei per unit time per unit surface area) is described as:

$$J = A_{kinetic} \exp(-\Delta G_{net}/(kT)) \quad (1.27)$$

From a molecular perspective, it is perceived that preferential orientation at a surface occurs. Solute molecules incline to orient the hydrophobic fragment of its structure towards a hydrophobic surface and the hydrophilic fragment of the molecule towards an hydrophilic medium and vice-versa for a hydrophilic surface.⁷ These molecular interactions may result in solute molecular pre-ordering or potentially generating local concentration to promote nucleation. However, the previously mentioned molecular interactions would be solute/solvent system specific and generalisation of molecular interactions is challenging.

1.4.2.3 Factors impacting fouling

(a) *Materials of construction*

With an industrial manufacturing setting, process equipment can be constructed and fabricated from a variety of different materials ultimately dependent on the designated purpose e.g. Hastelloy®, stainless steel, borosilicate etc. Different materials have inherently diverse properties comprising physicochemical, mechanical and thermal properties which contribute to a successful crystallisation campaign. As highlighted beforehand, abundant and extensive research has been conducted in the fouling of heat exchangers and, furthermore, the influence of different materials of construction (MOC) from which heat exchangers have been constructed of has been a notable area of research regarding inorganic solution fouling.

(i) *Metallic MOCs*

Typically, metallic MOCs have been investigated in heat transfer studies as heat exchange surfaces primarily due to their inherent high thermal conductivity. Additionally, these materials are robust and have been

traditionally utilised for decades within heat exchangers⁹⁶ and chemical processing equipment⁹⁷ successfully. Kazi explored heat transfer fouling on different heat exchanger pipe MOCs by visually observing the progressive deposition under the specific solution conditions.⁹⁸ The experimental set-up comprised of test pipes constructed from copper, aluminium, brass or stainless steel that were centrally located in a cylindrical tank which comprised a concentric vertical agitator that provided constant and uniform flow conditions near the explored pipe surface. The importance of a MOC's thermal conductivity in relation to fouling was demonstrated by Kazi where larger extents of fouling (mass deposited per unit area) were found with MOCs with increasing thermal conductivity values. Additionally, the investigated metallic substrates were also compared to sand-blast roughened counterparts to assess the impact of surface finishing upon fouling. It was found increasing the surface roughness resulted in increased fouling at given conditions. The importance of MOC thermal properties in addition to surface finishing in relation to fouling was highlighted within this study.

The fouling of metallic substrates by inorganic compounds was additionally explored by Förster and co-workers.²¹ MOCs explored included copper, aluminium, steel and brass with differences in fouling induction time were identified under identical process conditions (Figure 1.20). It was found the MOC with the largest surface energy, namely copper, had the lowest induction time. However, trends between determined induction time values and the surface energy of a MOC could not be correlated.

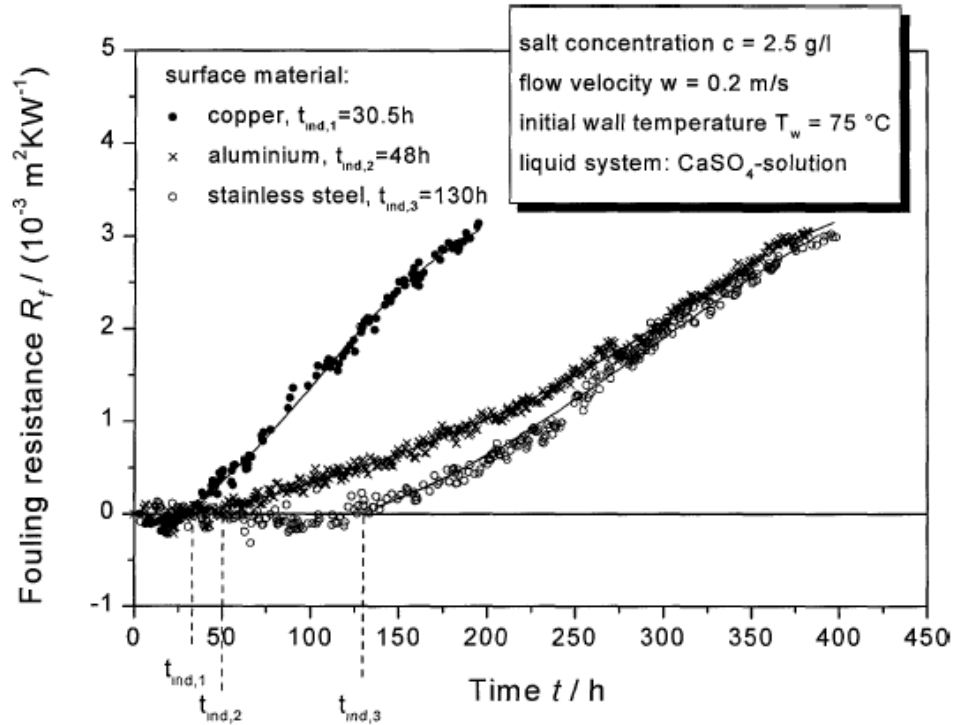


Figure 1.20: Fouling resistance curves versus time for a range of metallic MOCs under identical process conditions highlighting the impact of different MOCs upon fouling induction time.²¹

More recent research by Al-Janabi et al. explored various metallic materials (specifically austenitic alloys) and their heat transfer performance due to forced calcium sulphate fouling.⁹⁹ It was found that Hastelloy® C-276 and standard stainless steel had similar fouling induction times however SMO254 type stainless steel had a significantly larger induction time value under identical process conditions. The roughness effects of the investigated substrates was neglected within this research as the average roughness values (Ra) were within the range of $0.12 \text{ } \mu\text{m}$ to $0.18 \text{ } \mu\text{m}$ which have been proposed to most likely not influence fouling. The principal judgment from this research relates to the surface energy of MOCs. It was proposed that the electron donor component of the total surface energy of a substrate was significant for fouling in particular influencing the fouling rate. One explanation for this fouling behaviour relates to electron donor component values in which lower values

indicate strong interactions between the surface and the fouled deposit. This paper proposes that the total surface energy of a substrate as a single parameter in relation to fouling is debatable and its contributory components of surface energy require consideration.

The impact of different surface finishes of metallic materials on fouling have also been probed. Surface polishing alters the roughness profile of a surface in which surface roughness is defined as the randomly, closely spaced irregularities present at the material's surface.¹⁰⁰ From a chemical processing perspective, construction materials within equipment and instrumentation should be adequately smooth with the absence of problematic surface defects⁹⁷. In terms of engineering fundamentals, surface roughness can be undesirable as it can result in friction and drag. However, on the contrary, surface roughness can be desirable since it can potentially allow a given surface to increase convective heat and mass transfer owed to agitation within the viscous sub-layer.¹⁰¹ Notably transfer rates are highly dependent upon the nature of the roughened surface i.e. distribution of the roughened projections, shape, size and projection orientation.¹⁰²

Al-Janabi investigated shot peened stainless steel surfaces and its impact on calcium sulphate fouling during convective heat transfer.¹⁰³ The shot peening process involves bombarding the MOC surface with metal shots. This treatment improves stress-corrosion resistance properties of the MOC however increases the surface roughness. It was determined that the substrates with a larger roughness value (shot peened surfaces) had lower fouling induction time values in contrast to the smoother, original stainless steel. The significance of roughened surfaces in inducing nucleation were highlighted. Research by Geddert et al. explored the effect of different polishing treatments on stainless steel on the fouling of calcium sulphate as heat transfer surfaces.⁹ Explored treatments comprised using grinding papers with different grit sizes, polishing paste and electropolishing that created stainless steel surfaces of different roughness values. Average roughness depth values (Rz) of surfaces ranged from greater than 4 μm to less than 1 μm associated with electropolished stainless steel. It was found that the induction

time associated with electropolished steel was considerably larger than any of the mechanically polished surfaces in addition unmodified substrate (Figure 1.21). The notion of increasing surface roughness can potentially increase the number of nucleation sites with associated reduced required nucleation energy. However describing fouling with a single roughness parameter is uncertain as numerous are utilised and understanding the full contributions of roughness is necessary.

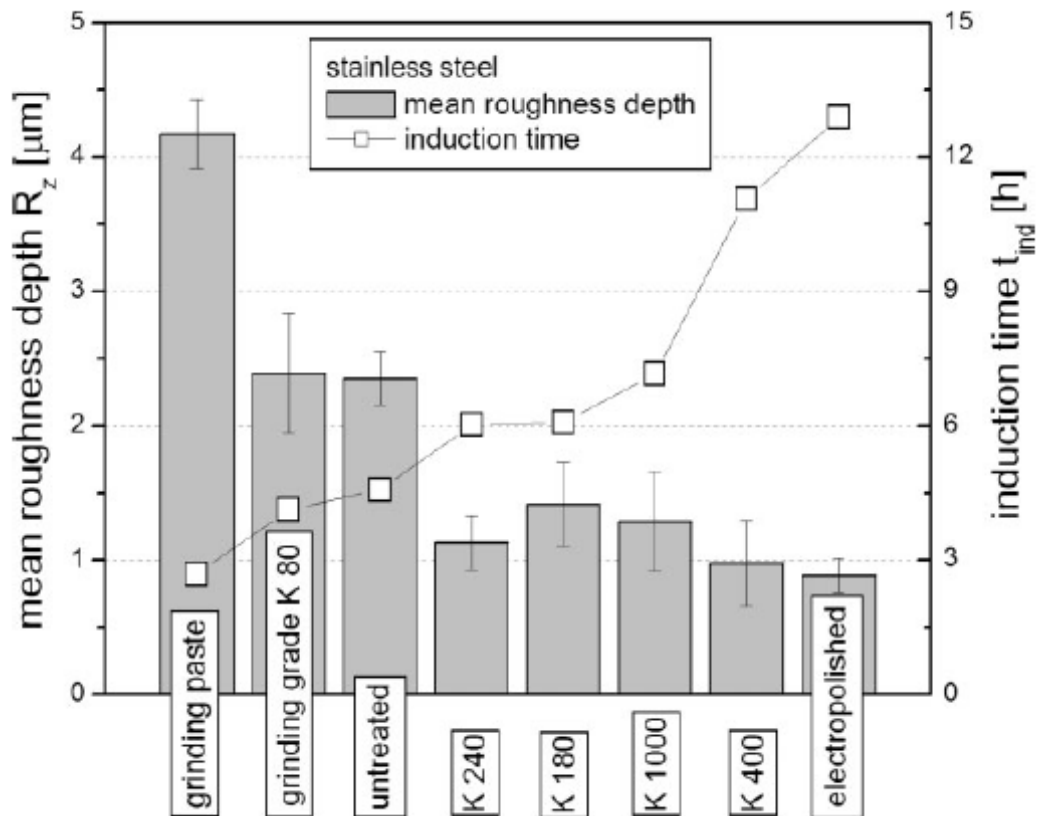


Figure 1.21: Influence of surface treatments upon surface roughness and fouling induction time.⁹

The impact of surface roughness upon adhesive strength of the fouling layer has additionally been explored by Keysar et al. who investigated the adhesive strength of calcium carbonate layers upon mild steel surfaces under well-defined conditions.⁹⁴ It was found that the surface roughness exerted a marked effect on the tenacity of the calcium carbonate deposit with the tensile stress needed to dislodge calcium carbonate deposits adhered to a rough surface

determined to be thirty times greater in contrast to requirements to dislodge calcium carbonate adhered to a smooth surface. Herz et al. demonstrated that the average surface roughness (R_a) has a distinct impact on determined heat transfer due to fouling.¹⁰⁴ It was observed that heat transfer coefficient values decreased faster as the surface roughness increased (Figure 1.22) with the prominent reason being that rougher surfaces have more nucleation sites resulting in faster fouling induction.

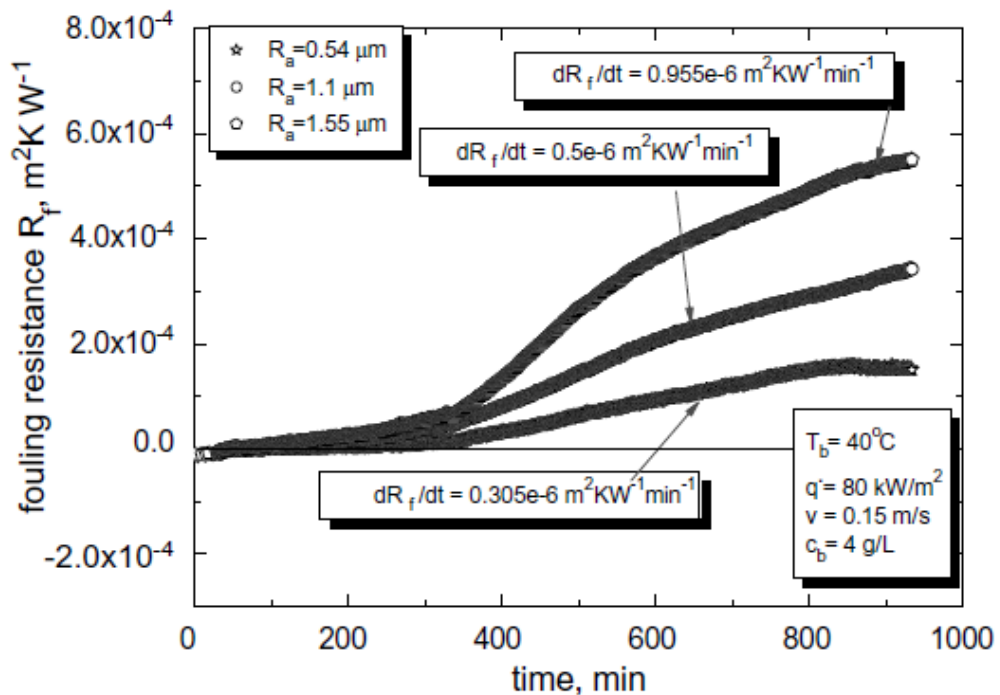


Figure 1.22: Fouling resistance curves versus time for different surface roughness (R_a) values of stainless steel substrates.¹⁰⁴

Bogacz et al. recently investigated the impact of modifying surface roughness, and resulting wetting properties, of stainless steel substrates.¹⁰⁵ Within this work it was found that the wettability of a substrate has a more significant influence on heat transfer fouling curves in comparison with surface roughness.

(ii) Other MOCs

In addition to heat transfer fouling studies of metallic materials, other MOC types have also been explored including polymers. Heat transfer surfaces typically require sufficient thermal characteristics notably thermal conductivity to allow adequate heat transfer across a surface. Polymer coatings of heat exchangers have been utilised to extend operation duration. However, the addition of polymer to a metallic surface decreases heat transfer efficiency in addition to altering other surface properties. The use of polytetrafluoroethylene (PTFE) as a coating for heat exchangers to mitigate crystallisation fouling has been highlighted by Zhao.¹⁰⁶ Numerous stainless steel surfaces were fabricated with different PTFE content coatings in which it was found that the mass per unit area of fouled calcium sulphate deposits for all coated substrates were lower in contrast to untreated stainless steel (Figure 1.23). Notably from this research it is proposed that the surface energy of the coating is significant in influencing the adhesion of calcium sulphate deposits.

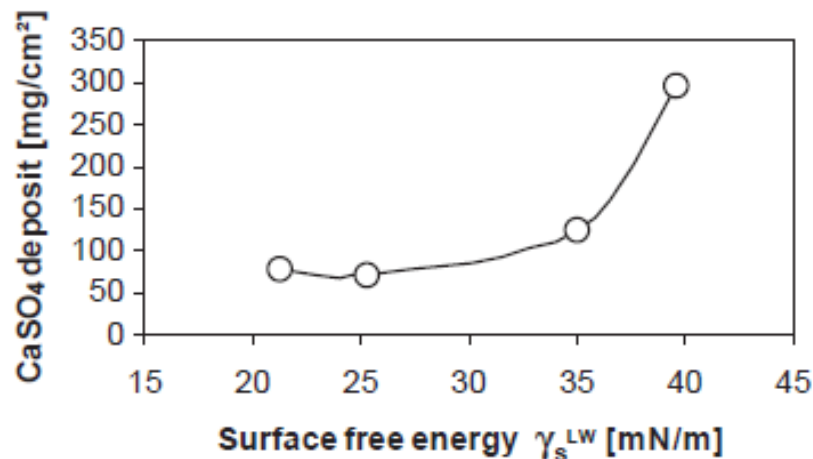


Figure 1.23: The impact of varying dispersive surface energy values of stainless steel/different PTFE-coated stainless steel substrates upon calcium sulphate deposition.¹⁰⁶

Drieser et al. explored the fouling of calcium sulphate on polyetheretherketone (PEEK) performing as a heat transfer interface within a batch crystallisation set-up.¹⁰⁷ It was concluded that PEEK surfaces had considerable advantages in terms of fouling kinetics and extent of fouling in contrast to the investigated

stainless steel material. In terms of fouling induction times, stainless steel fouled instantaneously with no induction period whilst, under identical process conditions, a probed PEEK surface composed of Aptiv® 1000 had a fouling induction time of approximately 10 hours highlighting its potential as a heat exchange material to mitigate fouling. It was emphasised that explaining fouling is not simplistic and is complicated by overlapping of energetic and topographical parameters. The utilisation of polymers as heat exchange surfaces is not novel. Rankin and Adamson explored the deposition of magnesium hydroxide upon various MOC surfaces including stainless steel, copper-nickel alloys and different Teflon™ polymer treated surfaces from flowing seawater evaporating under atmospheric boiling conditions. The initial fouling formation was demonstrated to be a strong function of the material's surface. However, as the fouling layer grows the fouling rate essentially becomes independent of the material surface. In terms of fouling adhesion to the investigated surfaces, it was found that there was very little difference between the various metallic surfaces of similar roughness however adhesion to Teflon™ branded surfaces were determined to be approximately ten times weaker in contrast to metallic surfaces.²²

Within a research laboratory setting, borosilicate is generally used in the construction of equipment including crystallisers. Tachtatzis et al. explored the fouling of L-glutamic acid (LGA) on the internal glass surface of an oscillatory baffled crystalliser (OBC) which acts as a heat transfer surface highlighting that even with the lack of physical features fouling at smooth heat transfer surfaces with lower thermal conductivity values can still foul.¹⁰⁸ LGA fouling upon borosilicate was also identified by Briggs and co-workers.¹⁸

Predominately research regarding the fouling of MOCs typically involves their utilisation as a heat transfer interface. However, fouling additionally occurs at interfaces here heat transfer is not its function such as materials used to construct impellers⁵³, baffles¹⁴ and other crystalliser fittings.¹⁸ Liang et al. investigated the influence of stirrer construction material and its operational parameters upon the primary nucleation of LGA within a batch crystalliser set-up. Retreat curve impellers employed were constructed from either Perspex®

(Poly(methyl methacrylate) (PMMA)) or stainless steel.⁵³ Authors observed evidence of crystals attached to the surface of both stirrers indicating nucleation initially started upon the surface of the stirrer instead of preferentially cooled regions located adjacent to the crystalliser wall. Overall, this research study revealed a heterogeneous nucleation mechanism involving a surface induced process upon the surface of a stirrer that resultantly became fouled. The surface properties and material of construction have an influential effect on the overall crystallisation process.

A number of fouling studies have been conducted by Vendel and Rasmuson to explore fouling mechanisms related to crystallisation fouling by exploring different MOCs.^{7,12} MOCs explored in both fouling studies were stainless steel and Teflon™ in which differences in fouling initiation were observed. Vendel and Rasmuson originally explored two initiation mechanisms namely catalytic nucleation and collision initiation.⁷ An experimental method was developed by which nucleation on a solid surface was investigated at controlled local supersaturation without the interference of particle deposition. In agitated solutions, crystals may form and deposit before they reach detectable size, when it becomes difficult to distinguish between particle deposition and crystal nucleation therefore solutions were quiescent. A variety of compounds were probed however it was determined that Teflon™ has a strong catalytic effect on inducing nucleation in comparison to stainless steel. It was proposed that Teflon™, a hydrophobic material, and reasonably hydrophobic molecules the crystal contact angle will be smaller and nucleation at the surface will be promoted. Collision initiation experimentation found differences between MOCs. Vendel and Rasmuson continued their research into collision initiation mechanisms of fouling at hydrodynamic conditions resembling those in an agitated crystalliser.¹² Stainless steel and Teflon™ were once again probed with more fouled crystals generated on roughened stainless steel in contrast to Teflon™.

(b) **Process conditions**

Alike to MOCs and exploring their inherent properties, modification of process conditions have also been explored within heat exchanger fouling research. Operational parameters that are acknowledged to influence fouling to a significant level include fluid velocity, fluid flow regime, surface/local temperature and bulk fluid temperature.^{17,19}

(i) **Hydrodynamics**

The influence of hydrodynamics on fouling has additionally been probed. Hydrodynamic conditions in relation to fouling has been explored by Förster et al. where stationary/constant and pulsating flow conditions were explored.²¹ For stationary flow conditions, an increase in fluid velocity resulted in an increase in fouling induction times. Pulsating flow conditions created a wide range of responses from instantaneous fouling with a negligible induction period to no detectable fouling detection after 500 hours. Wang recently explored crystallisation fouling of calcium carbonate in a double shell heat exchanger more specifically investigating the impact of different flow velocities/Reynolds numbers (Re) upon fouling resistance.¹⁰⁹ Wang determined that at lower Reynolds number flows ($Re < 2100$) the mean growth rate of fouling increased with increasing Reynolds number however at larger values ($Re > 2100$) the mean growth rate of fouling decreases with increasing Reynolds number. Bogcaz et al. explored different solution flow rates in the crystallisation fouling of magnesium sulphate heptahydrate in which it was found that fouling occurred firstly in the highest explored flow rates for all explored conditions.¹⁰⁵ Additionally, increasing solution flow rate also increased the fouled deposit's mass which is characteristic of a diffusion related mechanism. Fluid velocity can impact fouling via a number of ways. The transfer of solute molecules from bulk to surface interface is associated with diffusion controlled processes and increasing fluid velocity enhances diffusion process and resultantly causes more fouling. However in most instances as fluid velocity increases towards higher values fouling

decreases – increasing flow velocity increases the fluid shear stress at the surface which can remove more deposited crystalline material which is ultimately dependent on the adhesion strength.^{17,98} Chen et al. obtained agreeable results where fouling rate and asymptomatic fouling resistance values increased and fouling induction times decreased with decreasing fluid velocities¹¹⁰ as shown in Figure 1.24.

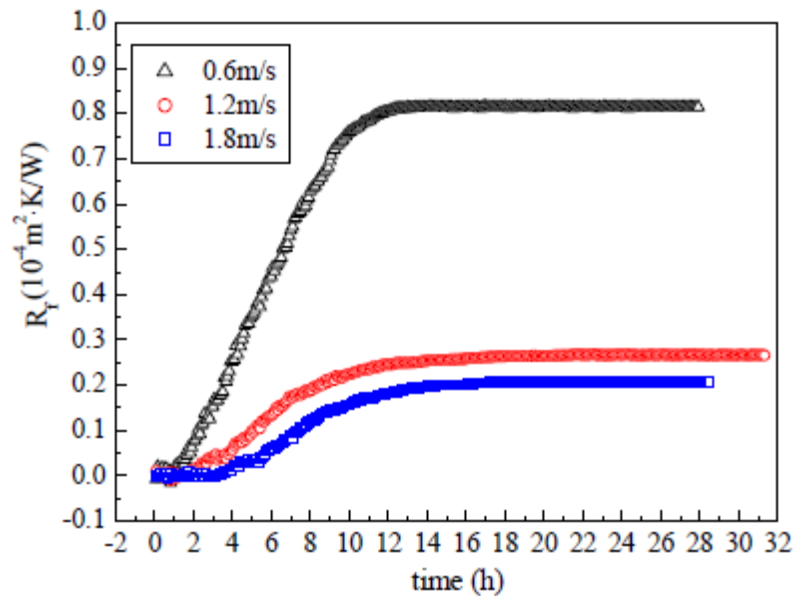


Figure 1.24: The influence of flow velocity upon fouling resistance curves for calcium carbonate fouling.¹¹⁰

(ii) Temperature

The surface temperature can also increase, decrease or have no impact upon fouling and is system dependent.^{17,98} For inverse soluble inorganic solutes increasing surface temperature increases fouling owing to larger concentration gradients however for normal solubility solutes cooling of the surface results in increased fouling. The surface temperature, in addition to contributions from the bulk solution temperature, dictate local supersaturation. Bansal and Müller-Steinhagen explored numerous process parameters which influence fouling one of which was the average heat exchanger wall temperature.¹¹¹ It was determined that larger average wall temperatures were associated with higher fouling rates. Additionally, this research also visually revealed that the location

where the hot stream entered the heat exchanger presented a larger extent of crystalline fouling due to a greater temperature difference (ΔT). Quan also examined the effect of surface temperature of a heat exchanger upon fouling resistance with respect to time in which it was determined that increasing the surface temperature increases fouling resistance values.¹¹² Drieser et al. also explored the impact of increasing substrate temperature which resulted in decreased fouling induction times, increased fouling rates and also increased fouling extent in terms of heat transfer.¹⁰⁷

In addition to the local surface temperature on which fouling can occur, the temperature of the bulk solution can impact fouling. For organic solutes decreasing the bulk solution temperature enhances the rate of crystal formation which ultimately can be deposited on a surface. Bulk crystallisation is governed by supersaturation which is dependent upon the bulk solution temperature. Pääkkönen et al. explored the impact of crystallisation on fouling upon stainless steel heat transfer surfaces.¹¹³ Within the research two different elements of fouling were investigated which included surface nucleation and composite fouling. In terms of experimental setup, composite fouling comprising particle deposition and surface nucleation was explored with no inline filter present whilst exclusively surface nucleation was explored by filtering out formed crystalline materials prior to substrate exposure. It was found that the combination of both surface crystal growth and particles deposited onto the surface via bulk crystallisation resulted in a significant increase in fouling resistance highlighting the importance of crystallising system understanding in particular to the generation of particles in bulk. The importance of fluid flow velocity and surface temperature are also demonstrated within this research. In addition to generating particles in suspension, the bulk solution temperature may contribute towards localised surface temperature and therefore impact local fouling via local surface nucleation.

(c) **Solution properties**

It is generally considered that fouling is solute and solvent system specific since fouling does not always ensue in addition to differing fouling responses under similar process conditions. Vendel and Rasmuson explored a variety of different organic and inorganic solutes and their fouling on stainless steel and Teflon™ substrates under identical conditions in which considerable differences in fouling behaviour between investigated fouling molecules was highlighted.⁷ Nývlt and Veverka investigated the fouling of various fouling molecules upon cooled surfaces in which different timescales for fouling to occur were identified as illustrated in Figure 1.25. A correlation between MSZW and time for fouling to occur was proposed for a variety of crystallising solutes with a narrow MSZW associated with a small experimental timescale for fouling to occur.¹⁵

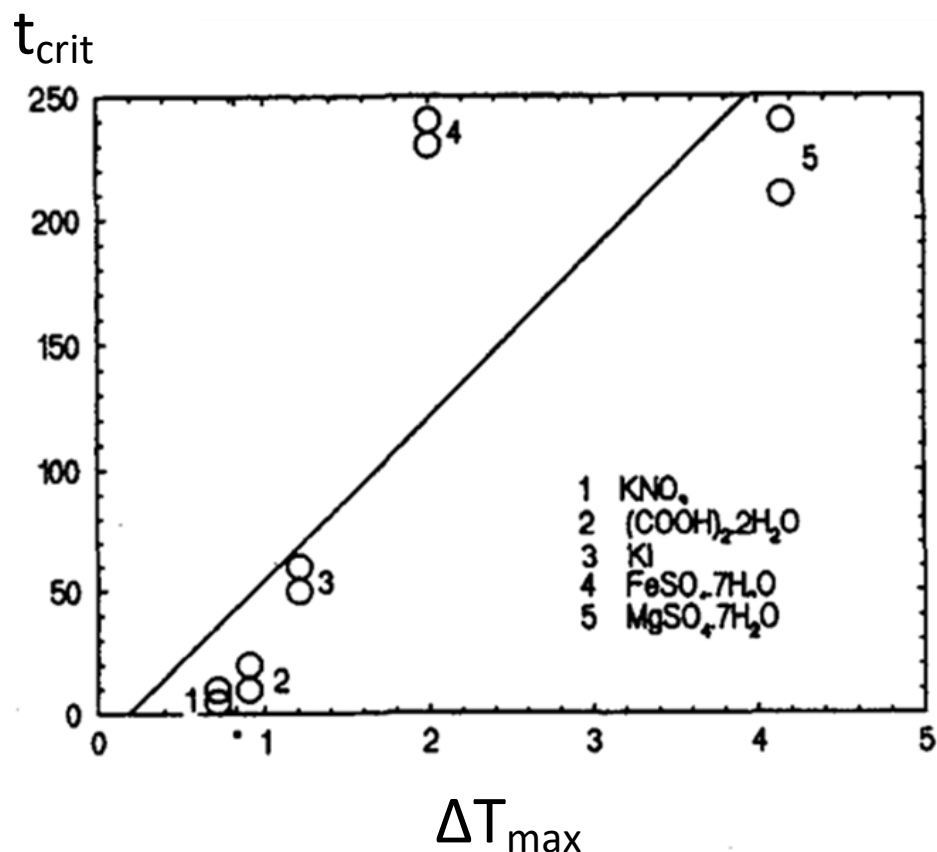


Figure 1.25: Nývlt and Veverka's plot illustrating critical time for scaling/fouling as a function of MSZW for various fouling molecules.¹⁵

The physicochemical properties of the solute and solvent molecule and their interactions ultimately contribute towards the generation of supersaturation which is essential for fouling to occur. The role of solvents and their properties are acknowledged to impact crystallisation processes such as agglomeration¹¹⁴, polymorphism¹¹⁵ and crystal morphology.¹¹⁶ Therefore, it is reasonable to assume it will additionally influence fouling.

1.4.2.4 Fouling mitigation

Fouling within a crystallisation process is anticipated to eventually occur throughout its operation. Mitigating fouling from occurring is highly desirable to extend a crystalliser's operation in particular for continuous campaigns. Continuous manufacturing plants are expected to operate for approximately 50 weeks successively a year according to one author underlining the necessity to prevent system failure.³¹ To combat fouling from occurring a number of approaches can be taken including mechanical and chemical methods. Mechanical methods often require a crystallisation process to be halted which are not suited for continuous operations. Generally mechanical methods only provide a partial solution with chemical methods more appealing with examples including the addition of additives, modification of pH and degassing.^{17,117} The use of chemical additives can potentially result in undesired product contamination or have an adverse effect on the crystallisation environment. For highly regulated organisations such as those within the pharmaceutical industry, the chemical additive approach to mitigate fouling is often dismissed. However, the addition of additives as a technique to mitigate fouling occurring has been successfully demonstrated by numerous authors in relation to heat exchanger fouling in addition to organic crystallisation research. Powell et al. examined the use of a common drug excipient, hydroxyl propyl methyl cellulose (HPMC), as an additive during the continuous crystallisation of paracetamol as a method to enhance crystallisation control.¹¹⁸ The presence of HPMC was found to suppress nucleation and crystal growth in addition to successfully mitigating fouling for

an extended period of time. This notable research would not require the removal of the additive as it may be employed as a drug excipient. A recent publication by Lapidot and Heng highlighted the addition of functionalised silica particles within a crystallising calcium sulphate system as a means to mitigate fouling.¹¹⁹

Surface modification of a substrate is an attractive approach to mitigate fouling occurring on crystalliser surfaces. Within research literature there are numerous reports highlighting the use of modified substrates to control and modify nucleation e.g. altering nucleation induction times¹²⁰ or polymorphic form.²⁴ Within heat exchanger studies surface modifications have been utilised to mitigate crystallisation fouling. In order to evaluate the anti-fouling potential of a surface modifications method, the impact on extending the fouling induction time must be assessed against the financial cost associated with such a modification.¹²¹ One such surface modification that has been extensively employed to mitigate fouling is coating surfaces in particular with polymers such as PTFE primarily due to its well established non-stick properties. However, low thermal conductivity, poor abrasion resistance and difficulty in adhering the polymer onto metallic substrates inhibits its industrial application in addition to its high financial cost.¹²²

The formation of a fouled deposit upon a surface can be considered in terms of attractive forces between the deposit and the surface. The first step of the fouling process on a heat exchange surface is the formation of a crystal phase on its surface from the solution. The phase transition from solution to solid is driven by the minimisation of the free energy of the crystallising system. Low levels of fouling are typically anticipated on substrates which have low surface energies such as PTFE, fluorinated ethylene propylene (FEP) and other hydrophobic related materials.¹²² However research by Förster et al. explored a variety of different polymer coatings as a means to mitigate fouling of heat exchangers in which it was determined no considerable difference in terms of fouling induction time between metallic substrates and fluorinated polymer coated substrates.²¹ It was proposed that the topography of the fluorinated polymer coatings was the principal reason for not observing distinct fouling

induction time differences with surface defects supporting the formation of stable nuclei.

In addition to coatings, other surface modifications have been probed to mitigate fouling. The intentional incorporation of impurities onto a surface via innovative surface modification techniques may be used to target lower surface energies and essentially present a barrier to fouling. Müller-Steinhagen et al. investigated SiF_3^+ ion implantation onto steel to reduce calcium sulphate fouling using a closed flow loop system.¹²² Müller-Steinhagen and co-workers determined that the implanted heat transfer surface was shown to reduce calcium sulphate dihydrate fouling significantly, with a measured increase in water contact angle of approximately 20° and a resultant reduction in wetting behaviour. However, the robustness of such surface modifications is debateable in particular regarding long term stability and, regarding pharmaceutical crystallisation processes, concern around fragments entering product stream. Superomniphobic surfaces have also been highlighted as one strategy to mitigate fouling due to their advanced repellent qualities.¹²³

The application of ultrasound has been applied for fouling mitigation. Within the last number of decades ultrasound technology has experienced a significant in development and utilisation including implementation at industrial manufacturing scales.¹²⁴⁻¹²⁵ Sonication has been utilised by a number of research investigators in particular concerning continuous crystallisation.^{14,126-127} Siddique et al. successfully conducted continuous sonocrystallisation campaigns of lactose monohydrate with no problematic fouling.¹²⁶ Sonocrystallisation has been demonstrated to influence nucleation including reductions in induction time and MSZW however it is challenging to predict exactly how sonication will impact a crystallisation process. There are two proposed methods in which sonication can impact fouling.^{126,128} The first method comprises the vibration of the surface which resultantly detaches adhered crystalline material. The second method involves the formation of cavitation bubbles near to the solid-liquid interface. The formed bubbles collapse resulting in shock waves that within the locality remove fouled

material. The effectiveness of sonication in mitigating crystallisation fouling is contentious as demonstrated by Narducci et al. where sonication had a notable effect in reducing fouling on non-cooled surfaces (Figure 1.26 (a) and (b)) however fouling was comparable for sonicated and non-sonicated cooled surfaces.¹⁴

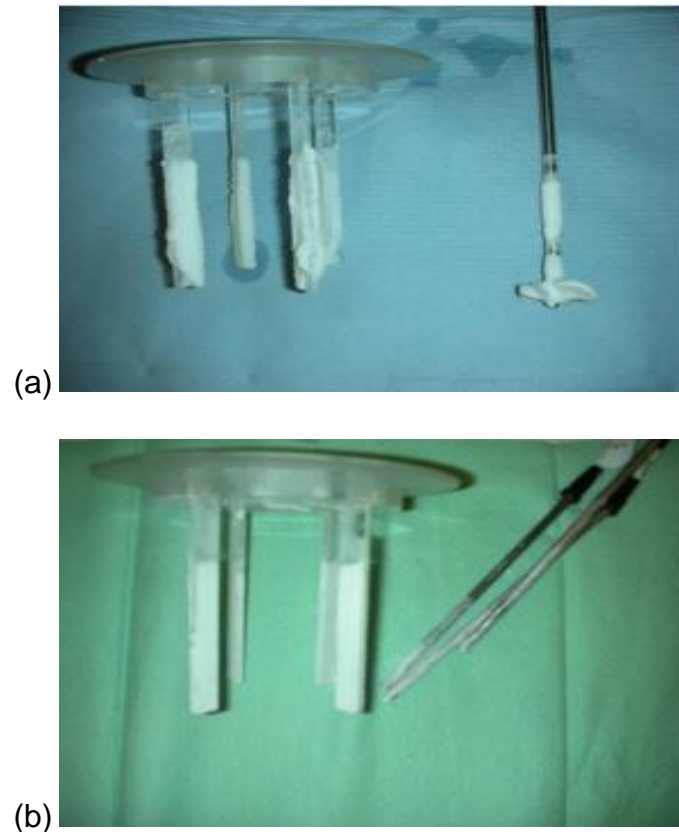


Figure 1.26: Images of fouled surfaces under (a) silent conditions and (b) sonication. Fouling was more prominent under silent conditions.¹⁴

Other techniques employed to mitigate or reduce fouling include changing the operational conditions. Notably however altering crystallising operating conditions to impact fouling will resultantly impact the crystalline product. Operational parameters which can be altered to contest fouling comprises the application of thermal shock (rapid increase or decrease in temperature) and increasing shear stress by pulsation, increase in flow velocity or reverse flow.⁹⁸ Additionally, the use of seed crystals is acknowledged as a strategy to prevent

fouling from occurring or limits its impact.^{18,129} Continuous seeding has been used to avoid fouling in successful continuous crystallisation campaigns.^{18,130}

1.4.2.5 Fouling measurement methods

Within fouling literature a number of different techniques to measure fouling have been utilised as summarised in Table 1.1. Additionally theoretically appropriate measurement techniques from related disciplines which are not routinely/have not been used to measure fouling are also detailed (Table 1.1). The most prevalently employed technique within heat exchanger fouling literature is assessing the impact of the fouling deposits on overall heat transfer coefficients and resultantly calculating fouling resistance (R_f). However, this type of measurement has not been performed routinely for organic crystallising systems. Other fouling measurements related to heat exchanger fouling include determining pressure drop and examining the fouled deposit via elementary techniques which are potentially applicable to organic crystallisation fouling. The use of imaging methods to monitor fouling has been routinely used including within organic crystallisation fouling. Tachtatzis et al. employed imaging methods in conjunction with statistical methods to detect early fouling indications which can allow corrective actions to be taken.¹⁰⁸ More sophisticated non-invasive measurements which have the potential to be utilised in measuring fouling have been highlighted Table 1.1 however their use is not established.

Table 1.1: Summary of measurements from literature utilised to describe fouling.

Fouling measurement	Description	Ref.
Fouling resistance/heat transfer measurement	Fouling resistance (R_f) can be calculated from deviations in overall heat transfer coefficient values via temperature trends across heat transfer surfaces. (See Equation 1.25). Fouling information obtained include fouling induction time (onset), rate of fouling and extent.	95,113 ,131- 132
Fouled deposit mass and mass coverage	Simple method to assess extent of fouling by measuring change in weight. Mass coverage and mass deposition rates can be determined.	81,133 -134
Fouled deposit thickness	A simple technique dependent on reasonable access to the fouled deposit. Techniques include the use of a micro-meter, travelling microscope or callipers to measure deposit thickness.	17,135
Fouled deposit morphology and deposit distribution	The use of microscopic techniques such as optical microscopy, atomic force microscopy or scanning electron microscopy to evaluate fouled single crystals and crystalline layer formation upon a surface. Additionally, the number of crystals formed on a surface can be determined.	7,136- 139
Pressure drop	Considered as an alternative to heat transfer measurements. Monitoring changes in pressure drop due to the presence of a fouled solid within a system. Measurements can be made using a differential pressure sensor.	17,140 -141

Table 1.1 continued...

<p>Progressive imaging of fouling</p>	<p>Images collecting at a given frequency to monitor the initiation and development of fouling. Imaging sources include the use of commodity webcams, particle imaging velocimetry measurement systems and microscopic imaging techniques. Information that can be eluded comprise induction time and growth rates in terms of area coverage.</p>	<p>7,95,1 08,142 -144</p>
<p>Use of process analytical technology (PAT) probes</p>	<p>The use of conventional PAT probes traditionally used to monitor crystallisation processes have also been explored to monitor fouling. However these techniques have not been established and are not traditionally employed.</p>	<p>145- 146</p>
<p>Acoustic fouling assessment methods</p>	<p>Quartz crystal microbalance (QCM) is a highly sensitive technique that can potentially detect thin layer deposits and the development of the fouling layer. It has limitations in implementing within a fouling system. Other acoustic methods have been used to detect fouling.</p>	<p>147- 149</p>
<p>Other non-invasive techniques</p>	<p>A number of developed methods have been demonstrated within research including tomography techniques and ultrasonic time domain reflectometry. These methods are not established within crystallisation fouling research however have been applied to other fouling disciplines.</p>	<p>150- 151</p>

1.4.2.6 Modelling crystallisation fouling

Modelling of crystallisation processes has received notable interest within recent years with conventional modelling approaches grounded on mass balance, energy balance and crystal population equations.⁶ Modelling related to crystallisation is challenging due to the large number of factors that can influence and contribute towards the process. Furthermore, fouling complicates prediction of the performance of a crystalliser primarily due to the uncertainty of when and where fouling initiates. Research by Peroni et al. highlighted the importance of having a fouling contribution incorporated within a crystallisation model to productively predict crystallisation behaviours and

outcomes.¹⁵² However, modelling of fouling is problematic due to the complexity of fouling deposit formation and lack of reproducibility from fouling measurements. Additionally, models to describe fouling often have a large number of assumptions. Nevertheless, fouling models have been generated by numerous authors. Recent research by Majumder and Nagy modelled a crystallisation process within a plug flow crystalliser and incorporated a fouling model in order to achieve a desired concentration profile in addition to adequate PSD.⁸ The fouling aspect of the generated model includes mechanistic processes comprising transfer of solute molecules towards the surface, integration of solute molecules into the fouled mass and also detachment. Having greater understanding of fouling mechanisms can lead to enhanced crystalliser modelling capabilities in particular concerning qualitative predictions.

1.4.2.7 Mechanisms related to crystallisation fouling

Although elementary processes related to crystallisation and particle interactions can be used to generally describe fouling, fundamental understanding of mechanisms involved in crystallisation fouling are currently limited. The stages involved in heat exchange fouling are well established comprising an induction phase and fouling phase as previously detailed. For organic crystallising fouling systems, the previously stated fouling stages have not been established however are considered to be relevant in addition to fouling occurring on non-heat transfer surfaces. Research by Vendel and Rasmuson proposed the sequential stages involved in crystallisation fouling in addition to highlighting important fouling initiation mechanisms. These initiation mechanisms are illustrated in Figure 1.27 in addition to elementary crystallisation and particulate processes.^{9,12}

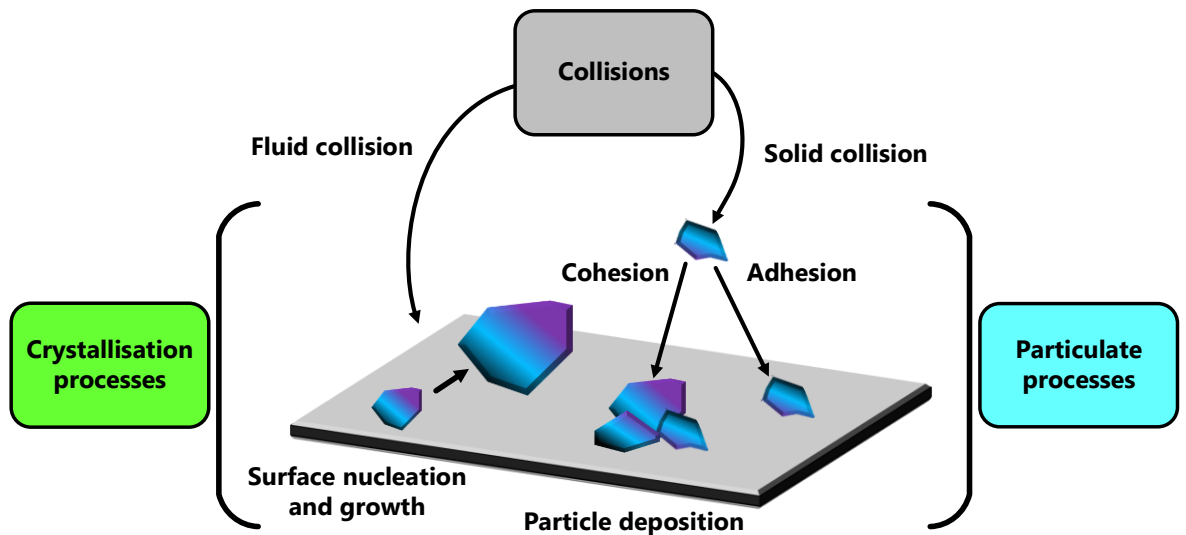


Figure 1.27: Adapted schematic figure highlighting initiation and growth mechanisms of crystallisation fouling involving fundamental crystallisation and particulate processes.^{9,12}

Vendel and Rasmuson originally explored two initiation mechanisms relating to crystallisation fouling namely collision induced nucleation and catalysed nucleation.⁷ It was determined from this work that the presence of a solid surface may catalyse primary nucleation with resulting fouling however this was only identified at higher levels of supersaturation. Additionally, within this research exploring fouling initiation via collision nucleation, it was identified that parent crystals that gently collide and slide down the solid surface can ultimately leave a trail of crystalline material on the surface. Surface-attached nuclei were generated at the surface at relatively low levels of supersaturation within the MSZW. The importance of secondary nucleation and hydrodynamic conditions within a crystallising system upon crystallisation fouling were highlighted. Relating to fouling mechanisms this research emphasises wall/surface nucleation and crystal/surface collisions as important initiation mechanisms however to what extent each contributes within a typical crystallisation campaign was not evaluated. Fouling initiation mechanisms were highlighted to be influenced by supersaturation in which catalysed induction was found at high levels of supersaturation. Additionally, within this

work a variety of different compounds were investigated in addition to different MOCs in which a wide range of fouling responses were identified (Figure 1.28). This raises queries regarding the importance of both the crystallising system and also the construction materials that are in contact with the crystallising system.

Compound	Steel Plate*	Teflon Plate*
Potassium bromide	Slide off at ΔT 3.0–5.0°C (2)	At bottom at ΔT 4.0°C (1)
Sodium sulfate	Slide off at ΔT 1.0–3.0°C (2)	At bottom at ΔT 1.5°C (1)
Adipic acid	Crust initiation at ΔT 4.0°C (1)	Crust initiation at ΔT 4.0°C (1)
Citric acid	Slide off at ΔT 8.0–15.0°C (5)	Crust initiation at ΔT 9.0–15.0°C (4)
Glycine	No nucleation at ΔT 4.0–7.0°C (2)	No nucleation at ΔT 4.0–8.0°C (3)
	Slide off at ΔT 8.0°C (1)	Crust initiation at ΔT 6.0°C (1)
Succinic acid	No nucleation at ΔT 5.0–6.0°C (2)	Crust initiation at ΔT 2.0–5.0°C (6)
	Crust initiation at ΔT 0.5–5.0°C (8)	No nucleation at ΔT 1.0°C (1)

Figure 1.28: Image of tabulated results from Vendel and Rasmuson’s research regarding collision initiation in which diverse fouling outcomes were identified for explored MOCs and solute molecules.⁷

Vendel and Rasmuson further researched fouling initiation mechanisms in particular establishing to what extent collision initiation of fouling would occur at hydrodynamic conditions resembling those in an agitated crystalliser.¹² Initiation of fouling was determined to occur at levels of supersaturation distinctly below the MSZW for all explored MOCs. On explored rough steel substrates, fouling initiation increased with increasing suspension flow rate towards the substrate, with increasing size of crystals suspended in the flow and also with increasing levels of supersaturation highlighting the contributions of process and system parameters upon initiation. A lower extent of fouling, in terms of number of fouled crystals, was initiated on smooth steel and Teflon™ substrates in contrast to explored rough steel substrates. The principal learning from this research that fouling can be initiated by crystals colliding with a given substrate highlighting its importance with a crystallisation process where generated crystals can collide with the surface of crystalliser equipment. This investigation further emphasises the importance of the hydrodynamics in crystallisers and the impact of operational parameters used within a crystallisation campaign has on initiating fouling.

Vendel and Rasmuson explored initiation mechanisms by using experimental techniques to explore each mechanistic process individually however fouling is anticipated to comprise a composite of mechanisms. Findings from inorganic fouling systems may have applicability to traditional normal solubility fouling systems in terms of mechanisms. Pääkkönen et al. investigated two fouling mechanisms namely surface nucleation and composite fouling (comprising surface nucleation and bulk generated particle deposition).¹³³ The composite fouling had a significant increase in fouling resistance in contrast to fouling due to surface nucleation alone. The learning from this research, in relation to Vendel and Rasmuson's work, emphasises the importance of not treating fouling as a single mechanistic process and that multiple mechanisms may be involved. Additionally it underlines the impact an additional fouling mechanism on the overall fouling process.

1.5 Motivation for research

At present the number of crystallisation fouling studies, notably fouling mechanism studies, are limited yet still remains a key operational issue.⁷ Proposed initiation mechanisms highlighted by researchers are relatively generic and it is not known to what extent each initiation mechanism occurs. Establishing what the most prominent fouling mechanism is for a given crystallisation process is required to propose specific mitigation strategies. In addition to fouling initiation mechanisms, fouling growth mechanisms are not traditionally probed however crystallisation and particle processes are considered again to be appropriate. Additionally, within a crystallisation process numerous parameters, as detailed in previously, are acknowledged to influence fouling however, similar to fouling mechanisms, the contribution of each parameter is not established and which parameters are considered as most important. Relating these parameters to fouling mechanisms allows for further fundamental fouling understanding. Ultimately by enhancing fouling mechanism understanding overall crystallisation process understanding will be enhanced (Figure 1.29). A series of suggestions on how to evaluate fouling

was expected as an outcome from this work in addition to proposing practical advice for future continuous crystallisation campaigns.

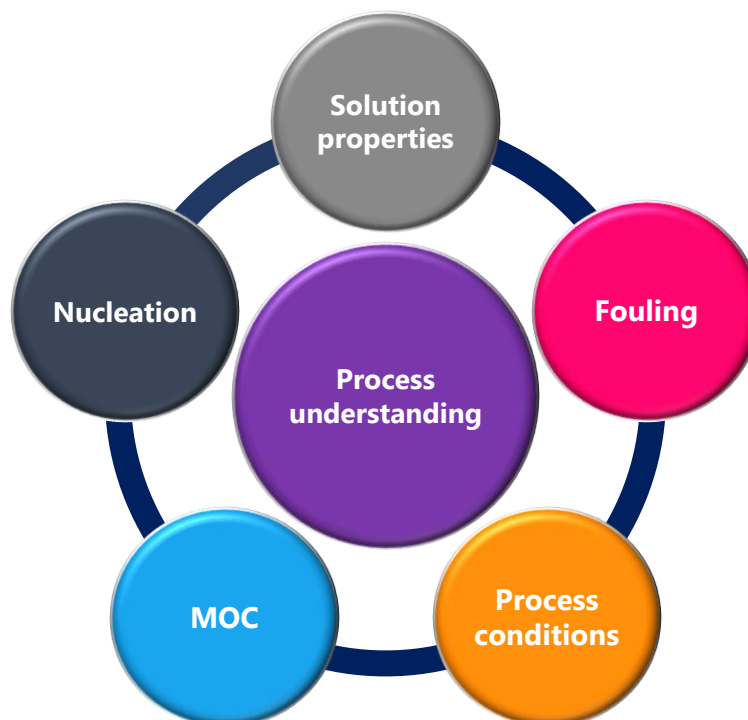


Figure 1.29: Schematic of the relationship between processes and parameters leading to process understanding.^{7,9,19,53,133,153}

Chapter 2. Aims and objectives

2.1 Aims

The overall aim of the research described within this thesis is to enhance the understanding of fouling mechanisms relevant to continuous crystallisation. The principal goal is to understand which factors influence crystallisation fouling and determine conditions where fouling occurs and relate these to fouling mechanisms. To achieve this a number of experimental approaches were conducted. Four research areas included MOC characterisation, crystallisation fouling investigations, assessment platform design and generation of fouling models. Ultimately a systematic approach to evaluate fouling was the targeted outcome for this work in addition to practical recommendations.

2.2 Objectives

A variety of objectives were targeted in order to meet the proposed thesis aims.

- The initial focus of research was regarding MOC characterisation in which a diverse array of MOCs used within process equipment were pursued.
 - Characterise using experimentally determined results and data from literature.
 - Experimentally characterise using contact angle goniometry and atomic force microscopy.
 - Create a MOC characterisation dataset.
 - Assess diversity via principal component analysis.
- To develop a number of fouling setups to probe fouling mechanisms.
 - Configure a small scale batch crystallisation setup to explore nucleation and fouling.
 - Develop and manufacture a continuous flow assessment platform for fouling.
- Explore a variety of different MOCs and process parameters within the small scale batch crystallisation setup.
 - Assess investigated parameters upon nucleation via statistical approach.
 - Assess investigated parameters upon fouling behaviour.
- Explore a variety of different MOCs, process parameters and solutions within the continuous flow fouling assessment platform.
 - Assess investigated parameters upon surface induced fouling on nucleation and growth via imaging and temperature methods.
 - Comparison of measurement methods.
- Develop predictive models for both setups and determine most influential parameters.
- Propose a fouling assessment methodology encompassing investigated fouling mechanisms.

Chapter 3. Materials and methods

3.1 Materials

A number of chemicals were utilised in this work. Chemicals used for crystallisation fouling experiments are detailed in Table 3.1. Chemicals utilised for other purposes within experimental chapters are highlighted where appropriate.

Table 3.1: List of chemicals used in subsequent crystallisation fouling experiments detailing purity and source location (abbreviations for chemicals used herein are detailed within brackets).

Chemical	Purity	Sourced from
Paracetamol (PCM)	≥ 98%	Sigma-Aldrich
Lovastatin (LOV)	Not stated	Molekula
Adipic acid (AA)	≥ 99%	Fluka
Aspirin (ASP)	≥ 99%	Sigma-Aldrich
Anhydrous carbamazepine (CBZ)	Not stated	Molekula
Deionised water	Not stated	In-house a Milli-Q integral 15 purification system (Millipore)
1-propanol	≥ 99.9%	Sigma-Aldrich
2-propanol (IPA)	≥ 99.5%	Sigma-Aldrich
Methyl isobutyl ketone (MIBK)	≥ 98.5%	Sigma-Aldrich
1-butanol	≥ 99%	BDH

A variety of different MOCs were investigated within this work which are detailed in Table 3.2. All explored MOCs were intended to be of equivalent thickness (1 mm). However, the nearest commercially available thickness value for silicon carbide (SiC) was 3 mm. All MOCs were explored as received in addition to selected surface treatments for probed metallic alloys. Metallic alloys which were selected for investigation were subjected to mechanical

polishing (280 grit polishing) and electropolishing (EP) (both conducted by MPE Limited). Investigated MOCs were either machined via company supplier or by in-house workshop to stated dimensions defined in Table 3.2.

Table 3.2: Investigated MOCs including details on thickness, source location and dimensions each MOC is machined to for subsequent experimental chapters.

MOC	Thickness (mm)	Source	Chapter 5 dimensions (mm)	Chapter 7 dimensions (mm)	Chapter 8 dimensions (mm)
Borosilicate	1	Scott Glass (Stirling)	-	-	Ø25
Quartz	1	Scott Glass (Stirling)	-	-	Ø25
Hastelloy® C276 as received (C276 as received)	1	Goodfellow (Cambridge)	-	-	Ø25
Hastelloy® C276 280 grit polished (C276 280 grit)	1	Goodfellow (Cambridge)	-	-	Ø25
Hastelloy® C276 electro polished (C276 EP)	1	Goodfellow (Cambridge)	-	-	Ø25
Polyether ether ketone (PEEK)	1	Goodfellow (Cambridge)	-	-	Ø25
Polytetrafluoroethylene (PTFE)	1	RS components (Corby)	71 x 8 rectangular coupon	Ø25	Ø25
Silicon carbide (SiC)	3	3M (Kempton, Germany)	-	-	Ø25
Stainless steel 316L as received (SS 316L as received)	1	Goodfellow (Cambridge)	71 x 8 rectangular coupon	Ø25	Ø25
Stainless steel 316L 280 grit polished (SS 316L 280 grit polished)	1	Goodfellow (Cambridge)	-	-	Ø25
Stainless steel 316L electro polished (SS 316L EP)	1	Goodfellow (Cambridge)	-	-	Ø25

3.2 Methods

The present thesis consists of three distinct research areas: MOC characterisation, statistical and computational approaches and crystallisation fouling experimental methods. Within this chapter each research approach will be explored with a particular emphasis on MOC characterisation methods. An overview of statistical approaches and crystallisation approaches are additionally highlighted with more detail regarding specific explored conditions provided in subsequent experimental chapters.

3.2.1 MOC characterisation

Numerous techniques were employed to characterise each unique MOC (including materials with selected surface treatments). Analytical techniques which were utilised included contact angle goniometry (CAG) and atomic force microscopy (AFM).

3.2.1.1 Contact angle goniometry

(a) *Introduction*

The angle at which the liquid interface meets a solid substrate is termed the contact angle ($\theta_{Droplet}$). Contact angle theory detailed earlier to describe heterogeneous nucleation (1.3.3.2 Heterogeneous nucleation) is applicable to a liquid droplet's contact angle. CAG is a technique which uses a probe solvent (e.g. water, ethylene glycol etc.) to quantify the wettability of a surface via Young's equation (Equation 3.1). Young's equation dictates there is a relationship between the contact angle, the surface tension of a probe liquid, the surface tension between the probe solvent and solid and the surface energy of the solid which is defined by:¹⁵⁴

$$\gamma_{sv} = \gamma_{sl} + \gamma_{lv} \cos \theta_{\text{Droplet}} \quad (3.1)$$

Where γ_{sv} , γ_{sl} and γ_{lv} are the solid-vapour, solid-liquid and liquid-vapour interfacial energies, respectively. With respect to utilising water as a probe liquid, determined contact angle values provide details on whether a surface is hydrophilic ($\theta < 90^\circ$) or hydrophobic ($\theta > 90^\circ$) as illustrated in Figure 3.4. The application of a solvent droplet onto a surface creates a droplet phase in which its shape is governed by intermolecular interactions of liquid molecules and total surface energy is minimised.¹⁵⁴

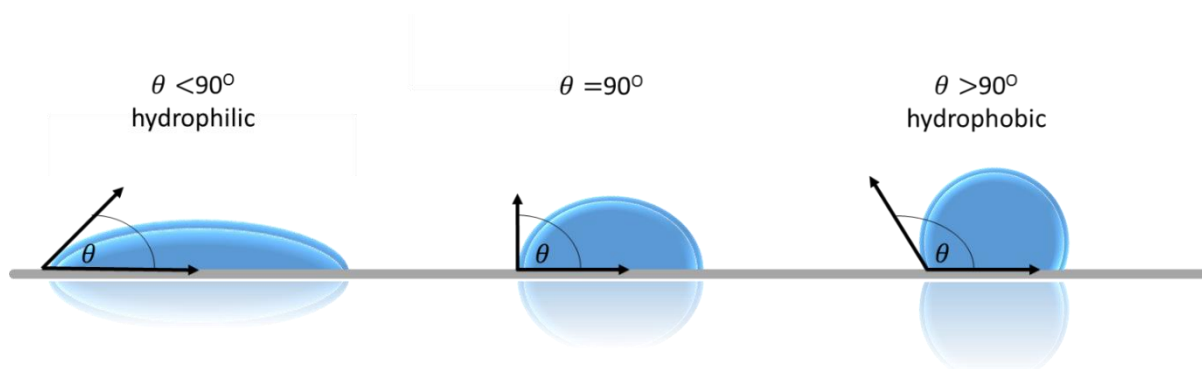


Figure 3.1: Schematic diagrams highlighting different wetting behaviours of water upon differing solid substrates.

A number of methods can be utilised to measure contact angles with the static sessile drop technique being the most practical.¹⁵⁵ In addition to obtaining wetting properties, determining the contact angle of selected probe solvents can be used to determine the surface energy (γ) of a given solid substrate (γ_s). The Good and van Oss acid-base method is an approach for calculating the surface free energy of a solid from determined contact angle values of at least three probe liquids. The Good and van Oss acid-base method requires γ_{sl} to be calculated prior to determining γ_s (or γ_{sv}). It determines the total surface free energy of a solid in addition to determining its dispersive and polar components.¹⁵⁶ According to the Lewis acid-base theory, polar interactions

occur between an electron acceptor and an electron donor. The geometric mean of these two opposing contributions are utilised in determining surface energy. The Good and van Oss method formula is defined as:

$$\gamma_{sl} = \gamma_{sv} + \gamma_{lv} - 2(\sqrt{\gamma_{sv}^{LW} \gamma_{lv}^{LW}} + \sqrt{\gamma_{sv}^+ \gamma_{lv}^-} + \sqrt{\gamma_{sv}^- \gamma_{lv}^+}) \quad (3.2)$$

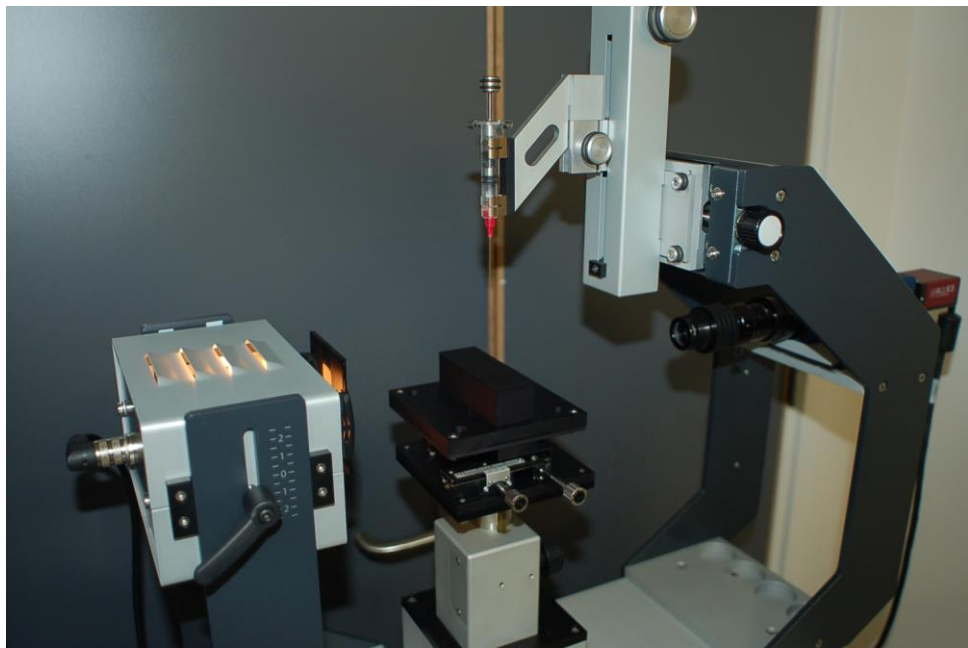
Where γ^{LW} , γ^+ and γ^- are interfacial tension contributions of dispersive component, polar electron acceptor component and polar electron donator component, respectively.

(b) **Methodology**

A Kruss DSA30 goniometer was employed to determine the contact angle formed by each unique MOC for a range of solvents by using the drop shape analyser ADVANCE software (Kruss) (Figure 3.2 (a) and (b)). The system was operated manually to create a droplet of 10 μ L that was left for a period of ten seconds on the surface prior to measurement. For each solvent and unique MOC explored at least ten replicates were conducted on at least three different samples to obtain average values at room temperature. Furthermore, the surface energy of each investigated material can be determined by probing solvents with varied polarity and obtaining associated contact angles. Probing solvents were water (HPLC grade, Sigma-Aldrich), diiodomethane (99%, contains copper as stabiliser, Sigma-Aldrich) and ethylene glycol (99.8%, Sigma-Aldrich). The method selected for determining surface energies and surface energy components was the Good and van Oss three-liquid formula¹⁵⁶ via an in-house Visual Basic program.¹⁵⁷ The three solvents employed in calculating surface energies and their associated surface energy components are displayed in Table 3.3. In addition to determining the total surface energy of each material (γ_s), the components that contribute to the total value including the dispersive and polar surface energy components were determined.



(a)



(b)

Figure 3.2: (a) CAG setup including software interface and (b) close up view of goniometer stage, light source, camera and droplet source.

Table 3.3: Probe solvents used to calculate surface energy values via CAG including liquid surface energy components.¹⁵⁸

Probing solvents	Surface energy components (mJ/m ²)			
	γ_l	γ_l^{LW}	γ_l^+	γ_l^-
Water	72.8	21.8	25.5	25.5
Diiodomethane	50.8	50.8	0	0
Ethylene glycol	48	29	1.92	47

3.2.1.2 Atomic force microscopy

(a) *Introduction*

Scanning probe microscopy (SPM) methods utilise a sharp probe to image and measure properties of an investigated material surface. One such scanning probe microscopy technique is AFM. AFM utilises a cantilever probe that scans over a selected investigated area and can generate a 3D image to provide height and topographical data of an investigated surface. A simple schematic of an AFM system is illustrated in Figure 3.3. The AFM probe is rastered in the x and y directions across a surface via a piezo-electric scanner. The probe scans across the sample and interacts with the structural features of a surface.¹⁵⁹ In order to detect very small displacements, an optical lever system is employed in which a laser beam is focused onto the end of the cantilever and reflects onto a photodiode detector. As the cantilever becomes displaced, the reflection angle of the laser beam also changes. An electrical signal based upon this displacement is then sent to a detector.¹⁶⁰ AFM typically operates in two modes namely contact mode and tapping mode. In tapping mode a cantilever oscillates at or close to the cantilever's resonance frequency as it rasters over a surface. This mode has several advantages including less time

at the surface, less drag and also less damage to sensitive samples. Contact mode is the most widely employed AFM method in which the probe is in contact with a surface in which the cantilever is fixed at constant force or constant height.¹⁶¹

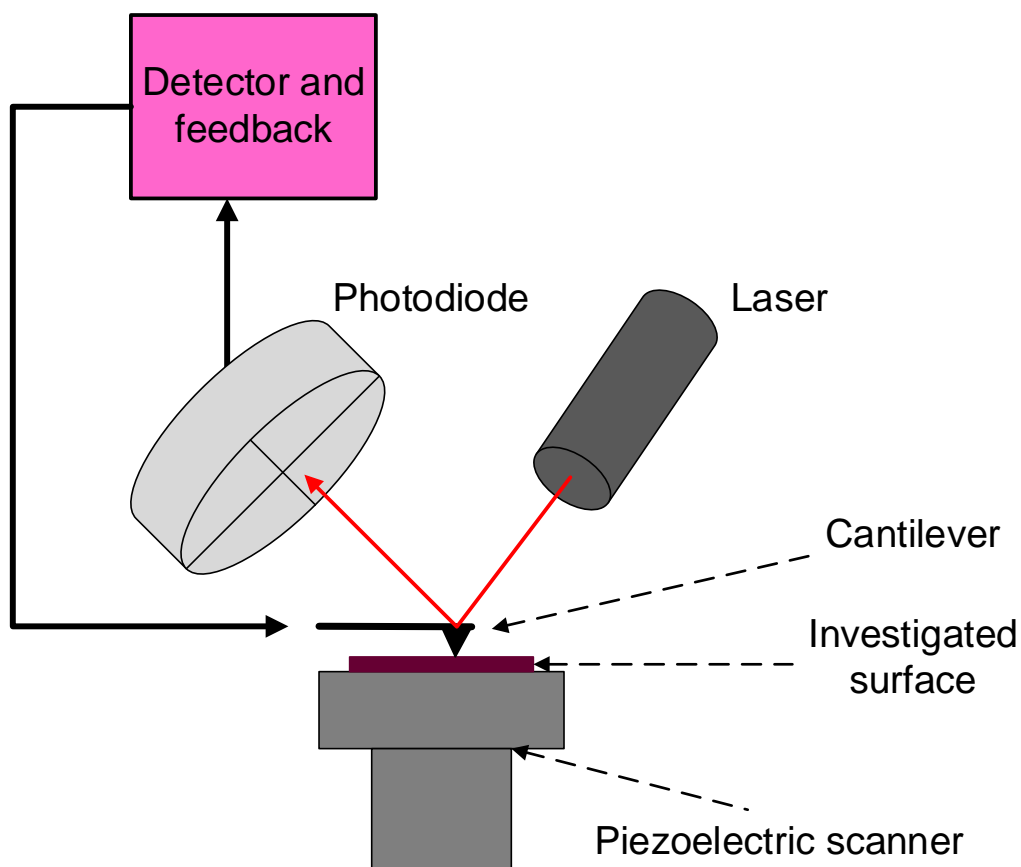


Figure 3.3: Schematic of an AFM system and necessary components.¹⁵⁹

(b) **Methodology**

AFM height micrographs for each MOC were obtained by using the Bruker Dimension FastScan AFM instrument which was equipped with the ICON scanner (Figure 3.4 (a) and (b)). AFM micrographs were acquired using ScanAsyst® mode at room temperature. ScanAsyst® is a PeakForce Tapping® based image optimization technique that generates high resolution AFM micrographs. ScanAsyst® air probes (Bruker) were used for all investigations with a nominal spring constant of 0.4 N/m and a nominal tip

radius of 2 nm. The scan rate employed was surface specific which varied between 0.0099 – 1 Hz due differences in topography. The selected area probed was 50 μm^2 . Generated micrographs were of 512 x 512 pixel resolution. All AFM data was analysed using NanoScope Analysis 1.5 software (Bruker). Additionally, first order flattening was applied to all height micrographs.

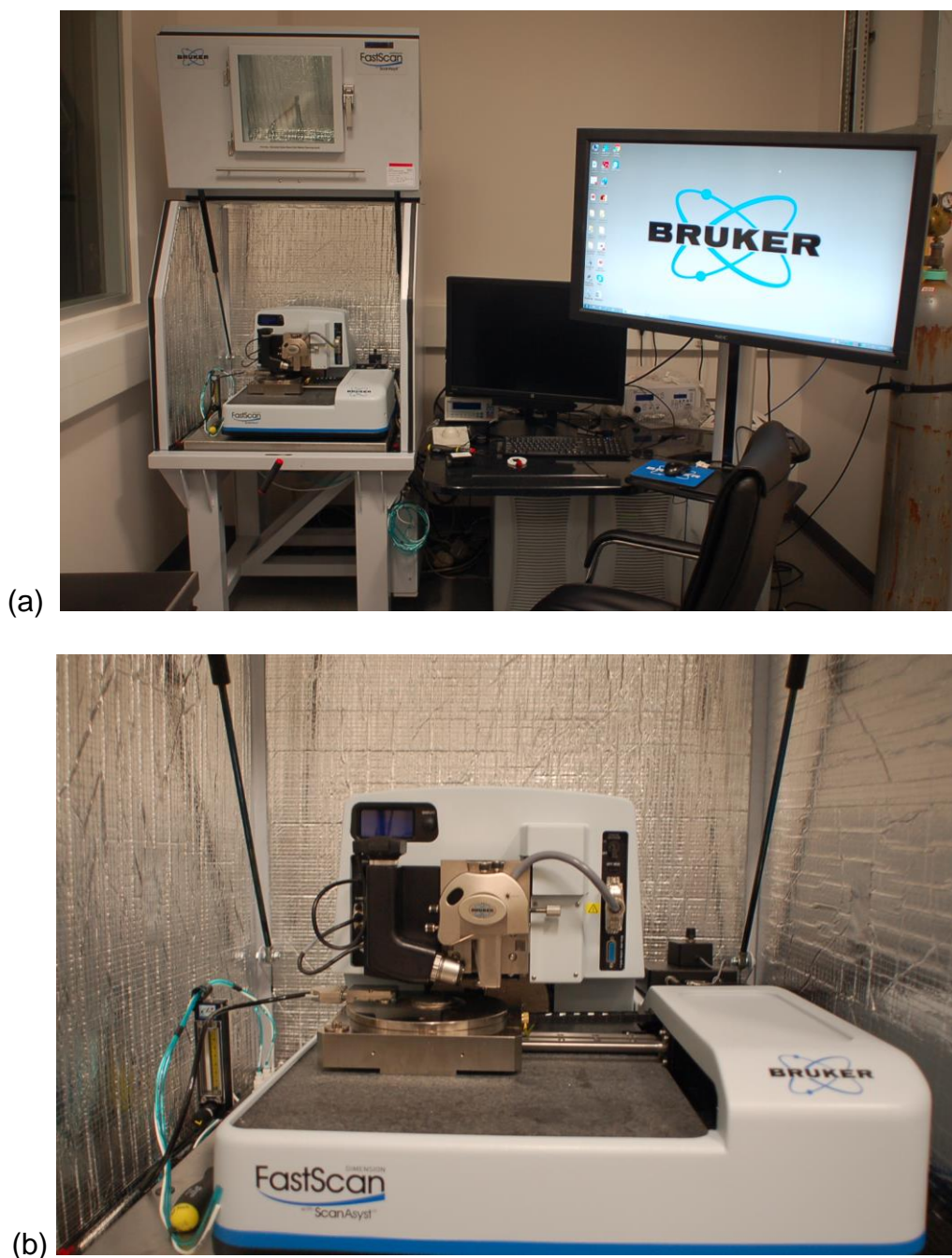


Figure 3.4: (a) Bruker FastScan AFM setup and (b) close up view.

In addition to obtaining height micrographs, the arithmetic average roughness (Ra) value was determined for each MOC which is defined as:

$$Ra = \frac{1}{N} \sum_{j=1}^N |Z_j| \quad (3.3)$$

Ra is the arithmetic average of the absolute of surface height deviation values between a mean plane and a given value. An average Ra value was determined based upon the Ra values of five individual micrographs for each unique MOC.

3.2.1.3 Other methods

A variety of other measurement methods to characterise each MOC were available e.g. hardness however were outwith the scope of the current study (as described in 4.1.3 Descriptors from literature). The following references provide more details for the interested reader.¹⁶²⁻¹⁶⁷

3.2.2 Statistical and computational approaches

A variety of different methods were employed to evaluate and model experimental data and experimental conditions. Approaches used included principal component analysis (PCA) and Design of Experiments (DOE). Computational fluid dynamics (CFD) was used to simulate conditions within given crystalliser configurations.

3.2.2.1 PCA

PCA is a statistical multivariate technique which is used to reduce the dimensionality of a dataset of quantitative dependent variables. The purpose

of PCA is to extract the important information detailed within a dataset into a set of new variables termed principal components.¹⁶⁸ Principal components are generated from linear combinations of the original data variables. The primary principal component generated relates to direction of limit bound variance and thereafter each principal component generated accounts towards the remaining variance. PCA allows the diversity or clustering of data to be assessed.¹⁶⁹⁻¹⁷⁰ Within this work PCA is conducted using SIMCA 14.1 software (UMetrics) to assess dataset diversity. Original data variables which had zero variance were removed from datasets for PCA.

3.2.2.2 DOE

DOE is a statistical method which incorporates planning, conducting, analysis and interpretation of experimental results via the influence of investigated parameters.¹⁷¹⁻¹⁷² Traditional laboratory experimental practices employ slow, labour intensive approaches whilst DOE methods typically reduce overall experimental workload and time whilst achieving similar or better experimental outcome. In DOE approaches, the type of experimental design employed is dependent upon the desired outcome i.e. screening to assess influence of each parameter, factorial designs to find detailed experimental processes and full factorial design with optimization to establish enhanced process detail for all investigated conditions.¹⁷² A number of designs can be used including full factorial, D-optimal and reduced combinatorial designs all of which have their inherent advantages and disadvantages in terms of information acquired, detail and timescale to perform.¹⁷²⁻¹⁷³ D-optimal and reduced combinatorial DOE designs were used within this work via MODDE Pro 11 software (UMetrics).

D-optimal designs are tailored for a given problem and are based upon an iterative search algorithm. The advantages of this type of design include exceptional flexibility and can be used where no classical design exists. D-optimal designs essentially maximise the information obtained within the selected experimental run sequence in relation to the selected model.¹⁷³ D-

optimal designs allow the estimation of parameters without bias and minimum variance whilst minimising the number of experiments required. D-optimal designs typically require less experimental runs in comparison to full factorial design (Figure 3.5).¹⁷⁴

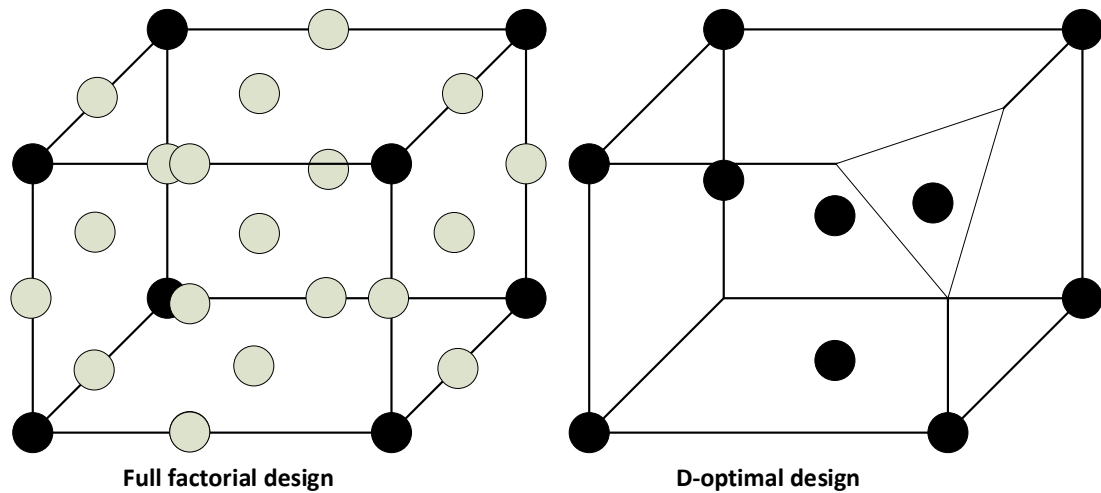


Figure 3.5: Examples of visual experimental designs for full factorial and D-optimal designs.

Reduced combinatorial designs are created using a strict combinatorial perspective in which all factors are subject to a balanced distribution. The proposed number of experiments is minimised within this design however enough detail is generated to allow adequate screening.¹⁷³

Statistics to describe each created model included (i) R^2 , (ii) Q^2 , (iii) model validity and (iv) reproducibility which are described in Table 3.4. R^2 and Q^2 are also relevant to PCA.

Table 3.4: Statistics employed by MODDE to describe generated models in addition to associated equations.¹⁷³

Statistic	Equation	Description
R^2	$1 - \frac{SS_{res}}{SS_{tot}}$	R^2 is a measure of how close experimental data is being to a fitted regression line i.e. measuring the goodness of fit.
Q^2	$1 - \frac{PRESS}{SS_{tot}}$	Q^2 is a measure of a model's predictive ability and is determined by cross validation.
Model validity	$1 + 0.57647 \log_{10} p_{lof}$	Model validity is calculated when replicated experiments have been conducted.
Reproducibility	$1 - \frac{MS_{pe}}{MS_{tot}}$	Reproducibility statistics is calculated when replicated experiments have been conducted.

Where:

SS_{res} = Sum of squares of the residual, corrected for the mean

SS_{tot} = Total sum of squares of Y corrected for the mean

$PRESS$ = Prediction residual sum of squares

p_{lof} = p -value for the lack-of-fit test

MS_{pe} = Mean square of the pure error

MS_{tot} = Total mean square of Y

Acceptable model statistic values have been described by Dennison and co-workers¹⁷⁵ and Bhatia et al.¹⁷⁶ which are detailed in Table 3.5.

Table 3.5: Accepted model statistics from literature.

Model statistic	Dennison and co-workers accepted statistic values¹⁷⁵	Bhatia and co-workers accepted statistic values¹⁷⁶
R^2	No information provided.	As near to 1 as possible.
Q^2	> 0.5	> 0.5 (> 0.1 can be classified as a significant model.)
<i>Model validity</i>	> 0.25	> 0.25 indicates an acceptable model. (< 0.25 suggests a lack of fit for the model.)
<i>Reproducibility</i>	> 0.5	Values < 0.5 indicates large error within the model and a lack of control within the experimentation.

3.2.2.3 CFD

COMSOL Multiphysics® 5.2a software (COMSOL) was used to simulate the fluid dynamics within a given structure under selected conditions. Models were constructed using measured dimensions obtained from investigated physical structures. Concentration and shear distributions were estimated using laminar flow and distribution of dilute species physics settings.

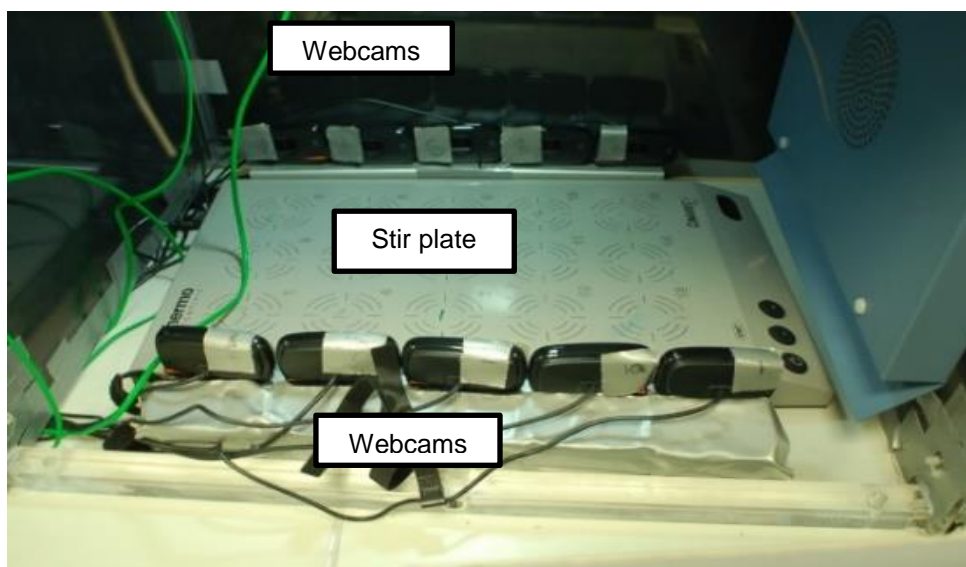
3.2.3 Crystallisation fouling experiments

Two crystallisation platforms were utilised to explore fouling which comprised (i) an in-house constructed small scale batch crystallisation set up and (ii) a continuous flow fouling assessment platform adapted from the Zebrafish platform (manufactured and designed by Cambridge Reactor Design (CRD)).

3.2.3.1 Small scale multiple batch crystallisation setup

To enable parallel experiments, an incubator was assembled to allow multiple samples to be observed under constant conditions. A setup was constructed to potentially modify and investigate a number of parameters namely environment temperature and agitation rate. Additionally, the setup also comprised imaging methods to monitor crystallisation events.

A fan incubator (Stuart S160D) was utilised to maintain a selected environment temperature which was blacked out to prevent exposure to external light sources. To maintain constant lighting for optical observation within the incubator, a compact axial white LED light (dimensions 50x50 mm, DCM Sistemas) was employed. Within the incubator, a 15-position stirrer plate (ThermoFisher Scientific) was used to control agitation rate. A series of Logitech C525 HD webcams (Logitech) were positioned within the incubator to monitor 10 stir plate positions (5 cameras parallel on each side) (Figure 3.6 (a)). The Logitech C525 HD webcams were capable of acquiring high resolution images (1280 x 720 pixels). Additionally, a black background was also employed to enhance imaging contrast (Figure 3.6 (b)). Other additional information including other materials, crystallisation methods and explored parameters are detailed in later chapters (see Chapter 5 Investigating nucleation and fouling processes in a batch crystallisation of paracetamol in water).



(a)



(b)

Figure 3.6: (a) Internal contents of the incubator with the multi-position stir plate with 5 webcams positioned either side. (b) Additionally for imaging purposes, a black background was used to enhance contrast allowing identification crystallisation events within an experimental vial.

3.2.3.2 Zebrafish platform

The Zebrafish platform is a corrosion test system that is manufactured and designed by Cambridge Reactor Design (CRD) as shown within Figure 3.7. The Zebrafish platform is a continuous recycle platform which consists of a

unique flow cell, gear pump, glass vessel and a Polar Bear Plus unit (CRD) which heats and cools the platform's glass vessel. The flow cell was designed to hold a test material coupon in which electrochemical conditions could be modified. Additionally the temperature of the investigated fluid and its associated flow rate can be accurately controlled. However, for proposed fouling studies within continuous flow a number of modifications were necessary which are described later (see Chapter 6 Development of a continuous flow assessment platform for fouling).



Figure 3.7: Library image of the Zebrafish platform.¹⁷⁷

Chapter 4. MOC characterisation and evaluation for fouling studies

4.1 Selection of materials of construction (MOCs) and characterisation

4.1.1 Introduction to materials of construction

In process development, the selection of process equipment and materials used in their construction requires consideration. For a given process, the most economical MOC that fulfils process and mechanical specifications over a stated operational duration should be utilised.¹⁷⁸ MOC considerations that require to be evaluated before use include:¹⁷⁸

- Mechanical properties (strength, stiffness, hardness etc.) and also its resistance to wear and tear.
- The influence of extremely high and low temperatures including thermal cycling upon the mechanical properties.
- Resistance to corrosive environments.
- Specific requirements for a stated process e.g. satisfactory thermal conductivity or electrical resistance.
- Availability in standard or specified sizes and dimensions.
- MOC cost and also the cost of fabrication.
- The capability of the material to be fabricated comprising welding and casting capability.

Another notable influential factor requiring consideration includes MOC robustness and the possibility of MOC contamination into the process product stream.¹⁷⁹⁻¹⁸⁰ For extreme process conditions, MOCs should be capable of handling such conditions whilst avoiding unwanted dangerous events from occurring e.g. high pressure build-up.¹⁸¹

Diverse MOCs can potentially be utilised for a given process ranging from traditional metallic alloys to plastic polymers to glass-like materials ultimately to meet the demands of a given process.¹⁸² Regarding crystallisation processes, a variety of materials can be used in the construction of a crystalliser platform with borosilicate⁵⁴, fluorinated ethylene propylene (FEP)¹⁸³

and stainless steel¹²⁶ prime examples from literature. Additionally, different MOCs have been used in the construction of auxiliary components and fittings associated with a crystalliser such as stirrer shafts, paddles and baffles.^{53,184} Furthermore MOCs used in the construction of PAT probes consist of several components such as optical windows¹⁸⁵ and housing unit materials for the probe¹⁸⁶ which are exposed to the crystallising solution.

The present research thesis proposed to investigate the influence of different MOCs upon fouling with the specific aim to further fundamental understanding of fouling mechanisms. A variety of MOCs with exceptionally different properties were targeted which have a role within crystallisation processes. Any MOC that is in physical contact with a crystallising solution was of interest from which a shortlist of MOCs was created. The MOC shortlist included traditional, routinely-used materials to more innovative materials that have been demonstrated in chemical processes within recent years which may have a use in crystallisation processes in the future.¹⁸⁷ MOCs proposed to be investigated within subsequent fouling research are highlighted within Figure 4.1.

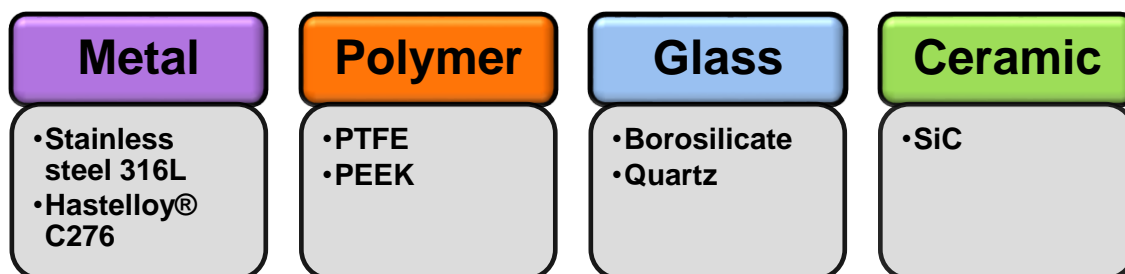


Figure 4.1: Different MOC types explored within this chapter including metals, polymers, glass-like materials and ceramics in addition to specific MOCs for each group.

The intention of this chapter was to assess the diversity of the previously highlighted MOCs by developing a MOC characterisation dataset. In order to assess MOC diversity, the properties of each MOC had to be determined. The characterisation of each MOC was conducted by an array of analytical

techniques in addition to acquiring established descriptors from research literature. MOC characterisation included acquiring quantitative data comprising physicochemical, thermal and mechanical properties.

4.1.2 Materials to be explored

A general description of each investigated MOC within this chapter is detailed herein.

4.1.2.1 Stainless steel 316L

Stainless steel is used extensively in manufacture of vessels¹⁸⁸ and other auxiliary components such as thermocouples.¹⁸⁹ Within the pharmaceutical and food industries, stainless steel 316L is commonly employed as a MOC in the construction of process equipment such as crystallisers (Figure 4.2).¹⁹⁰ In contrast with conventional steel, stainless steel does not willingly undergo corrosion or rust processes. The inherent resistance to corrosion associated with stainless steel is due to the elemental presence of chromium (content > 12%) with the larger the content of chromium, the greater resistance to oxidising corrosion conditions. Additionally, nickel is added to the alloy to enhance corrosion resistance due to non-oxidising conditions. Different grades of stainless steel exist in addition to a wide variety of finishes available. Both factors must be considered dependent upon the environment the alloy will be exposed to and for what operational duration.¹⁸² Within this study, stainless steel 316L was probed.



Figure 4.2: A commercially available COBC constructed from stainless steel 316L by Alconbury Weston Ltd.¹⁹¹

Stainless steel 316L also contains molybdenum in addition to the other compositional metallic components to further improve its resistance to reduction conditions. This ultimately allows the exposure of stainless steel 316L to solutions containing chlorides.¹⁸² In addition to stainless steel's corrosion resistance properties, it has ideal physical and mechanical properties that allow it to perform as an excellent MOC for process equipment. Stainless steel 316L is a robust material with excellent tensile properties in addition to having exceptional welding properties allowing the creation, fabrication and formation of reactors and other equipment components. The thermal conductivity properties of stainless steel have been exploited in the construction of heat exchangers due to its high thermal conductivity.¹⁹² Stainless steel has been extensively researched as a heat transfer surface in heat exchanger studies where fouling is a frequent observation.^{20,193-194} Herein stainless steel 316L is denoted by SS 316L or stainless steel.

4.1.2.2 Hastelloy® C276

Hastelloy® is a metallic alloy manufactured by Haynes International and is composed primarily of nickel in addition to containing molybdenum, chromium and iron to lesser quantities. Similar to stainless steel, Hastelloy® also has a variety of different types and grades with varying elemental content. Hastelloy® C22 has been used in the construction of PAT probes¹⁹⁵ which has minor variations in elemental composition compared to other grades such as Hastelloy® C276. For the purposes of this thesis, Hastelloy® C276 was explored to represent this variety of material as Hastelloy® C22 could not be sourced. Hastelloy® C276 has an exceptional resistance profile against corrosion with tungsten added to the alloy to enhance its resistance to highly corrosive, acidic environments. The large compositional content of nickel and molybdenum in Hastelloy® C276 allows resistance to pitting and crevice corrosion within a reducing environment. The inclusion of chromium, similar to stainless steel, promotes resistance to oxidising conditions. In terms of fabrication, Hastelloy® C276 has resistance to grain boundary generation caused by welding which allows this welded component to be utilised as is for most chemical processes without any further surface treatment.¹⁹⁶⁻¹⁹⁷ Similar to stainless steel, Hastelloy® C276 has been investigated as a heat transfer surface due to its notable thermal conductivity. Fouling has also been experienced upon heat exchangers.¹⁹⁸ Herein Hastelloy® C276 is denoted by C276.

4.1.2.3 PTFE

PTFE is a synthetic fluorinated polymer manufactured from the compound tetrafluoroethylene (Figure 4.3). It is a hydrophobic thermoplastic that is used commonly in an industrial setting primarily to confer its repellent/anti-stick quality commonly as a coating or as a fabricated component.¹⁸² Within an industrial setting, PTFE is commonly used as machined parts such as bellows¹⁹⁹ or baffles²⁰⁰ or as a surface coating for parts such as impellers²⁰¹ or temperature probes.⁵⁴ PTFE can be worked at temperature approaching

250°C. In terms of chemical resistance, PTFE is resistant to most compounds with the notable exceptions of alkali metal melts/solutions and fluorinated compounds at extreme conditions i.e. high temperature and pressure which will not realistically be found for routine crystallisation processes. One major disadvantage of PTFE, as a construction material, is its associated expense in which it is deemed expensive relative to other polymers. Additionally PTFE it is regarded as a difficult MOC to manufacture and manipulate.¹⁸² Another dilemma around employing PTFE as a MOC is its wear and tear propensity with PTFE fragments always a concern in particular if entering the product stream and causing product contamination as demonstrated by Pham and co-workers.¹⁸⁰

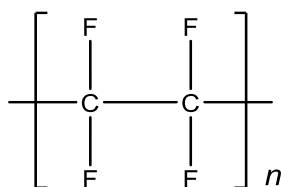


Figure 4.3: Repeating chemical monomer unit for PTFE.

4.1.2.4 PEEK

PEEK is a polymer MOC that has been used for many engineering applications due to its advantageous material properties. PEEK has a stable chemical structure (Figure 4.4) which uniquely provides the material with excellent mechanical, thermal and chemical resistance properties. PEEK can be exposed to temperatures around 200°C for sustained periods of time without any damaging effects.²⁰² PEEK can be made into reinforced carbon fibre components. Alike to PTFE, PEEK is an expensive MOC.²⁰³ It is commonly used as a MOC in the construction of small, precision components associated with crystalliser equipment.^{18,26}

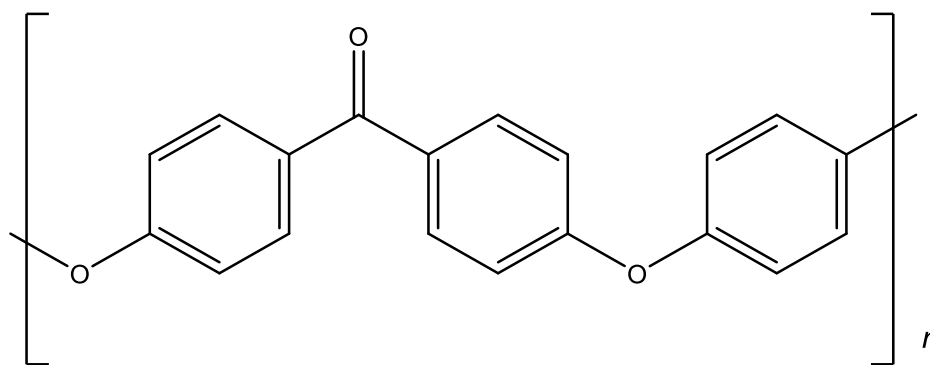


Figure 4.4: Repeating chemical monomer unit for PEEK.

4.1.2.5 Borosilicate

Borosilicate is a glass type which is routinely used in the construction of vessels in particular for the small-scale manufacture of speciality molecules.¹⁷⁸ The main advantages of borosilicate as a MOC include its relatively inexpensive cost, can be used at elevated temperatures (up to 700°C) and allows operators/researchers to observe internal contents due to its transparent nature allowing processes including crystallisation to be monitored.¹⁰⁸ Another important property of borosilicate is its low thermal expansion coefficient which resultantly increases its resistance to thermal shock. Borosilicate glass has an excellent chemical resistance profile with water, organic compounds and salt-containing solutions suited to borosilicate glassware. However borosilicate cannot be subjected to hydrofluoric acid or strong caustic solutions at extreme conditions e.g. elevated temperature. However these conditions would not be commonplace within crystallisation processes.¹⁸²

One negative aspect of borosilicate is its inherently low thermal conductivity in contrast to other MOCs. However, in certain circumstances, borosilicate's thermal conductivity is sufficient for allowing necessary heat transfer for cooling crystallisation i.e. meeting target internal temperature setpoints.¹⁸ Additionally borosilicate is subject to fracture and can easily be broken under constant pressure which provides a long term robustness issue.²⁰⁴

4.1.2.6 Quartz

Quartz is an amorphous material that is composed principally of silicon dioxide. Quartz has a larger operating temperature range in contrast to borosilicate. The optical properties of quartz are exceptional in contrast to other glasses owing to its superior purity.²⁰⁵ Quartz has a wide transparency range that extends from the near infrared (NIR) to the ultraviolet (UV) region making this MOC ideal for optical windows used within spectroscopic probes.²⁰⁶ Quartz is a chemically inert material and, comparably to borosilicate, has exceptional resistance to thermal shock.

4.1.2.7 Silicon carbide

Silicon carbide (SiC) is a ceramic MOC that has been researched and exploited over the last few decades notably in the construction of reactor vessels for fine chemicals. Flow chemistry reactors constructed with SiC have been commercialised by companies including ESK, Boostec and Chemtrix (Figure 4.4) which allow chemical reactions to be performed in a continuous method.²⁰⁷⁻²⁰⁸ Additionally, reactions which are not achievable within borosilicate or metallic reactors due to corrosive reactions can be conducted in a continuous process within SiC sintered reactors due to their outstanding corrosion and chemical resistance profile. SiC reactors additionally absorbed microwave energy which has a specific role for microwave related chemical reactions. The inherent thermal properties of SiC make it an excellent MOC where considerable heat transfer is required due to its large thermal conductivity in addition to its thermo-mechanical stability. SiC has a substantially large melting point of $\sim 2700^{\circ}\text{C}$ and a considerably low thermal expansion coefficient that allows operation at more extreme conditions.²⁰⁹ The selected grade of SiC for this research was grade C which is principally employed in the construction of SiC flow reactors.



Figure 4.5: Protrix® SiC flow reactor produced by Chemtrix.²¹⁰

4.1.3 Descriptors from literature

The selection of MOCs for subsequent fouling studies was grounded on current use within industrial chemical and crystallisation processes. A unique dataset containing MOC properties was to be generated which included quantitative descriptors from literature and, where appropriate, determine quantitative descriptors experimentally. Parameters which could not be quantified experimentally which were obtained from literature included:

- Thermal properties e.g. thermal conductivity and specific heat capacity.
- Mechanical properties e.g. Young's modulus.

The initial proposal for obtaining MOC descriptors was to acquire as many relevant properties to characterise each MOC in detail. Although other MOC descriptors from literature were available, incomplete datasets and incomparable data resulted in the exclusion of particular descriptors e.g. MOC hardness. In addition, selected material descriptors were not included which were deemed not to influence the crystallisation process e.g. electrical properties.

4.1.3.1 Thermal conductivity

Thermal conductivity (λ) is a measure of a material's capacity to permit the movement of heat due to a temperature gradient and its quantitative value describes how proficient a material can conduct thermal energy.^{6,211} Metallic alloys are generally good conductors of heat whilst polymer materials such as PTFE are described as poor heat conductors.²¹² Thermal conductivity is a significantly important material property in particular regarding cooling crystallisation processes where sufficient heat transfer is required. Thermal conductivity values at room temperature (RT) for each MOC from literature are detailed in Table 4.1 where magnitudes of difference are identified between MOCs.

Table 4.1: Thermal conductivity values for each MOC from a variety of literature sources (References detailed within table).

MOC	Boro-silicate	Quartz	C276	PEEK	PTFE	SiC	SS316L
λ (W/m.K) at RT	2	1.46	10.2	0.25	0.25	130	14
Reference	213	214	198	214	214	215	216

4.1.3.2 Specific heat capacity

The specific heat capacity (C_p) of a substance is the quantity of energy per unit mass required to raise its temperature by 1°C.⁶ It provides an indication of how demanding or undemanding a material is to raise its temperature in terms of energy input. The specific heat capacity values at RT for each MOC from literature sources are detailed in Table 4.2. The polymer materials have the largest specific heat capacity values proposing that these materials require larger inputs to increase the material's temperature. The metallic alloys have

the lowest associated specific heat capacity values which states that these materials are undemanding in increasing their temperature.

Table 4.2: Specific heat capacity values for each MOC from literature sources (References detailed within table).

MOC	Boro-silicate	Quartz	C276	PEEK	PTFE	SiC	SS316L
C_p (J/kg.K) at RT	800	705	425	1340	1000	690	502
Reference	217	214	198	214	214	215	216

4.1.3.3 Young's modulus

Young's modulus (E) or modulus of elasticity is a mechanical property of a material which is a measure of its stiffness.²¹⁸ The Young's modulus of a material is determined from the slope of its stress–strain curve within the elastic deformation region.²¹⁹ Young's modulus values at RT obtained from literature sources are shown in Table 4.3.

Table 4.3: Young's modulus values for each MOC from literature sources. (References detailed within table).

MOC	Boro-silicate	Quartz	C276	PEEK	PTFE	SiC	SS316L
E (GPa) at RT	64	73	205	3.85	0.55	430	200
Reference	217	214	99	214	214	215	214

Young's modulus values for each MOC highlighted mechanical property diversity with magnitudes of difference identified. The two investigated polymer MOCs have the lowest values which suggest these materials have low resistance to deformation in contrast other materials. The increase in Young's modulus correlates to an increase in material stiffness which is reflected in the investigated materials with the largest values including the metallic alloys and SiC.

4.1.4 Descriptors required to be determined experimentally

4.1.4.1 Introduction

A number of additional MOC properties were determined by employing a series of analytical techniques to acquire quantitative descriptors to further supplement the exclusive MOC characterisation dataset. Although each material has been characterised to variable extents in other research, the MOCs which are to be investigated in subsequent fouling experiments are uniquely specific to this research therefore each MOC including their different finishes were characterised. Descriptors obtained from literature were deemed to be constant even for different surface finishes. Each MOC was subjected to a series of techniques comprising microscopy methods, surface roughness assessment, wetting behaviour and surface energy analysis.

4.1.4.2 Materials and methods

(a) *Materials*

Investigated MOCs are detailed in Chapter 3 (see 3.1 Materials). MOC coupons were cleaned with dilute Hellmanex III (Helma) surfactant aqueous solution in an ultrasonic bath for 30 minutes. Prior to each analytical technique, individual MOC coupons was rinsed with methanol and water in triplicate and dried under gaseous nitrogen.

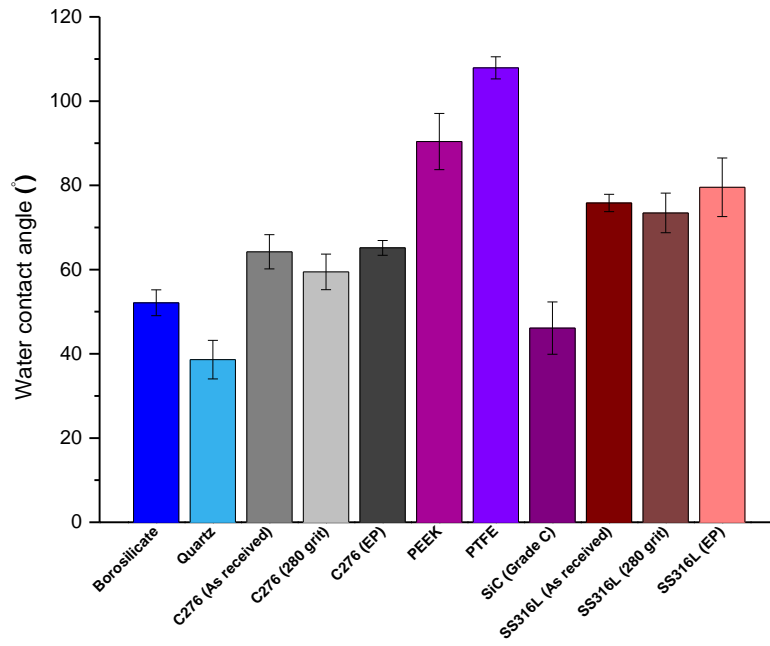
(b) **Methods**

The methodology for each characterisation technique including CAG (with surface energy analysis) and AFM (with Ra surface roughness assessment) are described in detail within Chapter 3 (3.2.1.1 (b) Methodology and 3.2.1.2(b) Methodology).

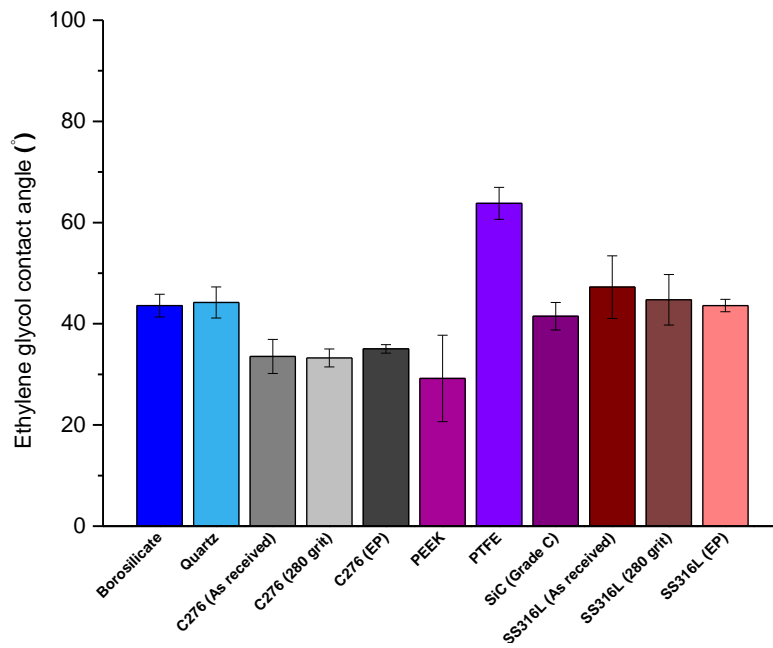
4.1.4.3 Results and discussion

(a) **CAG and surface energy**

CAG was performed for all unique MOCs to acquire qualitative wetting and energetic data for the MOC characterisation dataset. Average contact angles were determined for each MOC using three solvents namely water, ethylene glycol and diiodomethane (see 3.2.1.1(b) Methodology) which are illustrated in Figure 4.6 (a), (b) and (c). Average water contact angles determined ranged from 38.6° for borosilicate towards values of 108° associated with PTFE highlighting the different wetting behaviours of the investigated MOCs. Investigated polymers had the largest water contact angles in which both PEEK and PTFE are classified as hydrophobic which is in agreement with current literature.²²⁰⁻²²¹ Average contact angles for ethylene glycol and diiodomethane additionally yield a range of quantitative values underlining different surface wetting behaviours for polar and non-polar solvents, respectively. The influence of different polishing methods upon contact angle measurements was small and non-significant for all probe solvents. The effect of increasing surface roughness increases the surface area of liquid-solid contact and alters subsequent contact angle due to modified interactions as described by Wenzel.²²²



(a)



(b)

Figure 4.6: Bar charts of average contact angle values (with standard deviations) for (a) water, (b) ethylene glycol and (c) diiodomethane.

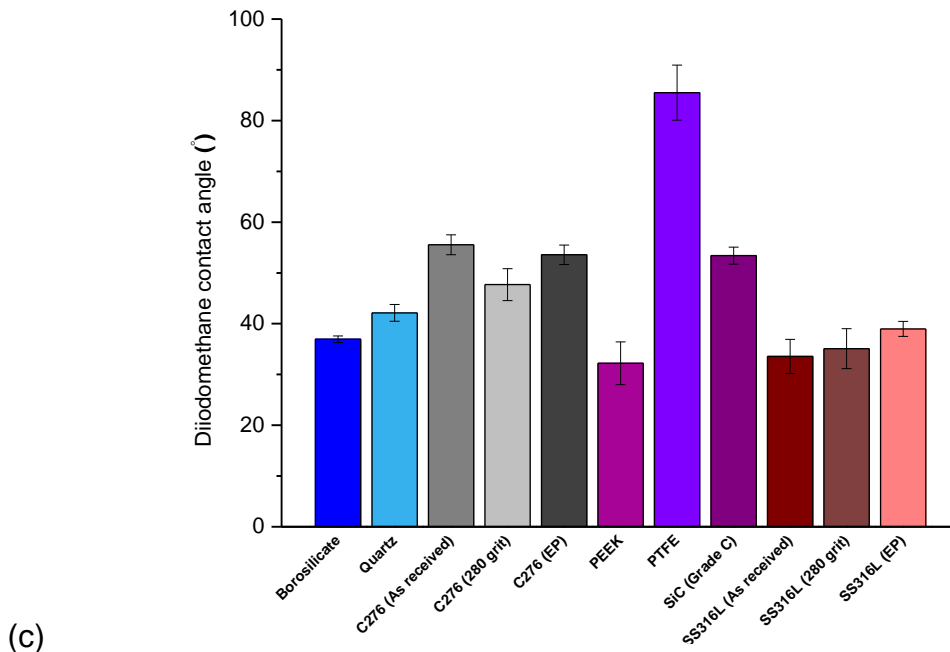


Figure 4.6 continued...

The total surface energy of each unique MOC was determined using average contact angle values for probed solvents. The Lifshitz van der Waals (γ_s^{LW}) and acid-base (γ_s^{AB}) surface energy components contributing to the total surface energy of each unique MOC are displayed in Figure 4.7. All MOC total surface energy values varied between 36 mJ/m² and 44 mJ/m² with the exception of PTFE which had a distinctly lower surface energy value of 18 mJ/m². The influence of polishing methods had a small impact upon total surface energy via altering droplet contact angles.

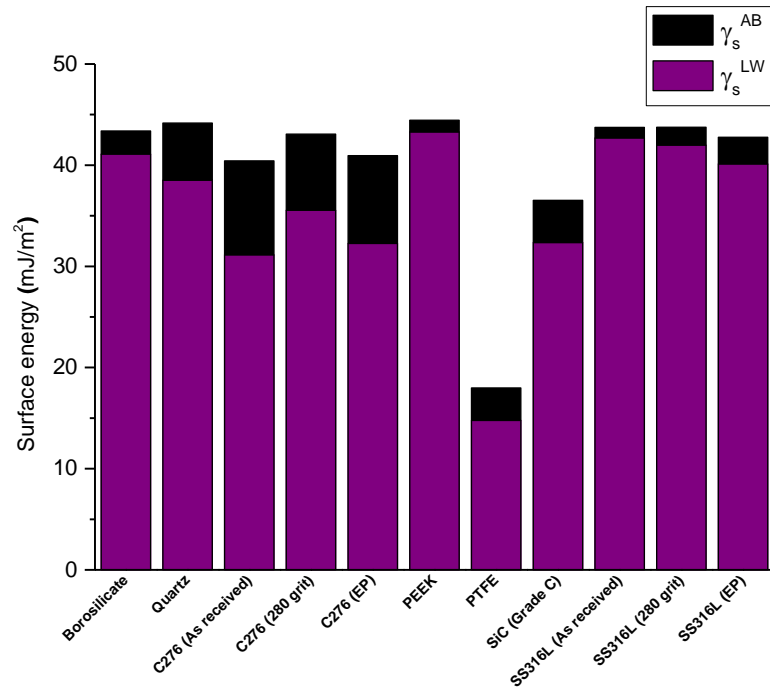


Figure 4.7: Total surface energy including Lifshitz van der waals (γ_s^{LW}) and acidic-base (γ_s^{AB}) components for each unique MOC.

(b) **AFM**

AFM micrographs were obtained to acquire (i) surface topographical details and (ii) Ra roughness data associated with each unique MOC (see 3.2.1.2(b) Methodology).

(i) **AFM height micrographs**

Acquired AFM height micrographs demonstrated a diverse array of surface topographies. Glass-like MOCs, namely borosilicate and quartz, had smooth surface features with submicron defects detected. These were anticipated to be residual dirt for borosilicate and, for quartz, identified defects were due to mechanical polishing (Figure 4.8 (a) and (b)). Both MOCs can be defined as micro-scale homogenous surfaces.

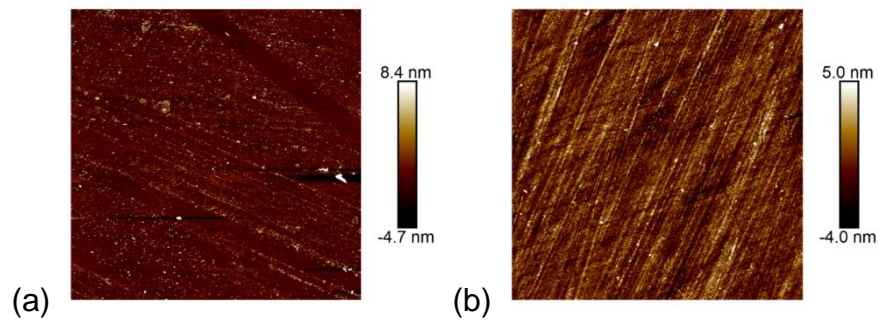


Figure 4.8: AFM micrographs of (a) borosilicate and (b) quartz [scan area: $50 \mu\text{m}^2$].

The surface structure of investigated metallic alloys varied considerably (Figure 4.9 and 4.10). Stainless steel 316L received from suppliers had a grain like structure consisting of nano-scale crevices (Figure 4.9 (a)). Mechanically polished stainless steel has a distinctly different surface topography which is rough and forms single direction troughs due to the polishing technique used (Figure 4.9 (b)). Electropolished stainless steel 316L presented an extremely flat structure with some nano-scale surface features. Electropolished stainless steel had a distinctly different topography compared to as received material (Figure 4.9 (c)).

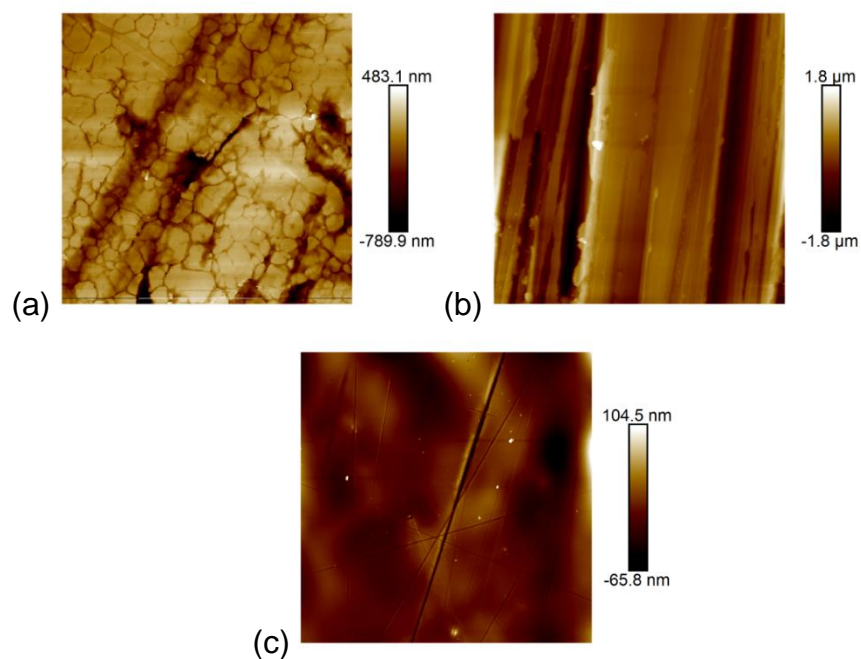


Figure 4.9: AFM micrographs of stainless steel 316L (a) as received, (b) 280 grit mechanically polished and (c) electropolished [scan area: $50 \mu\text{m}^2$].

Acquired Hastelloy® C276 AFM micrographs reveal a different surface topography for as received material compared to stainless steel yet the polishing treatments yield comparable topographies to their counterparts (Figure 4.10 (a), (b) and (c)). Hastelloy® C276 received and unmodified from the supplier has a relatively smooth surface. However, it consists of a number of grooves and surface defects with pits and fine scratches.

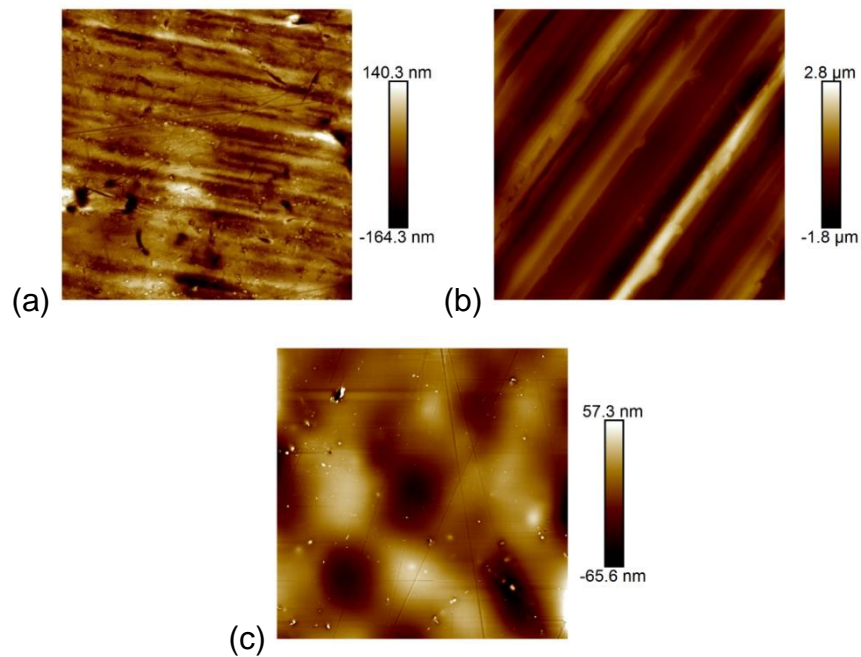


Figure 4.10: AFM micrographs of Hastelloy® C276 (a) as received, (b) 280 grit mechanically polished and (c) electropolished [scan area: $50 \mu\text{m}^2$].

Investigated polymer MOCs, namely PTFE and PEEK, have different topographies in contrast to the glass related and metallic MOCs. Each polymer also differs between each other (Figure 4.11). PTFE has an uneven, heterogeneous surface with nanoscale and microscale features detected (Figure 4.11 (a)). It contains groove like features on its surface from where it has been machined. The surface properties of PEEK are distinct with an uneven, irregular surface roughness with microscale surface features projected out from its surface (Figure 4.11 (b)).

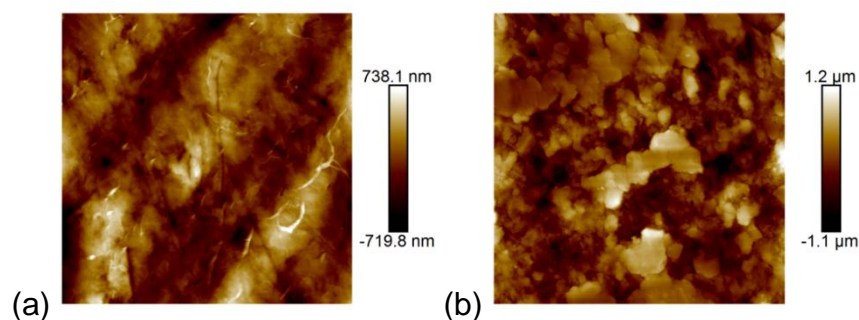


Figure 4.11: AFM micrographs of (a) PTFE and (b) PEEK [scan area: $50 \mu\text{m}^2$].

The surface topography of SiC as shown in Figure 4.12 yields a drastic surface structure that appears rough with very little repeating structure to it. It can be observed that individual SiC particles of different sizes have been adhered together to form a solid which is the basis of its surface via sintering. It is classified as a heterogeneous surface with a large number of crevices and gaps on its surface.

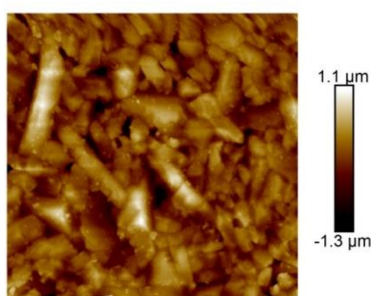
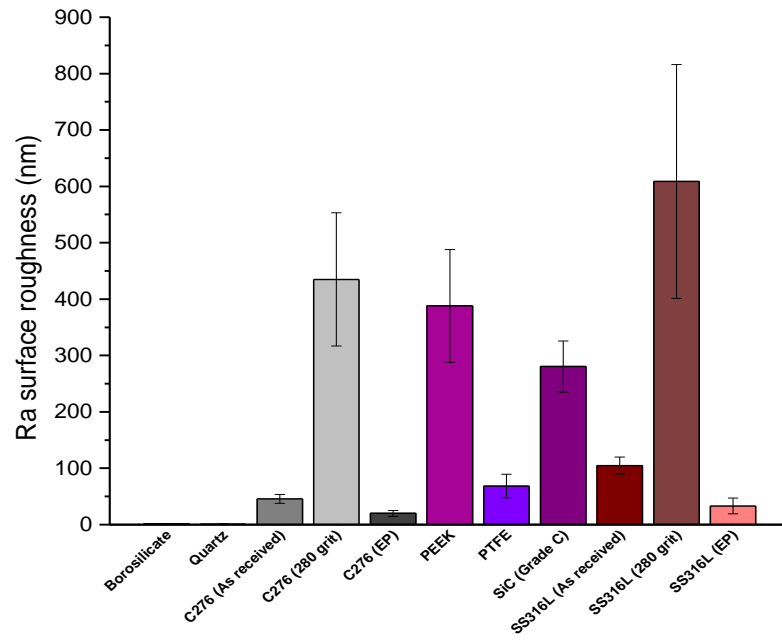


Figure 4.12: AFM micrograph of SiC [scan area: $50 \mu\text{m}^2$].

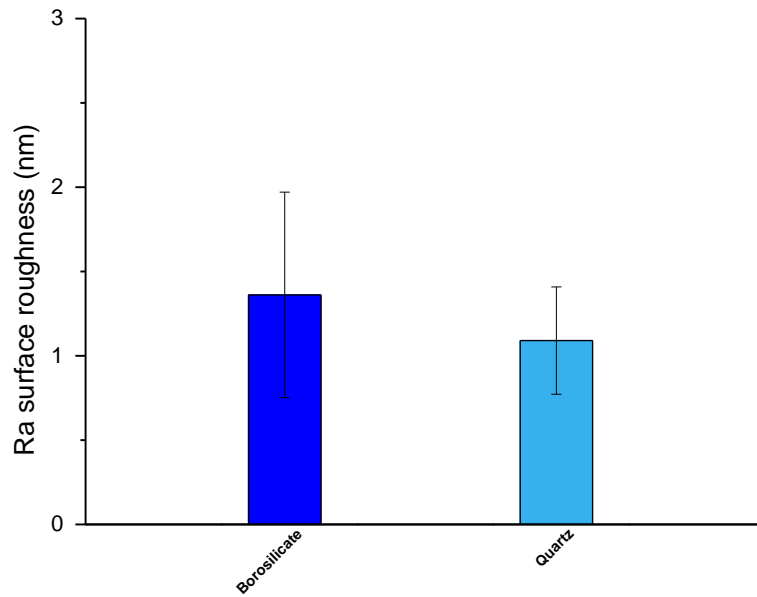
(ii) Surface roughness measurement

The average submicron Ra roughness values that represents randomly investigated $50 \mu\text{m}^2$ sections for each unique MOC are displayed in Figure 4.13 (a) and (b). It was found that the average Ra values varied considerably between each MOC and also between surface treatments. Average Ra values for borosilicate and quartz were exceptionally small ($Ra = \sim 1 \text{ nm}$) representing

a smooth, homogenous surface for each (Figure 4.13 (b)). Determined Ra values for investigated metallic alloys underlined the importance of polishing upon surface roughness. As received Hastelloy® C276 and stainless steel 316L had respective average Ra roughness values of 45 nm and 104 nm whilst electropolishing treatment resulted in notably lower Ra values of 19 nm and 33 nm, respectively. Electropolished metallic alloys had significantly smaller Ra values reflecting a superiorly smoother surface. The influence of mechanical 280 grit polishing upon the investigated alloys resulted in a significantly larger Ra surface roughness in addition to increasing their associated standard deviation highlighting a more irregular, heterogeneous surface. A similar observation was identified by Hilbert and co-workers in which different surface treatments of stainless steel resulted in different Ra values where increasing Ra results were associated with larger standard deviations.²²³ The investigated polymers, PTFE and PEEK, have large differences in surface Ra values with PEEK having a larger average value with a wider standard deviation value suggesting a heterogeneous surface. SiC had a smaller Ra value compared to PEEK yet was considerably rougher than the remaining unmodified MOCs.



(a)



(b)

Figure 4.13: Average Ra surface roughness values for (a) all unique MOCs explored and (b) glass-like MOCs.

4.2 Assessment of MOC diversity

4.2.1 Overview of material properties

For each unique MOC, experimentally determined quantitative descriptors in addition to acquired literature data were collated to generate an exclusive MOC characterisation dataset which is detailed in Table 4.4. It was proposed that the MOC dataset should be evaluated to assess the diversity of investigated MOCs in addition to highlighting the MOC spread. The variance within the data of Table 4.4 was assessed via principal component analysis.

Table 4.4: MOC characterisation quantitative dataset comprising experimental determined results (blue columns) and literature values (green columns).

Parameter MOC	Roughness [Ra] (nm)	Water contact angle [θ] ($^{\circ}$)	Total surface energy [γ_s] (mJ/m ²)	Thermal conductivity [λ] at RT (W/m.K)	Specific capacity heat [C_p] (J/kg.K)	Young's modulus [E] (GPa)
Borosilicate	1.36	52.12	43.38	2	800	64
Quartz	1.09	38.6	44.16	1.46	705	73
C276 as received	45.67	64.22	40.42	10.42	425	205
C276 (280 grit)	434.9	59.45	43.07	10.42	425	205
C276 (EP)	19.98	65.15	40.95	10.42	425	205
PEEK	388	90.4	44.44	0.25	1340	3.85
PTFE	68.44	107.9	17.98	0.25	1000	0.55
SiC	280.3	46.1	36.52	130	690	430
SS 316L as received	104.7	75.82	43.74	16.3	502	200
SS 316L (280 grit)	608.6	73.45	43.75	16.3	502	200
SS 316L (EP)	33.15	79.53	42.75	16.3	502	200

4.2.2 Assessment of MOC diversity

Principal component analysis (PCA) was conducted as a method to assess variance within the MOC characterisation dataset (see 3.2.2.1 PCA). Allesø and co-workers employed PCA as a statistical method to assess solvent diversity used within a polymorph screen highlighting its application in assessing differences within a given quantitative dataset.²²⁴ Two principal components were used in this analysis. The use of the first two principal components describes 65.6% of the variance within the dataset.

A bi-plot containing scores and loadings information is displayed in Figure 4.14 consisting of the 1st and 2nd components. Cluster groupings of MOC is identified in particular for the glass-like materials and metallic MOCs with SiC, PEEK and PTFE discretely unique. The objective from this statistical analysis was to assess each MOCs range of properties via PCA. Figure 4.14 shows that the investigated MOCs are distinctly diverse in terms of quantitative descriptors. Additionally the positioning of the coloured MOC descriptors support each MOC's position.

From Figure 4.14 it is shown the dataset is diverse and as a collection should be investigated for a wide spread fouling study (see Chapter 8 Multivariate modelling of fouling responses and parameter evaluation). However, it was anticipated that selected fouling studies would only probe a small selection of MOCs. Two distinctly different MOCs from Figure 4.14 were stainless steel (as received) and PTFE which were selected for initial fouling studies (Chapter 5 Investigating nucleation and fouling processes in a batch crystallisation of paracetamol in water and Chapter 7 Fouling assessments in novel flow platform).

The generated PCA biplot describes the interrelationship between MOC descriptors e.g. an inverse correlation was identified between water contact angle and surface energy whilst a direct correlation between water contact angle and specific heat capacity was identified.

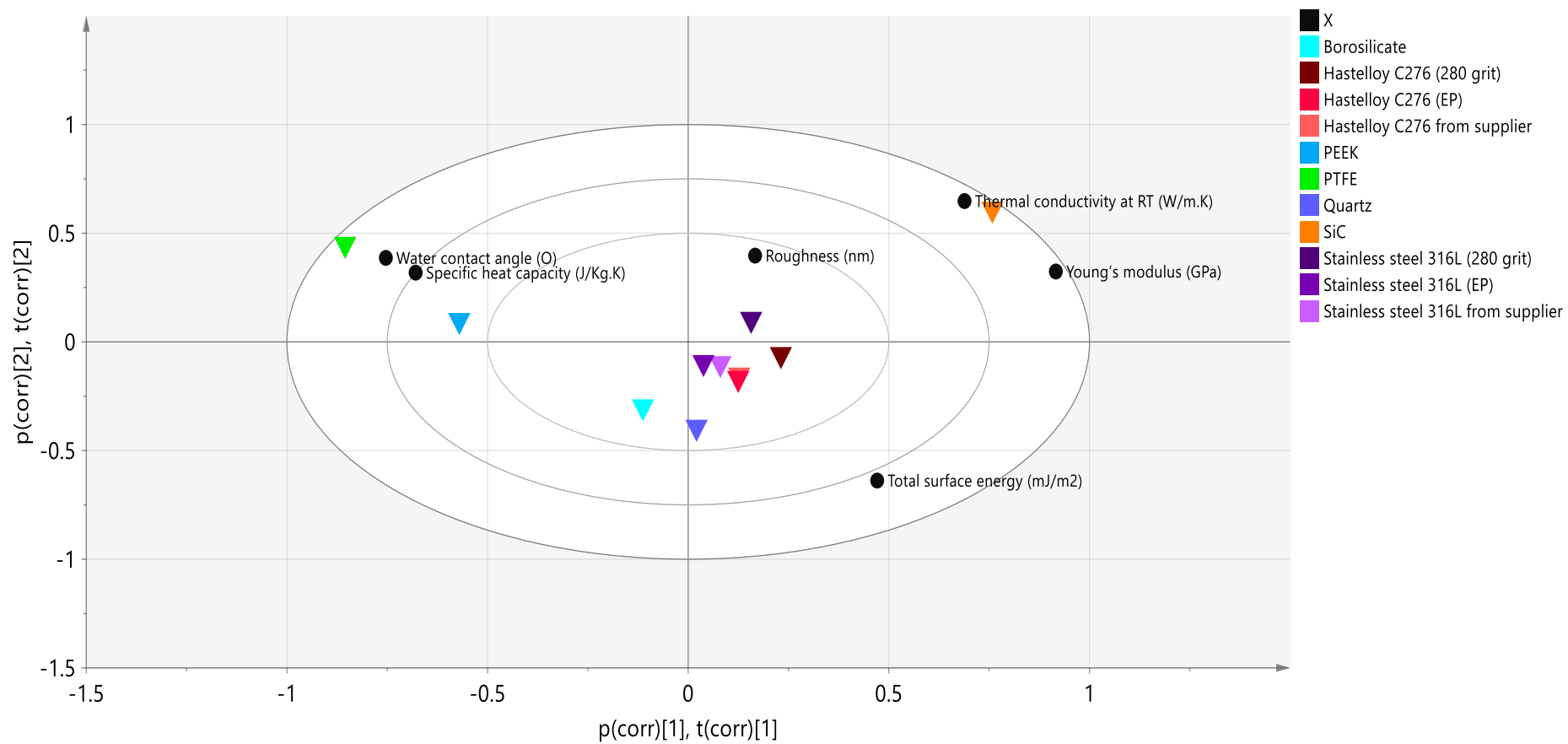


Figure 4.14: Biplot containing MOC descriptors (black circles) and distribution of unique MOCs (coloured inverse triangles). Metallic MOCs and glass-like MOCs are both individually grouped whilst other MOCs are uniquely different.

4.3 Summary

The purpose of this work was to establish an unique dataset describing various MOCs relevant to crystallisation processes. This comprised both determining qualitative MOC descriptors experimentally in addition to acquiring data from literature sources. The benefit of this exclusive MOC dataset allows future fouling research outcomes to be related to a diverse set of MOC properties. Additionally, the development of a MOC characterisation dataset and consequently PCA biplot provides a measure of how different MOCs are from one another when comparing to all MOCs within the dataset. This work provides a meaningful tool to enable the assessments and selection of MOCs.

The outcome from the generated dataset and bi-plot informed on which MOCs should be explored in subsequent fouling studies. Although some clustering was identified, it was decided that all investigated MOCs should be subject to fouling studies due to their unique properties in addition to differing material types. The outcome from the PCA analysis did not warrant any exclusions and also highlights relationships between MOC descriptors.

Chapter 5. Investigating nucleation and fouling processes in a batch crystallisation of paracetamol in water

5.1 Introduction

Nucleation is the critical step in controlling a crystallisation process (see 1.3.3 Nucleation mechanisms).⁵⁷ In terms of primary nucleation, heterogeneous nucleation is induced by the presence of a foreign surface with true homogenous nucleation generally accepted as a rare event under practical conditions. From an industrial perspective, secondary nucleation is commonly exploited where seed crystals are added to avoid any reliance on primary nucleation and enhance process robustness.²²⁵ However heterogeneous nucleation is typically found in industrial crystallisation processes where seeding has not been employed and rely upon foreign surfaces to induce nucleation.⁶

Theoretically, heterogeneous nucleation can occur on any surface in contact with a supersaturated solution. There is repeated evidence of heterogeneous nucleation initiating upon the internal surfaces within a crystalliser leading to fouling.^{18,53} However identifying where nucleation initiates upon the surface is a challenge. The influence of different MOCs upon nucleation kinetics primarily upon MSZW values has been demonstrated by a number of studies in which different MOC surface properties were used to explain the observed effects.^{53,184} Liang et al. investigated the impact of impellers constructed from different MOCs within a batch stirred vessel upon the MSZW associated with the cooling crystallisation of L-glutamic acid (LGA) in water. Impellers constructed of stainless steel were found to have a narrower MSZW in contrast to Perspex® impellers with significant differences determined for a range of explored process conditions. Nucleation upon the stirrer surface was presumed to be the initial nucleation mechanism. The energy required to form a critically stable LGA nuclei on stainless steel was lower than Perspex® due to a smaller associated free energy ratio (Φ) (See 1.3.3.2 Heterogeneous nucleation) which was concluded to be the principal cause for differences in nucleation kinetics. Liang also highlighted that surface induced nuclei were subject to detachment. If hydrodynamic shear forces exceeded adhesion forces, LGA particles could detach and become suspended within the bulk.

The suspended LGA particles were liable to attrition where hydrodynamics and the hardness of MOC are of importance.⁵³ Collisions between agitator and suspended particles are significant in relation to secondary nucleation in which the probability of a collision is directly proportional to the rotational agitation rate.⁶ Ni and Liao determined the MSZW for different crystallisation conditions within a batch OBR in which baffle inserts composed of different MOCs, namely stainless steel and polyvinylidene difluoride (PVDF), were investigated. Ni and Liao found crystallisation conditions involving stainless steel baffles had smaller MSZW ($\Delta T_{MSZW} = 18^{\circ}\text{C}$) in contrast to PVDF ($\Delta T_{MSZW} = 24^{\circ}\text{C}$) with the effect attributed to differences in surface roughness.¹⁸⁴

In addition to traditional MOCs influencing nucleation kinetics, nucleation studies investigating innovative research materials have been conducted. A publication by Diao et al. explored the effect of different polymer substrates on the nucleation induction times of aspirin from solution.¹²⁰ It was found that poly(4-acryloylmorpholine) and poly(2-carboxyethyl acrylate) cross linked with divinylbenzene substrates significantly reduced aspirin induction times in contrast to other less polar polymers explored e.g. polystyrene highlighting the importance of physicochemical interactions between substrate and solute molecules in influencing nucleation processes. The presence of poly(4-acryloylmorpholine) directed nucleation upon its surface as shown in Figure 5.1 (a) in contrast to its absence (Figure 5.1 (b)) where bulk nucleation occurs. Authors proposed surface energetics, notably polar interactions, as their main reasoning for differences in aspirin induction times. This work additionally demonstrates the presence of additional functional surfaces within a crystallisation process can considerably alter prominent nucleation processes.

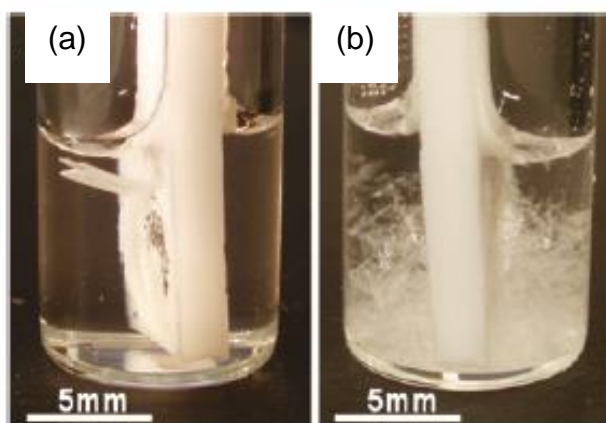


Figure 5.1: Aspirin crystals (a) nucleated on the poly (4-acryloylmorpholine) surface whilst the absence of this polymer surface (b) resulted in bulk nucleation.¹²⁰

In addition to different material substrates influencing heterogeneous nucleation, the impact of process parameters has been researched extensively notably the effect of supersaturation and degree of mixing/agitation. Supersaturation is the key driving force for nucleation to occur with increasing supersaturation resulting in increased rate of nucleation via CNT (see 1.3.3.1 Homogeneous nucleation) as detailed by several researchers.^{6,226} Kulkarni and co-workers investigated the impact of different supersaturation ratios upon induction time probability distributions from which kinetic ($A_{Kinetic}$) and thermodynamic (B_{Therm}) nucleation rate parameters were determined (see 1.3.3.1 Homogeneous nucleation).²²⁷ The impact of agitation on nucleation is considered to be complex with authors proposing increasing agitation can reduce the tendency of nucleation occurring or even reach a plateau.⁶ The influence of agitation has been shown by Liu and Rasmuson to reduce the induction time for butyl paraben in ethanol solutions across a range of stirring rates with a resultant increase in nucleation kinetics.²²⁸ Mitchell and co-workers determined a linear decrease in induction time with increasing agitation rate.²⁰⁰ Within a stirred batch crystalliser, the agitation rate relates to the energy dissipation ($\frac{P}{V}$) within the vessel.¹⁸² Liu and Rasmuson established a linear correlation between energy dissipation and induction time for butyl

paraben.²²⁹

$\frac{P}{V}$ can be calculated from:¹⁸²

$$\frac{P}{V} = \frac{P_0 \rho N_s^3 D_s^5}{V_L} \quad (5.1)$$

Where

$\frac{P}{V}$ = Energy dissipation (power per unit volume) (W/m³)

P_0 = Dimensionless power number of the agitator

ρ = Fluid density (kg/m³)

N_s = Speed of the stirrer (rps)

D_s = Diameter of stirrer (m)

V_L = Volume of liquid (m³)

Crystal nucleation upon a surface can also be associated with the initiation of crystallisation fouling.⁷ Liang et al. identified within their work that nucleation occurred upon the rough surface of the impeller anchor before being fully encased in crusts. Crystallisation fouling is acknowledged to comprise a number of mechanistic processes as highlighted previously (see 1.4.2.7 Mechanisms related to crystallisation fouling). However, fundamental understanding remains a challenge. Further understanding of the relationships between nucleation mechanisms, fouling mechanisms and process parameters are key towards improving process understanding and the design of robust crystallisation processes.

An experimental method was created to explore the processes of nucleation and fouling and probe the influence of two distinctly different MOCs (stainless

steel and PTFE; as shown in Figure 4.14) and process parameters upon fouling during the cooling crystallisation of paracetamol (PCM) (Figure 5.2). Furthermore by probing and understanding the impact of experimental parameters further insight into relevant fouling mechanisms could be deduced.

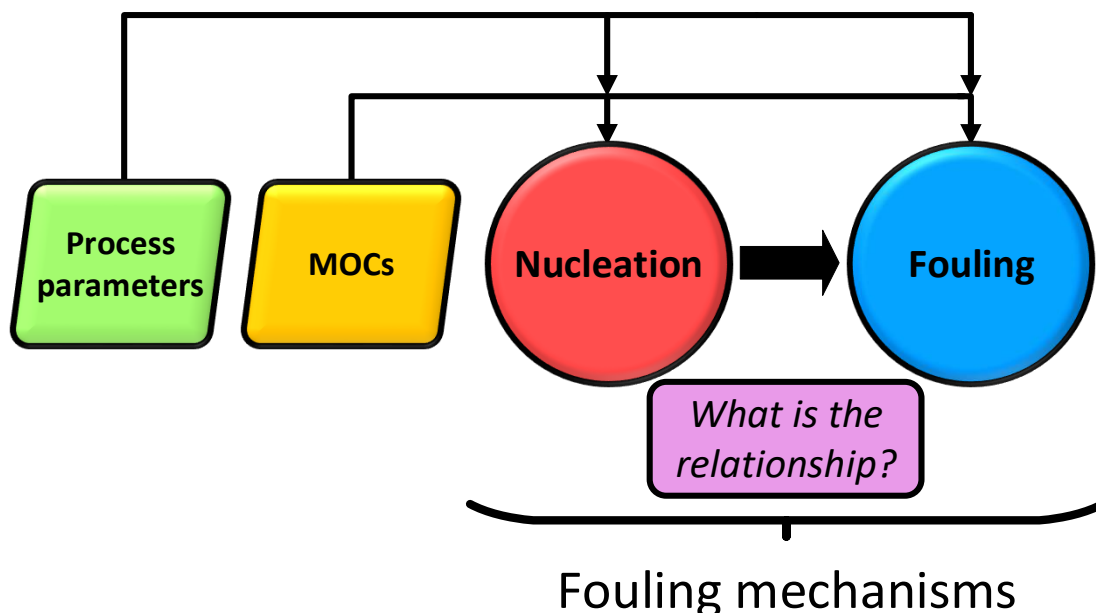


Figure 5.2: Schematic summarising the aim of this experimental chapter. Various process parameters and different MOCs were to be explored and investigate their influence on both nucleation and fouling. Understanding the relationship between nucleation and fouling with respect to further mechanistic understanding was desired.

5.2 Materials and methods

5.2.1 Materials

Materials used in this experimental chapter including chemicals, MOCs and equipment are detailed in Chapter 3. PCM in water was the selected investigatory crystallising system within this work in which its solubility curve is shown in Figure 5.3. The chemical structure of PCM is illustrated in 5.4. Crystallisation campaigns involving PCM have reported problematic fouling

during operation as highlighted by several authors^{118,230-231} hence its investigation within this chapter.

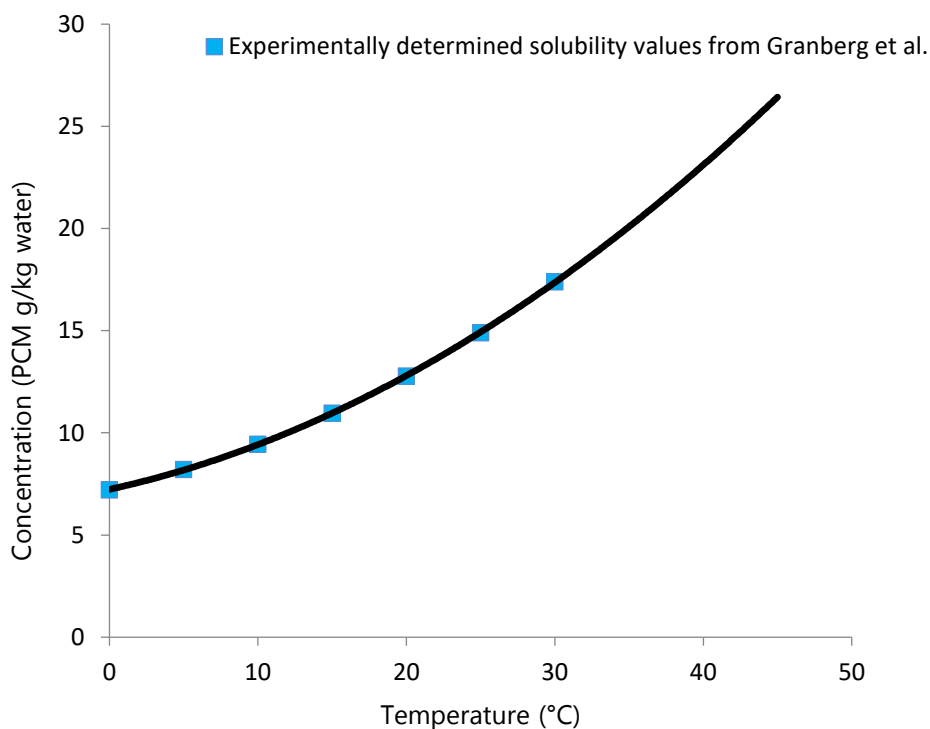


Figure 5.3: Temperature-dependent solubility curve for PCM in water.²³²

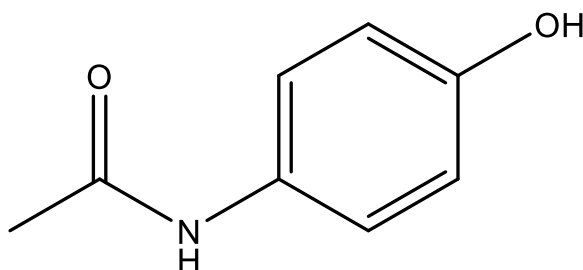


Figure 5.4: Molecular chemical structure of PCM.

5.2.2 Methods

5.2.2.1 Basic crystallisation setup and investigatory method

A crystallisation setup was constructed to investigate the effects of two key process parameters: supersaturation and agitation rate. Additionally, the setup

also comprised an imaging system to constantly monitor crystallisation events (see 3.2.3.1 Small scale multiple batch crystallisation setup).

A methodology was established to investigate supersaturation, agitation rate and different MOCs upon crystallisation events: nucleation and fouling. The crystallisation batch setup comprised of a series of glass borosilicate vials (volume = 8 ml) which contained a PTFE-coated magnetic stir bar (Figure 5.5). The MOC coupons to be investigated were inserted vertically as illustrated in Figure 5.5 to a predetermined spatial configuration (insertion depth from air/solution interface = 24 mm). The top of each sample vial was sealed with a PTFE cap and paraffin film.

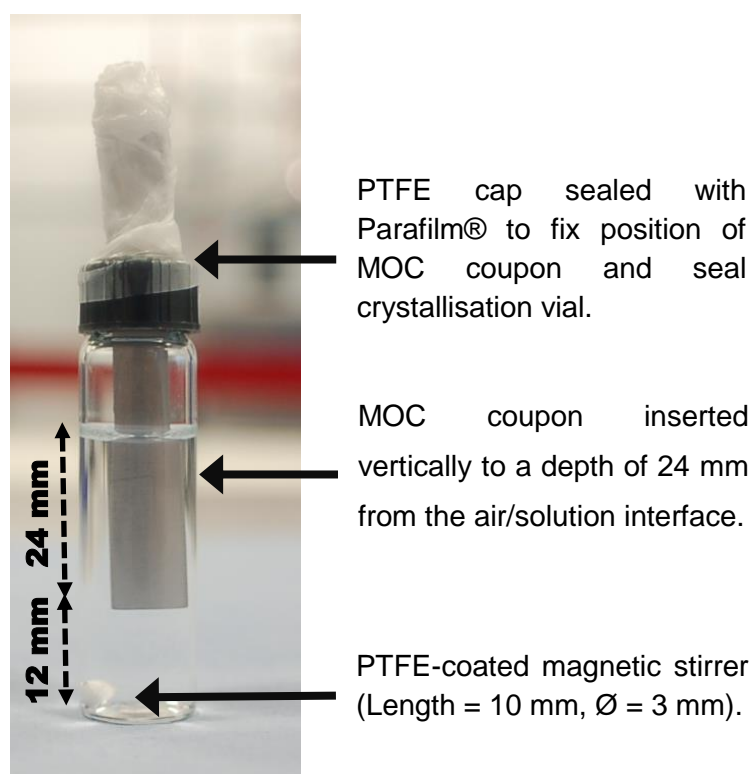


Figure 5.5: An example batch crystallisation vial containing an inserted MOC coupon at a designated spatial configuration.

In the preparation of investigatory crystallisation vials, stock PCM solutions were heated to 45°C and held for 30 minutes to ensure full dissolution. After

dissolution, 6 ml of PCM solution was added to each investigatory vial (via a 0.2 µm PTFE membrane syringe filter (Millipore)) which were maintained at 45°C for an additional 10 minutes thereafter. Vials were immediately transferred to the preheated incubator which was maintained at 30°C. All experimental vials were assumed to cool instantaneously due to the small crystallisation volume cooling from 45°C to 30°C. At 30°C the solubility of PCM in water is 17.39 g/kg water²³² and solution concentrations required to generate supersaturation ratios of 1.2, 1.3 and 1.4 at 30°C are detailed in Table 5.1.

Table 5.1: PCM in water concentrations required to generate supersaturation ratios of 1.2, 1.3 and 1.4 for crystallisation experiments at 30°C.

Supersaturation	PCM in water concentration (g/kg solvent)
1.2	20.87
1.3	22.61
1.4	24.35

Individual vials were added to each designated positioning on the utilised stir plate located within the incubator. In a typical experiment conducted, 10 vials and their contents were investigated. To monitor crystallisation events occurring within each investigated vial, images were acquired every 15 seconds using YAWCAM software (YAWCAM). Each webcam was positioned and focused upon a planar surface of investigated MOCs whilst monitoring the surrounding bulk solution (see Figure 3.5 within 3.2.3.1 Small scale multiple batch crystallisation setup).

5.2.2.2 Nucleation kinetics

Two nucleation kinetics measurements were determined within this research: induction time data and nucleation rate. For each investigated condition, induction time values were determined by visual detection via a series of

recorded images. The time difference between the addition of vials into the incubator until the point where solutions became turbid was considered as the induction time. Constant supersaturation was assumed once all vials had been added into the incubator. Induction time (t_{ind}) can be expressed as:⁶

$$t_{ind} = t_r + t_n + t_g \quad (5.2)$$

Where t_r , t_n and t_g represent the system's relaxation time, time to form stable nuclei and time to grow to a detectable size, respectively. An eight hour time limit was applied. Induction times were determined for a range of parameters specifically supersaturation, agitation rate and different MOCs as detailed in Table 5.2. Experiments were conducted for all process conditions where the MOC coupon was absent from the crystallising vials.

Table 5.2: Parameters explored for induction time experiments.

Parameters	Conditions investigated
Supersaturation at 30°C	1.2, 1.3 and 1.4
Agitation rate (AR)	130, 350 and 700 rpm
MOC	Stainless steel 316L (SS) and PTFE

Twenty induction time values were targeted to represent each explored condition. Induction time datasets obtained were then analysed via the Kruskal-Wallis test (MINITAB software (MINITAB)) to assess the statistical significance of differences between the measured induction time datasets. The Kruskal-Wallis test is a non-parametric analytical technique used to evaluate significant differences by testing whether two or more independent samples come from identical populations.²³³ It is of particular usefulness for data

populations which are not normally distributed. The Kruskal-Wallis test requires:²³⁴

- Sample populations should have distributions with similar shapes and equal variances.
- Samples must be random and independent.
- Individual sample should contain of five or more measurements within its population.

Nucleation rates (J) were also calculated for each explored condition using associated average induction times. An inverse relationship between induction time and nucleation rate is defined as:²³⁵

$$\ln t_{ind} = -\ln JV \quad (5.3)$$

Where

- t_{ind} = Induction time (s)
- J = Nucleation rate ($\#/m^3.s$)
- V = Solution volume (m^3)

5.2.2.3 Fouling behaviour

A second series of experiments using the conditions investigated to determine nucleation kinetics was carried out. Fouling upon MOC coupons was investigated by carefully removing from individual vials at given time intervals (2.5, 5.0, 7.5 and 10.0 minutes post-nucleation) to assess fouling with time whilst not disturbing any deposited crystalline matter. Each condition was explored in duplicate. Fouled material coupons were dried overnight in a vacuum oven for further analysis. A DOE approach was considered with a D-optimal design employed to investigate process parameters for stainless

steel and PTFE (see 3.2.2.2 DOE). Process parameters explored for both stainless steel and PTFE are detailed in Table 5.3. Both MOCs were additionally explored at a near-central design space point (supersaturation ratio 1.3, agitation rate 350 rpm).

Table 5.3: Experimental design for D-optimal DOE investigating supersaturation, agitation rate, exposure time after nucleation and MOCs.

Supersaturation	Agitation rate (rpm)	MOC	Sample times after nucleation (mins)
1.2	130	PTFE	2.5, 5.0, 7.5 and 10.0
1.2	700	PTFE	2.5, 5.0, 7.5 and 10.0
1.2	130	Stainless steel	2.5, 5.0, 7.5 and 10.0
1.2	700	Stainless steel	2.5, 5.0, 7.5 and 10.0
1.3	350	Stainless steel	2.5, 5.0, 7.5 and 10.0
1.3	350	PTFE	2.5, 5.0, 7.5 and 10.0
1.4	130	PTFE	2.5, 5.0, 7.5 and 10.0
1.4	700	PTFE	2.5, 5.0, 7.5 and 10.0
1.4	130	Stainless steel	2.5, 5.0, 7.5 and 10.0
1.4	700	Stainless steel	2.5, 5.0, 7.5 and 10.0

The measurement fouling responses used for the DOE were (i) total mass deposition upon MOC coupon (mass deposited on all planes; Figure 5.6) and (ii) fouling area coverage on one selected surface (either plane 1 or 2; Figure 5.6).



Figure 5.6: Schematic representing an investigatory MOC coupon specifically highlighting the five planes on which fouling can occur.

Total mass deposition was determined by washing each fouled surface with small volumes of methanol and dried via a vacuum oven. The fouling area coverage was determined by obtaining micrographs using the Morphologi G3 (Malvern). The Morphologi G3 disperses dry particles onto a slide from which particle size and shape information can be obtained.²³⁶ However the Morphologi G3 was employed within this work to collect a series of micrographs of the fouled MOC coupon. Micrographs were collected at 2.5x magnification and merged into a single image (Figure 5.7) which contains all fouled PCM deposits present upon the selected investigatory plane. Image analysis was performed using MATLAB software (MathWorks) to determine the number of fouled pixels at the specified intensity range and converted into a total fouled area coverage (area per pixel = $8.35 \times 10^{-6} \text{ mm}^2$) via an in-house generated algorithm. Average mass deposition, area coverage and mass coverage plots against time were determined and linear fouling rates were obtained. Models were generated for each fouling response.

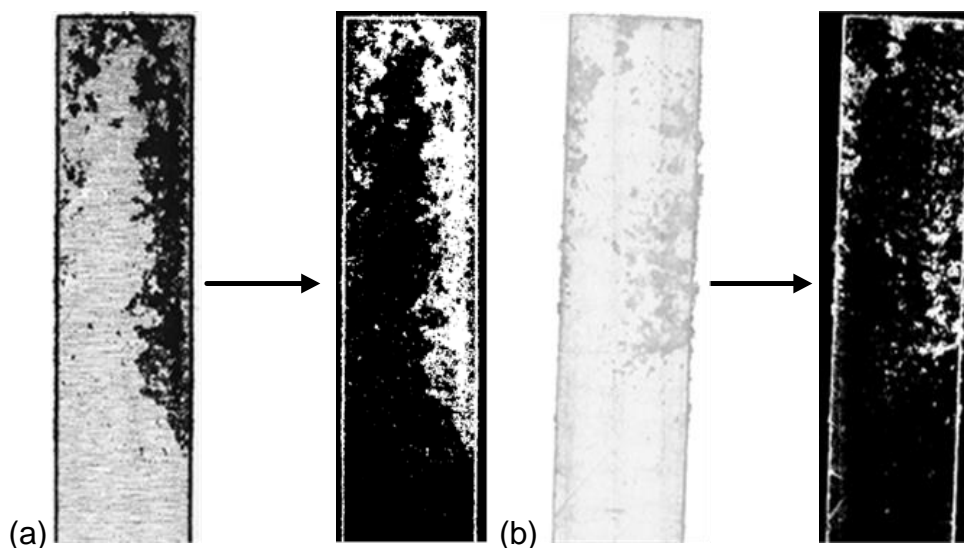


Figure 5.7: Example of merged images of fouled MOC coupons in addition to images after image analysis via MATLAB for (a) stainless steel and (b) PTFE.

5.2.2.4 CFD analysis

CFD analysis was performed as described in 3.2.2.3 CFD to predict shear rates within an investigatory MOC-containing vial. Shear rates were determined for the bulk solution and also within the locality of the MOC coupon for all investigated agitation rates.

5.3 Results and discussion

5.3.1.1 Nucleation kinetics

The effect of supersaturation, agitation rate and each MOC coupon on nucleation was the initial research interest. Note that not all investigated vials for each explored condition nucleated within the allocated eight hour experiment time window (Figure 5.8) highlighting the stochastic nature of nucleation. This led to an unequal population for each dataset. One prime example is the investigatory condition comprising supersaturation 1.2 and agitation rate of 130 rpm where only 35% of 14 stainless steel investigatory vials nucleated within 8 hours in contrast to PTFE containing vials where 77%

of 22 investigated vials nucleated. Vendel and Rasmuson found Teflon™ had a catalytic nucleation effect for adipic acid and glycine solutions whilst stainless steel was not identified to have this induction effect which may offer an explanation to observed nucleation percentage differences between stainless steel and PTFE as seen in Figure 5.8. The number of vials sampled for each explored condition was varied in which notably PTFE had a larger total sampled number in comparison to stainless steel vial numbers. Consequently a situation arises where there is an increased probability for nucleation occurring within 8 hours for PTFE due to its larger sample size. The sample number for each condition ranged between 10 to 30 samples which is considered to effectively represent the distribution of induction time data. The number of samples to represent explored conditions varied widely within induction time research with Kulkarni and co-workers²²⁷ using 144 replicates to determine induction time data for isonicotinamide in ethanol whilst Ilevbare et al.²³⁷ determined induction times in triplicate for each explored condition in the investigation of selected APIs. The effect of increasing supersaturation and agitation rate across all data shows a potential trend in increasing nucleation percentage however is not consistently found.

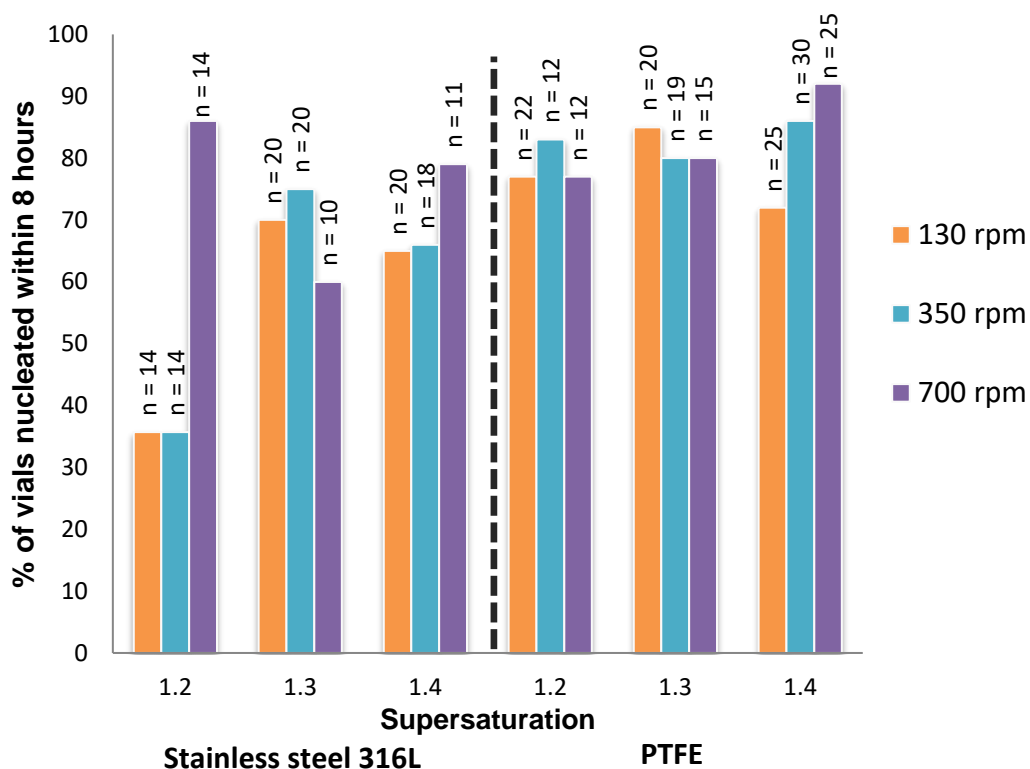


Figure 5.8: Percentage of experimental vials that nucleated within 8 hours for all explored conditions where n represents the total number of studied vials (n ranging from 10 to 30).

Nucleation does not appear to be affected significantly by the presence of the two MOC (Figure 5.8). This finding suggests that the initiation of nucleation is occurring within the bulk solution, rather than at any of the surfaces in contact with the solution. This is consistently observed regardless of which process condition was explored. Examples of acquired images are displayed in Figure 5.9 which indicate the cloud points of both stainless steel (Figure 5.9 (a) and (b)) and PTFE (Figure 5.9 (c) and (d)), respectively, under identical conditions.

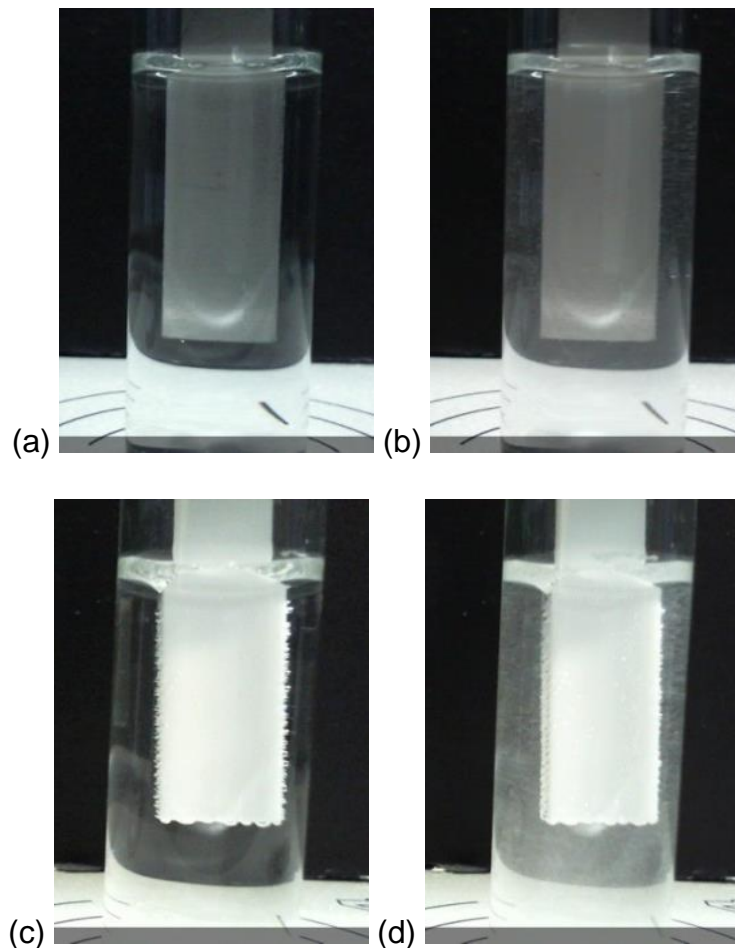


Figure 5.9: Recorded images obtained of the nucleation point of PCM in water for supersaturation ratio 1.3 at an agitation rate of 350 rpm for stainless steel ((a) and (b)) and PTFE ((c) and (d)). Images (a) and (c) are the first image obtained once the prepared vials were added into the incubator with (b) and (d) the nucleation point from which the time difference (induction time) was obtained. The addition of PTFE into the investigatory vial resulted in bubble formation at its surface as observed in image (c). Once agitation begins the surface of PTFE becomes wetted.

Although heterogeneous nucleation by the MOC was not confirmed, heterogeneous nucleation is the likely primary nucleation mechanism (1.3.3.2 Heterogeneous nucleation). No statistically significant differences between groups were identified in Figure 5.8 indicating the heterogeneous nucleation process is occurring due to impurities in the solution and the influence of the borosilicate vial. The detection method for nucleation was by visual observation via webcams hence visual ability to identify the location of nucleation was limited. Research by Little et al. utilised commodity webcams

to study the nucleation of glycine from aqueous solutions in which the minimum observable crystal size was estimated to be around 110 μm which highlights the sensitivity of webcam based techniques.²³⁸ Nucleation may have initiated at other locations at the sub-micron scale which would not be detected within the present work. Nucleation may have occurred at the MOC coupon surface, at other materials in contact with PCM solution or even within bulk however this was not established. It was expected that nucleation would occur readily upon the stainless steel surface due to a higher roughness value and providing a higher number of nucleation sites.¹⁹ However as shown by Vendel and Rasmuson, fluoropolymer surfaces can catalyse the nucleation of selected organic molecules whilst stainless steel had no influence⁷ highlighting nucleation uncertainty involving these two MOCs. Alternatively, nucleation may have initiated at the surface of a MOC which nuclei rapidly detach due to shear therefore it cannot be confirmed where nucleation began. However on the basis of the data presented in Figure 5.8, the dominant nucleation process is not affected by the investigated MOC surfaces.

For each condition, an unequal number of induction time values were generated. In order to facilitate comparison and analysis, boxplots were generated for each studied condition to highlight differences in the spread of induction times (Figure 5.10) and assess data distribution. No significant differences were considered with a high degree of overlap, in particular comparing different MOCs under identical process conditions. Similar to results identified within Figure 5.8, the lack of distinct influence of MOCs on induction time suggests bulk nucleation mechanisms dominate in contrast to surface-induced nucleation (Figure 5.10). A correlation is identified with increasing supersaturation and resulting decreasing induction time as is also noted for increasing agitation rate. A large proportion of the generated boxplots have a skewed distribution as shown in Figure 5.10. The distribution of induction time data is shown to be influenced by different supersaturation ratios as demonstrated by Jiang et al.²³⁹ for *m*-aminobenzoic acid. The influence of the number of datapoints contributing to boxplots and related induction time ranges were noted with boxplots associated with larger numbers

of datapoints having larger ranges. This is observed in particular for PTFE boxplots (Figure 5.10). Although differences are observed within Figure 5.10, there is no evidence of significant differences for the two MOCs tested based upon the boxplots.

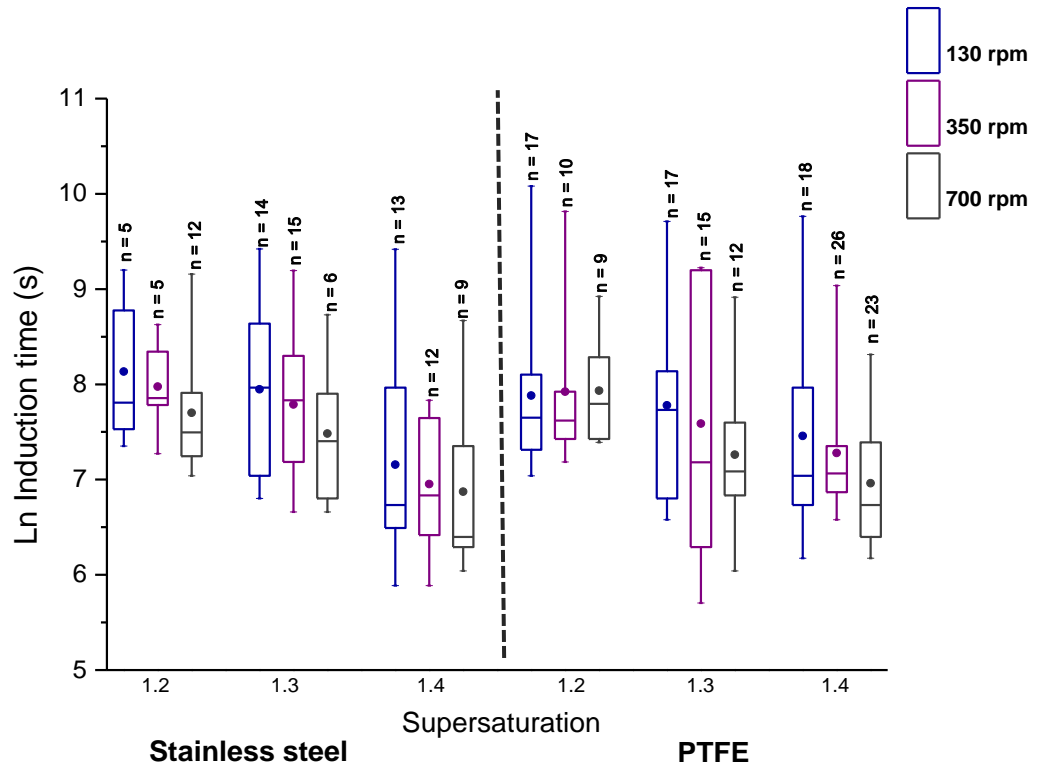
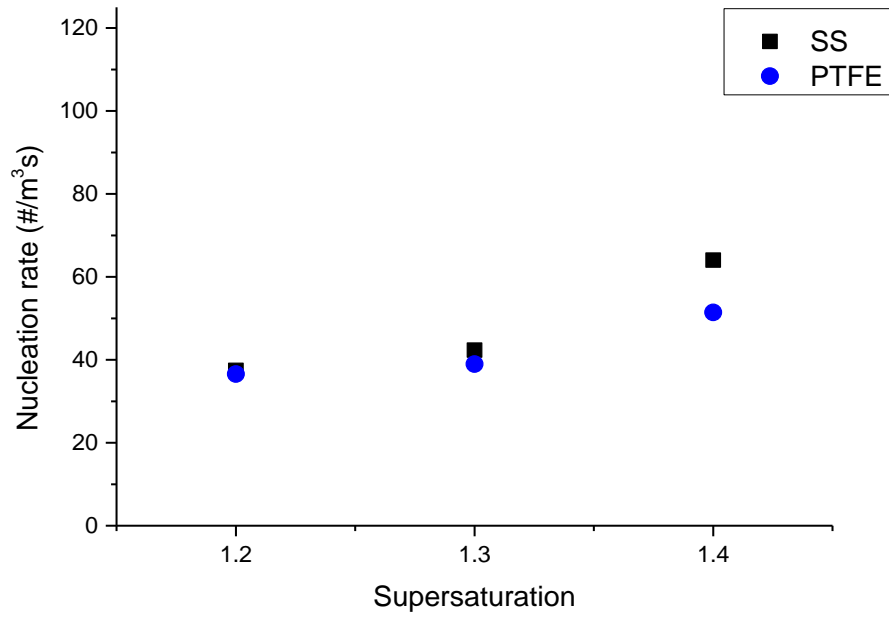
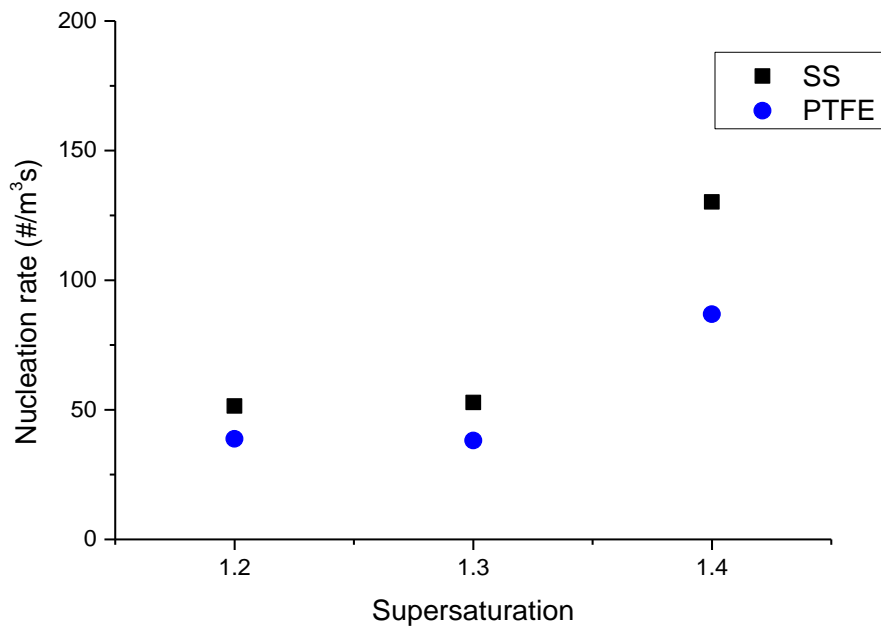


Figure 5.10: Boxplots for all investigated conditions. The data plotted highlights minimum and maximum values for dataset in addition to 25%, median and 75% quartile values. Mean values are denoted by a filled circle icon. n represents the number of investigated vials.

The nucleation rate was determined for each condition from calculated average induction times using Equation 5.2. Nucleation rate values are shown in Figure 5.11 for all explored supersaturation ratios, MOCs and agitation rates (Figure 5.11 (a) 130 rpm, (b) 350 rpm and (c) 700 rpm).

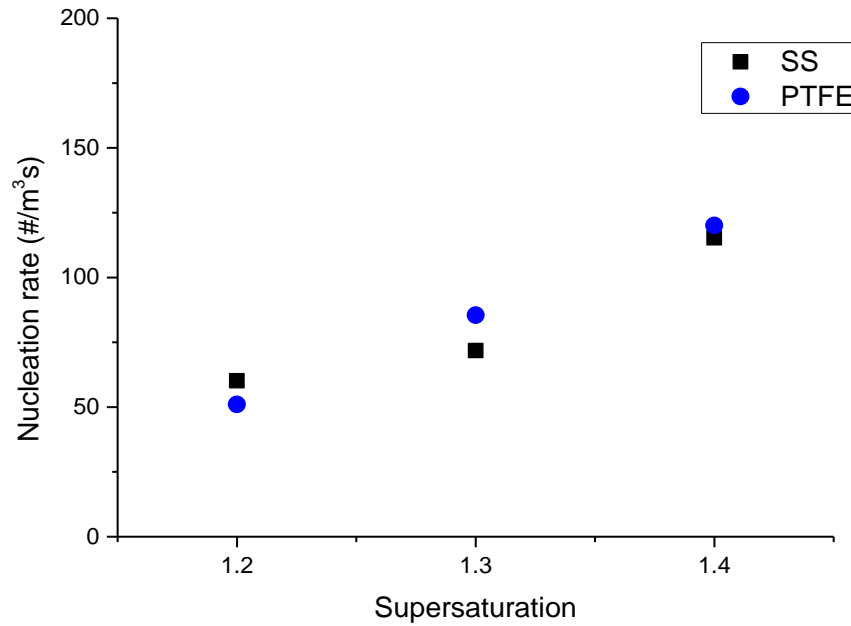


(a)



(b)

Figure 5.11: Nucleation rate calculated from average induction time values for investigated MOCs, supersaturation ratios and agitation rates of (a) 130 rpm, (b) 350 rpm and (c) 700 rpm.



(c)

Figure 5.11 continued...

It is observed that supersaturation and agitation rate had a distinct impact upon nucleation rate which was to be expected. Figure 5.11 demonstrates that increasing supersaturation results in an increase in nucleation rate which relates to CNT^6 and is defined by Equation 1.14. Mitchell and co-workers also established a similar trend in which nucleation rates were estimated to increase for PCM in ethanol with increasing supersaturation.²²⁶ Additionally the influence of increasing agitation rate on nucleation rate was evident however reaches a plateau phase at 350 rpm with no apparent increase in nucleation rate afterwards. This effect had been previously highlighted by Mullin previously.⁶ Small variations in nucleation rate were found between investigated MOCs for all explored conditions. The nucleation rate of PCM for investigated conditions involving stainless steel were expected to be larger than PTFE due to rougher surface topography allowing more nucleation sites in addition to research using stainless steel being demonstrated to influence on nucleation rate as in research by Liang and co-workers.⁵³ Differences in nucleation rates were found for stainless steel and Perspex® impellers for LGA

nucleation in which stainless steel predominately had larger nucleation rate values. Additionally Liang explored the impact of agitation on nucleation rate for each stirrer MOC in which no notable increase in nucleation rate was observed with increasing agitation.⁵³ Increasing agitation rate consequently increases the shear conditions within a crystallising system. Forsyth and co-workers determined a relationship between increasing average shear rate and increasing nucleation rate of glycine within a Couette flow cell crystalliser set up.²⁴⁰ It was noted within Figure 5.11 that the absence of a MOC coupon for several conditions resulted in considerably larger nucleation rates compared to the presence of MOCs. This is contrary to findings by Forsyth et al.²⁴⁰ where increasing the solid surface area contact to crystallising volume ratio increased glycine nucleation rate. It was highlighted that increasing the exposure surface area increases the number of potential nucleation site for subsequent nucleation. However these findings relate to a Couette flow cell where the hydrodynamic conditions are different compared to the small batch crystalliser used herein and hence are not directly related to added surfaces within the present study.

The Kruskal-Wallis test can be used to determine if there are statistically significant differences between two or more independent variable groups upon a continuous variable (see 5.2.2.2 Nucleation kinetics). The Kruskal-Wallis test was performed to evaluate what parameters had a significant effect upon induction time which could not be established based upon routine inspection of generated boxplots (Figure 5.10). Callahan and Ni employed the Kruskal-Wallis test as a statistical method to assess the significance of crystalliser configuration upon the crystal percentage similarity to crystal seeds used.¹⁹⁹ Application within crystallisation research is limited however it merits further application in this case notably due to the absence of normal distributions in the majority of datasets (Figure 5.10).

Induction time datasets were compared and analysed. The Kruskal-Wallis test results are detailed in Table 5.4:

Table 5.4: Kruskal-Wallis test results detailing p-values and assessment for significance upon induction time. Significance effects were deemed with resultant p-values ≤ 0.05 .

Dataset	Parameter	p-value	Significant difference (p-value ≤ 0.05)
All data	Supersaturation	0.000	Significant
	Agitation rate	0.08	Not significant
	MOC	0.652	Not significant

The relationship between supersaturation and induction time has been well established by a number of investigators^{200,241-242} which is in agreement with the results detailed in Table 5.4 where significance was identified for all datasets. Increasing agitation rate may be expected to decrease induction time, as demonstrated by Liu and Rasmuson in the case of butyl paraben nucleation.²²⁸ Kruskal-Wallis test results found that agitation rate did not have a significant effect upon nucleation. The impact of MOCs on induction time was determined to be non-significant. The addition of a MOC coupon into a crystallising system was hypothesised to decrease subsequent induction times. Theoretically the addition of a MOC coupon increases the exposed solid surface area in contact with the solution's volume therefore increasing the likelihood of nucleation to occur on a surface. The addition of a MOC coupon within investigated vials perform partly as a baffle. Liu et al.²²⁹ investigated the influence of stainless steel baffle inserts upon average induction time values. It was found that stainless steel baffle inserts reduced associated induction times for butyl paraben in comparison to baffle-free experiments underlining the importance of additional solid projectiles within a crystallising system.²²⁹ Different extents of induction time reduction due to baffle insertion were identified for different agitators/paddles and respective agitation rates. Mitchell et al. found the addition of baffles constructed from PTFE resulted in a reduction in induction times of between 20 to 50 minutes in contrast to induction times associated with the set up without baffles present.²⁰⁰ It was therefore reasonable to foresee the addition of a MOC coupon would decrease induction times and have a significant effect.

No significant difference was identified in induction time overall between the two MOCs namely stainless steel and PTFE. The properties of each MOC vary considerably as indicated in Table 4.4 in which stainless steel has a rougher topography, greater wetting behaviour and a larger surface energy in relation to PTFE. However, relating specific surface properties to nucleation is questionable with contrasting information from literature involving surface roughness^{19,53} and surface energy^{7,53} contributions. The effect of different MOCs upon primary nucleation within research literature is uncommon with secondary nucleation typically further explored. Differences in nucleation kinetics via altering MSZW due the presence of different MOCs has been demonstrated by Liang et al.⁵³ where stainless steel and Perspex® were investigated which was related to their different inherent properties. The presence of different MOCs was suggested would result in altered induction times however using stated nucleation detection techniques did not reveal any significant differences.

5.3.2 Fouling studies

5.3.2.1 General observations

Across the conducted experiments a number of features were observed. PCM particles suspended after bulk nucleation tended to deposit onto the coupon surface (Figure 5.12 and Figure 5.13). This was observed for both MOCs albeit to different extents and is explored further in later sections (5.3.2.2 DOE results). Deposition of PCM particles onto the coupons occurred promptly after nucleation and was found to be dynamic during the experiment with crystalline material detaching from and reattaching over time (Figure 5.12).

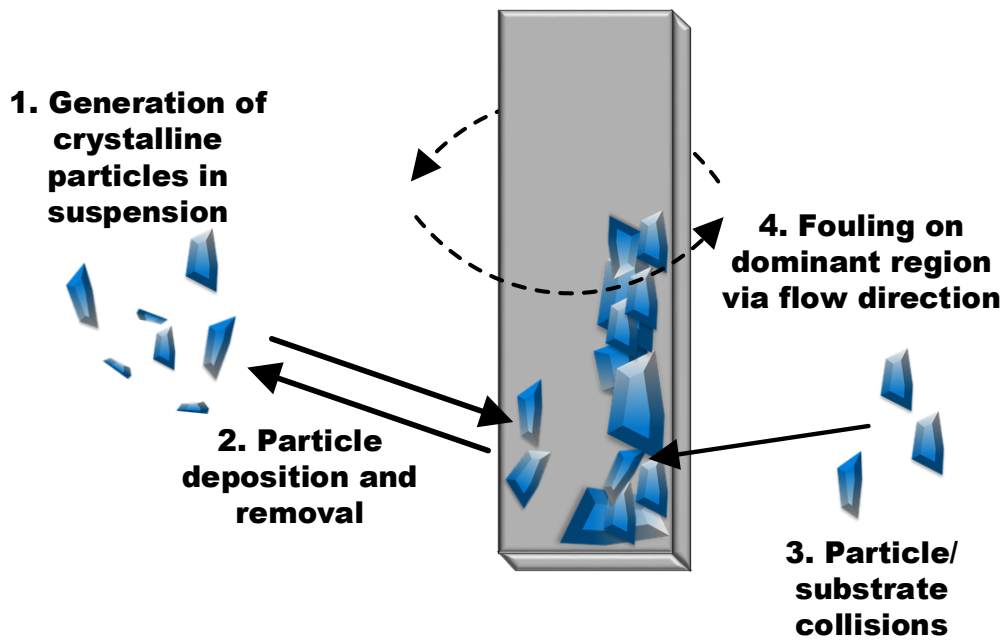


Figure 5.12: Schematic highlighting the relationship between nucleation and MOC fouling for the crystallising PCM in water solution.

Observed fouling was not symmetrical and, on each major face, a dominant region was mirrored on the opposite face. This is expected to relate to local flow patterns around the coupon. The influence of agitation is anticipated to impact the adhesion and cohesion processes of PCM particles and explored MOCs. Research by Sharma and co-workers investigated the detachment of colloidal particles of size range between 5 μm to 40 μm from glass and copper substrates in which a critical flow velocity and consequential force was identified after which particles would be removed.²⁴³ Ålander and co-workers highlighted that PCM agglomeration is influenced by fluid shear rate via increasing agitation rate in which agglomeration can be enhanced or decreased.²⁴⁴ Agglomeration consists of collisions and particle adhesion processes therefore findings relating to PCM agglomeration can be partly applied to PCM particle and MOC substrate interactions.

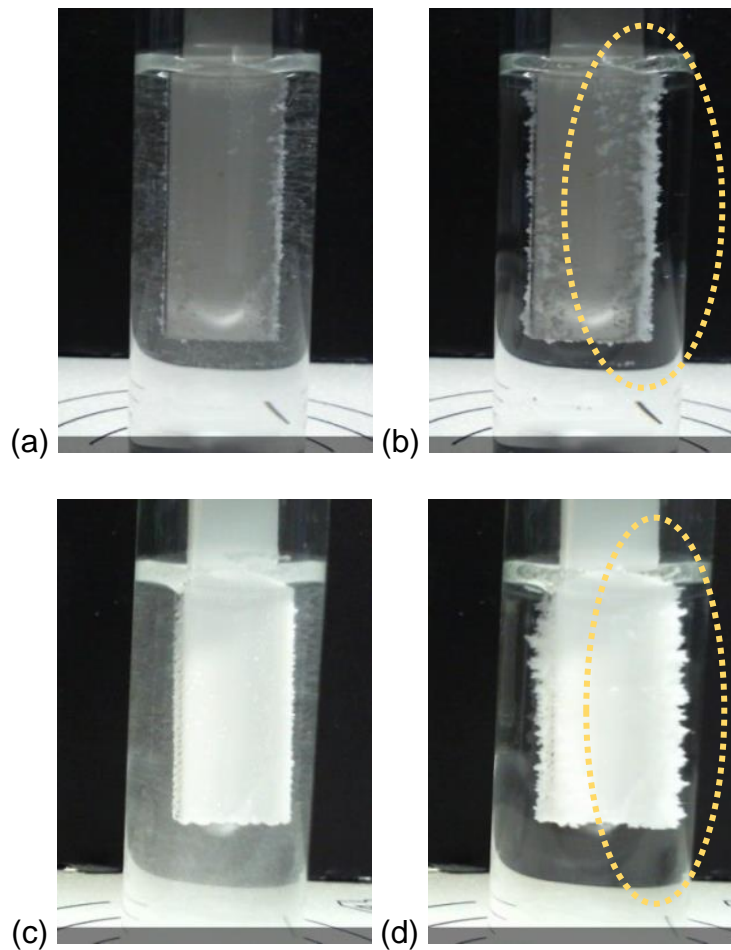


Figure 5.13: Images of stainless steel and PTFE at the nucleation point in a saturated solution of PCM in water ((a) and (c), respectively) showing the different extents of fouling after 10 minutes at supersaturation 1.2 and 700 rpm. [Yellow dashed outline highlights the dominant location where fouling mainly occurs].

CFD simulations were computed to determine shear rates within the bulk fluid and at the coupon surface (Table 5.5) where larger shear rates were found within the bulk solution (see 3.2.2.3 CFD). The distribution of shear upon the MOC coupon varied with increasing agitation rate in addition to larger shear present mainly in one locality and also in the direction of fluid flow (Figure 5.14). These findings relate to the distribution of fouled particles as seen in Figure 5.13 and further support the present research findings.

Table 5.5: Table of simulated average shear rates within the bulk solution and at coupon surface.

Agitation rate (rpm)	Shear rate bulk average (1/s)	Shear rate coupon average (1/s)
130	6.2474	0.97458
350	21.292	10.599
700	46.973	31.117

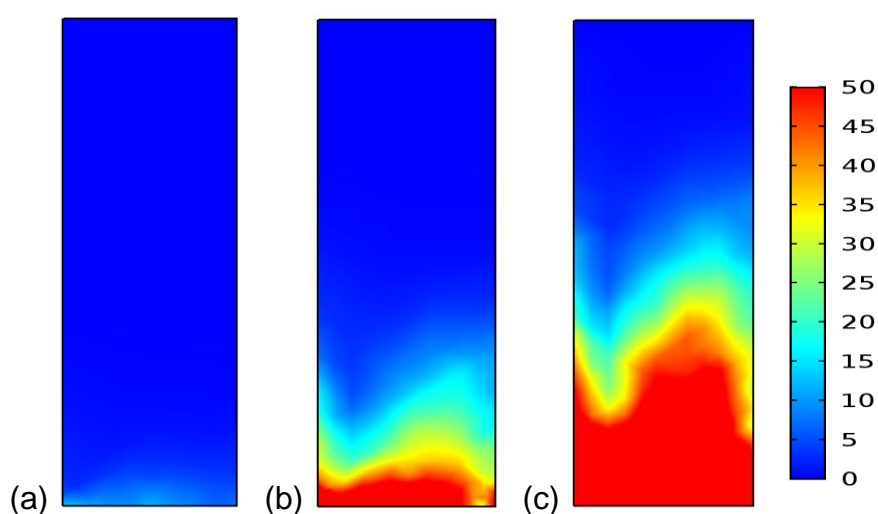


Figure 5.14: Shear rate distribution simulated upon exposed MOC coupon at agitation rates of (a) 130 rpm, (b) 350 rpm and (c) 700 rpm.

5.3.2.2 DOE results

Models for each fouling response were generated for all experimental data by applying logarithmic transformations and fitting transformed data via multiple linear regression (MLR). Models for each fouling response were generated by using individual factors and factor-factor interactions. Models were edited by removing non-significant terms to improve model statistics. A summary of fit plot for each model is detailed in Figure 5.15 which describes statistics to assess the strength and robustness of a model. Summary statistics and acceptable values are described in detail in 3.2.2.2 DOE. All fouling models

had R^2 and Q^2 that were termed acceptable based upon Table 3.4. Model reproducibility values illustrated in Figure 5.15 were satisfactory (as detailed in Table 3.4) however model validity values for all fouling model responses were all -0.2. The model validity term within MODDE software is capped at -0.2 and the reason for this value is due to the large number of replicates resulting in the model becoming oversensitive. The value for model validity is not satisfactory however on the basis of respectable model statistics generated fouling models are still valid. Each fouling response will be investigated including associated model contour plots, expressions and other fouling data interpretations.

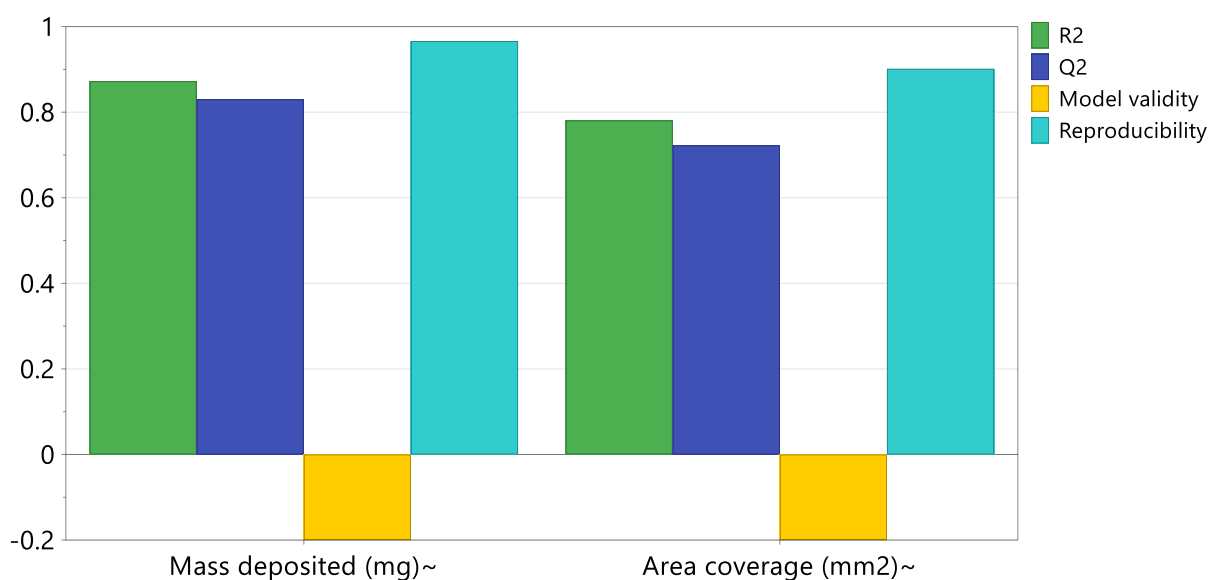


Figure 5.15: Summary of fit plot for each fouling response model.

(a) ***Total mass deposited***

The influence of MOCs, investigated process conditions and exposure time upon PCM fouling mass are presented in Figure 5.16, Table 5.6 and Figure 5.17. Average total mass values of fouling PCM are illustrated in Figure 5.16 which shows fouling mass is influenced by different parameters to varied extents. Average fouling mass is dependent on increasing exposure time to

fouling conditions, increasing supersaturation and increasing agitation rate with resultant increasing fouling PCM mass. Figure 5.16 also illustrated the influence of different MOCs on PCM mass deposition in which larger fouling mass values were found for stainless steel in contrast to PTFE at larger agitation rates whilst other experimental conditions were identical. However at lower agitation rates differences in fouling trends with time for each MOC were comparable (Figure 5.16).

A contour plot was generated for PCM fouling mass which illustrates the previously highlighted relationships between supersaturation, agitation rate and exposure time that resulted in larger total fouling mass values (Figure 5.17). Notable differences were found between the contour plots for each investigated MOC. Larger fouling mass values involving stainless steel were identified in contrast to PTFE in particular concerning larger agitation rates whilst at lower agitation rates the contour plots for stainless steel and PTFE were comparable. The fouling mass unscaled model expressions for stainless steel and PTFE are detailed in Equation 5.5 and Equation 5.6, respectively, which can be used as a prediction tool.

$$\begin{aligned}
\text{Mass deposited}_{SS} & & (5.5) \\
& = (-0.641011S - 0.000222486AR - 0.51969MOC_{SS} \\
& - 0.221371t + 0.00137946S*AR + 0.281873S*MOC_{SS} \\
& + 0.244361S*t + 0.000571836AR*MOC_{SS} + 2.38776E^{-5}AR*t \\
& - 0.0138436MOC_{SS}*t) - 0.250164
\end{aligned}$$

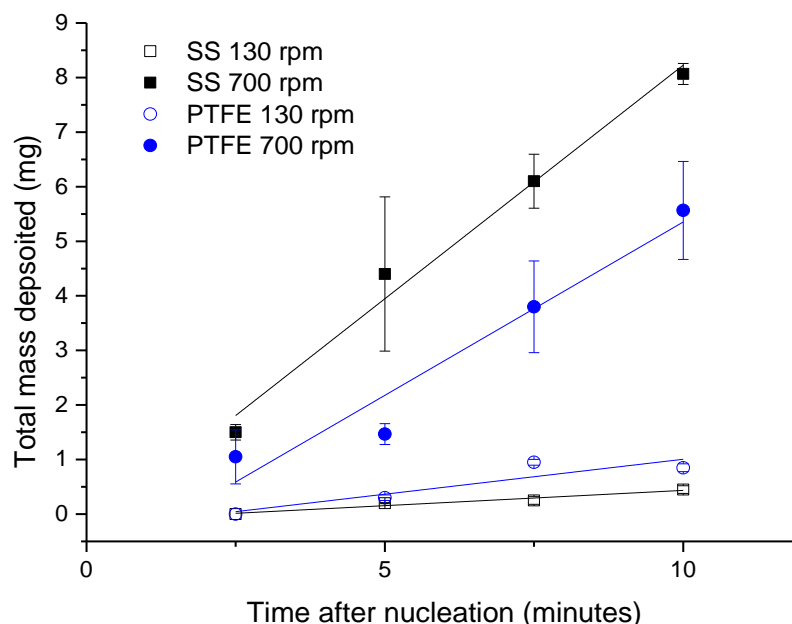
$$\begin{aligned}
\text{Mass deposited}_{PTFE} & & (5.6) \\
& = (-0.641011S - 0.000222486AR + 0.51969MOC_{PTFE} \\
& - 0.221371t + 0.00137946S*AR - 0.281873S*MOC_{PTFE} \\
& + 0.244361S*t + 0.000571836AR*MOC_{PTFE} \\
& + 2.38776E^{-5}AR*t + 0.0138436MOC_{PTFE}*t) - 0.250164
\end{aligned}$$

Where:

S	=	Supersaturation ratio
AR	=	Agitation rate (rpm)
MOC_{SS}, MOC_{PTFE}	=	Material of construction (stainless steel and PTFE)
t	=	Time (minutes)

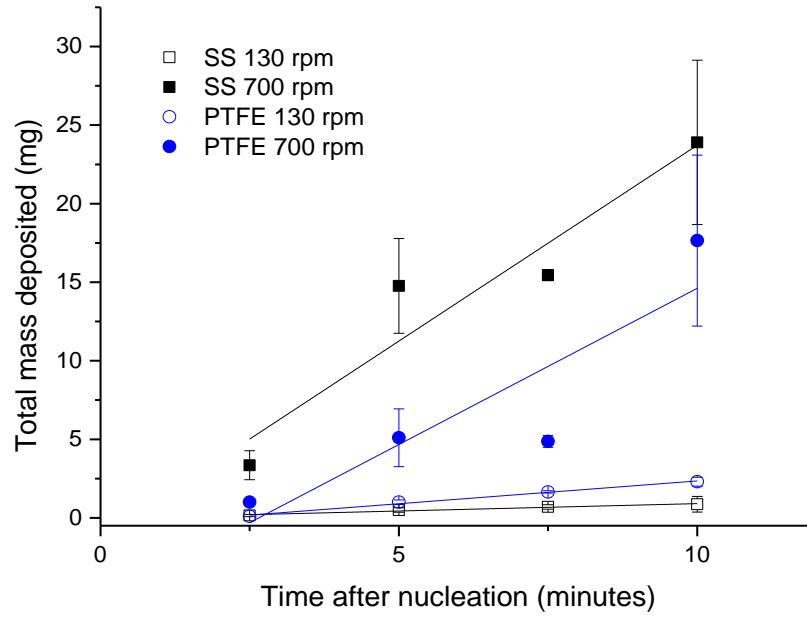
It is considered that PCM particles deposit upon each coupon from the bulk PCM aqueous solution in contrast to surface nucleation and growth. There is evidence from literature highlighting differences in particle deposition upon various substrates. Rosmaninho et al. investigated the deposition of calcium phosphate particles in a batch set-up upon stainless steel and also PTFE-containing coated substrates (Ni-P-PTFE coating on stainless steel). It was found the mass of calcium phosphate particles deposited upon stainless steel was significantly larger than stainless steel substrates with Ni-P-PTFE coatings. Additionally Rosamaninho and co-workers conducted particle detachment experiments in which Ni-P-PTFE coated substrates had a greater removal percentage of calcium phosphate particles in contrast to stainless steel which may provide an explanation to the observed PCM fouling

behaviour.¹³⁴ However different proposals were identified by Vendel and Rasmuson in which it was suggested Teflon™ formed stronger adhesions between its surface and investigated organic crystals in contrast to stainless steel. This theory is proposed on the basis that crystals were hydrophobic in nature and strongest adhesion arises between a hydrophobic surface and hydrophobic crystal face. Both particle adhesion and surface catalytic nucleation is governed by the work of adhesion.⁷ Proposals by Vendel and Rasmuson are based upon hydrophobic crystalline material interacting with a hydrophobic surface however pure hydrophobic interactions are rare and typically include a hydrophilic element.

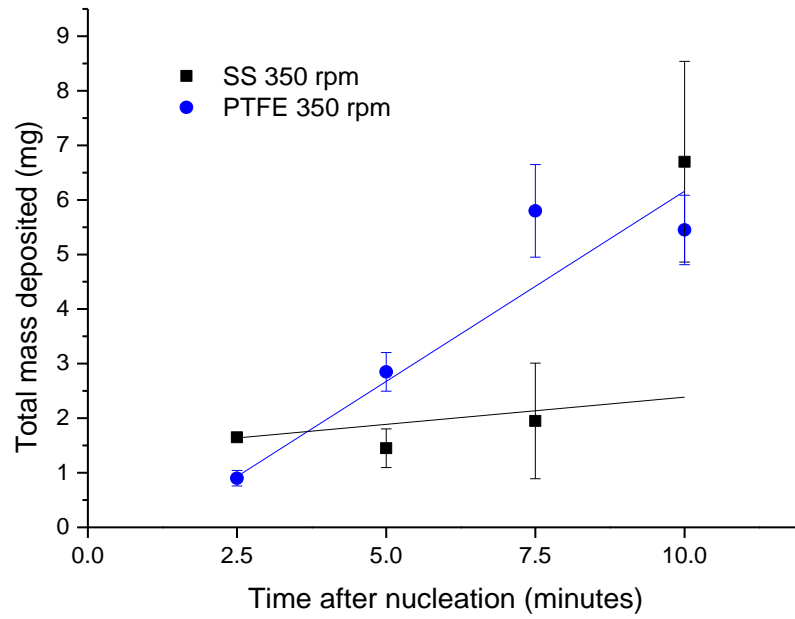


(a)

Figure 5.16: Average total mass deposited upon MOC material coupons at 2.5 minute time intervals over 10 minutes for different agitation rates (130 rpm and 700 rpm) at supersaturation (a) 1.2 and (b) 1.4. Error bars represent standard deviation values and a non-weighted line of best fit was applied where Y intercept is not restricted and employed for all data. A near centre condition (supersaturation 1.3 and 350 rpm) was additionally investigated based upon experimental design as shown in image (c).



(b)



(c)

Figure 5.16 continued....

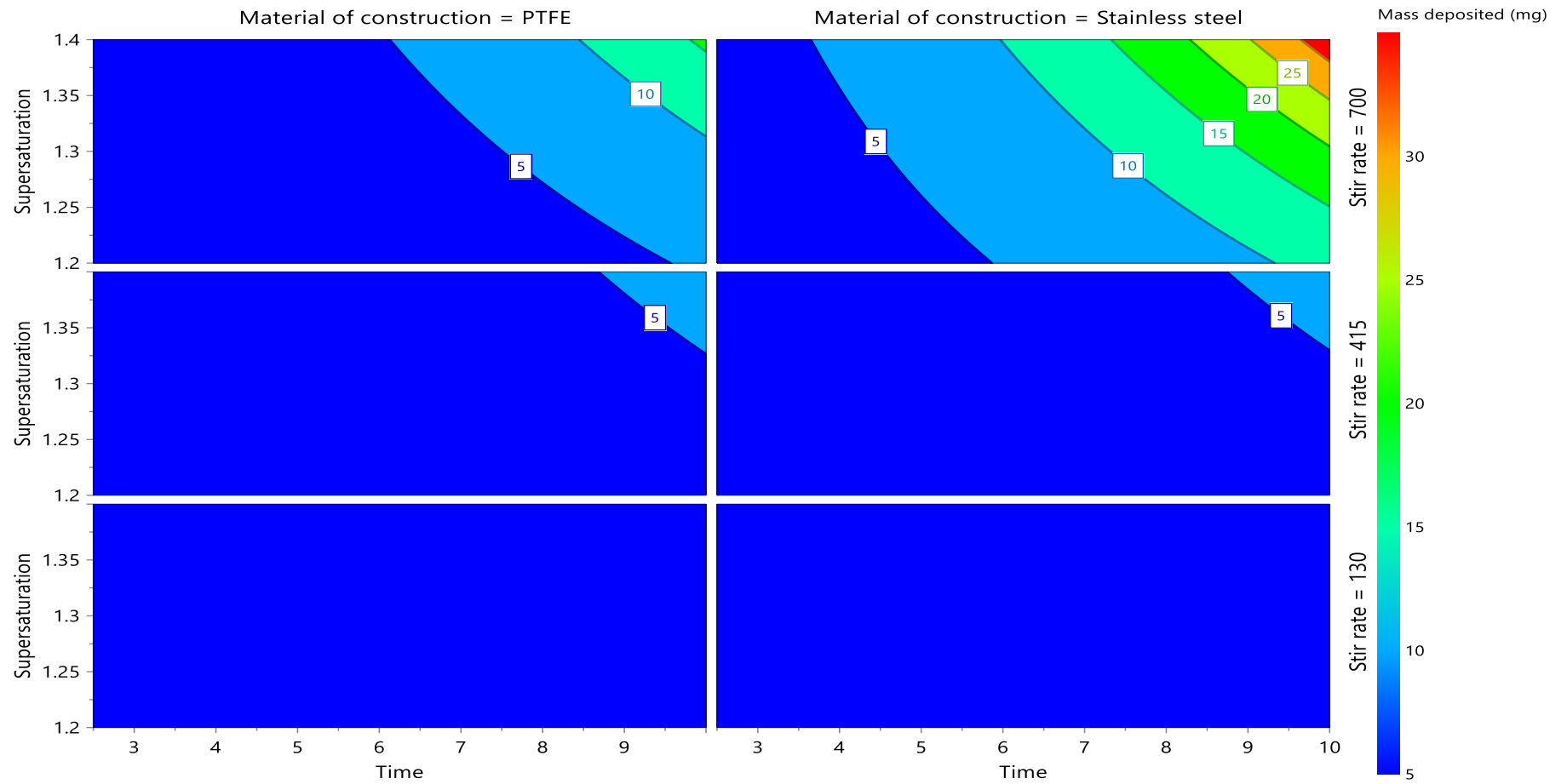


Figure 5.17: 4D response contour plot for total mass deposited model (model expressions are detailed in Equation 5.5 and Equation 5.6).

(b) **Area coverage**

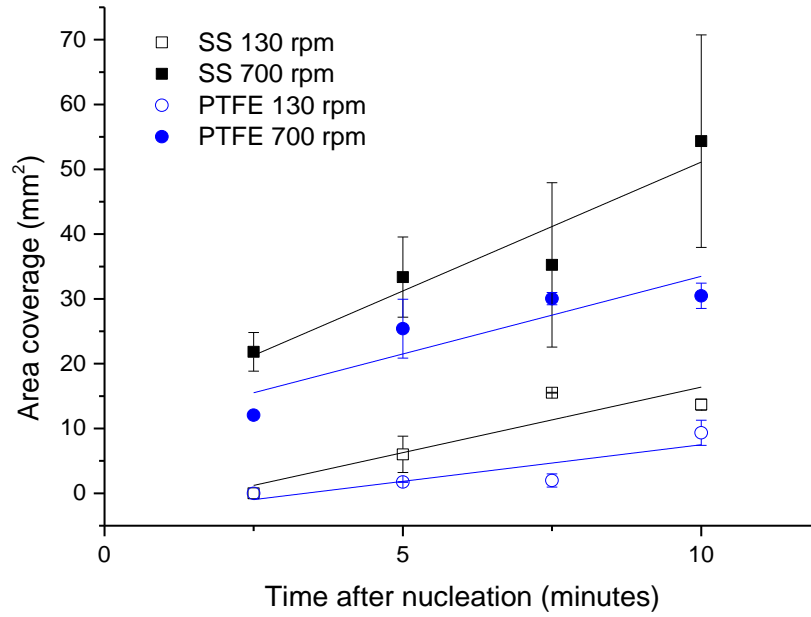
The influence of investigated MOCs, process conditions and exposure time upon the fouling area coverage due to PCM particle deposition are detailed in Figure 5.18, Table 5.7 and Figure 5.19. Figure 5.18 shows the average fouling area coverage deposited upon each investigated MOC at selected conditions for two supersaturation ratios (1.2 and 1.4). From Figure 5.18 it is shown, that for both MOCs, larger average area coverage values were obtained when subjected to a larger agitation rate of 700 rpm in contrast to lower agitation. Similar to trends identified for average fouling total mass deposited at higher and lower agitation rates investigated were found for average fouling area coverage highlighting the importance of particle mass transfer. There is a progressive increase in area coverage with respect to time for all MOCs explored at 700 rpm. The impact of increasing supersaturation upon fouling area coverage was not confirmed. However there was evidence of increased fouling area coverage with increasing supersaturation. It was hypothesised that increasing supersaturation would increase respective PCM nucleation rate (Equation 1.14) and consequently number of particles available to deposit/cover a MOC coupon. Increasing the number of generated particles in suspension potentially allow more particles to adhere to the MOC coupon. Average area coverage due to PCM particle deposition was found to be larger for stainless steel than that of PTFE across investigated conditions however significance is not considered. It is determined that stainless steel has larger area coverage in comparison to PTFE in particular for explored conditions for supersaturation ratio 1.4. Vendel and Rasmuson explored the fouling of stainless steel and Teflon™ (fluorinated polymer substrate) via an impinging jet to mimic particulate collision conditions within a crystalliser in which was found stainless steel had more crystals adhered to its surface than Teflon™ substrates¹² – this capability of stainless steel to adhere particles may explain its associated larger area coverage. One explanation involving MOC properties is the influence of surface roughness in which roughened surface encourages particulate fouling due to particle entrapment.²⁴⁵ Within research literature area coverage measurements have not been utilised in crystallisation

and fouling studies however related measurements such as crystal density have been employed. Research by Diao et al. used crystal area density as a measurement to assess nucleation on various polymer substrates.¹²⁰

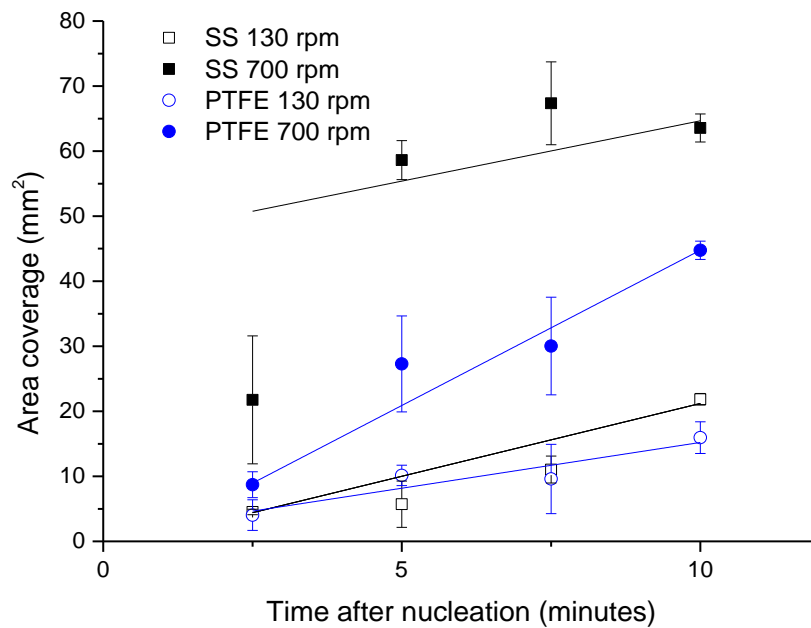
Contour plots generated for the area coverage fouling model reveal increasing supersaturation, agitation rate and fouling exposure time after bulk nucleation resulted in larger area coverage (Figure 5.19) in which notable differences in contour plots are observed for different agitation rates and different MOCs. The fouling area coverage model expressions for stainless steel and PTFE are detailed in Equation 5.7 and Equation 5.8, respectively.

$$\begin{aligned}
 \text{Area coverage}_{SS} & & (5.7) \\
 &= (0.518559S + 0.00241038AR + 0.0740077MOC_{SS} \\
 &\quad - 0.0116891t - 0.000849713S*AR + 0.0756056S*t \\
 &\quad + 5.96034E^{-5}AR*MOC_{SS} - 3.52816E^{-5}AR*t) - 0.45238
 \end{aligned}$$

$$\begin{aligned}
 \text{Area coverage}_{PTFE} & & (5.8) \\
 &= (0.518559S + 0.00241038AR - 0.0740077MOC_{PTFE} \\
 &\quad - 0.0116891t - 0.000849713S*AR + 0.0756056S*t \\
 &\quad - 5.96034E^{-5}AR*MOC_{PTFE} - 3.52816E^{-5}AR*t) - 0.45238
 \end{aligned}$$

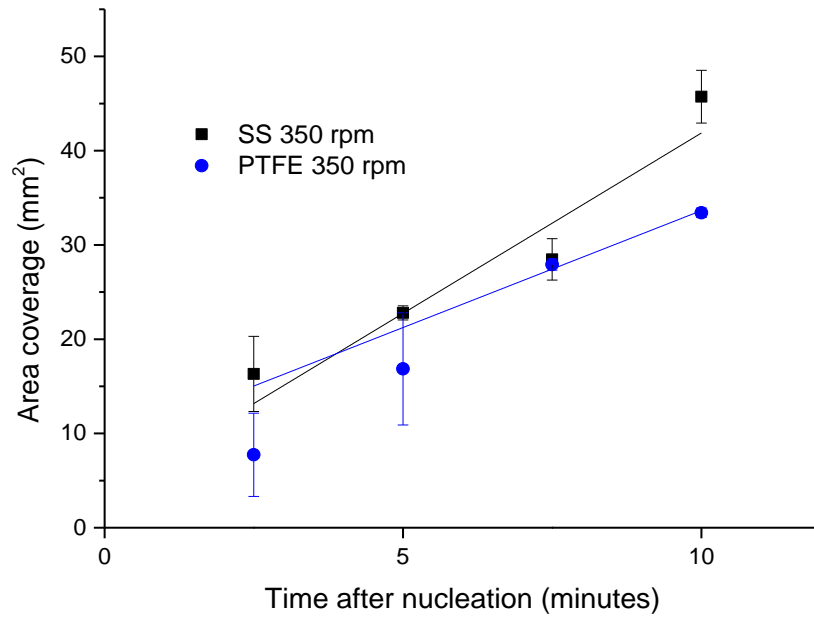


(a)



(b)

Figure 5.18: Average area coverage upon MOC material coupons at 2.5 minute time intervals over 10 minutes for different agitation rates (130 rpm and 700 rpm) at supersaturation (a) 1.2 and (b) 1.4. Error bars represent standard deviation values. A non-weighted line of best fit was applied where Y intercept is not restricted and employed for all data. A near centre condition (supersaturation 1.3 and 350 rpm) was additionally investigated as shown in image (c).



(c)

Figure 5.18 continued

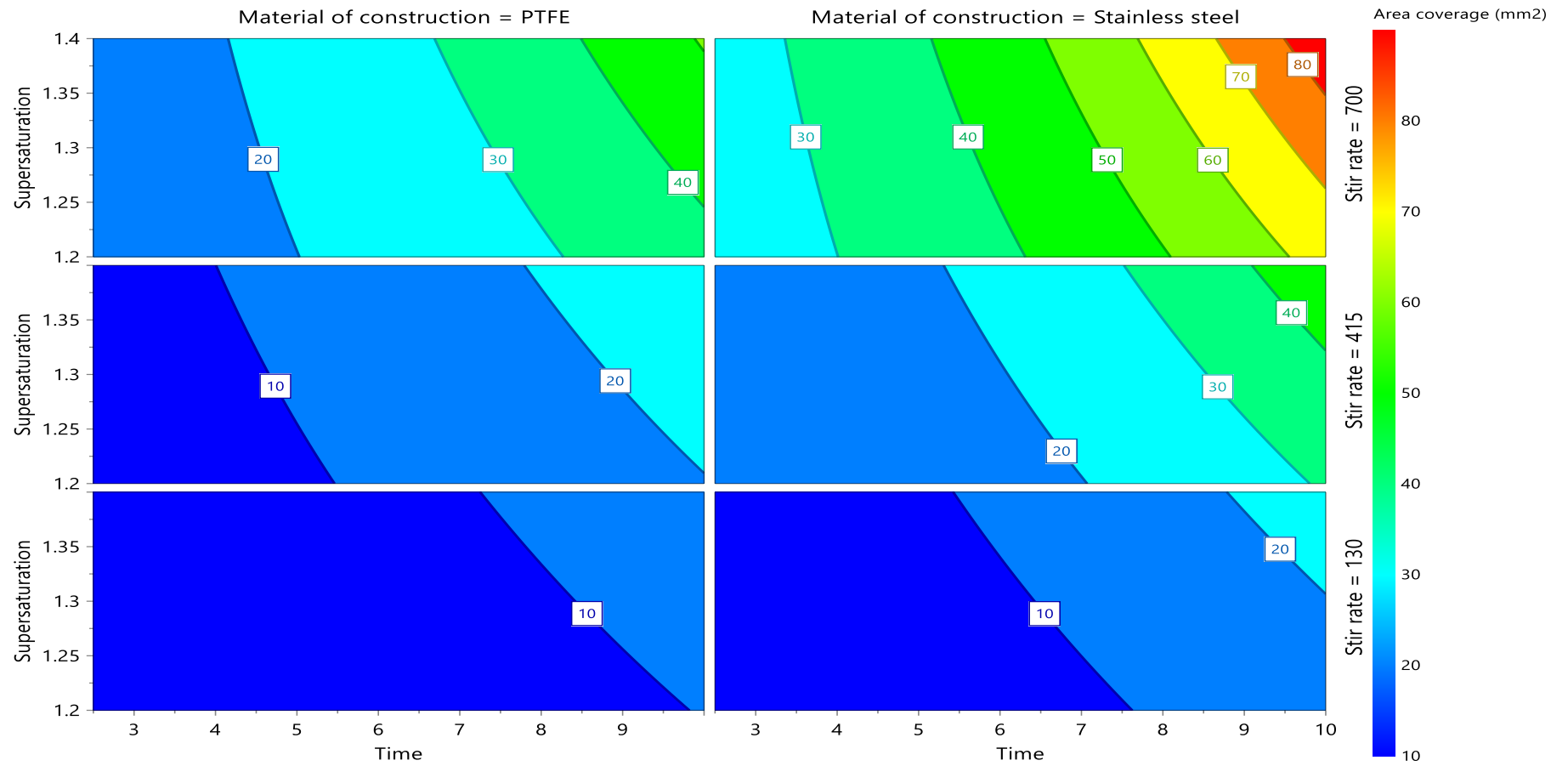


Figure 5.19: 4D response contour plot for fouling area coverage model (model expressions are detailed in Equation 5.7 and Equation 5.8).

(c) **Model validation**

Although each fouling response model had adequate descriptive statistics, a number of random validation experiments were conducted within the designated fouling design space. Validation experimental conditions used comprised investigating supersaturation ratio 1.2, agitation rate of 700 rpm and stainless steel and PTFE were both probed. Table 5.6 reveal the additionally determined experimental results for stainless steel and PTFE respectively, in terms of total mass deposited, area coverage and mass coverage over the initial 10 minutes post bulk nucleation. Additionally Table 5.6 reveal the model predicted results for all fouling responses. It was found that for all fouling responses, the predicted values within Table 5.6 are in close proximity to the experimentally determined results highlighting each model's validity in fouling prediction.

Table 5.6: Experimental and predicted fouling response results related to (a) stainless steel and (b) PTFE over the initial 10 minutes after bulk nucleation for supersaturation ratio 1.2 and agitation rate of 700 rpm.

(a) Time after nucleation (mins)	Total mass deposited (mg)	Total mass deposited predicted (mg)	Area coverage (mm ²)	Area coverage predicted (mm ²)
2.5	1.1	2.45	18.73	24.83
5.0	2.5	3.77	25.3	33.95
7.5	6.2	5.79	20.47	46.42
10.0	7.8	8.91	56.42	63.46

(b) Time after nucleation (mins)	Total mass deposited (mg)	Total mass deposited predicted (mg)	Area coverage (mm ²)	Area coverage predicted (mm ²)
2.5	1.15	1.05	11.90	14.57
5.0	1.4	1.89	19.65	19.92
7.5	2.5	3.41	25.3	27.24
10.0	5.9	6.15	34.25	37.25

5.4 Summary

The purpose of the present research was to establish fundamental understanding of the relationship between nucleation and fouling and reveal specific mechanistic insights under the conditions tested. A method was designed using inexpensive commodity webcams to investigate the influence of MOCs on nucleation and fouling. Further understanding of nucleation and fouling mechanisms can be applied to any crystallisation campaign. However application of this knowledge to continuous crystallisation is highly desirable where process understanding is essential. Nucleation and fouling mechanisms were probed under different supersaturation and agitation rates in the presence of either stainless steel or PTFE coupons. A relationship between nucleation and fouling was recognised in which the generation of PCM particles within the bulk was followed by particle deposition onto the MOC coupon. Although surface nucleation was not identified it cannot be neglected.

The applicability of the Kruskal-Wallis test to assess the significance of process parameters and different MOC on nucleation was demonstrated. Induction time and nucleation rate differences were identified for PCM in water in terms of explored supersaturation ratios and agitation rates. The influence of different MOCs upon bulk induction time was not found to be significant. Additionally different MOCs had no notable effect upon bulk nucleation rate.

The principal fouling mechanism was highlighted to be particle deposition via collisions between PCM particles and MOC surface. PCM fouling was influenced by supersaturation and agitation rate notably in terms of mass deposition and area coverage. Differences in fouling behaviour were found between different MOCs under identical process conditions. The importance of material surface properties upon fouling was underlined in which the properties of stainless steel were subject to larger extents of fouling in contrast to PTFE. However relating specific material properties to fouling behaviour was not established. A model encompassing all explored process parameters

and MOC was created highlighting each parameters contribution with excellent model statistic measurements and has been successfully validated.

From a process understanding perspective, the importance of crystalliser operational parameters and the physical experiences particulates undergo within the crystalliser can directly contribute towards fouling. Learnings from this research can be related to MOC in contact with a supersaturated solution that do not perform as heat transfer surfaces e.g. a PAT probe. However further research is necessary regarding the fouling of MOC utilised for heat exchange within a crystalliser environment.

The methodology and setup used within this work is useful as a rapid screen to test fouling phenomena within batch systems where the deposition propensity of a solute particle can be evaluated for a range of MOC. Modifications of the utilised setup via other imaging approaches could provide greater insight into nucleation and fouling initiation mechanisms e.g. microscopic 3D observations.

Chapter 6. Development of a continuous flow assessment platform for fouling

6.1 Introduction

Assessment of fouling mechanisms within a batch crystallisation system was performed within Chapter 5. Evaluating fouling mechanisms in continuous flow is desirable from which fouling mechanistic processes within batch and continuous systems can be assessed. The Zebrafish platform (as detailed in 3.2.3.2 Zebrafish platform) was specifically designed to investigate corrosion processes in which different process parameters, solutions and MOCs could be probed. The properties and functionality of the Zebrafish platform highlights its potential application for crystallisation fouling studies. In order for fouling to be investigated in continuous flow, a number of modifications to the Zebrafish platform were proposed. These are discussed herein regarding the development of the continuous flow fouling assessment platform (C-FAP).

6.2 Proposed modifications

In conjunction with CRD, a number of proposed modifications were discussed and conducted to allow fouling studies to be conducted. The objective was to develop a platform which would be representable of a heat transfer surface within a cooling crystallisation process.

Modifications which were made to the Zebrafish platform (Figure 6.1) included:

- A new bespoke flow cell design.
- The addition of a cold stream in contact with the rear of an investigated MOC coupon to induce fouling on the solution side coupon surface.
- The addition of thermocouples to monitor the (i) solution temperature before and after cell entry and also to monitor the (ii) cold stream temperature before and after contact with the rear of MOC coupon.

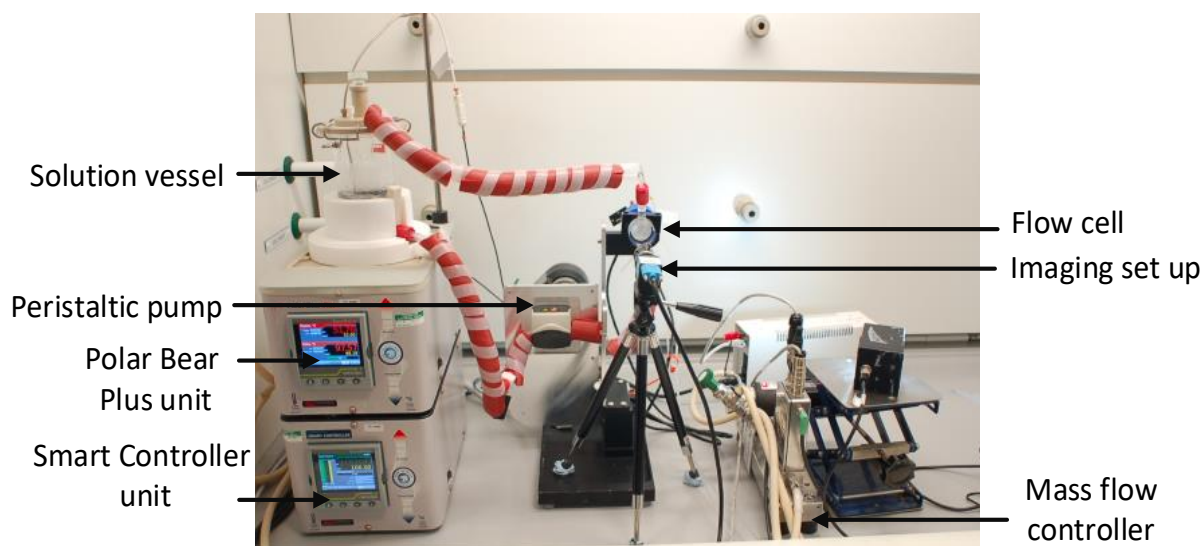


Figure 6.1: Image of the C-FAP set-up comprising a number of modifications.

6.2.1 Flow cell design

A number of obstacles were present with the Zebrafish platform's conventional electrochemical flow cell for it to be used for fouling studies (Figure 6.2). The proposed novel flow cell should allow for imaging and thermal measurement capabilities. The conventional flow cell required a number of modifications including:

- Replacing one of the electrodes with an optical glass window to allow internal monitoring via imaging. The optical window allows the fouling of a selected MOC to be monitored.
- The electrochemical flow cell contained a number of additional ports which served no purpose for fouling research and were consequently removed.
- The conventional flow cell accommodated an investigatory MOC coupon, via a PTFE housing component, which interfaced the internal environment of the flow cell and an electrode (Figure 6.2) – a minor modification was conducted allowing the investigated MOC to be exposed to the flow cell internal environment whilst the removal of the electrode component (Figure 6.3). A PEEK insert which allowed the

temperature of an investigated MOC coupon to be altered via a cooling fluid (Figure 6.3) was introduced to replace the electrode.



Figure 6.2: Library image of conventional corrosion flow cell for Zebrafish including electrode positions and several ports.¹⁷⁷

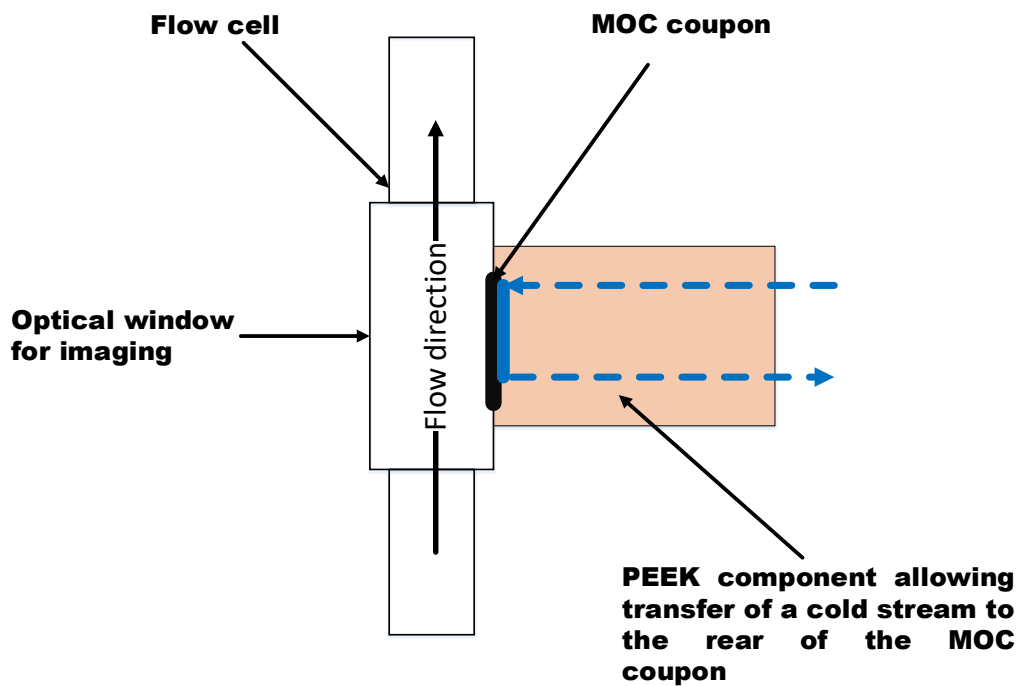


Figure 6.3: Schematic highlighting proposed alterations to conventional corrosion flow cell [not illustrated to scale].

Implemented flow cell modifications however did not result in fouling induction at extreme conditions after initial fouling trials. Computational fluid dynamic (CFD) simulations were performed using a model of the flow cell structure (3.2.2.3 CFD) to assess the distribution of diluted species towards the MOC coupon/solution interface (Figure 6.4). A key modification to the flow cell was altering its entry and exit angle (increase entry and exit gradient by 20°) to enhance directional flow towards the surface of the MOC coupon (Figure 6.5). CFD results highlight some changes in species concentration however fouling trials found this modification induced fouling upon the MOC coupon.

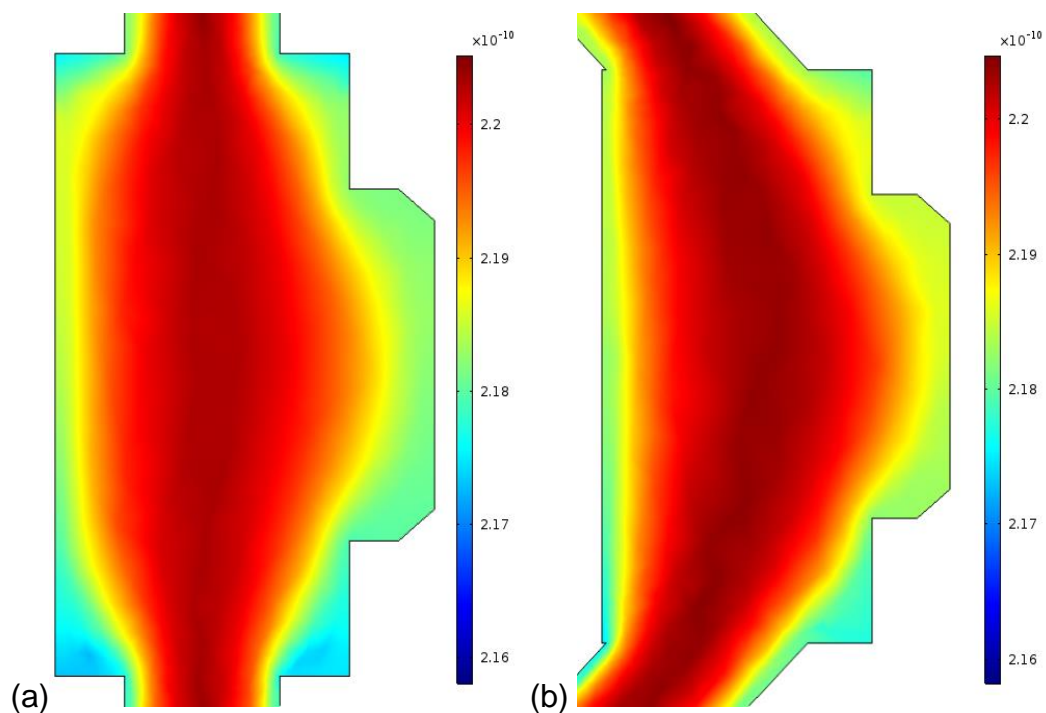


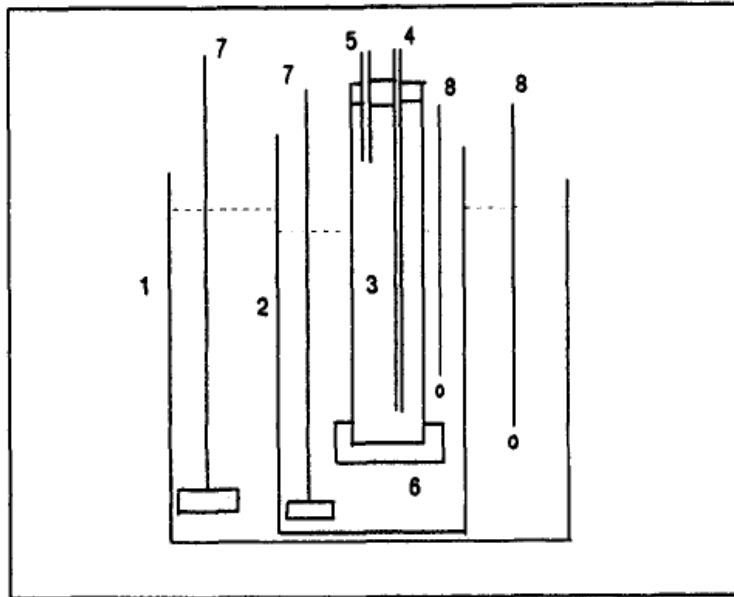
Figure 6.4: CFD diluted species distribution of (a) original flow cell design and (b) modified flow cell design.



Figure 6.5: Final flow cell design based upon CFD results highlighting the modified entry and exit angles. Additional ports for Pt100 sensor were incorporated which are detailed in 6.2.3 Thermocouple addition.

6.2.2 Cold stream incorporation

The C-FAP was inspired upon a fouling evaluation set up proposed by Mullin⁶ and was demonstrated by Nývlt and Veverka¹⁵ as shown in Figure 6.6. Within this set up a continually cooled insert was used to induce fouling on its surface under defined process and solution conditions. Conditions could be assessed in which fouling occurs in terms of the temperature difference between the bulk solution and cooled projection (ΔT), supersaturation and solution flow rate. Cooled projections e.g. cold finger were also used by Abohamra and Ulrich to induce potassium sulphate fouling on various MOCs including TeflonTM, steel and glass.²⁴⁶ Within the C-FAP, cooling of the MOC coupon was used to initiate fouling upon its surface. To provide cooling of a MOC coupon surface, a Julabo F25 chiller unit (Julabo) was employed in conjunction with a Bronkhorst mini CORI-FLOW® (Bronkhorst) system to control coolant mass flow rate. The coolant entry and exit from the MOC coupon was directed by the previously highlighted PEEK component within the flow cell in counter-current configuration. The coolant selected was water.



Apparatus with cold finger for encrustation studies. 1 ... thermostatted vessel, 2 ... vessel with studied suspension, 3 ... cold finger made of steel, 4 ... cooling water inlet, 5 ... cooling water outlet, 6 ... insulated bottom, 7 ... stirrers, 8 ... thermometers

Figure 6.6: Cold finger technique fouling assessment set up used by Nývlt and Veverka.¹⁵

6.2.3 Thermocouple addition

Pt100 temperature sensors were incorporated into the C-FAP for numerous purposes. Four Pt100 temperature sensors were added across the modified flow cell to monitor the circulating solution temperature before ($T_{SOL\ inlet}$) and after ($T_{SOL\ outlet}$) cell entry and also monitor cold stream temperature before ($T_{COL\ inlet}$) and after ($T_{COL\ outlet}$) contact with the rear of a MOC coupon (Figure 6.7). Determining the temperature difference across the flow cell theoretically allows heat transfer and the impact of fouling upon it to be evaluated via fouling resistance (see 1.4.2.1 Overview of fouling literature and measurements). Additionally the entry flow cell Pt100 sensor provides feedback to the Polar Bear Plus unit (CRD) to drive heating/cooling of the vessel in order to obtain a constant selected set point entry temperature. The controller temperature feedback system uses a proportional–integral–derivative (PID) algorithm. PID control is the most dominant control system for automation.²⁴⁷ The advantages of PID control include its simplicity, applicability and ease of use.²⁴⁸ One

disadvantage of employing a PID algorithm for temperature control is the potential for temperature overshoot in which takes substantial time to reach a steady value.²⁴⁹

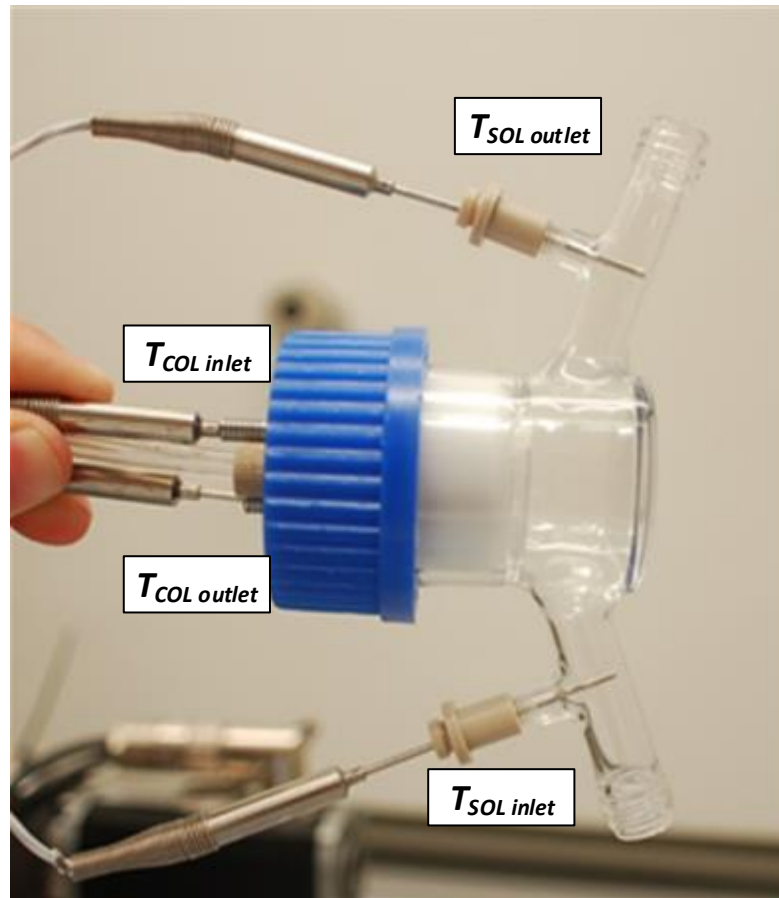


Figure 6.7: Addition of Pt100 sensors to monitor the temperature of the solution and cold stream entering and exiting the bespoke flow cell.

A number of assumptions were made. It is assumed the temperature difference across the investigated MOC (ΔT_{MOC}) is the same as the two entry temperature values of the hot ($T_{SOL\ inlet}$) and cold stream ($T_{COL\ inlet}$). It is assumed that all investigated MOCs have identical heat transfer behaviour and reach maximum heat transfer instantly.

6.2.4 Additional modifications

The platform's tubing was changed from standard silicon tubing to tubing which is chemically compatible with a wide range of organic solutes and solvents. Tubing which was employed within the C-FAP included GORE STA-PURE PFL reinforced fluoroelastomer tubing (Gore) [3.2 mm OD; 1.6 mm ID] and rigid PTFE tubing (RS components) since potentially aggressive solvents were to be explored in subsequent experiments. The Zebrafish's original gear pump was replaced with a peristaltic pump (DriveSure PMD24CI114 (Watson-Marlow)) primarily to allow suspensions of particles to potentially be explored. Another addition to the platform was the incorporation of a Smart Controller unit (CRD) which, in conjunction with Eurotherm iTools software (Eurotherm), continuously acquires and stores Pt100 sensor temperature data concurrently. An imaging set up (Figure 6.8) was constructed with a USB 3.0 monochrome industrial camera (Sony), a commodity camera tripod and a compact axial white LED light (dimensions 50x50 mm) (DCM Sistemas) to enhance imaging contrast (Figure 6.8). YAWCAM software (www.yawcam.com) was employed to obtain images at a given frequency.

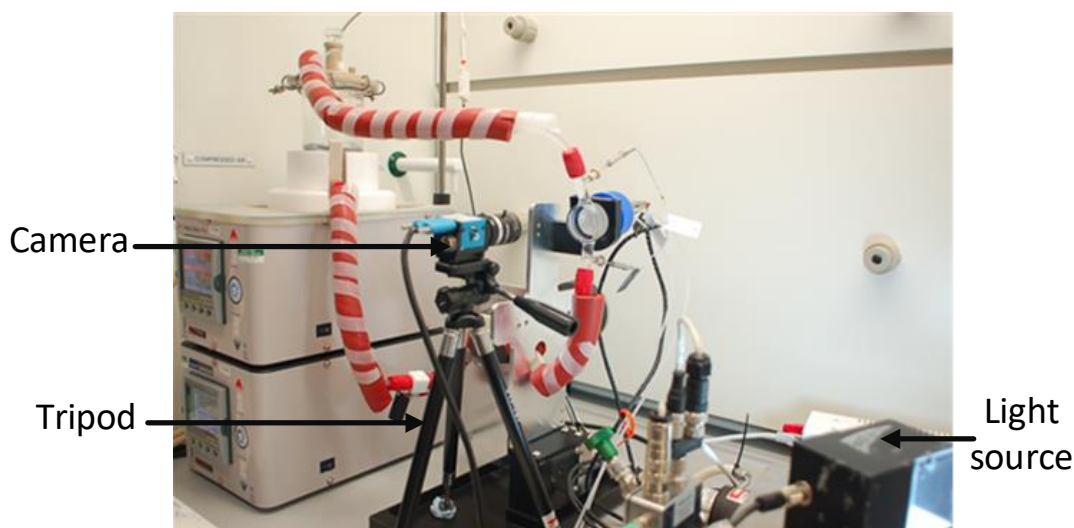


Figure 6.8: Imaging setup comprising a light source, commodity tripod and camera.

6.3 Capabilities

The C-FAP allows a number of fouling measurements to be made including fouling resistance (R_f) via differences in heat transfer, fouling induction time and fouling growth rate are described in greater detail (see Chapter 7 Fouling assessments in novel flow platform). In addition, fouled material on the investigated MOC can be easily removed from the continuous flow environment allowing offline analysis of the fouled material including mass measurement and microscopy techniques. The process conditions within the platform can be well defined in terms of solution flow rate, solution entry temperature, cold stream mass flow rate and cold stream temperature. The temperature difference across the MOC can be controlled. Within the flow cell any MOC coupon of designated dimensions can be examined in which its rear side is cooled to induce fouling. Although the pump within the platform was altered, the platform struggled to keep particles in suspension under normal flow conditions. Particle settling was an issue within the bespoke flow cell (Figure 6.9). For practical purposes the application of the platform is fixed for solutions. Flow rates greater than terminal velocity would be necessary for particle suspension.²⁵⁰

The operational capabilities of the C-FAP are detailed in Table 6.1. The C-FAP has the ability to perform other surface investigations related to crystallisation highlighting its practicality. Examples of such investigations are detailed in Table 6.2.

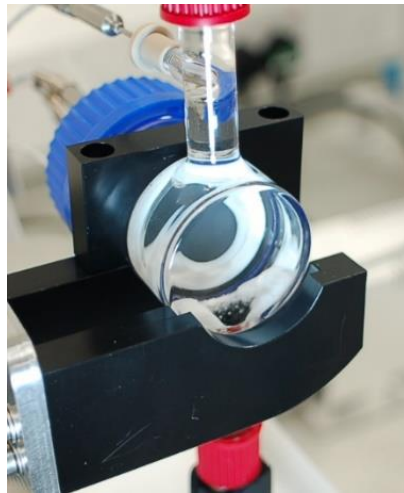


Figure 6.9: Settling of PCM particles during the circulation of a PCM suspension via a peristaltic pump.

Table 6.1: Capabilities and technical data of the adapted crystallisation fouling Zebrafish platform.

Parameter	Operational capabilities
Vessel volume	500 ml
Flow cell volume	20 ml
Solution flow rate	20 – 100 ml/min
Water coolant flow rate (M_{COL})	0 – 100 g/min
Exposed MOC coupon area on solution side (A_{MOC})	2.01 cm ²
MOC backside temperature (with respective $T_{COL\ inlet}$)	2.5°C – 40°C (12.5°C – 36°C)
Solution temperature entering flow cell ($T_{SOL\ inlet}$)	25°C – 60°C
Controller temperature resolution with Pt100 sensor	0.05°C

Table 6.2: Potential investigations in which the C-FAP has the capacity to conduct.

Investigation	Description
Polymorph screen	Explore different substrates acting as templates to influence polymorph nucleation. The influence of solution flow, solution temperature and substrate cooling can be probed.
Single crystal growth rate	Crystal growth of an adhered single crystal to a substrate can be determined via 1D and 2D growth rates.

6.4 Validation of C-FAP

The first solution investigated within the C-FAP platform was PCM in 3-methyl-1-butanol in which different temperature gradients ($\Delta T_{MOC} = 17.4^{\circ}\text{C}$, 23.5°C and 28.7°C [dictated by the coolant temperature]) across the coupon were explored in addition to different MOCs (C-276 as received and borosilicate). The experimental outcome was to assess differences in fouling induction time by imaging for all conditions explored. No fouling was identified on borosilicate whilst PCM fouling was present on C-276 only at the ΔT_{MOC} values of 23.5°C and 28.7°C (Figure 6.10). Determined fouling results reveal differences under explored conditions and validate its use as a fouling assessment platform. This assessment was a rapid screen however provided further insight into fouling. A more thorough study is conducted within Chapter 7 to assess the application of the C-FAP.

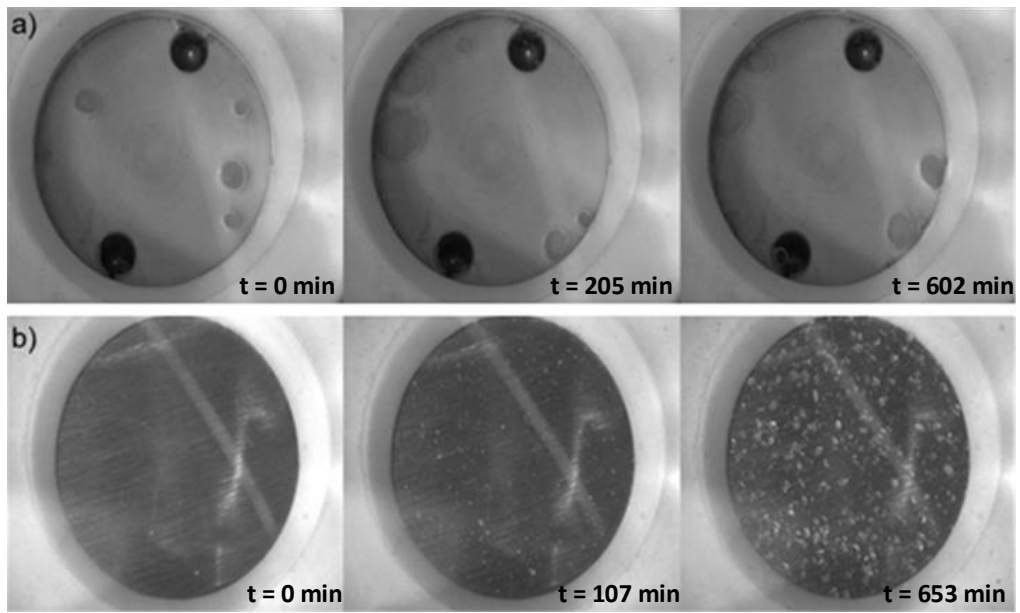


Figure 6.10: Sequential images over a 12 hour period for (a) borosilicate and (b) C-276 as received at $\Delta T_{MOC} = 28.7^\circ\text{C}$.

Chapter 7. Fouling assessments in novel flow platform

7.1 Introduction

Continuous crystallisation processes have numerous advantages over traditional batch processing including improved product quality, reduction in process inventories and enhanced process control.^{26,41} Converting a batch crystallisation process into continuous operation requires a great deal of consideration prior to its implementation into a fully operational campaign.

Developing and establishing systematic approaches to evaluate individual crystallisation aspects has been performed successfully previously. Systematic approaches have been employed in polymorph screening²⁵¹⁻²⁵², solvent selection²⁵³⁻²⁵⁴ and crystalliser setup²⁵⁵⁻²⁵⁶ to methodically arrive to an outcome. However, encompassing individual crystallisation processes and aspects to arrive at a rational crystallisation design (Figure 7.1) is not routinely conducted yet would be highly advantageous. The concept of developing a workflow to arrive to a logical crystallisation design outcome has been demonstrated by Wibowo and Ng.²⁵⁷ Workflows have also been designed in converting batch process into continuous. Teoh and co-workers provided a methodology to assess the feasibility of converting fine chemical batch processes into continuous operation in addition to defining key decision-making stages during the assessment.⁴²

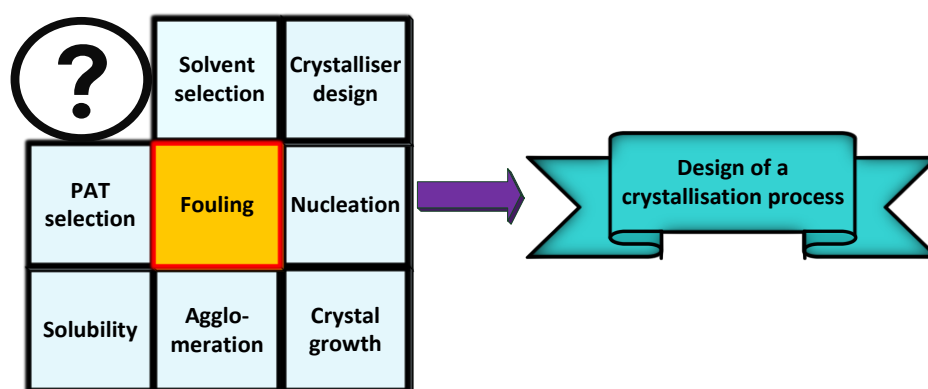


Figure 7.1: Selected examples of crystallisation processes and aspects contributing towards the logical design of a crystallisation process. However, fouling contributions are often neglected. Required details are process dependent therefore provided examples are not exhaustive.

Continuous crystallisers are normally designed to operate for extended time periods. However, at some stage throughout a crystallisation campaign, fouling is expected to occur.^{6,26} The presence of significant fouling within a continuous crystalliser would require the campaign to be halted as subsequent continuation would lead to unstable processing conditions.^{8,108} During continuous crystallisation, conditions within crystalliser are at non-equilibrium in which fresh crystallising solution is constantly in contact with a given surface. Rashid et al. utilised solubility, MSZW, growth and nucleation data to inform the design of both batch and continuous crystallisation campaigns for the API, ibuprofen. Breakage and agglomeration kinetics were considered in this crystallisation design however the influence of fouling was not considered.²⁵⁸ Generally the fouling propensity and behaviour of a crystallising system is not probed prior to the initiation of a crystallisation campaign and is often neglected without any comprehensive understanding. Briggs and co-workers altered the cooling crystallisation of LGA to mitigate fouling by the use of seeds in comparison to previously relying upon heterogeneous nucleation where fouling was prominent.¹⁸ Establishing the fouling propensity and fouling behaviour of a crystallising system would be valuable to allow a successful campaign to operate with fouling potential well understood and limit the undesirable effects of fouling.

Evaluating the fouling potential of a crystallising system prior to initiating a crystallisation campaign is highly beneficial to enhance process understanding and ultimately prevent process system malfunction whilst meeting process and product specifications. The experimental setup developed in Chapter 5 provided a rapid method for fouling assessment notably for MOC comparison under identical process conditions. However this setup did not probe the influence of cooling across a MOC i.e. ΔT_{MOC} upon crystallisation fouling. Additionally the experimentation was not conducted within continuous flow. Research by Geddert et al. employed a continuous flow setup to explore calcium sulphate fouling on different MOC heat transfer surfaces under well-defined thermal and hydrodynamic conditions (Figure 7.1).⁹² The C-FAP was developed to evaluate the fouling propensity of a crystallising system in

continuous flow upon a cooled surface by promoting nucleation and subsequent growth upon an investigatory MOC which is described in Chapter 6. These conditions may be representative of experiences within a continuous crystallisation campaign i.e. cooling across borosilicate within a COBC.

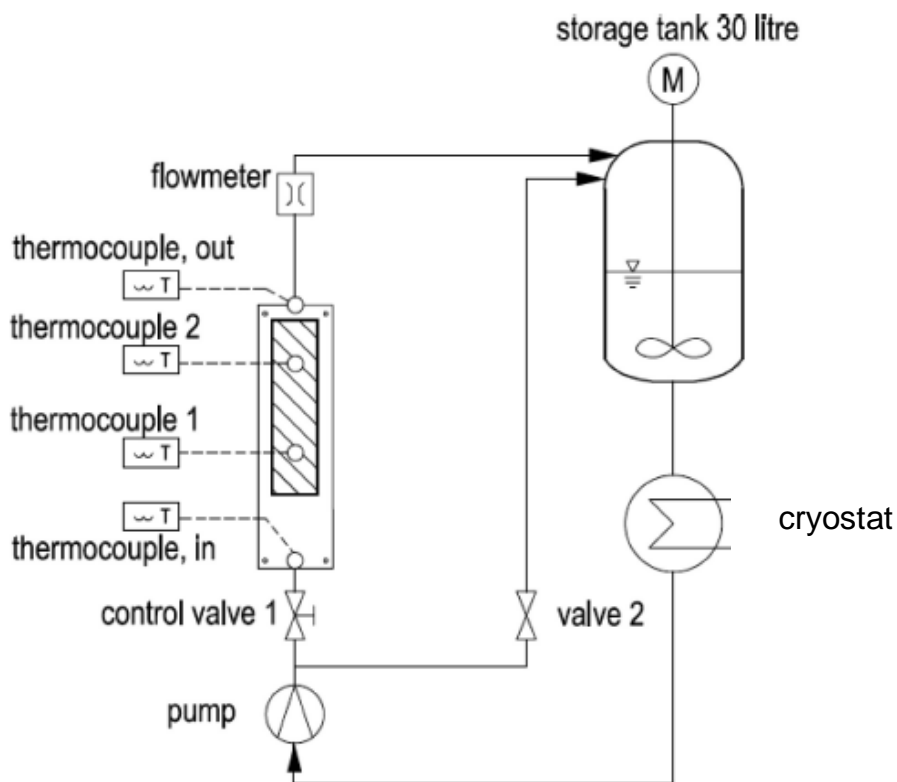


Figure 7.2: Continuous flow unit for fouling experiments utilised by Geddert and co-workers.⁹² The temperature difference (ΔT) across the flow cell can be calculated in addition to calculating fouling resistance values.

The C-FAP was designed to allow a variety of different parameters to be investigated namely solution flow rate, solution temperature, different investigatory MOCs, MOC coupon temperature difference (ΔT_{MOC}) and also the ability to probe different solution systems (as detailed in 6.3 Capabilities). In addition to exploring the fouling propensity of an investigated crystallising system, understanding fouling progression is also beneficial in particular in situations where fouling initiation is inevitable.

Within heat transfer fouling studies, fouling resistance (R_f) measurements are used to determine the fouling induction time which identifies when fouling deposits begin to impact heat transfer.^{9,17} Considerable crystalline deposits may be present on the heat transfer surface before heat transfer is affected. Other methods have been employed to determine induction times. The first detection of crystalline material within a crystallising system under constant supersaturation is the traditional technique for determining an induction time.^{6,250} This technique can also be applied to initial identification of fouling deposits upon a surface and, likewise, can similarly be termed as the fouling induction time.¹⁰⁸ Comparing each induction time definition would be beneficial in establishing which technique is more applicable to continuous crystallisation process understanding in addition to assessing C-FAP's capabilities (Figure 7.3).

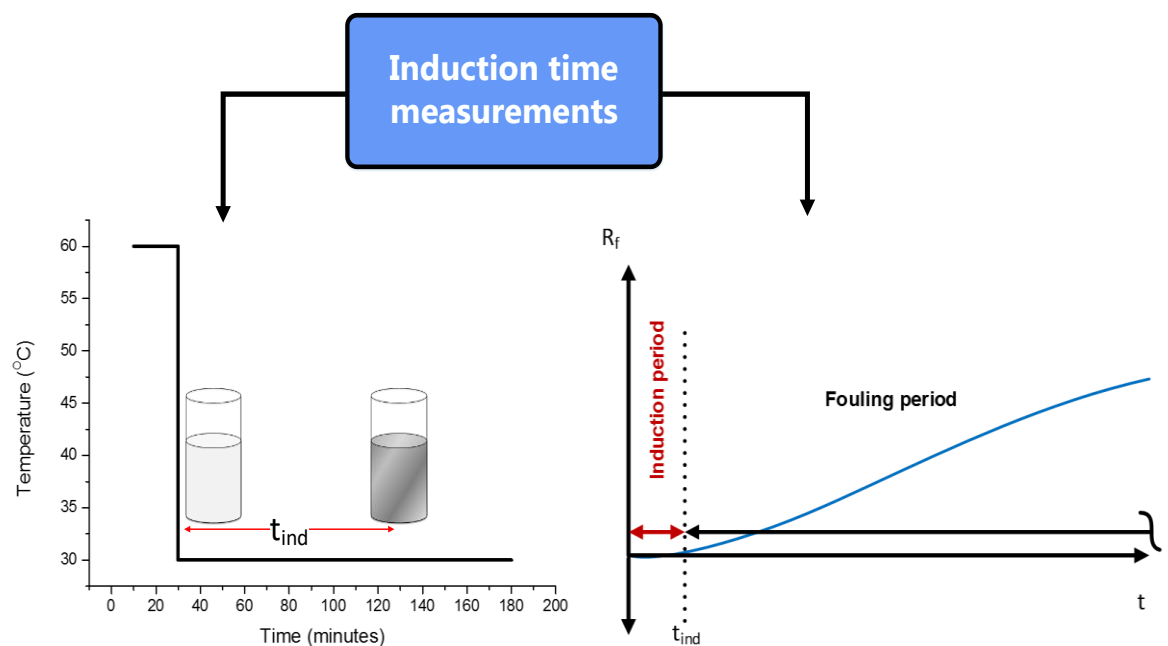


Figure 7.3: Induction time measurements related to fouling including imaging and temperature measurements. For both measurements, induction times and growth kinetics can be determined.

The dominant fouling mechanism from Chapter 5 was particle deposition for explored conditions. The influence of cooling the two diverse investigatory

MOCs (stainless steel and PTFE) on fouling was not probed. Herein the C-FAP was designed to probe surface induction and growth fouling mechanisms which was evaluated using stainless steel and PTFE as test MOCs. An experimental method was generated to explore the influence of supersaturation, different ΔT_{MOC} , solution flow rate and different MOCs upon fouling behaviour within the C-FAP. In addition to exploring and contrasting fouling induction times, fouling growth kinetics were determined to assess the influence of explored system parameters on subsequent growth. The C-FAP was briefly assessed within Chapter 6 to confirm fouling would take place and differences were identified. However, a comprehensive assessment was necessary. Overall the proposed measurements were proposed to validate the C-FAP and its application for future fouling investigations.

7.2 Materials and methods

7.2.1 Materials

The C-FAP is described within Chapter 6. The investigated solution within the C-FAP was PCM in water. MOCs coupons and their dimensions explored within this work are detailed in Chapter 3.

7.2.2 Methods

7.2.2.1 Solution preparation and C-FAP setup

Both understaturated and supersaturated PCM in water solutions were investigated in this work. The solubility of PCM in water at 52°C is 31.488 g/kg solvent (polynomial fit using data from Granberg et al.²³²). Undersaturated (supersaturation ratio = 0.96) and supersaturated (supersaturation ratio = 1.07) solutions were freshly prepared for each fouling experiment. Investigated PCM in water solutions were heated to 55°C to ensure full dissolution for at least 30 minutes prior to addition into the C-FAP.

The configuration of the C-FAP is described in Chapter 6. The C-FAP was circulated with blank solvent (deionised water) prior to the addition of solution which was subsequently heated to and maintained at the set-point temperature of 52°C i.e. $T_{SOL\ inlet}$. The purpose of heating and circulating blank solvent was to heat the internal surfaces within the platform. The addition of the investigatory solution without preheated surfaces could result in unwanted system nucleation that would require a significant period of time to dissolve. The C-FAP was then drained and 250 ml of heated PCM solution was added. Once the solution circulation temperature became constant at 52°C, the cold water stream was initiated at a flow rate of 50 g/min and counter-current to solution flow. Once the coolant entry temperature ($T_{COL\ inlet}$) decreased to a minimum and became constant, fouling measurement methods were initiated. A 24 hour time limit was applied in which if fouling had not initiated during this time, the experimental run was ended and conditions were deemed not to foul. Conditions explored within this chapter are detailed in Table 7.1 in which each investigatory condition was conducted at least in duplicate.

Table 7.1: Conditions explored including process parameters and MOC probed for C-FAP assessment.

Exp No	Coolant entry temp ($T_{COL\ inlet}$) with respective ΔT_{MOC}	MOC coupon	Solution flow rate	Solution supersaturation
1	12.5°C ($\Delta T_{MOC} = 39.5^\circ\text{C}$)	Stainless steel 316L	50 ml/min	0.96
2	17.5°C ($\Delta T_{MOC} = 34.5^\circ\text{C}$)	Stainless steel 316L	50 ml/min	0.96
3	25°C ($\Delta T_{MOC} = 27^\circ\text{C}$)	Stainless steel 316L	50 ml/min	0.96
4	12.5°C ($\Delta T_{MOC} = 39.5^\circ\text{C}$)	Stainless steel 316L	50 ml/min	1.07
5	17.5°C ($\Delta T_{MOC} = 34.5^\circ\text{C}$)	Stainless steel 316L	50 ml/min	1.07
6	25°C ($\Delta T_{MOC} = 27^\circ\text{C}$)	Stainless steel 316L	50 ml/min	1.07
7	12.5°C ($\Delta T_{MOC} = 39.5^\circ\text{C}$)	Stainless steel 316L	100 ml/min	0.96
8	17.5°C ($\Delta T_{MOC} = 34.5^\circ\text{C}$)	Stainless steel 316L	100 ml/min	0.96
9	25°C ($\Delta T_{MOC} = 27^\circ\text{C}$)	Stainless steel 316L	100 ml/min	0.96
10	12.5°C ($\Delta T_{MOC} = 39.5^\circ\text{C}$)	Stainless steel 316L	100 ml/min	1.07
11	17.5°C ($\Delta T_{MOC} = 34.5^\circ\text{C}$)	Stainless steel 316L	100 ml/min	1.07
12	25°C ($\Delta T_{MOC} = 27^\circ\text{C}$)	Stainless steel 316L	100 ml/min	1.07

Table 7.1 continued...

13	12.5°C ($\Delta T_{MOC} = 39.5^\circ\text{C}$)	PTFE	50 ml/min	0.96
14	17.5°C ($\Delta T_{MOC} = 34.5^\circ\text{C}$)	PTFE	50 ml/min	0.96
15	25°C ($\Delta T_{MOC} = 27^\circ\text{C}$)	PTFE	50 ml/min	0.96
16	12.5°C ($\Delta T_{MOC} = 39.5^\circ\text{C}$)	PTFE	50 ml/min	1.07
17	17.5°C ($\Delta T_{MOC} = 34.5^\circ\text{C}$)	PTFE	50 ml/min	1.07
18	25°C ($\Delta T_{MOC} = 27^\circ\text{C}$)	PTFE	50 ml/min	1.07
19	12.5°C ($\Delta T_{MOC} = 39.5^\circ\text{C}$)	PTFE	100 ml/min	0.96
20	17.5°C ($\Delta T_{MOC} = 34.5^\circ\text{C}$)	PTFE	100 ml/min	0.96
21	25°C ($\Delta T_{MOC} = 27^\circ\text{C}$)	PTFE	100 ml/min	0.96
22	12.5°C ($\Delta T_{MOC} = 39.5^\circ\text{C}$)	PTFE	100 ml/min	1.07
23	17.5°C ($\Delta T_{MOC} = 34.5^\circ\text{C}$)	PTFE	100 ml/min	1.07
24	25°C ($\Delta T_{MOC} = 27^\circ\text{C}$)	PTFE	100 ml/min	1.07

7.2.2.2 Fouling measurements

Once fouling conditions were initiated and cooling entry temperatures became constant, two measurement methods were conducted concurrently: sequential imaging and temperature monitoring.

(a) *Fouling induction time and fouling growth rates via imaging*

Imaging was used to determine two quantitative fouling measurements: fouling induction time and fouling growth rates. The imaging setup is detailed in Chapter 6 (6.2.4 Additional modifications) which was positioned to image the entire exposed MOC through the flow cell. Images of investigated MOCs were obtained at a frequency of 60 seconds. Visual observation was employed as the fouling detection method (Figure 7.4 (a) and (b)). Once the first signs of surface nucleation were detected, the time interval from once the cold stream temperature becomes constant to the identification of surface nucleation was measured as the induction time.

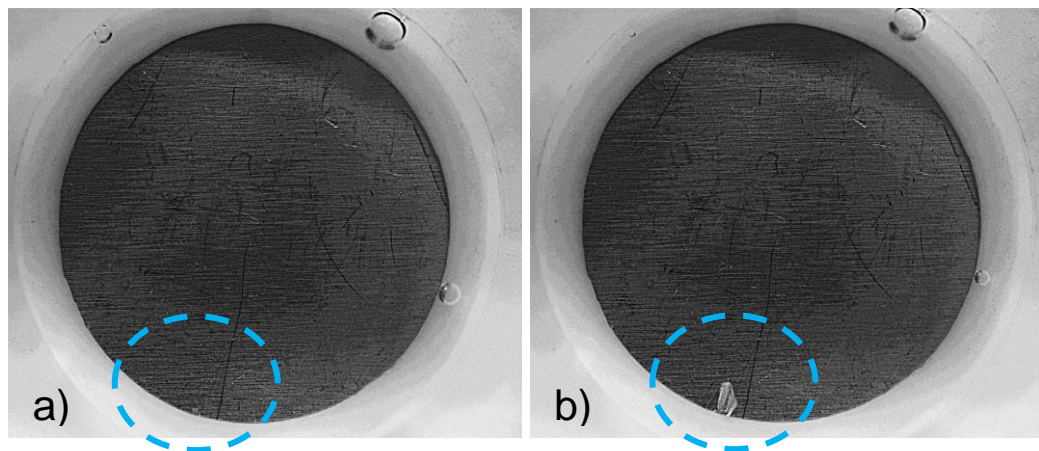


Figure 7.4: An example of PCM nucleation upon stainless steel where (a) the first indications of nucleation are difficult to detect with real time. The reliance on retrospectively serial imaging (b) where identifiable crystals were present was essential to determine accurate induction time values. [Position of nuclei within the dashed blue oval].

Following the identification of surface nucleation upon MOCs under investigated solution concentrations, supersaturation ratios and solution flow rates, PCM fouling growth kinetics were evaluated by determining the area

coverage of the fouled PCM with time. ImageJ software (National Institute of Health) was used to determine the number of pixels associated with fouling. These were converted into a true fouled area. The area associated with each pixel was determined for each unique experimental run since camera positioning was liable to minor movement. Using the average pixel number diameter (based upon 4 diameters [1 horizontal, 1 vertical and 2 diagonal values]) and the true exposed MOC diameter (16 mm), the pixel area value was determined. The cumulative fouled area was determined at 5 minute intervals post nucleation to account for additional surface nucleation and combining of distinct growing masses. Linear growth rates over the initial 120 minutes after nucleation were determined.

(b) ***Temperature profiles and heat transfer performance***

The temperature of the investigated PCM solution entering ($T_{SOL\ inlet}$) and exiting ($T_{SOL\ outlet}$) the flow cell in addition to the cold stream's temperature before ($T_{COL\ inlet}$) and after ($T_{COL\ outlet}$) contact with the rear of the investigated MOC coupon were recorded every 60 seconds (see 6.2.3 Thermocouple addition). Temperature profiles were obtained to (i) assess whether changes in heat transfer can be detected and, if detected, (ii) determine the effect of fouling on heat transfer efficiency. Within heat exchanger fouling research literature, the impact of fouling on heat transfer was quantified by determining the overall heat transfer coefficient (U) with time with the fouling resistance (R_f) which is defined in Equation 1.25. The measurement of fouling resistance is routinely conducted for inorganic system fouling in heat exchangers however has not been routinely demonstrated for small organic molecules within cooling crystallisation processes. Briançon et al. utilised temperature differences to determine the decline in overall heat transfer coefficient due to fouling associated with the crystallisation of adipic acid.¹³ It was anticipated that determining R_f will allow the fouling induction time and growth kinetics to be determined.

Determining fouling resistance with time is traditionally used to identify the fouling induction time. Within heat transfer studies, the fouling induction time is defined as the time difference between experimental start up and when fouling initially impacts heat transfer via overall heat transfer coefficient⁹ (1.4.2.1 Overview of fouling literature and measurements) which differs to the conventional crystallisation induction time definition (Equation 5.2). However, within this work the fouling induction time relates to once the coolant stream becomes constant and the initial identification that heat transfer is impacted i.e. same start point as imaging methods. Therefore, direct comparisons can be made.

To calculate the fouling induction time, fouling resistance measurements are calculated at a frequency of 60 seconds. Fouling resistance (R_f) is defined by:

$$R_f = \frac{1}{U_f} - \frac{1}{U_o} \quad (1.24)$$

Where U_f and U_o are the overall heat transfer coefficients when the surface has become fouled and when the surface is clean at experimental start up, respectively. The overall heat transfer coefficient values associated with fouled and clean surfaces can be calculated from:⁹⁵

$$Q = UA_{MOC}\Delta T_{LMTD} \quad (7.1)$$

Where

Q	=	Heat transfer rate (W)
U	=	Overall heat transfer coefficient (W/(m ² .K))
A_{MOC}	=	Heat transfer surface area (m ²)
ΔT_{LMTD}	=	Logarithmic mean temperature difference (K)

In order to calculate U , Q requires to be known first at the same time frequency. Q can be determined for a counter current system using:⁹⁵

$$\begin{aligned} Q &= M_{SOL} C_{pSOL} (T_{SOL\ inlet} - T_{SOL\ outlet}) \\ &= M_{COL} C_{pCOL} (T_{COL\ outlet} - T_{COL\ inlet}) \end{aligned} \quad (7.2)$$

Where

M_{SOL}, M_{COL} = mass flow rate of hot solution and cold fluid stream, respectively (kg/s)

C_{pSOL}, C_{pCOL} = specific heat values of hot solution and cold fluid stream, respectively (kJ/(kg.K))

$T_{SOL\ inlet}, T_{COL\ inlet}$ = inlet temperatures of hot solution and cold fluid stream, respectively (K)

$T_{SOL\ outlet}, T_{COL\ outlet}$ = outlet temperatures of hot solution and cold fluid stream, respectively (K)

Q can be calculated by investigating the heat transfer into the cold stream since the mass flow rate, temperatures and specific heat (water = 4.184 kJ/kg.K)²⁵⁹ of the coolant are known. The logarithmic mean temperature difference (ΔT_{LMTD}) for counter-current heat exchange is calculated using:²⁶⁰

$$\Delta T_{LMTD} = \frac{\Delta T_1 - \Delta T_2}{\left(\ln \frac{\Delta T_1}{\Delta T_2} \right)} \quad (7.3)$$

Where

ΔT_1 = $T_{SOL\ outlet} - T_{COL\ inlet}$

ΔT_2 = $T_{SOL\ inlet} - T_{COL\ outlet}$

The C-FAP has the capability to monitor:

- Inlet temperatures of hot solution ($T_{SOL\ inlet}$) and cold fluid ($T_{COL\ inlet}$) stream across the flow cell.
- Outlet temperatures of hot fluid ($T_{SOL\ outlet}$) and cold stream ($T_{COL\ outlet}$) across the flow cell .
- Mass flow rate of the cold stream (M_{COL}).

Therefore, U can be calculated as ΔT_{LMTD} and Q can be determined at a given frequency within the C-FAP. The exposed MOC heat transfer area (A_{MOC}) remained constant for all experiments at a value of 0.000201 m². Since U is determined at a given frequency the fouling resistance (R_f) could be calculated and plotted against time. The application of fouling resistance within a fine chemical crystallisation process has been demonstrated within a batch type crystalliser system by Nývlt and Veverka.¹⁵ It is therefore reasonable to anticipate fouling resistance is applicable to continuous crystallisation processes.

7.3 Results and discussion

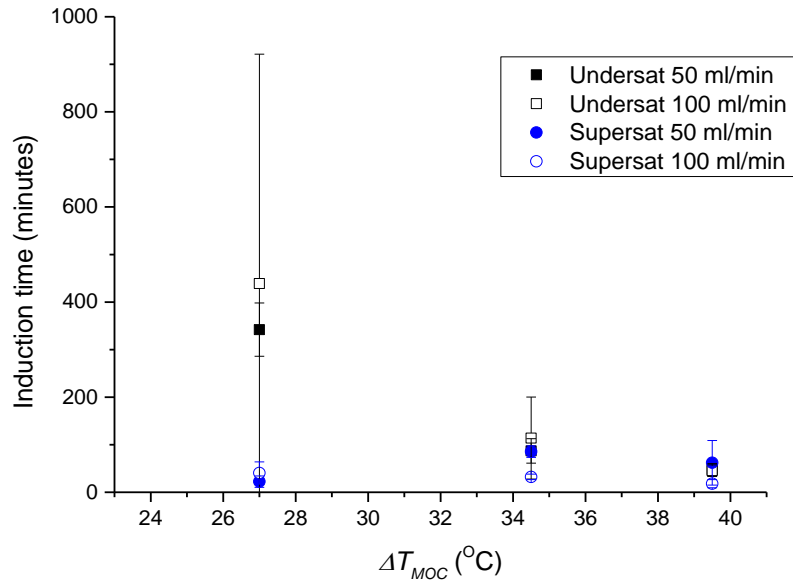
The C-FAP was developed as an evaluation platform to probe surface induced fouling mechanisms in which system parameters could be modified and controlled. Results described herein demonstrate the C-FAP's applicability and practicality as an assessment tool for fouling.

7.3.1 Fouling induction time and fouling growth rates via imaging

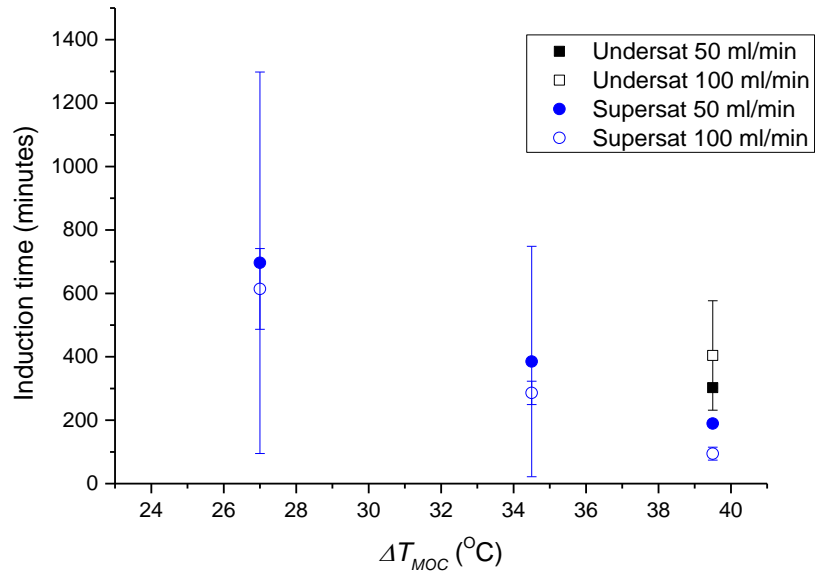
7.3.1.1 Induction time

Two fouling measurements were obtained by imaging namely fouling induction time and fouling growth rates. The average fouling induction times for all investigated conditions involving (a) stainless steel and (b) PTFE are plotted

against ΔT_{MOC} within Figure 7.5. It was found for stainless steel that induction times from different supersaturated solutions were comparable across all process conditions suggesting the influence of the additional cooling input and flow rate was insignificant. Distinct differences in induction times associated with stainless steel for undersaturated solutions were found – larger average induction times were identified for smaller ΔT_{MOC} values i.e. less driving force to generate local supersaturation.²⁶¹⁻²⁶² The influence of solution flow rate was again deemed insignificant. The importance of surface cooling was evident in creating local supersaturation at the MOC for an undersaturated solution. For PTFE, fouling was only identified for two of the tested conditions when probing undersaturated PCM feed solutions ($\Delta T_{MOC} = 39.5^\circ\text{C}$; flow rate 50 ml/min and 100 ml/min) however induction times were identified for all supersaturated conditions. Therefore, comparisons between each MOC's induction times using supersaturated solution could be only conducted as illustrated Figure 7.6 where notable differences between average induction times were observed. It was found increasing ΔT_{MOC} , i.e. local supersaturation, resulted in a decreased standard deviation associated with the average induction time. Research by Jiang and ter Horst determined that increasing supersaturation resulted in a decreased spread of induction time values which supports observations within the present work.²³⁹ Comparisons of undersaturated solution induction times could not be successfully compared since PTFE related fouling experiments could not generate supersaturation to induce fouling for all experiments.



(a)



(b)

Figure 7.5: Average induction time values (with standard deviation values) for all explored conditions for (a) stainless steel and (b) PTFE.

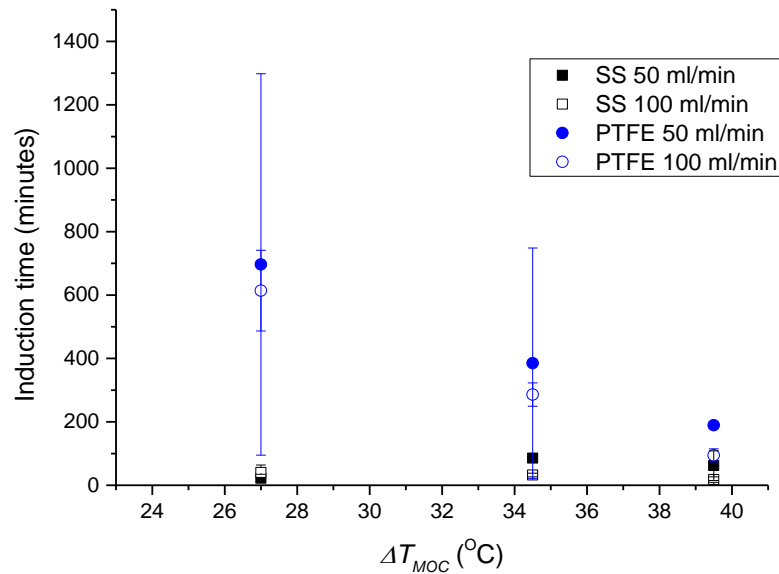


Figure 7.6: Average induction time values (with standard deviation values) for supersaturated PCM solutions associated with stainless steel and PTFE.

It was found that employing supersaturated feed solutions in comparison to undersaturated feed resulted in lower average induction time values which is to be anticipated (Figure 7.5). Zhao highlighted fouling may still occur upon a surface where locally it is supersaturated but principally undersaturated within the bulk solution.¹⁹³ Undersaturated solutions solely relied upon cooling across the MOC coupon to induce fouling upon its surface with no transport of particles generated in the bulk to the surface. Exposure to supersaturated solutions can result in fouling in the absence of local excess cooling. However, fouling can occur to a greater extent (as identified in Figure 7.6) in the presence of a cooled surface with increasing temperature differences resulting in increasing local supersaturation at the surface. It was found for all supersaturated solution conditions that surface nucleation occurred rather than initiating within the bulk solution. One limitation in investigating supersaturated feed solutions was the likelihood of bulk nucleation and crystallisation occurring in addition to the surface attached PCM crystals acting as seed material.

The impact of solution flow rate, and consequently flow velocity, upon fouling induction time was insignificant for conditions tested (Figure 7.6). However, the influence of flow velocity upon fouling induction time via fouling resistance determination has been identified by numerous authors^{133,142} to increase with increasing flow velocity. However, the hydrodynamic conditions explored within this work were limited due to the restricted range of flow rates (see 6.3 Capabilities).

Differences in average fouling induction time between stainless steel and PTFE for undersaturated feed solutions under identical process conditions (Figure 7.5) must be attributed to the properties of each MOC. The most influential MOC properties that contributes to differences in induction time remains unknown. The influence of increasing ΔT_{MOC} between the surface temperature and the bulk solution temperature mostly decreases the determined average induction time which highlights the importance of heat transfer across the MOC's surface. Therefore, it can be deduced that there is experimental evidence that the thermal properties of each MOC (as detailed in Table 4.4) are of significance. Stainless steel, in contrast to PTFE, has a larger thermal conductivity and lower specific heat capacity indicating heat transfer across the stainless steel coupon would be greater and consequently result in a larger local supersaturation generated at its surface. The majority of the undersaturated solution conditions explored for PTFE did not result in any fouling induction indicating inadequate heat transfer across the coupon to create sufficient local supersaturation. This result further reinforces the importance of the thermal properties of individually explored MOCs. Considerable differences were found comparing stainless steel and PTFE for supersaturated solution conditions (Figure 7.6) with the larger induction times associated with PTFE whilst stainless steel had comparable induction times across all investigated conditions.

In addition to relating these findings to MOC thermal properties, other material properties must have a role in surface nucleation including wettability, surface energy, surface roughness etc.^{6,94} Both stainless steel and Teflon™ have the

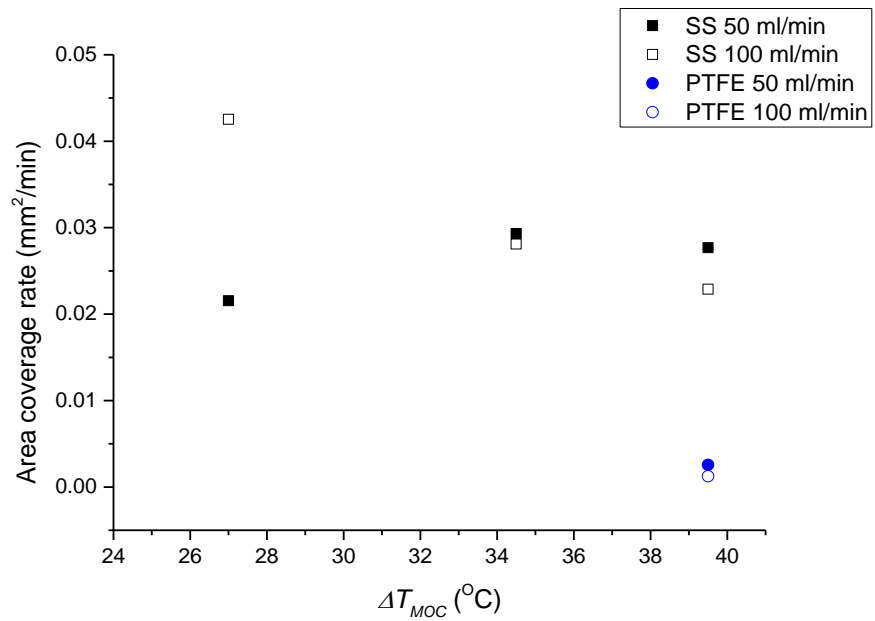
capacity to catalyse nucleation upon their surfaces as demonstrated by Vendel and Rasmuson albeit at larger levels of supersaturation with different compounds.⁷ Comparisons between stainless steel and PTFE-coated stainless steel heat exchangers and potential fouling was explored by Zettler and co-workers.²⁸ It was shown that stainless steel had a fouling induction time of approximately 800 minutes whilst no fouling was identified for PTFE-coated heat exchangers. Authors proposed the positive effect of PTFE on fouling was due to its inherent lower surface energy with no reference to the insulation effects of PTFE.

Within the present work heat transfer is vitally important in impacting induction time. The prominent fouling mechanism is surface nucleation which was due to local cooling and local supersaturation generation. However, the role of surface catalysis needs to be further explored. Exploring undersaturated PCM in water solutions target solely surface induced nucleation and growth whilst supersaturated solutions mainly explore surface induction however bulk nucleation and deposition may also occur under different conditions.

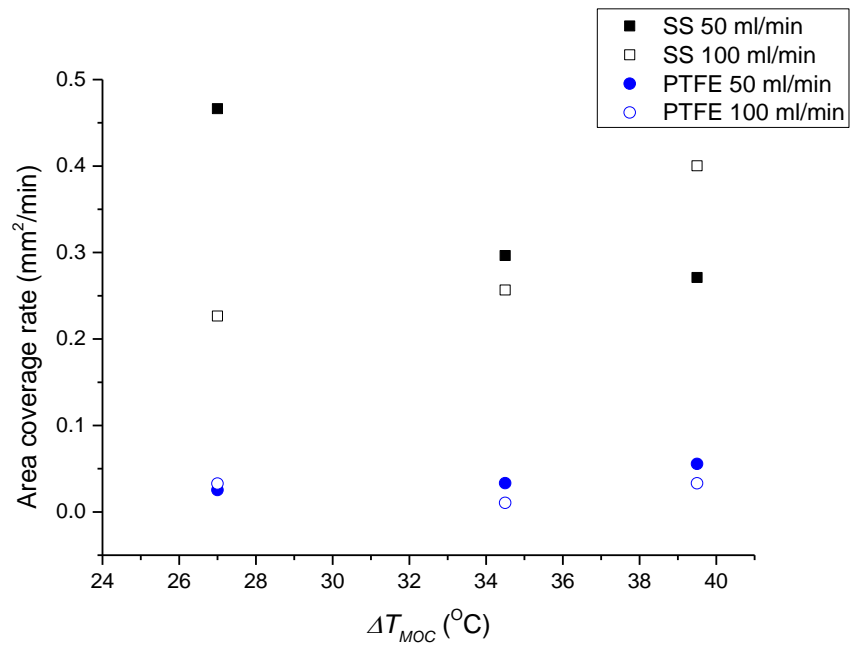
7.3.1.2 Fouling growth via area coverage

The growth kinetics of PCM crystals on each MOC were probed over the first 120 minutes post nucleation (Figure 7.7 (a) and (b)). Area coverage rates were determined since measuring growth rates of individually formed crystals was unrealistic with continual growth leading to complex formations as illustrated in Figure 7.8. Additional challenges included crystal detachment and secondary nucleation due to detached particle/MOC contact. Therefore, the cumulative area coverage of all fouled deposits with time was determined allowing a relative fouling growth rate to be established and compared. Within literature the application of crystalline material coverage as a measurement to determine growth kinetics is not routine. Shih et al. expressed the fouling of gypsum on different membrane substrates as an area coverage value.²⁶³ Additionally gypsum fouling growth on a reverse osmosis membrane has been investigated by Uchymiak and co-workers in which growth was expressed as

crystal number density and also as percentage area coverage fouled.²⁶⁴ Linear fouling area coverage rates were determined for each investigated condition and expressed in terms of temperature difference. Differences in area coverage rate were identified in particular for different MOCs and solution concentration (i.e. undersaturated or supersaturated). However, the influence of ΔT_{MOC} and solution flow rate on area coverage rate was not as clear (Figure 7.7).



(a)



(b)

Figure 7.7: Area coverage rate values for (a) undersaturated and (b) supersaturated PCM in water solutions under explored conditions.

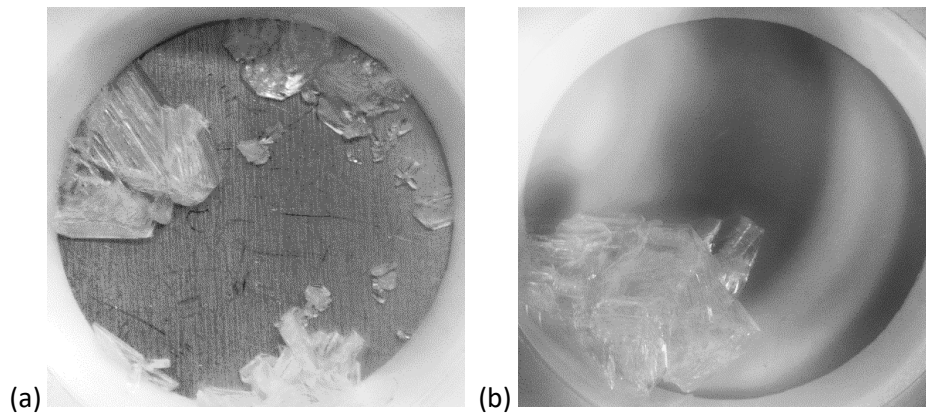


Figure 7.8: Example of images of PCM nucleation and subsequent growth upon (a) stainless steel and (b) PTFE.

Traditionally growth rates are not measured for fouling and generic fouling rates are described in terms of mass deposition or fouling resistance. Crystal growth rates of single PCM crystals has been demonstrated by Omar et al. where the impact of operating conditions, namely temperature and supersaturation, on growth rate was probed.²⁶⁵ The individual effects of increasing supersaturation and increasing temperature were found to increase selected directional growth rates. Omar's results support the present research findings relating to the differences identified for area coverage rates between undersaturated and supersaturated trends where differences exist (Figure 7.7). The influence of supersaturation upon the growth rate of paracetamol was demonstrated by Ó'Ciardha.²⁶⁶ Equation 1.23 highlights the importance of supersaturation upon crystal growth. However, the influence of increasing the ΔT_{MOC} could not be confidently explained where no clear trend is found. It is expected increasing ΔT_{MOC} would result in increased growth rates due to the greater local supersaturation generated. Pääkkönen et al. explored the fouling of calcium carbonate upon stainless steel heat exchanger.¹³³ It was found fouling deposition kinetics were considerably influenced by larger temperature differences between bulk solution and surface temperature. The area coverage rate was determined over a duration of 120 minutes therefore extending the growth time may yield a different outcome. For example supersaturated solutions after this timescale may nucleate within the bulk

resulting in various growth processes occurring simultaneously (Figure 7.9). Particle settling was the main problem with the use of saturated solutions in the C-FAP. In an ideal situation exploring both particle deposition and surface induction would be more beneficial and realistic to experiences within a crystalliser. For a supersaturated solution surface induction and bulk nucleation can occur concurrently although would preclude the use of imaging applied in this work.

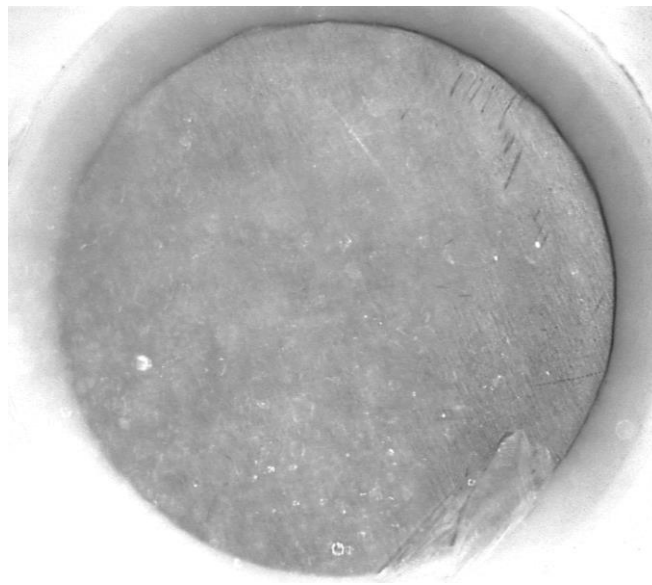


Figure 7.9: Image highlighting PCM crystals growing upon the stainless steel surface with bulk nucleation and growth occurring concurrently.

Pääkkönen explored surface induced fouling and composite fouling comprising surface induction and particle deposition in which the additional impact of particle deposition has a significant effect on the fouling deposition rate.¹³³ It was anticipated that increasing ΔT_{MOC} would increase area coverage rate due to increased local supersaturation however nucleation processes during this time cannot be neglected. The effect of solution flow rate was insignificant for PTFE associated area coverage rates however considerable differences were found for stainless steel albeit random (Figure 7.7). It was expected that increasing flow rate would reduce growth kinetics with Pääkkönen

demonstrating a reduction in fouling deposition rate with increasing flow velocity.¹³³ The influence of different MOCs upon fouling growth rates has been explored by authors including Dreiser¹⁰⁷, Al-Janabi⁹⁹ and Geddert⁹ which is determined via fouling resistance curve gradient. Comparison in fouling growth rates vary considerably with distinct differences identified¹⁰⁷ whilst other work reveals only minor differences.⁹⁹ Notably the influence of different MOCs upon area coverage rate for both explored solutions was the most significant finding. Within crystal growth and fouling literature, the effect of different substrates upon crystal area coverage growth has not been routinely conducted. Identified differences between stainless steel and PTFE in terms of area coverage rates for explored conditions can be potentially related to differing thermal properties. The present methodology for determining relative fouling area growth rates does not comprise the growth of one single crystalline entity is influenced by the presence of several concurrent entities via formation and detachment processes. Stainless steel has the potential to permit enhanced nucleation due to its thermal, physicochemical and topographical properties allowing the generation of nuclei from which crystal growth can occur – this includes rough, grain-like topography, good wetting properties and large thermal conductivity values. Crystal growth of PCM on PTFE is significantly reduced than its stainless steel counterpart under identical conditions which must be related to PTFE's surface and thermal properties.

7.3.2 Fouling resistance

7.3.2.1 Investigation of heat transfer to identify fouling in a continuous crystallisation process

A case study is described herein to demonstrate the applicability of identifying deviations in heat transfer as a means to identifying fouling during a continuous crystallisation campaign. Determining differences in heat transfer has been applied to batch crystallisation processes previously.^{13,15} The Rattlesnake continuous crystalliser platform (manufactured by CRD) is a COBC that has been successfully utilised in the continuous crystallisation of lactose

monohydrate (Figure 7.10).¹²⁶ The Rattlesnake platform employs a double water filled, shell and tube jacket to provide temperature control within the internal volume of the crystalliser. The primary shell jacket allows hot fluid flow from a hot circulator in a co-current configuration whilst the secondary coil allows the coolant fluid flow from a cold circulator in a counter-current configuration. The combination of both jacket components provides a smooth temperature profile across the crystalliser's length which is advantageous for cooling crystallisation.¹²⁶

However, initial experimental trials using this crystalliser experienced fouling which was identified by deviations in heater and chiller pump speeds, temperatures and power input as a means to maintain a constant internal vessel temperature. Fouling of lactose monohydrate was identified between Module 2 and Module 3 (Figure 7.10). A continuous cooling seeded crystallisation campaign of lactose monohydrate in water was conducted continuously for 32 hours within the Rattlesnake platform in which experimental conditions are detailed in Table 7.2.

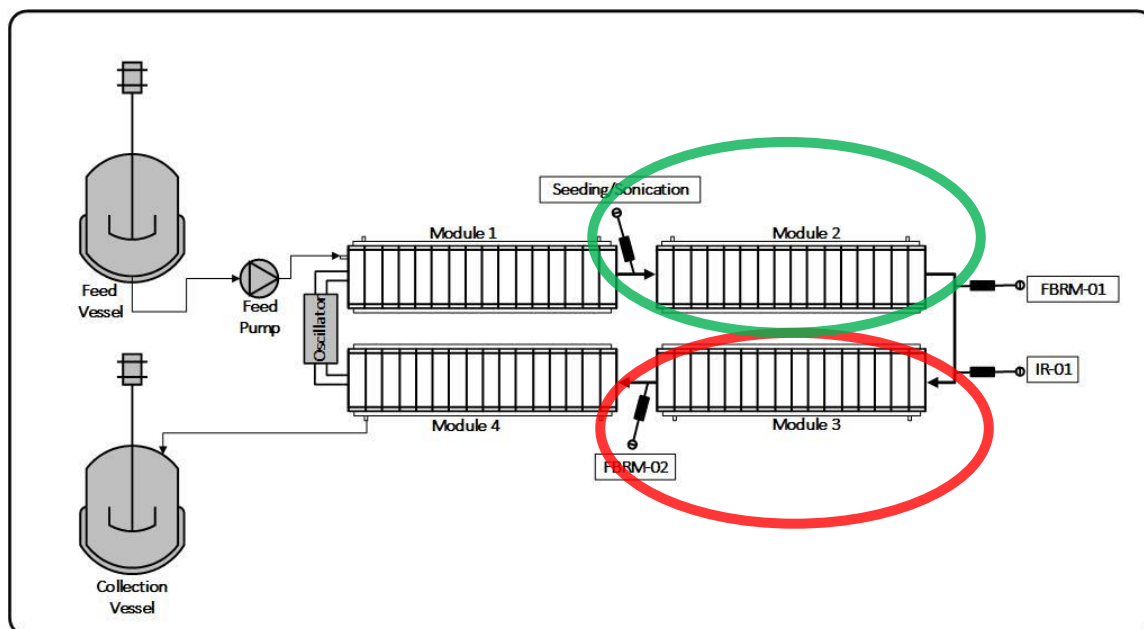


Figure 7.10: Schematic of the Rattlesnake COBC in which fouling was identified within Module 2 and 3, respectively (green and red oval).

Table 7.2: Table of conditions explored within the Rattlesnake continuous crystalliser for lactose monohydrate in water.

Parameter	Condition explored
Feed solution concentration	38 g/100g solution
Seed loading	2%
Seed size	D50:48 μm (span = 1.2)
Feed flow rate	40 ml/min
Seed Flow rate	3 ml/min
Supersaturation	1.6
Residence time	5 hours
Cooling profile	60°C to 15°C

Prior to any identified lactose monohydrate fouling, a number of trends were recorded including:

- Temperatures of the feed solution and the hot circulation fluid from Module 2 to Module 3.
- Pump speeds for the hot circulation and also for Module 2 cold pump.

Figure 7.11 illustrates the temperature and pump trends during the initial few hours of crystalliser start up. Within this time it is observed that all trends begin to stabilise and do not deviate drastically. During continuous cooling crystallisation these trends should remain constant to generate a consistent product via steady state operation.

Figure 7.12 also shows a number of trends approximately after 24 hours from the timescale of trends in Figure 7.11. It can be observed in Figure 7.12 that erratic and variable trends are present highlighting present operation is not at steady state. The feed solution within Module 3 were set to a fixed temperature however what was measured varied considerably. To compensate for differences in internal temperature and circulator temperature, the hot and cold pump speed increased considerably to overcome insulation effects of fouling.

Although this example is not simplistic it highlights that heat transfer can be used to detect fouling occurring within a real continuous crystallisation campaign. Calculating the fouling resistance with time could not be quantified for this example however its application for identifying fouling in continuous crystallisation processes remains valid.

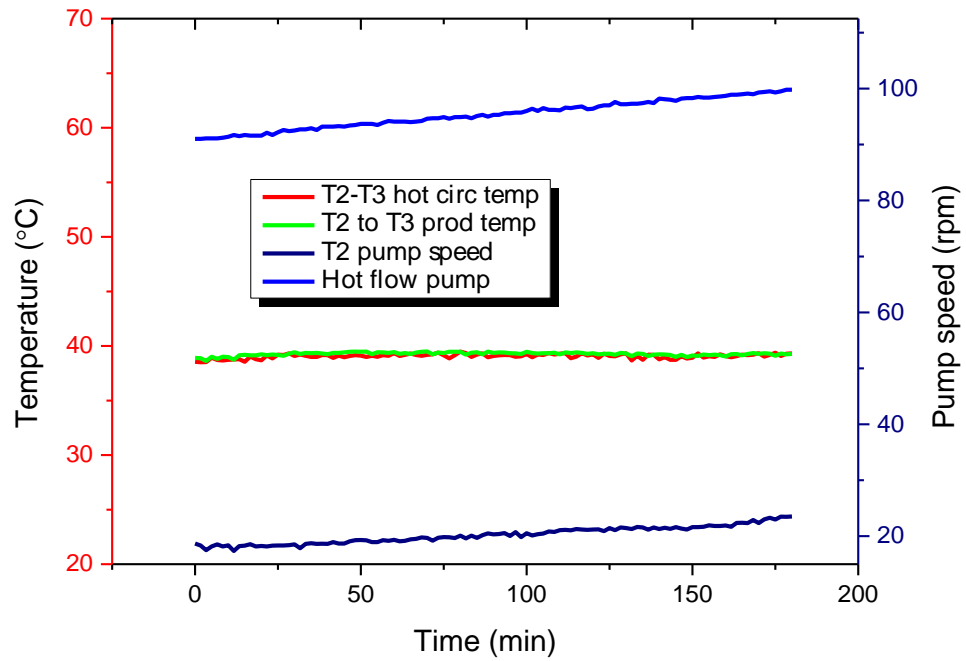


Figure 7.11: Temperature and pump speed trends related to the continuous crystallisation of lactose monohydrate between Module 2 and Module 3 within the Rattlesnake platform.

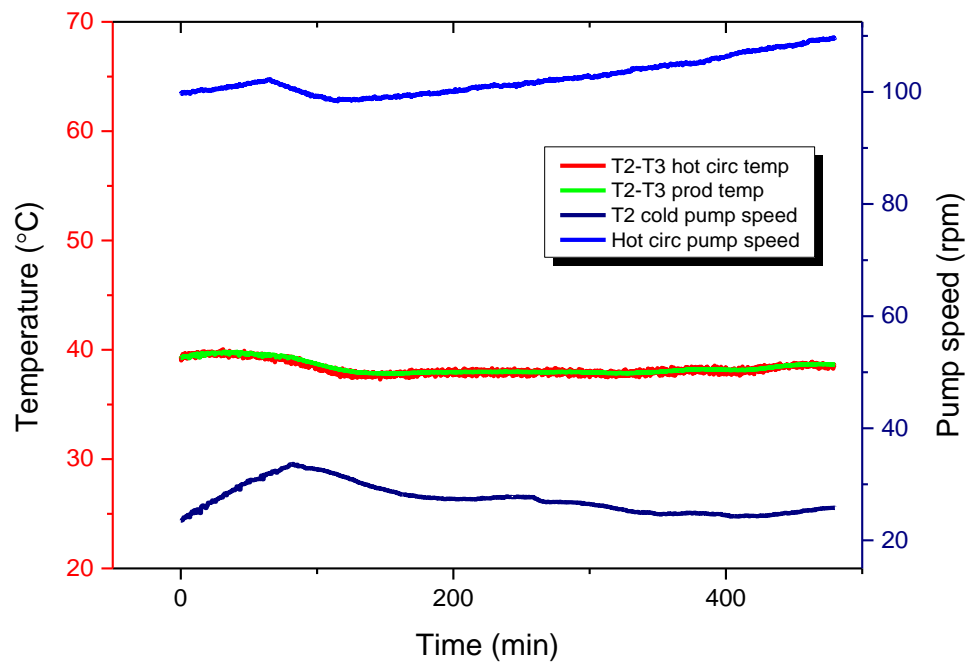


Figure 7.12: Temperature and pump speed trends associated between Module 2 and Module 3 of the Rattlesnake where fouling was identified i.e. 24 hours after initial operation (Figure 7.11).

7.3.2.2 C-FAP data – comparison

Although fouling resistance could not be calculated using temperature data within the previous section (7.3.2.1 Investigation of heat transfer to identify fouling in a continuous crystallisation), crystallisation fouling was demonstrated to impact heat transfer during a continuous crystallisation process. The C-FAP was specifically designed to have the capability to determine temperature values necessary to calculate the fouling resistance as described earlier (6.2.3 Thermocouple addition and 7.2.2.2(b) Temperature profiles and heat transfer performance). Experimental fouling trials were conducted to assess whether calculating fouling resistance could be applied within the C-FAP. Determining the fouling resistance fouling induction times can be determined. Test data was based upon the most extreme conditions for fouling to occur. Results where fouling was prominent (i.e. largest temperature difference ($\Delta T_{MOC} = 39.5^{\circ}\text{C}$) involving stainless steel, using an undersaturated PCM in water solution and a solution flow rate of 50 ml/min) are demonstrated herein. A comparison between the two fouling induction time definitions was conducted for the present example. Figure 7.13 shows the temperature trends across the fouling flow cell have some fluctuations however remain reasonably stable. The fouling induction time and full MOC coverage time points from imaging are detailed in Figure 7.14. At first observations no apparent effect on heat transfer is observed where nucleation occurred after 57 minutes and complete area coverage after 606 minutes.

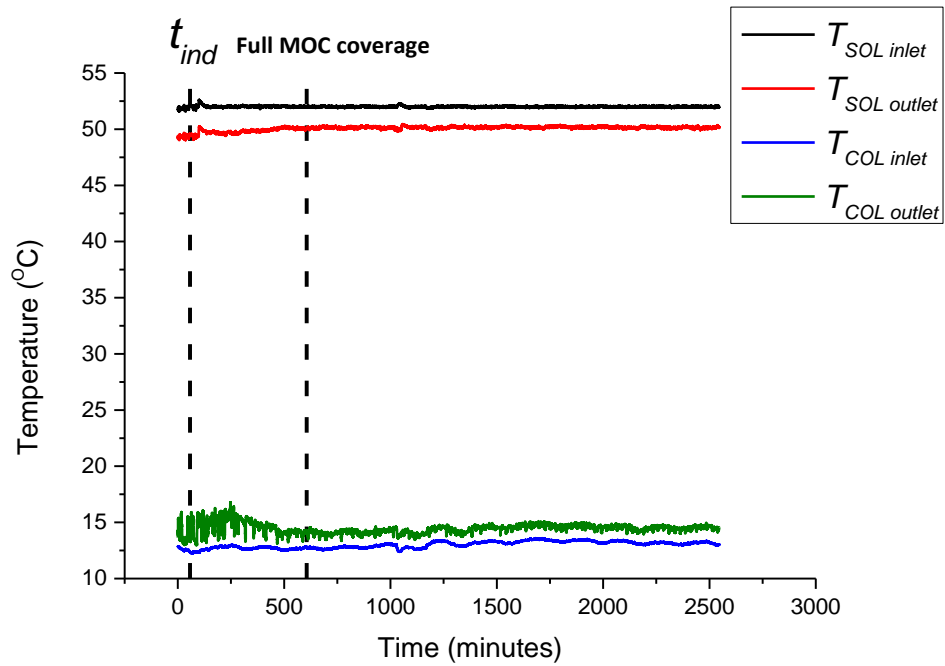
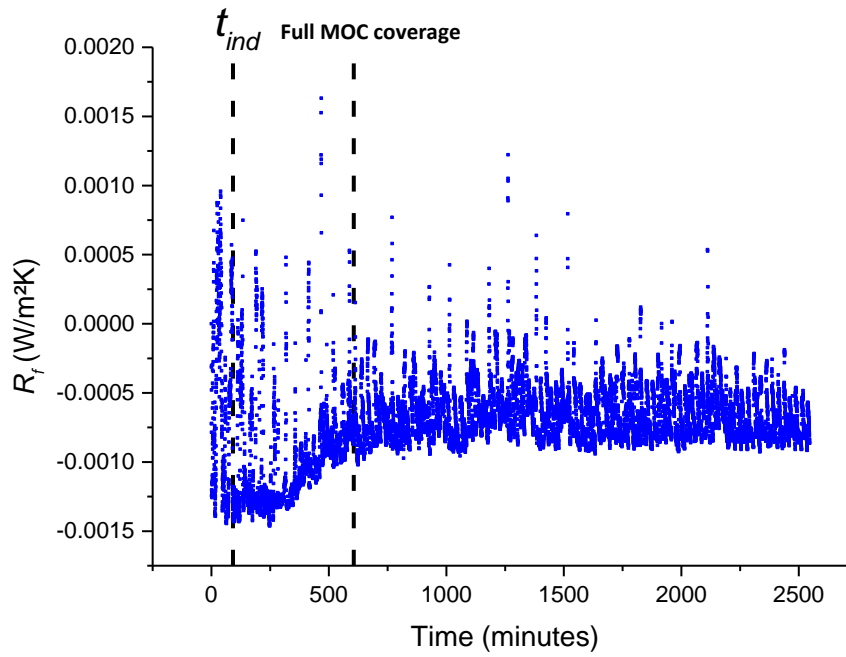


Figure 7.13: Temperature profiles of inlet and outlet hot solution and coolant thermocouples highlighting induction time and complete area fouling coverage (from imaging).

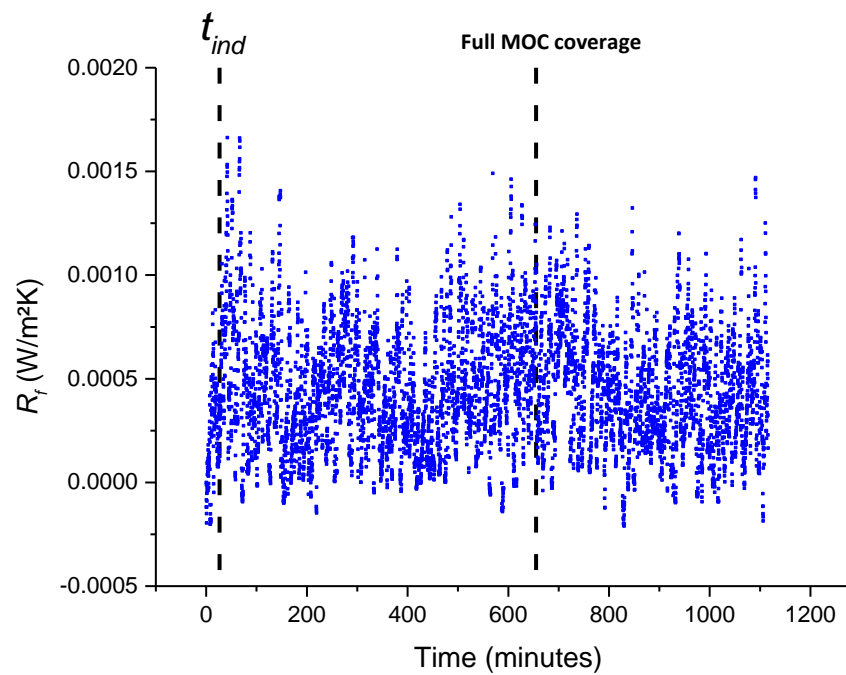
Using the temperature values obtained (and Equation 1.25, Equation 7.1, Equation 7.2 and Equation 7.3) the heat flux and overall heat transfer coefficient can be determined with respect to time. The fouling resistance was determined with respect to time in Figure 7.14 (a) which reveals considerable fluctuations highlighting unreliable ability to determine heat transfer across the flow cell. It is observed in the initial periods of Figure 7.14 (a) there is a degree of oscillation which is considered to be due to the PID feedback control. The fouling resistance curve based upon temperature trends from Figure 7.13 is shown in Figure 7.14 (a). A steady positive value is not identified which proposes a more sensitive method is required. Approaches to enhance the applicability of this technique include increasing the heat transfer surface area in relation to working volume in addition to altering the position of thermocouple to measure temperature within the locality of the flow cell. The flow rate selected for the cold stream was high with respect to the operating cold volume at the rear of the MOC. This feature may be another reason for not identifying

changes in heat transfer. Another consideration regarding utilising this method as a fouling detection and measurement method is evaluating the heat loss to other areas associated with the flow cell which may be magnitudes larger than the heat transfer at the MOC coupon. To emphasise the lack of sensitivity and reproducibility associated with this approach another fouling resistance curve was generated for identical explored conditions shown in Figure 7.14 (b). Figure 7.14 (b) reveals an inconsistent trend where no different features are identified in relation to imaging fouling induction time and total area coverage.

A comparison between imaging and heat transfer methods for determining fouling induction time found imaging methods identified the first detection of crystals on the MOC surface whilst heat transfer methods were not successful. Heat transfer methods for identifying the initiation of fouling was not identified highlighting a lack of sensitivity. Additionally even when exposed MOC surface was fully covered with PCM crystalline material no identified change in heat transfer was observed. This lack of sensitivity again demonstrates against its use within the C-FAP as an evaluation tool. Additionally the use of heat transfer methods within continuous crystallisation campaigns as an initial fouling detection method may not be suitable since considerable fouling deposits may already be present. Other fouling detection methods are more appropriate in identifying initial fouling within a continuous crystalliser such as image based methods described by Tachtatzis and co-workers.¹⁰⁸



(a)



(b)

Figure 7.14: (a) Example of a fouling resistance curve with respect to time based upon temperature trends of Figure 7.13 in which can be described as variable however an increasing trend is found between induction time (t_{ind}) and full MOC coverage. (b) Another example of a fouling resistance curve for the same conditions explored within image (a) highlighting lack of reproducibility and sensitivity.

7.4 Summary

The C-FAP was developed as an assessment platform to evaluate the influence of different MOCs, process conditions and solution properties notably degree of supersaturation on fouling behaviour. In this work a crystallising solution that is known to cause fouling related issues was explored to highlight the C-FAP's applicability to evaluate fouling. The C-FAP can perform two different measurement techniques namely imaging and heat transfer measurements.

The use of imaging to determine fouling induction times and relative growth kinetics was established in which distinct differences were identified for explored conditions comprising different process, solution and MOC parameters. However, the application of heat transfer measurements to determine fouling behaviour measurements was not a successful owing to the limited sensitivity. Future practical applications should use undersaturated feed solutions to minimise the risk of uncontrolled or secondary processes. Additionally the present research directed future practical applications in which undersaturated solutions should only be used within the C-FAP since supersaturated solutions are unstable once surface nucleation occurs.

The most appropriate induction time and growth rate measurements related to the C-FAP were determined from sequential imaging. The extent of influence on explored parameters for fouling induction time varied in which temperature difference (ΔT), degree of solution saturation and MOC properties all had significant effects. The effect of solution flow rate was deemed not to be significant. However, a wider range of flows may show different results. Relative growth rates were found to be considerably influenced by degree of solution saturation and MOC whilst other parameters influenced to lesser extents. The application of area coverage rates was a novel approach to describing fouling growth kinetics.

From a fouling mechanistic perspective, the C-FAP was designed to explore fouling on different MOCs acting as heat transfer interfaces and attempt to

mimic conditions experienced within a crystalliser. The application of cooling across the MOC coupon generates local supersaturation at the MOC's surface which will promote crystallisation within this region. The C-FAP also has the potential for explored MOCs to initiate fouling due to catalytic effects however this is unlikely within this study since high supersaturation is often required. The C-FAP also has the potential to explore suspensions however modifications to prevent particle settling is necessary. The two investigated MOCs within this chapter yielded vastly differing results highlighting the importance of heat transfer surface properties in influencing the fouling initiation and growth. It can therefore be confirmed that the C-FAP has demonstrated its validity as a fouling assessment platform in which investigatory parameters can be explored systematically.

Chapter 8. Multivariate modelling of fouling responses and parameter evaluation

8.1 Introduction

The influential importance of process parameters and MOCs on surface induced crystallisation fouling of PCM in continuous flow was demonstrated within Chapter 7. However, the extent of influence for each parameter was not considered therefore establishing the relative importance of parameters explored on fouling behaviour was out with the study. The C-FAP was demonstrated as a practical screening platform for the assessment of surface induced fouling where different MOCs, solutions and process parameters could be probed. The range of explored conditions within Chapter 7 was limited. Exploring a larger range of parameters specifically parameter interactions would highlight the most significant parameters influencing fouling with a specific emphasis on surface induction and growth mechanisms. Systematically evaluating a wide range of different MOCs, process conditions and solution properties for detailed fouling studies within the C-FAP would require substantial time and resource input in order to carry out. Within the pharmaceutical industry both time and resources are restricted therefore other approaches would be beneficial. One such approach benefiting the pharmaceutical industry is the application of modelling. Model types such as CFD²⁶⁷, discrete element modelling (DEM)²⁶⁸, finite element modelling (FEM)²⁶⁷ and artificial neural networks (ANN)²⁶⁹ have been applied to pharmaceutical processes to enhance insight into process operation and mechanistic perspectives. Predictive methods such as random forest classifications¹⁷⁰ and multivariate approaches²⁷⁰ have been applied to pharmaceutical sciences. The development of predictive frameworks provides an alternative method to traditional experimental approaches. Examples of predictive approaches related to a crystallisation process include predicting crystallinity²⁷¹, crystal structure²⁷², polymorphism²⁷³ and solution solubility.²⁷⁴ Developing a prediction framework for fouling would be highly beneficial notably in the early stages of process development.

Fouling is not commonly involved as a model term in the modelling of crystallisation processes (see 1.4.2.6 Modelling crystallisation fouling). Peroni

and co-workers highlighted the importance of including a fouling term within crystallisation models ultimately to improve the prediction of crystallisation processes and associated outcomes.¹⁵² Modelling of fouling with continuous crystallisers has received considerable interest. A recent model describing potassium aluminium sulphate fouling within a continuous crystalliser has been proposed by Majumder. Majumder and co-workers developed a model that coupled progressive fouling formation, population balance and energy balance to predict fouling thickness and its resultant effect on the modelled product PSD.⁸ The fouling component of the generated model attempted to include generic mechanistic processes including the transfer of solute molecules towards the surface, the integration of solute molecules into the fouled mass and detachment. This generic fouling model can encompass a variety of fouling initiation mechanisms.¹² However, specifics of each initiation mechanism in addition to subsequent growth are not covered.⁸ Current modelling research by Koswara and Nagy explored developing models to limit fouling occurring within a plug flow continuous crystalliser via heating and cooling cycles.²⁷⁵

Modelling of fouling upon heat exchange surfaces has been conducted routinely with models generated to describe a variety of fouling responses such as fouling resistance²⁷⁶, mass deposition rates²⁷⁷ and fouling induction time.²⁷⁸ Typically fouling model terms utilise specific process parameters to describe a fouling measurement for a given experimental setup such as surface temperature, surface thermal conductivity, bulk concentration, local surface concentration and bulk temperature.^{19,113,279} Fouling models generally do not encompass a wide variety of differing model terms to describe a fouling response however substrate properties, solution properties and process parameters are all known to influence fouling to an extent.⁹ In addition to predicting fouling behaviour, the generation of fouling propensity models are desirable but are sparse within the literature. Wallhäußer et al. utilised an ANN approach to predict the propensity of milk protein fouling upon a stainless steel heat exchanger. It was found that the generated model was 98.58% accurate at predicting fouling propensity highlighting the model's value as a predictive

tool. A methodology to predict inorganic fouling upon a PVDF membrane distillation system was proposed by Warsinger and co-workers which considered temperature, solution concentration and flow conditions in model generation. A model was created to predict specific operational conditions where fouling will or will not occur ultimately aiding process design.²⁸⁰ At present no fouling models exist comprising process, solution and MOC property terms. Research by Wang and Tang explored membrane fouling in which hydrodynamic properties, membrane properties and solution chemistry were systematically investigated.²⁸¹ The prospect of having models capable of predicting (i) whether fouling is likely to occur and also (ii) predicting fouling behaviour based upon the previously highlighted properties would be highly advantageous.

Herein a number of models to describe fouling responses were generated based upon experimental data acquired using the C-FAP specific for surface induced fouling. Solution composition, process and MOC parameters were included in the screening approach and assessment. Pharmaceutically relevant fouling models were targeted that could be applicable universally to other organic solute molecules and solvents in which fouling could be assessed. Theoretically a new investigatory solution can be assessed using newly generated fouling models prior to further testing and progression towards a crystallisation campaign. Additionally details involving compatibility issues between solute, solvent and MOC can be assessed with created models. In order to generate a universal range of novel fouling models, a diverse array of system descriptors were necessary. Recommendations regarding the choice of MOCs and operating conditions with a continuous crystallisation process can be based upon the properties of the crystallising solution i.e. molecular structure of solute and solvent.

In addition to prediction, determined fouling models and their contributory model terms will highlight the most influential parameters impacting each fouling response. The advantage of establishing important influential

parameters can ultimately be related to the mechanistic processes of surface induced fouling (Figure 8.1).

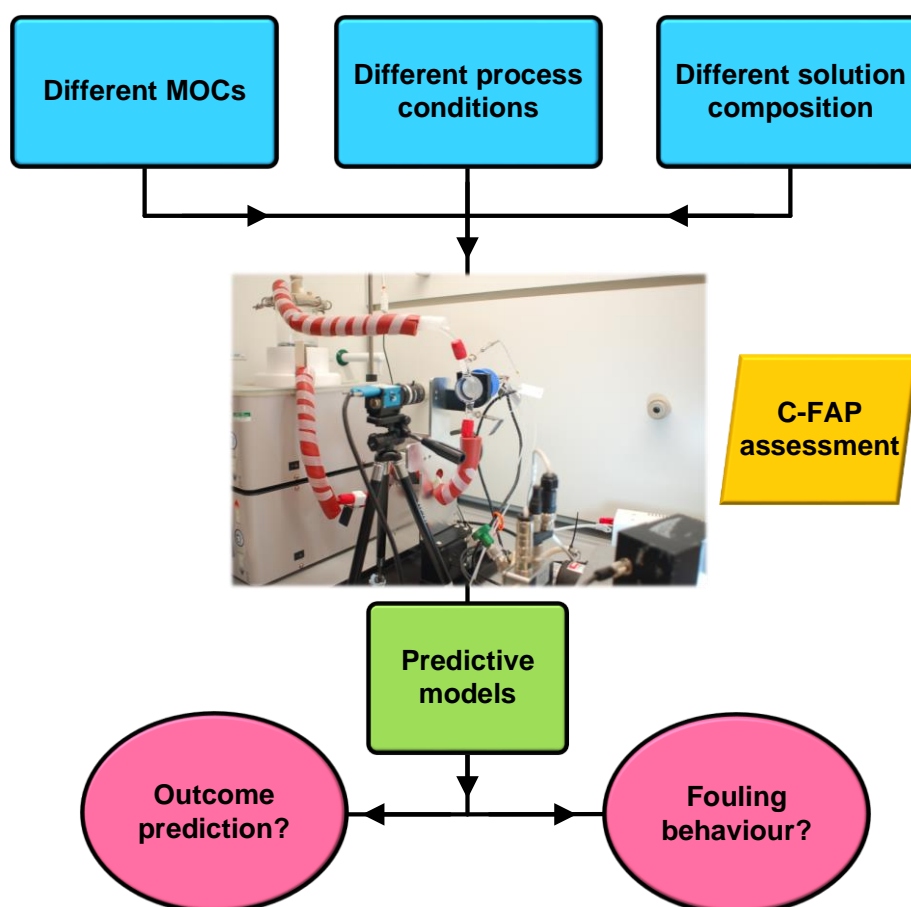


Figure 8.1: The proposed investigatory system parameters to be explored within the C-FAP to create predictive fouling models and establish the most influential parameters for each model.

8.2 Materials and methods

8.2.1 Materials

The C-FAP setup is detailed in both Chapter 6 and Chapter 7. A variety of different solutes (Figure 8.2) and solvents (Figure 8.3) (which are detailed in 3.1 Materials) were investigated to acquire experimental fouling data subsequently used to generate fouling models. Selected solutes comprised of pharmaceutically relevant compounds comprising APIs and drug excipients

with different molecular and physicochemical properties. Solvents selected within this work are typically considered for selection within the pharmaceutical industry due to their green chemistry and their use is highly relevant for reaction and crystallisation processing.^{253,282} Solutions were targeted that were pharmaceutically relevant and where associated solubility curves were available. The solubility curves of each probed solution are shown in Figure 8.4. MOCs coupons explored within this chapter are detailed in Chapter 3 (3.1 Materials). The assessment of diversity for each unique MOC was conducted in Chapter 4 (4.2.2 Assessment of MOC diversity) from which all unique MOCs were selected for investigation. Table 8.1 shows all selected MOCs explored within this work including MOC descriptors associated with each.

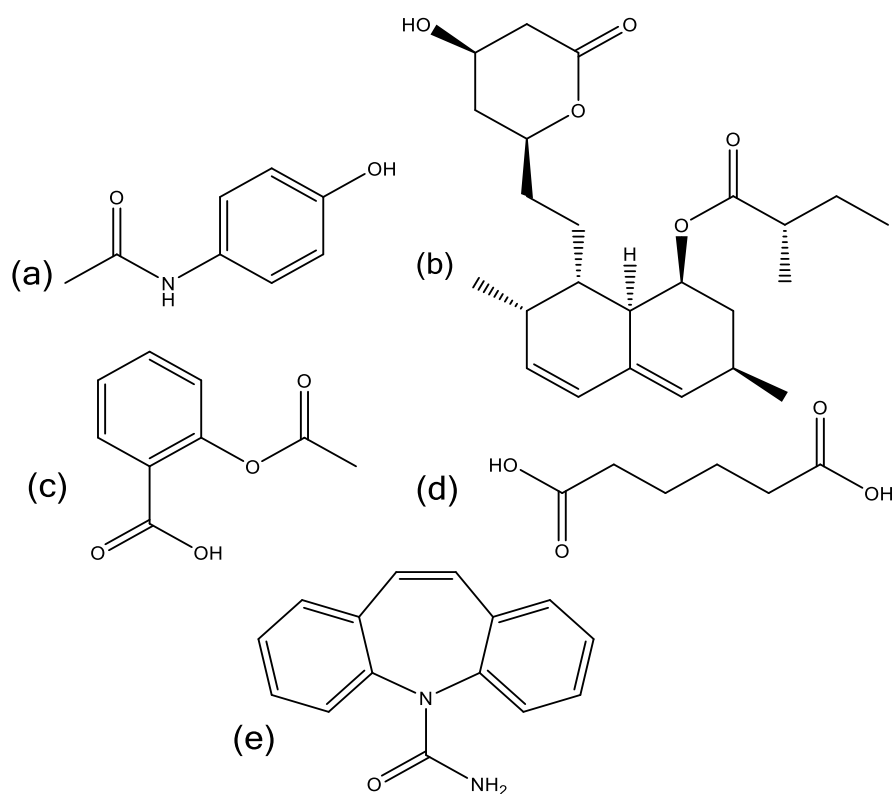


Figure 8.2: Molecular chemical structure of solutes used in this study comprising (a) PCM, (b) lovastatin (LOV), (c) aspirin (ASP), (d) adipic acid (AA) and (e) carbamazepine (CBZ).

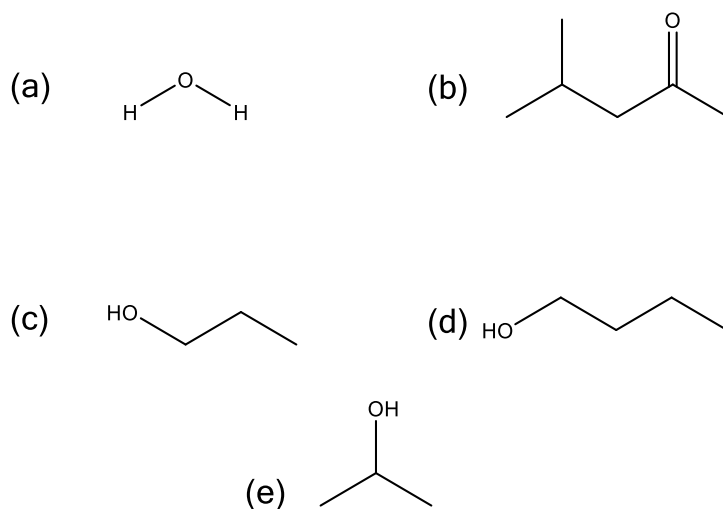


Figure 8.3: Molecular chemical structure of solvents used in this study including (a) water, (b) methyl isobutyl ketone (MIBK), (c) 1-propanol, (d) 1-butanol and (e) 2-propanol (IPA).

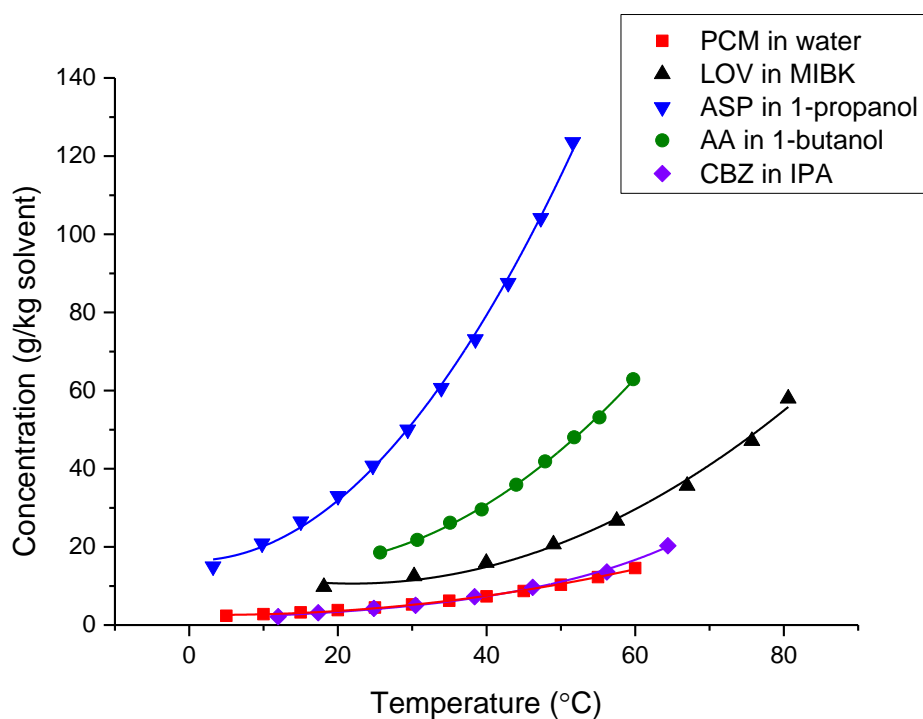


Figure 8.4: Solubility curves for the solute/solvent pairs tested in this study comprising PCM in water (red curve)²³², LOV in MIBK (black curve)[determined experimentally], ASP in 1-propanol (blue curve)²⁸³, AA in 1-butanol (green curve)²⁸⁴ and CBZ in IPA (violet curve).²⁸⁵

Table 8.1: Replicate of Table 4.4 highlighting all investigated MOCS including associated descriptors.

Parameter MOC	Roughness [Ra] (nm)	Water contact angle [θ] ($^{\circ}$)	Total surface energy [γ_s] (mJ/m ²)	Thermal conductivity [λ] at RT (W/m.K)	Specific capacity heat [C_p] (J/kg.K)	Young's modulus [E] (GPa)
Borosilicate	1.36	52.12	43.38	2	800	64
Quartz	1.09	38.6	44.16	1.46	705	73
C276 as received	45.67	64.22	40.42	10.42	425	205
C276 (280 grit)	434.9	59.45	43.07	10.42	425	205
C276 (EP)	19.98	65.15	40.95	10.42	425	205
PEEK	388	90.4	44.44	0.25	1340	3.85
PTFE	68.44	107.9	17.98	0.25	1000	0.55
SiC	280.3	46.1	36.52	130	690	430
SS 316L as received	104.7	75.82	43.74	16.3	502	200
SS 316L (280 grit)	608.6	73.45	43.75	16.3	502	200
SS 316L (EP)	33.15	79.53	42.75	16.3	502	200

8.2.2 Methods

8.2.2.1 Solute and solvent classification and diversity assessment

The diversity of solutes and solvent molecules explored within this work were evaluated using PCA as detailed in Chapter 4 (see 4.2.2 Assessment of MOC diversity). A varied array of solute and solvent molecules were targeted to create a pharmaceutically relevant design space. Solute and solvent molecular descriptors were obtained from MOE software (Chemical Computing Group) which included 2D and 3D molecular descriptors. All available descriptors were used for assessing diversity for solutes and for solvents. Descriptors which had zero variance were removed prior to PCA.

8.2.2.2 Crystallisation fouling experiments and fouling outcomes

(a) *Design overview*

Fouling experiments were conducted using the C-FAP. A reduced combinatorial design (3.2.2.2 DOE) was employed via MODDE software (Umetrics) that comprised of (i) 11 unique MOCs (see 4.2.2 Assessment of MOC diversity), (ii) 4 different investigatory solutions, (iii) 3 different temperature differences (ΔT_{MOC}) across the MOC coupon (as detailed in 6.2.3 Cold stream incorporation) and (iv) 2 different solution flow rates (see Table 8.1). Cold stream flow rate was fixed at 50 g/min.

Table 8.2: Different parameters to be explored to generate fouling models namely different MOCs, solutions, temperature differences across explored MOCs and solution flow rates.

Parameter	Different parameter explored
MOC	Borosilicate, quartz, C276 as received, C276 (280 grit), C276 (EP), PEEK, PTFE, SiC, SS 316L as received, SS 316L (280 grit) and SS 316L (EP)
Solution	PCM in water, lovastatin in MIBK, aspirin in 1-propanol and adipic acid in 1-butanol
ΔT_{MOC} (°C)	27, 34.5 and 39.5
Solution flow rate (ml/min)	50 and 100

A conventional DOE approach involving all parameter combinations would consist of hundreds of experimental runs which is unrealistic in terms of time and resources. Reduced combinatorial design allows the screening of a large number of investigatory parameters relatively quickly which will direct what factors have the largest contribution towards a resultant model. Accurate predictions cannot be conducted with this type of screening in which enhanced prediction capabilities would require a more thorough DOE approach.

Each MOC, solute and solvent explored within this work was described in terms of the quantitative descriptors (see 4.2.2 Assessment of MOC diversity and 8.3.1 Diversity of experimental study). A maximum number of 32 factors within a dataset in MODDE software was possible. Therefore, descriptors most likely to affect fouling based on physicochemical considerations were selected. The selected descriptors to describe investigated MOCs, solutes and solvents are detailed in Table 8.3. Solute and solvent descriptors were selected to

include interactions such as hydrogen bonding²⁸⁶, polarity²⁸⁷ and van der Waals (vdW) forces²⁸⁸ which have been proposed to influence fouling from membrane studies. Additionally, other descriptors were selected which have previously been probed to impact fouling including molecular mass, size and charge.²⁸⁷ MOC descriptors encompassing roughness, thermal, physical, energetic and physicochemical properties were chosen to represent each MOC. The specific reduced combinatorial experimental design is detailed within Table 8.4.

Table 8.3: Employed MOC, solute and solvent descriptors within the reduced combinatorial experimental design used to describe each parameter (with shorthand terms).

Parameter	Descriptors used for each parameter									
MOC	Surface roughness (Ra)	Water contact angle (θ)	Total surface energy (γ_s)	Thermal conductivity (λ)	Specific heat capacity (C_p)	Young's modulus [E]				
Solute	Molecular mass (SWeight_molecularmassolute)	Log octanol/water partition coefficient (log P)	Total charge of molecule (Fcharge)	Aqueous solubility at 25°C in mol/L (logS)	Sum of the atomic polarizabilities (Sapol)	Number of hydrogen bond acceptors and donators (a_donacc)	Approximation to the sum of VDW surface areas of polar atoms (vsa_pol)	Approximation to the sum of VDW surface areas of hydrophobic atoms (vsa_hyd)	Water accessible surface area (ASA)	van der Waals volume (Svdw_vol)
Solvent	Molecular mass (LIQMolecular Weight)	Water accessible surface area (LIQASA)	Sum of the atomic polarizabilities (LIQapol)	Number of hydrogen bond donor atoms (LIQa_don)	Number of hydrogen bond acceptor atoms (LIQa_ace)	Number of hydrophobic atoms (LIQa_hyd)	van der Waals volume (LIQvdw_volume)	Molecular mass density (Density)		

Table 8.4: Experimental conditions selected by the reduced combinatorial experimental design including parameter descriptors for assessment in the C-FAP.

Exp No	Investigated system	Flow rates (ml/min) †	ΔT_{MOC} (°C) †	Ra roughness (nm) \diamond	Water contact angle (°) \diamond	Total surface energy (mj/m ²) \diamond	Thermal conductivity at RT (W/m.K) \diamond	Specific heat capacity (J/Kg.K) \diamond	Young's modulus (GPa) \diamond	SWeight_molecul armassolute*	Slog p (o/w)*	Fcharge*
1	Borosilicate/PCM_Water	100	39.5	1.36	52.12	43.38	2	800	64	151.17	0.89	0
2	Borosilicate/ASP_1-Propanol	50	27	1.36	52.12	43.38	2	800	64	179.15	1.64	-1
3	Quartz/AA_1-Butanol	50	27	1.09	38.6	44.16	1.46	705	73	144.13	0.6	-2
4	Quartz/LOV_MIBK	100	34.5	1.09	38.6	44.16	1.46	705	73	404.547	4.06	0
5	C276 AS REC/PCM_Water	50	27	45.67	64.22	40.42	10.42	425	205	151.17	0.89	0
6	C276 AS REC/ASP_1-Propanol	100	39.5	45.67	64.22	40.42	10.42	425	205	179.15	1.64	-1
7	C276 280 GRIT/AA_1-Butanol	50	39.5	434.9	59.45	43.07	10.42	425	205	144.13	0.6	-2
8	C276 280 GRIT/LOV_MIBK	100	27	434.9	59.45	43.07	10.42	425	205	404.55	4.06	0
9	C276 EP/PCM_Water	100	39.5	19.98	65.15	40.95	10.42	425	205	151.17	0.89	0
10	C276 EP/ASP_1-Propanol	50	34.5	19.98	65.15	40.95	10.42	425	205	179.15	1.64	-1
11	PEEK/AA_1-Butanol	100	34.5	388	90.4	44.44	0.25	1340	3.85	144.13	0.6	-2
12	PEEK/LOV_MIBK	50	39.5	388	90.4	44.44	0.25	1340	3.85	404.55	4.06	0
13	PTFE/PCM_Water	50	34.5	68.44	107.9	17.98	0.25	1000	0.55	151.17	0.89	0
14	SiC/ASP_1-Propanol	50	34.5	280.3	46.1	36.52	130	690	430	179.15	1.64	-1
15	SS316 AS REC/AA_1-Butanol	100	34.5	104.7	75.82	43.74	16.3	502	200	144.13	0.6	-2
16	SS316 280 GRIT/LOV_MIBK	50	27	608.6	73.45	43.75	16.3	502	200	404.55	4.06	0
17	SS316 EP/PCM_Water	100	27	33.15	79.53	42.75	16.3	502	200	151.17	0.89	0
18	C276 AS REC/PCM_Water	50	27	45.67	64.22	40.42	10.42	425	205	151.17	0.89	0
19	C276 EP/ASP_1-Propanol	50	34.5	19.98	65.15	40.95	10.42	425	205	179.15	1.64	-1
20	PTFE/PCM_Water	50	34.5	68.44	107.9	17.98	0.25	1000	0.55	151.17	0.89	0

Table 8.4 continued....

Exp No	LogS [†]	Sapol [†]	a_donac [‡]	vsa_pol [‡]	vsa_hyd [‡]	ASA [‡]	Svdw_vo [‡]	LIQMolecular Weight [◊]	LIQASA [◊]	LIQapolo [◊]	LIQa_dono [◊]	LIQa_ace [◊]	LIQa_hydo [◊]	LIQvdw_volo [◊]	Density [◊]
1	-1.23	22.79	4	32.82	107.8	342.48	203.72	18.02	117.85	2.136	1	1	0	33.68	1
2	-1.97	23.72	1	40.7	103.31	355.29	219.31	60.1	228.03	11.42	1	1	3	95.71	0.803
3	-0.2705	19.10	0	54.27	63.23	326.39	171.09	74.12	259.38	14.51	1	1	4	120.14	0.8098
4	-4.23	70.25	4	40.7	298.54	656.77	578.91	100.16	291.94	19.36	0	1	5	161.65	0.801
5	-1.23	22.79	4	32.82	107.8	342.48	203.72	18.02	117.85	2.136	1	1	0	33.68	1
6	-1.97	23.72	1	40.7	103.31	355.29	219.31	60.1	228.03	11.42	1	1	3	95.71	0.803
7	-0.2705	19.10	0	54.27	63.23	326.39	171.09	74.12	259.38	14.51	1	1	4	120.14	0.8098
8	-4.23	70.25	4	40.7	298.54	656.77	578.91	100.16	291.94	19.36	0	1	5	161.65	0.801
9	-1.23	22.79	4	32.82	107.8	342.48	203.72	18.02	117.85	2.136	1	1	0	33.68	1
10	-1.97	23.72	1	40.7	103.31	355.29	219.31	60.1	228.03	11.42	1	1	3	95.71	0.803
11	-0.2705	19.10	0	54.27	63.23	326.39	171.09	74.12	259.38	14.51	1	1	4	120.14	0.8098
12	-4.23	70.25	4	40.7	298.54	656.77	578.91	100.16	291.94	19.36	0	1	5	161.65	0.801
13	-1.23	22.79	4	32.82	107.8	342.48	203.72	18.02	117.85	2.136	1	1	0	33.68	1
14	-1.97	23.72	1	40.7	103.31	355.29	219.31	60.1	228.03	11.42	1	1	3	95.71	0.803
15	-0.2705	19.10	0	54.27	63.23	326.39	171.09	74.12	259.38	14.51	1	1	4	120.14	0.8098
16	-4.23	70.25	4	40.7	298.54	656.77	578.91	100.16	291.94	19.36	0	1	5	161.65	0.801
17	-1.23	22.79	4	32.82	107.8	342.48	203.72	18.02	117.85	2.136	1	1	0	33.68	1
18	-1.23	22.79	4	32.82	107.8	342.48	203.72	18.02	117.85	2.136	1	1	0	33.68	1
19	-1.97	23.72	1	40.7	103.31	355.29	219.31	60.1	228.03	11.42	1	1	3	95.71	0.803
20	-1.23	22.79	4	32.82	107.8	342.48	203.72	18.02	117.85	2.136	1	1	0	33.68	1

† denotes process parameters, ◊ denotes MOC descriptors, ‡ denotes solute descriptors, ◊ denotes solvent descriptors

(b) ***C-FAP setup and operation***

Feed solutions were undersaturated ($S = 0.98$) for all solutions with supersaturation generated locally at the MOC coupon surface by varying ΔT_{MOC} . The crystallisation fouling methodology is described elsewhere (Chapter 7) including setup and initiation of measurements (7.2.2.1 Solution preparation and C-FAP setup). A 24 hour time limit was applied in which if fouling had not initiated during this time, the experimental run was ended and conditions were deemed not to foul.

(c) ***Fouling measurements***

Three fouling measurements were made using the C-FAP for each explored condition: fouling induction time (via imaging), maximum area coverage rate (via imaging) and total mass deposited 24 hours after surface nucleation (gravimetry).

The method for determining fouling induction time via imaging is detailed in Chapter 7 (see (a) Fouling induction time and fouling growth rates via imaging). The concept of determining maximum area coverage rates was grounded upon methods employed within other research disciplines. Area coverage rates have not been measured in crystallisation studies historically whilst are frequently used in microbiological research. Microbiological area coverage growth within a fixed area such as a petri dish follows a sigmoidal growth curve.²⁸⁹⁻²⁹⁰ Research by Uchymiak et al. explored the area coverage of gypsum upon a membrane surface which has a sigmoidal trend when plotted with time.²⁹¹ A maximum area coverage rate can be identified where the gradient is at its largest (red line) as illustrated in Figure 8.5. Crystal growth rates are acknowledged to be influenced by different solvent compositions as demonstrated by Ó'Ciardhá et al.²⁶⁶ ultimately altering the solution composition. Therefore, each investigated solution's crystal growth rate will vary which was anticipated within this work. Each crystallising system's growth rate were anticipated to be different therefore area coverage was determined

over an extended period of time i.e. 24 hours after nucleation to ensure the maximum area coverage rate was determined. The total mass deposited upon the investigated MOC for each explored condition was determined by removal and weighing by difference.

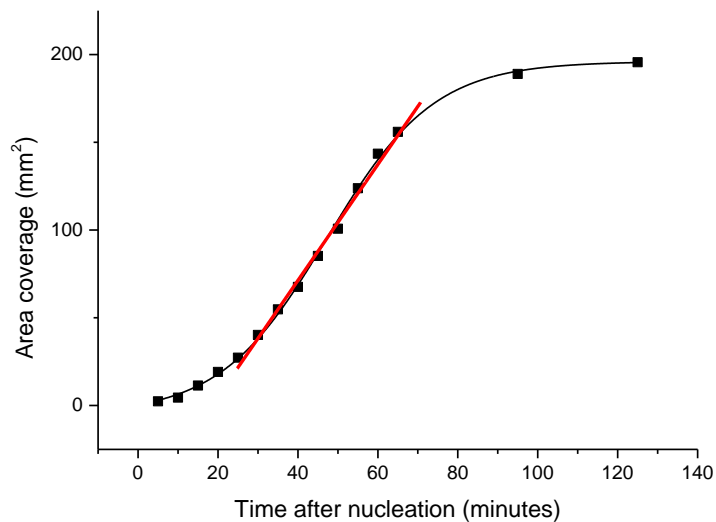


Figure 8.5: An example of a fouling area coverage against time after nucleation sigmoidal plot. The maximum gradient is denoted by the red line from which an area coverage rate can be determined.

(d) ***Model fitting with experimental fouling data***

Response models were generated for each fouling response (as detailed in (c) Fouling measurements). The predictive capabilities of each model was also assessed and they were used as a basis to assess the relative importance of the experimental and calculated descriptors. Furthermore a prediction fouling model was developed which could indicate the relative risk of fouling occurring based on all the descriptors. For generated models, data acquired from the reduced combinatorial design was used with partial least squares regression (PLS) fitting applied using MODDE (UMetrics) (as detailed in 3.2.2.2 DOE). In total 4 predictive models were created (Figure 8.6). Validation experiments were performed to assess generated models in which are detailed later on.

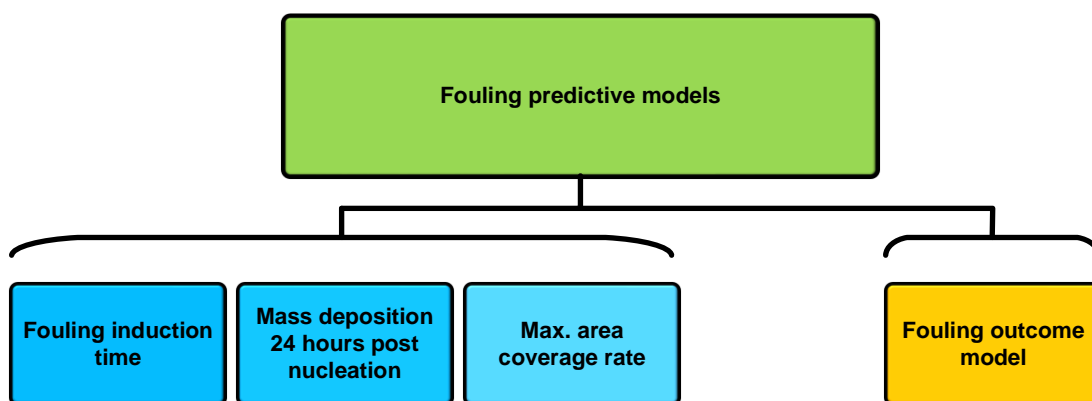


Figure 8.6: Two different model types to be generated within this chapter including specific fouling behaviour models and a definitive fouling outcome model.

8.3 Results and discussion

8.3.1 Diversity of experimental study

PCA was conducted for all solutes and solvents explored in addition to the external validation solution components (CBZ in IPA). Performing PCA of the investigated solutes (Figure 8.7) and solvents (Figure 8.8) allows the assessment of two aspects: (i) the diversity of all molecules in the study and (ii) the external validation solute and solvent system fits within the original design space i.e. confirm that the external validation is of an acceptable range.

Figure 8.7 illustrates the degree of diversity in the solute molecules. The selected validation solute (carbamazepine) is well within the range. The selected solvents show, as expected, a range of diversity however the three alcohols are closely grouped, consistent with the minor variations in their structure and related properties.

The results from the PCA demonstrated the selected molecules have a reasonable degree of physicochemical similarity and are well suited to the fouling study. Additionally Figure 8.9 highlights investigated MOCs were distinctly diverse (Replicate of Figure 4.11).

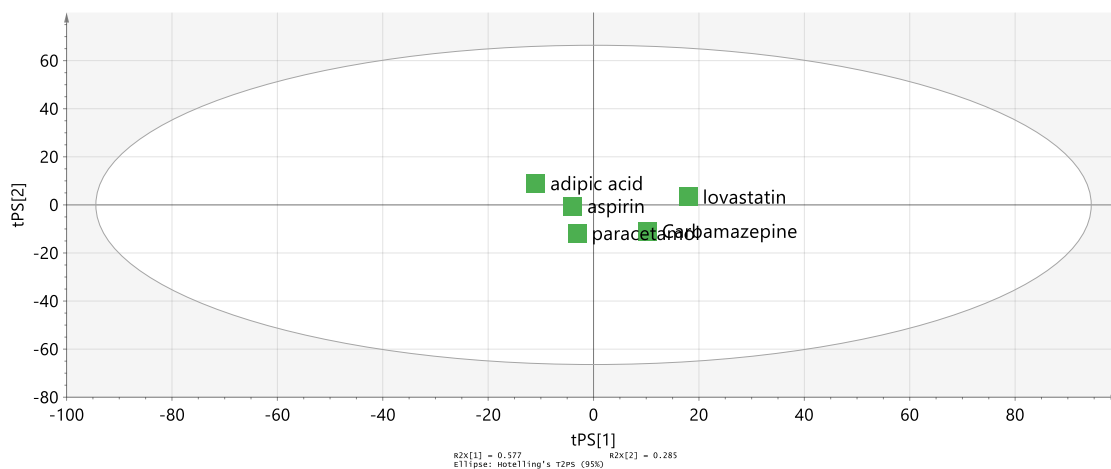


Figure 8.7: PCA scores plot for 1st and 2nd component generated for solute molecules to be investigated. External validation solute was located marginally out with the grouping yet within the Hotelling's ellipse [1st component $R^2 = 0.577$, 2nd component $R^2 = 0.285$, variance described = 86.2%].

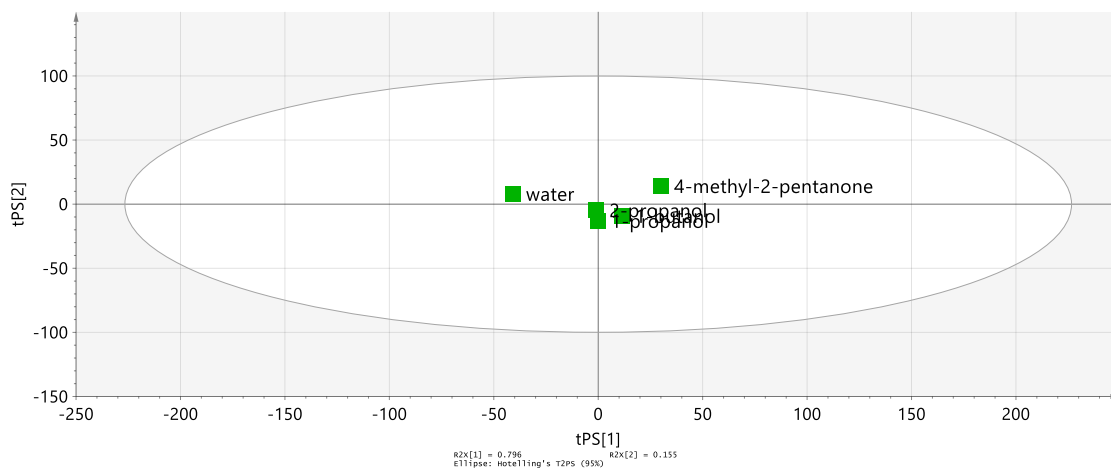


Figure 8.8: PCA scores plot for 1st and 2nd component generated for solvent molecules to be investigated. The external validation solute is located within the solvent grouping [1st component $R^2 = 0.796$, 2nd component $R^2 = 0.155$, variance described = 95.1%] (4-methyl-2-pentanone denotes MIBK and 2-propanol denotes IPA).

Table 8.5: Fouling behaviour results for each experiment number as detailed in Table 8.3. Grey shaded rows indicate experiments where no fouling had occurred within the 24 hour timescale.

Experiment number	Crystal induction time (minute)	Mass 24 hours after nucleation (mg)	Maximum growth rate (mm ² /min)
1	127	466.5	0.145
2	0	0	0
3	0	0	0
4	12	237.7	7.23
5	32	490.8	0.266
6	23	697.4	10.871
7	11	542	3.32
8	26	134	0.339
9	62	578	0.532
10	910	387.9	1.703
11	72	226.4	0.355
12	0	0	0
13	0	0	0
14	4	586.7	4.392
15	17	478.6	6.727
16	47	492	0.09
17	255	567	0.426
18	46	627.9	9.466
19	274	406.9	0.352
20	0	0	0

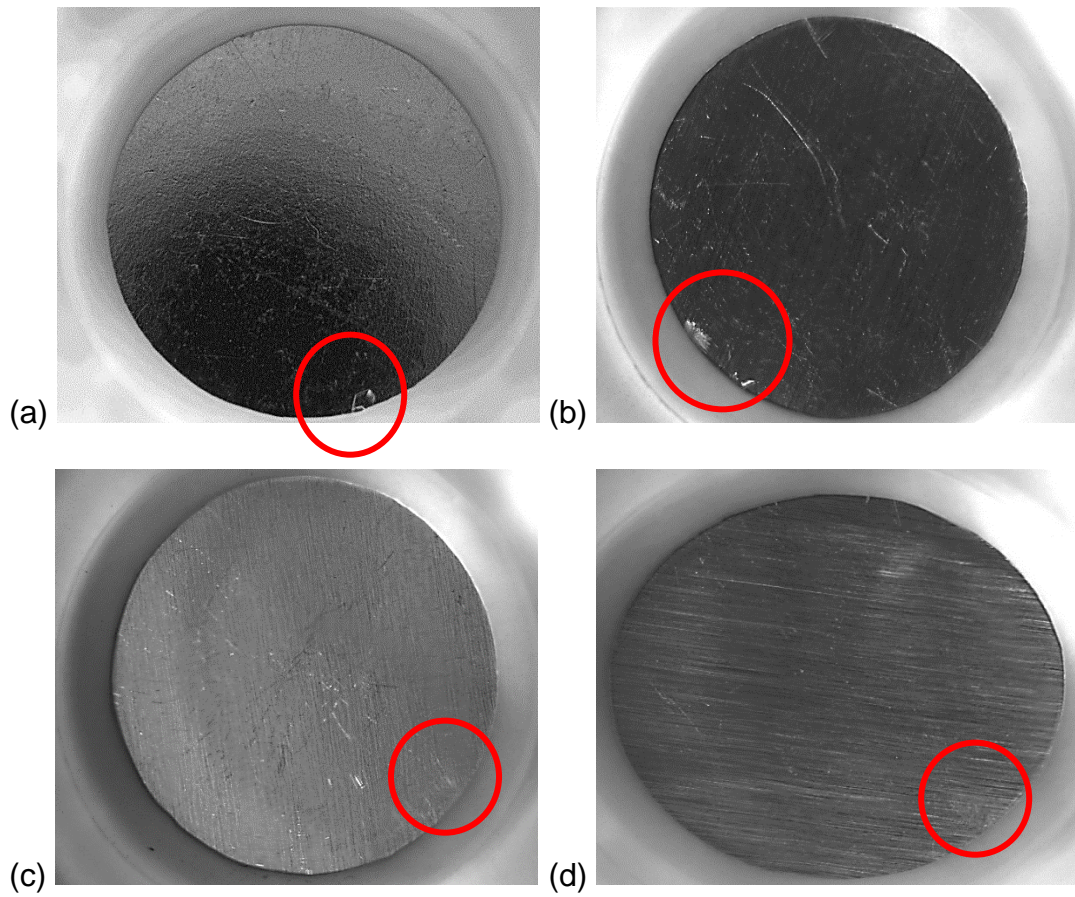


Figure 8.10: Selected images highlighting the initial formation of crystalline material that was used for determining induction time values specifically (a) PCM [Exp 9], (b) LOV [Exp 8], (c) ASP [Exp 6] and (d) AA [Exp 7]. Red oval shows the location of nucleation initiation.

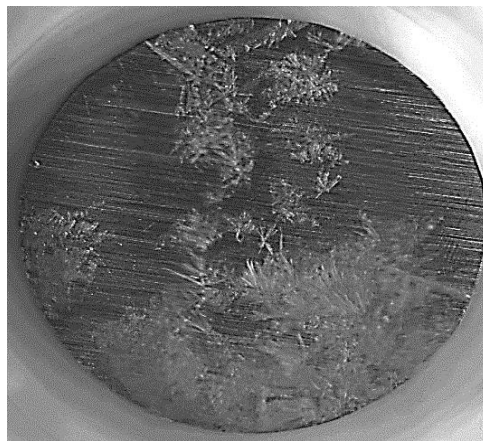


Figure 8.11: Image of AA growth revealing the needle-like morphology and large number of growth locations.

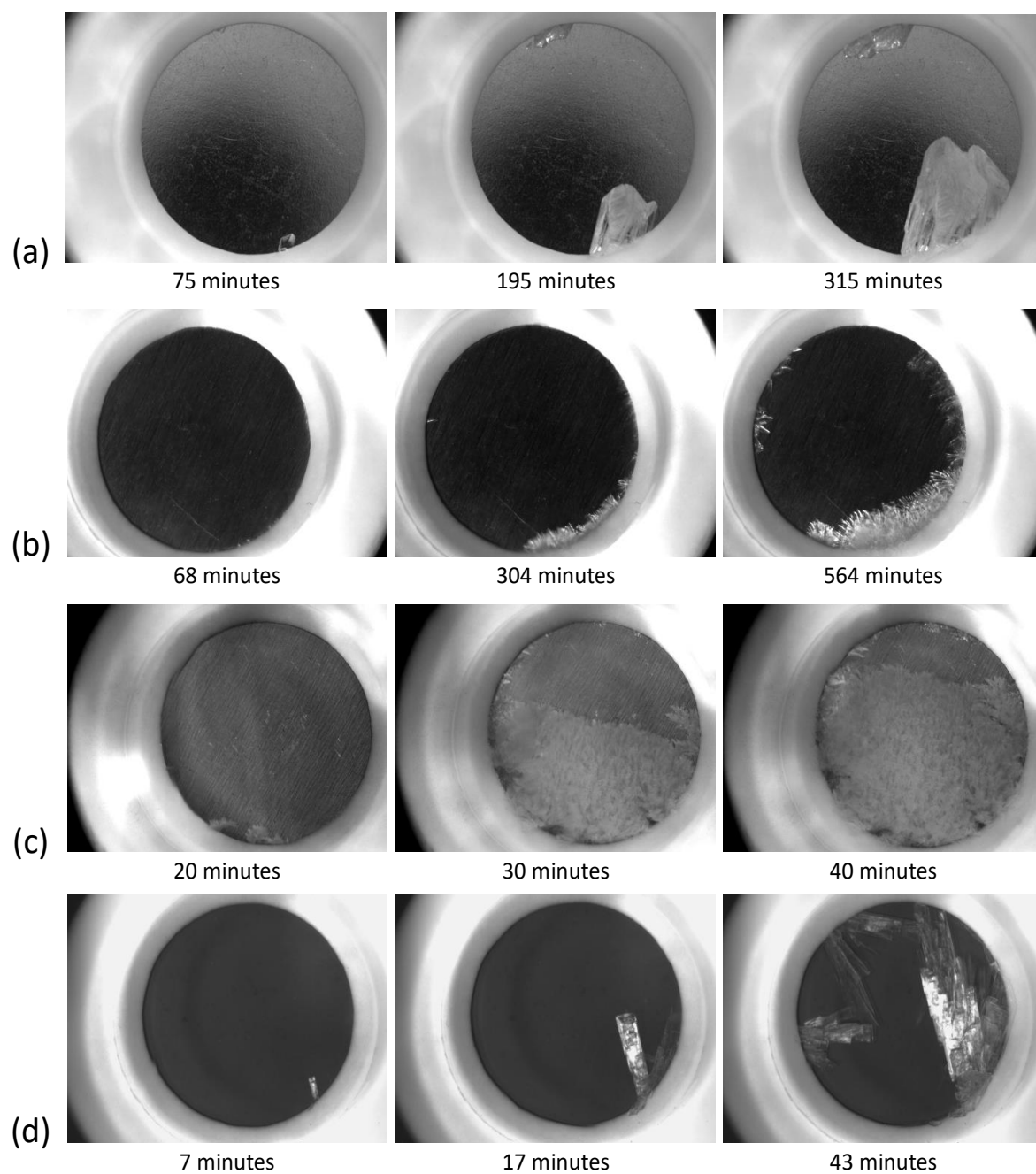


Figure 8.12: Series of images collected at several time point once experiments were initiated for (a) PCM in water [Exp 9], (b) LOVA in MIBK [Exp 16], (c) AA in 1-butanol [Exp 16] and ASP in 1-propanol [Exp 14]. Time values associated with each image specifies time-point after experiment was initiated.

Growth rate information data could be attained by determining the fouling area coverage over an extended time period towards complete MOC coverage. As anticipated, sigmoidal area coverage growth curves were identified albeit to different extents. Maximum area coverage rates were determined (Table 8.4) however it is worth noting that area coverage rates are not absolute and are only relative to other experimental runs.

8.3.3 Fouling behaviour screen

8.3.3.1 Model generation and evaluation

Experimental fouling results detailed within Table 8.4 were used to create three fouling response models to describe (i) fouling induction time, (ii) mass deposition after 24 hours post-nucleation and (iii) maximum area coverage rate. Five experiments were excluded from the model since no fouling had occurred within the designated 24 hour timescale. PLS models for each fouling response yielded satisfactory R^2 values. However, other relevant model statistics deemed each model as unreliable notably in terms of prediction (Q^2) as shown in Figure 8.12 (reference values detailed in 3.2.2.2 DOE). Reproducibility statistics as shown in Figure 8.12 are diverse with excellent statistics for fouling induction time, satisfactory for mass deposited and extremely poor reproducibility for maximum area coverage rate. No model validity statistic is present due to the insufficient number of replicates conducted. Models were constructed using factors and factor-factor interactions. Each model was edited to remove factors and factor-factor interactions to improve model statistics however no notable improvement was observed through systematic removal.

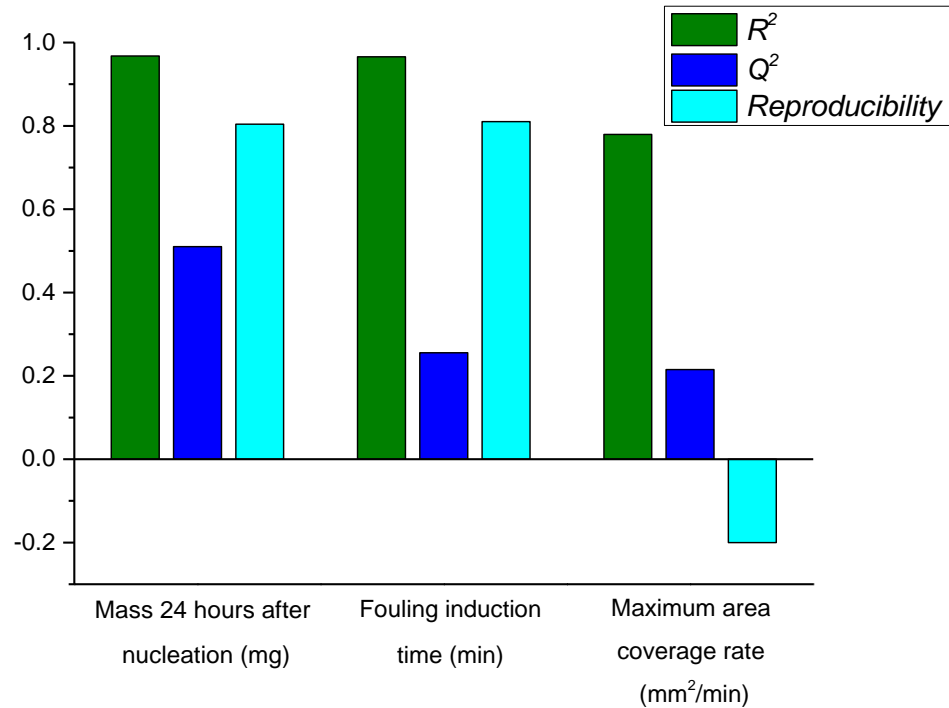


Figure 8.13: Summary of fit plots for each fouling response model.

For each fouling response model, associated effects plots were analysed to determine the top 10 influencing factors/interactions contributing towards the model which are detailed in Table 8.6.

Table 8.6 reveals a number of findings in relation to the determined fouling models and additionally fouling mechanisms. The first notable finding relates to model contributions in which factor-factor interactions were prominent in contrast to single factor terms. A large degree of overlap in influential factors and interactions was identified across all fouling behaviour models. The importance of MOC properties is apparent in Table 8.6 notably the contribution of thermal conductivity, specific heat capacity, total surface energy and Young's modulus in factor-factor interactions. The influence of process parameters namely temperature difference i.e. ΔT_{MOC} and solution flow rate were additionally important in influencing fouling behaviour models via factor-factor interactions. The importance of solute and solvent parameters upon fouling was also underlined, albeit to a lesser extent as detailed by effects

contributions, with a number of shape and interaction descriptors included in Table 8.6. Mechanistically the C-FAP was designed to investigate surface induced fouling via nucleation and crystal growth on the probed MOC coupon. Therefore, explored system parameters can potentially be related to mechanisms of surface nucleation and subsequent growth.

Table 8.6: The top 10 greatest factors and factor interactions contributing towards each fouling response model. Effects contributions for each generated detailed within square brackets.

Top 10 factors/interactions influencing model	Fouling induction time	Mass deposition after 24 hours post nucleation	Maximum area coverage rate
1	$C_p * \Delta T_{MOC}$ [1.05]	$C_p * \Delta T_{MOC}$ [277.2]	$\lambda * \Delta T_{MOC}$ [0.95]
2	$\lambda * \Delta T_{MOC}$ [0.94]	$\lambda * \Delta T_{MOC}$ [185.15]	$C_p * \Delta T_{MOC}$ [0.78]
3	$\gamma_S * \Delta T_{MOC}$ [0.39]	$\gamma_S * \Delta T_{MOC}$ [145]	$\gamma_S * \Delta T_{MOC}$ [0.44]
4	$E * \Delta T_{MOC}$ [0.38]	$E * \Delta T_{MOC}$ [91.2]	$E * \Delta T_{MOC}$ [0.23]
5	flow rate * C_p [0.35]	flow rate * γ_S [57.41]	flow rate * C_p [0.2]
6	$\lambda * v_{sa_hyd}$ [0.34]	flow rate * C_p [53.14]	flow rate * γ_S [0.19]
7	$\lambda * LIQASA$ [0.34]	flow rate * Ra [47.12]	ΔT_{MOC} [0.19]
8	$\lambda * Svdw_vol$ [0.32]	$\Delta T_{MOC} * a_donacc$ [45.87]	flow rate * density [0.19]
9	$\lambda * Sapol$ [0.31]	$\Delta T_{MOC} * flow\ rate$ [43.1]	flow rate * Ra [0.18]
10	$\lambda * ASA$ [0.31]	ΔT_{MOC} [42.74]	$\Delta T_{MOC} * flow\ rate$ [0.18]

In this chapter, the generation of local supersaturation was essential to induce nucleation on the MOC surface via local cooling. The influence of ΔT_{MOC} was expected to impact fouling behaviour since altering the temperature difference would directly influence the local supersaturation at the MOC/solution interface. This has been demonstrated by Pääkkönen et al. in which the calcium carbonate deposition rate increased with increasing temperature differences across the heat transfer surface.¹³³ The influence of flow rate on fouling behaviour was not predicted to be considerable as explored rates did not differ greatly. However the influence of flow rate was deemed to be an important model term. Research by Bogacz and co-workers found that the mass of magnesium sulphate heptahydrate fouling within a flow cell increased with increasing flow rate from 500 ml/min to 1500 ml/min.¹⁰⁵ It can be established that temperature difference and flow rate are key to controlling fouling behaviour notably in influencing the initiation and progression of surface induced fouling.

Additionally each model was strongly influenced by a variety of MOC properties. It is acknowledged that the surface energy of a MOC influences nucleation upon its surface as described by Equation 1.15, Equation 1.16 and Equation 1.17. Work by Geddert and co-workers explored MOCs with various surface energy values and their relation with fouling induction time in which no distinct relationship is observed.⁹ A similar result is observed by Bohnet et al.²⁹² The surface energy of a MOC can effect further deposition and growth processes after nucleation as described by Zhao and co-workers¹⁰⁶ and Al-Janabi et al.²⁹³ for mass deposition and heat transfer fouling rate, respectively. Its role within the generated models is therefore expected. MOC thermal properties such as thermal conductivity and specific heat capacity were expected to influence fouling responses as the investigated fouling process requires sufficient heat transfer to create supersaturation. The role of Young's modulus in influencing generated model was highlighted in Table 8.6. Young's modulus has been involved in a fouling adhesive strength model underlined by Wu.⁹³ However, Young's modulus has not been researched extensively and its mechanistic role in fouling is not known. Remarkably surface roughness

was not considered an important MOC descriptor in influencing fouling response models. One major finding for all models was the absence of roughness effects upon fouling behaviour. It was anticipated MOCs with increasing Ra would increase fouling behaviour i.e. lower induction times, larger growth rate and larger fouled mass primarily. There is abundant research describing the influence of surface roughness upon fouling.^{104-105,117,294} Recent work by Bogacz found that the fouling mass of magnesium sulphate heptahydrate increased with increasing Ra surface roughness with larger effective contact area and more available nucleation sites proposed explanations for this effect.¹⁰⁵ These effects were not found within this work.

The role of solute and solvent descriptors are also shown to be influential in the model. The important solute properties include (i) Approximation to the sum of VDW surface areas of polar atoms (ii) Water accessible surface area (iii) Sum of the atomic polarizabilities. The important solvent properties include number of hydrogen bond donators and van der Waals volume but does not provide important relationships.

8.3.3.2 Validation of model

Although fouling behaviour models generated were not anticipated to be sufficiently accurate, each model's validity was assessed. To assess the validity of generated models both internal and external validations were conducted. Internal validations were performed using conditions which have not been previously conducted within the original experimental design and assessing fouling measurements against predictions via MODDE (UMetrics). An external validation was performed by using a different crystallising system namely CBZ in IPA for several experimental conditions. CBZ and IPA were assumed to be within the original design space therefore applicable to be used as a validation system.

(a) ***Internal validation***

Details of experimental conditions and experimental results with predictions are displayed in Table 8.5. Comparison between the determined and predicted results yielded wide differences in values. This was to be expected for a screening type model. However, generated models yielded some value in predicting the extent of each fouling response rather than accurate predictions. Table 8.7 revealed the ranking order for both experimental and model datasets i.e. smallest to largest value in which comparisons revealed a degree of ranking order prediction. This was shown for induction time datasets however some variation was identified for the other two fouling responses. The limited quantitative prediction capability for each model was validated by respective Q^2 values (see Figure 8.12). A more detailed DOE approach would be necessary for a quantitative prediction model.

(b) ***External validation***

Details of experimental conditions, experimental results and predictions for the external validation are detailed in Table 8.6. Similar to the internal validation, comparisons between the experimentally determined results and predictions vary quite considerably in particular when predicting fouling induction times. The ranking order was also detailed in Table 8.8 in which a similar outcome to Table 8.7 was found with ranking order prediction was demonstrated for induction time datasets.

(c) ***Assessment of model's validation***

Both methods of validation revealed the quantitative predictive capabilities of each fouling response model was poor with magnitudes of difference between predictions and real data identified. However, each model's predictive capabilities do provide an estimate in ranking order for each fouling response which has never been conducted previously. The predictive ranking order capability was validated successfully for predicting induction time order.

Further work in this area is essential to generate a reliable model for qualitative values. In particular the importance of replicates needs to be considered since crystallisation events notably nucleation are highly unpredictable and values can vary drastically. Conducting replicates will enhance the statistics surrounding a DOE approach.

Table 8.7: Internal validation experiments including determined and predicted fouling measurements. Ranking order from smallest to largest value ranged from 1 to 5 within square brackets.

Investigated system	Solution flow rate (ml/min)	ΔT_{MOC} (°C)	Induction time (mins)	Model induction time (mins)	Mass after 24 hours (mg)	Model mass after 24 hours (mg)	Maximum growth rate (mm ² /min)	Model maximum growth rate (mm ² /min)
SiC/PCM_water	100	27	405 [5]	159.7 [5]	472 [4]	459.9 [4]	0.33 [1]	2.23 [3]
SS 316 280G/AA_1-butanol	100	39.5	9 [1]	2 [1]	684.1 [5]	611.1 [5]	6.05 [5]	14.32 [5]
PEEK/AA_1-butanol	50	39.5	52 [4]	96.8 [4]	412.1 [2]	183 [1]	0.55 [2]	0.28 [1]
SS 316 EP/LOV_MIBK	100	27	16 [2]	14.1 [2]	468.4 [3]	271 [2]	1.65 [4]	0.65 [2]
Borosilicate/LOV_MIBK	50	34.5	37 [3]	41.6 [3]	196.4 [1]	411.2 [3]	1.09 [3]	3 [4]

Table 8.8: External validation experiments including determined and predicted fouling measurements. Rank order from smallest to largest value ranged from 1 to 5 within square bracket.

Investigated system	Solution flow rate (ml/min)	ΔT_{MOC} (°C)	Induction time (mins)	Model induction time (mins)	Mass after 24 hours (mg)	Model mass after 24 hours (mg)	Maximum growth rate (mm ² /min)	Model maximum growth rate (mm ² /min)
C276 AS REC/CBZ_IPA	100	39.5	4 [1]	5.5 [1]	217.6 [2]	598.3 [3]	2.41 [3]	3.04 [2]
PEEK/CBZ_IPA	50	39.5	165 [3]	2631 [3]	135.1 [1]	351.4 [1]	1.12 [1]	0.01 [1]
Quartz/CBZ_IPA	100	34.5	51 [2]	17.1 [2]	246.1 [3]	450.5 [2]	2.21 [2]	4.12 [3]

8.3.4 Definitive fouling outcome model

In addition to modelling fouling responses and fouling behaviour, a model was created to determine which factors or factor interactions are important in influencing the definitive fouling outcome i.e. whether fouling occurs or does not develop. Data detailed in Table 8.5 was employed in which experiments with fouling responses were labelled 1 and non-fouling experiments were labelled 0 (i.e. Experiments 2, 3, 12, 13 and 20). The model was fitted using experimental data and fitted with PLS. The summary of fit plot is shown in Figure 8.14 in which R^2 and reproducibility statistics were excellent. Q^2 statistics were acceptable since difference between R^2 and Q^2 is less than 0.3 (see 3.2.2.2 DOE).

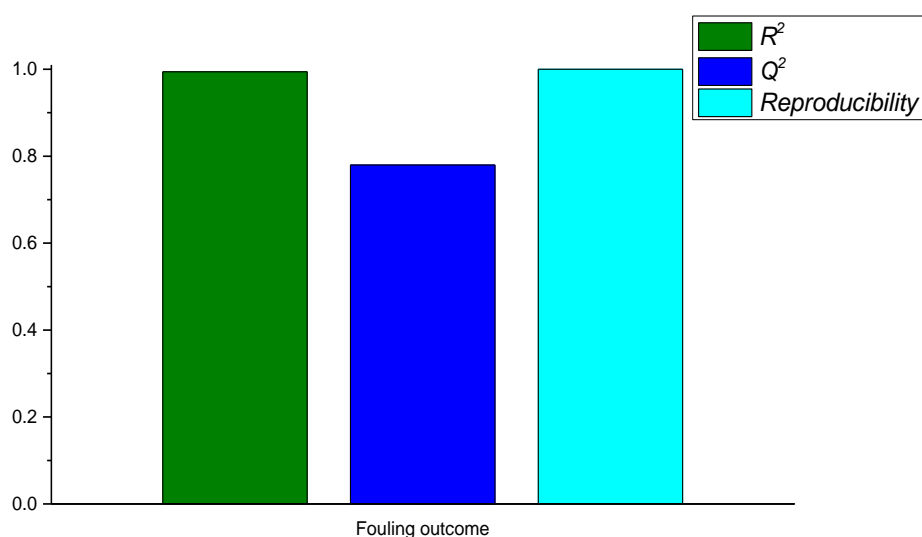


Figure 8.14: Summary of fit plot for the definitive fouling outcome model.

In contrast to the 10 most influences for fouling responses, the definitive fouling outcome model consisted of a variety of different influential parameters including MOC and solute properties. However one notable difference is the water contact angle contribution towards the model. The hydrophilicity of MOCs are considered to be important in influencing whether fouling occurs or

doesn't occur. Another MOC property which is deemed to impact this model considerably is thermal conductivity which is to be expected. Similar to generated fouling response models, surface roughness was not considered an important descriptor in influencing fouling propensity. One major difference is the influence of solute properties compared to fouling outcome models which were dominated by MOC properties and process parameters. Solute descriptors which were deemed to be important including overall molecule charge, Van der Waals surface area associated with polar atoms, aqueous solubility and hydrogen bonding acceptors and donators.

Table 8.9: Top 10 factors and factor interactions contributing towards definitive fouling outcome. Effects contributions for each generated model within square brackets.

Top 10 factors/interactions influencing model	Fouling outcome
1	$\lambda * C_p$ [0.29]
2	$\Delta T_{MOC} * \theta$ [0.18]
3	$\lambda * \Delta T_{MOC}$ [0.14]
4	$\Delta T_{MOC} * \gamma_S$ [0.12]
5	$\theta * a_{donacc}$ [0.09]
6	$\theta * Fcharge$ [0.09]
7	$\lambda * vsa_{pol}$ [0.09]
8	E [0.08]
9	$\theta * vsa_{pol}$ [0.07]
10	$\Delta T_{MOC} * a_{donacc}$ [0.07]

8.4 Summary

The purpose of the present research was to determine which parameters influence surface induced crystallisation fouling within the C-FAP for various pharmaceutically relevant systems. This was achieved by generating a number of models via three main groups of parameters: solution properties, process parameters and MOC properties. Each parameter was represented by a number of relevant descriptors. Two distinct types of fouling model were generated specifically fouling behaviour models and a definitive fouling outcome model from, for which each model, the largest contributions can be determined.

The generated fouling behaviour models all had similar factor and factor-factor interaction contributions. The most important contributions to all models consisted of MOC properties e.g. surface energy, thermal conductivity, specific heat capacity and Young's modulus in addition to process parameters such as ΔT_{MOC} and solution flow rate. Surface roughness was not considered to have a considerable effect upon fouling behaviour models. Secondly, the influence solution properties have a considerable contribution to the model however MOC properties and process parameters have the greatest impact as identified from the effects plot scores.

Efforts were made to validate the generated fouling behaviour models using internal and external validations. Comparison between experimentally determined and validation quantitative fouling behaviour results vary considerably highlighting poor prediction capability. However, predicting ranking order for a series of quantitative fouling behaviour data was shown to be useful notably for predicting the order for induction time values. Ordering rank prediction results provide a quick assessment of fouling behaviour which can be applied to within the PCA design space. Fouling behaviour models could be enhanced by conducting a more detailed DOE approach in addition to conducting replicates.

Creation of a definitive fouling outcome model was attempted within this chapter. The notion behind the proposed model is to determine which parameters are associated with the initiation of fouling. Similar to the fouling behaviour models, the prediction statistics of the definitive fouling outcome model are acceptable. The most influential parameters to influence whether fouling occurs or does not occur comprises MOC properties such as water contact angle, thermal conductivity, surface energy, specific heat capacity and Young's modulus), process parameters (ΔT_{MOC}) and solute properties. The influential parameters differ to fouling behaviour models. The solute properties contributing to the model included the charge, polar surface area, hydrogen bonding acceptors and donators and compound solubility. In terms of surface induced nucleation and growth, the induction is reliant upon the MOC properties, process parameters and notably the solute properties.

The notion of having modelling capabilities to describe fouling is highly desirable as a means to predict fouling propensity and behaviours. At present little modelling research has been conducted describing fouling. Fouling terms have been included into crystallisation models as a means to predict its impact on an element of a crystallisation process such as PSD. The models described within the generated models were practical however could be significantly improved. No other research has encompassed MOC properties, solution properties and process parameters to generate novel fouling models. As detailed earlier all fouling models could be enhanced by conducting a more detailed DOE study to obtain more accurate predictions. Additionally incorporating specific descriptors describing solution concentrations would be advantageous in addition to ensuring all explored MOCs were of equivalent thickness which was not achieved herein.

Chapter 9. Conclusions and future work

9.1 Summary of thesis

The basis of this thesis was to enhance understanding of fouling within crystallisation processes notably in relation to continuous crystallisation. A variety of experimental approaches were conducted to probe fouling and associated mechanisms. The principal research parameter investigated to further fouling understanding was different MOCs and their inherent properties. A variety of MOCs employed for chemical processing equipment were investigated and characterised in the generation of a novel MOC characterisation dataset. PCA highlighted the MOCs in the characterisation dataset presented a reasonably diverse set suited for subsequent fouling experiments (Chapter 4). The MOC PCA plot would be of interest for manufacturing industries as a tool to compare different MOC to drive materials development and also for comparing different material properties within the dataset. Two MOCs which were identified as distinctly different were stainless steel and PTFE which were subsequently probed in further detail in Chapters 5 and 7. All MOCs were investigated within Chapter 8 to assess the range of behaviours they display.

Chapter 5 investigated stainless steel and PTFE under selected process parameters looking at both nucleation and fouling of paracetamol in water solution within a small scale batch crystallisation setup. Nucleation studies found supersaturation had a significant influence upon induction time using the Kruskal-Wallis statistical test. However agitation and MOCs were deemed not to have a significant effect on bulk nucleation induction time. Distinct differences in nucleation rate were identified for different supersaturations and agitation rates whilst MOC properties had a limited effect. Surface nucleation was not identified under these conditions and bulk nucleation was the dominant nucleation process. The prominent fouling mechanism was shown to be particle deposition which was influenced by explored process parameters. In contrast to the influence of MOC on nucleation, considerable differences were identified between stainless steel and PTFE in which fouling was more prominent for steel under identical conditions. The importance of

MOC properties was demonstrated for particle fouling within Chapter 5 in terms of mass deposition and area coverage. Although this work focused on batch crystallisation, learning can be applied to other crystallisation methods i.e. where there is the presence of an agitated suspension. The MOC coupons can be related to projections within a crystallising system such as the introduction of PAT probes, baffles, connections, temperature probes etc. in particular for continuous crystalliser equipment (Figure 9.1). The present experimental set-up can probe particle deposition and potentially surface nucleation on different MOCs or coated MOCs which could be used in the construction of PAT probes or baffles from which different crystallising solutions and fouling behaviour can be evaluated. A fouling model for each fouling response was generated in which its predictive capabilities were validated. The application of these models can direct the selection of operational conditions to minimise fouling.



Figure 9.1: Significant fouling present upon the casing of an FBRM probe which had been introduced into a crystallising system.

The assessment of fouling within continuous flow was targeted to resemble conditions within a continuous crystalliser. No commercially available assessment setup was available. Therefore, a fouling assessment platform was designed in conjunction with CRD by developing their Zebrafish platform (Chapter 6). The C-FAP was specifically designed to detect and monitor fouling via imaging and temperature measurements. MOCs could be investigated within a bespoke flow cell where fouling was induced by a cold stream at the rear of the MOC substrate. Within the C-FAP fouling could be probed by exploring different process parameters, solutions and MOC properties highlighting its potential as a tool to evaluate fouling due to cold induction.

The use of the C-FAP as a fouling assessment platform was demonstrated within Chapter 7. PCM in water solution was explored as the initial assessment system in addition to exploring stainless steel and PTFE which were explored within Chapter 5. In comparison to Chapter 5, cold induction was used to induce fouling and subsequent growth. Fouling was assessed by determining fouling induction time and fouling growth kinetics by imaging and determining fouling resistance via temperature. The application of the fouling resistance method was not sufficiently sensitive to reliably detect fouling. Chapter 7 highlighted different MOCs, process parameters and degree of supersaturation all had considerable influence on fouling induction time and kinetics. The application of fouling resistance within the C-FAP would require substantial fouling deposits to effect heat transfer therefore limiting its application to early detection. Chapter 7 compared MOCs against each other to inform crystallisation process design e.g. construction material of crystalliser and components. Future operation design of the C-FAP was influenced by the use of supersaturated solutions within Chapter 7 which eventually led to unstable operation. This identified optimal operating ranges for the C-FAP and the use of undersaturated feed solutions to allow stable operation.

Chapter 8 utilises the C-FAP to explore a wide range of MOC, solution and process parameters upon fouling induction time, mass deposition and

maximum area coverage growth rate. The intention of this chapter was to determine the most influential parameters for each fouling response. A reduced combinatorial experimental design was used to obtain a fouling dataset from which fouling models were generated. A range of pharmaceutically relevant solutes and solvents were used to create the predictive models. MOCs, solutes and solvents were described in terms of chemoinformatic and measured descriptors. The most influential parameters governing each fouling response model comprised MOC descriptors such as surface energy and thermal conductivity in addition to process parameters including ΔT_{MOC} and flow rate. Solution properties were also identified to influence each fouling response model. In addition each fouling response model was tested against internal and external validations from which accurate quantitative predictions were not found. However, generated models provided some predictive capabilities notably in comparing investigated systems via ordering rank. This provides an opportunity for direct comparisons between two crystallising systems. Further work in developing each model would provide an excellent resource to assess fouling behaviour of a system within the designated design space. In addition to generated fouling response models, a definitive fouling outcome model was attempted to define what parameters dictate the occurrence of fouling. MOC properties, notably water contact angle, in addition to process parameters were identified to be important measures consistent with CNT. The influence of solute properties was also highlighted. Further development of accurate predictive models for fouling initiation and behaviour would provide an excellent resource in process design.

Throughout all experimental chapters, the importance of MOC properties was demonstrated to influence fouling considerably for different fouling mechanisms. MOCs had not previously been researched extensively with respect to organic crystallisation fouling however they have a significant role. The impact of process conditions, as anticipated, greatly influenced fouling mechanisms. A summary is illustrated in Figure 9.2.

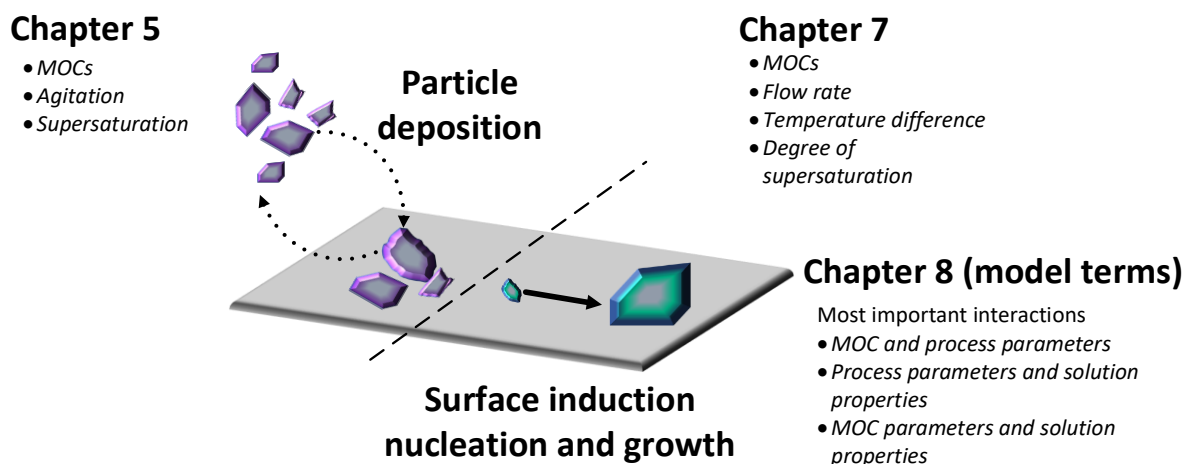


Figure 9.2: Summary of crystallisation fouling processes investigated within this thesis with explored factors identified to influence respective mechanisms.

9.2 Recommendations and future work

A number of approaches were undertaken to investigate fouling and fouling mechanisms leading to a variety of recommendations. In addition to these recommendations relating to the use of fouling assessment approaches, future work to further enhance fouling understanding has also been proposed. Based upon the current fouling assessment approaches a number of recommendations to their use were proposed (Figure 9.3) including a specific fouling assessment framework or workflows.

The initial recommendation involves the use of fouling models as a means to predict fouling behaviour in addition to predicting whether fouling will occur for a specific design space. The current models provide some insight into the rank order of importance however are not quantitatively accurate. The order ranking allows comparisons between different crystallising systems to be conducted. Further work notably in terms of experimental design and replicates would provide improved and more extensive fouling models. Predicting the fouling behaviour of a crystallising system could considerably reduce the reliance of empirical fouling experimental methods saving time and resources. There is a need to improve production processes within the pharmaceutical sector with financial and resource constraints.²⁹⁵

Once the likely fouling tendencies of a system has been predicted, it is recommended that crystallising solution is investigated with a variety of MOCs using process conditions which are typical within a batch process or temperature ranges likely to be relevant to a continuous crystallisation campaign. The use of the small scale batch crystallisation setup (Chapter 5) provides a rapid assessment opportunity for particle deposition i.e. from particles suspended in solution to deposition onto the surface. The small scale batch crystallisation setup would be particular useful for investigating MOCs involved in the fabrication of probes including temperature probes and PAT probes. It could be beneficial to assess fouling behaviour of any MOC projection within a crystallising system in which a temperature difference is not present across the MOC. The use of this assessment approach is highly recommended regardless of which crystallisation method is selected to evaluate particle deposition. At present the C-FAP does not explore particle deposition therefore the application of the small scale batch crystallisation setup is valid.

Next the crystallising solution of interest and selected MOCs should be assessed within the C-FAP. Using the C-FAP as currently configured for fouling evaluation provides detail on surface induction which would potentially be experienced within a continuous crystalliser. The C-FAP's flow cell could potentially be modified to allow particle suspensions to be explored which is more representative within a crystalliser. Establishing results from the C-FAP in relation to what is observed within a continuous crystalliser would be advantageous.

The combination of all approaches provides a systematic framework for evaluating the fouling propensity and behaviour of a crystallising solution. Additionally directly assessing different MOCs and process conditions will provide indications for subsequent crystallisation campaigns i.e. to steer the selection of materials and conditions to avoid. Additionally, further development to enable minimalisation, parallelisation and/or automation of these experimental methods would be ideal.²⁹⁶

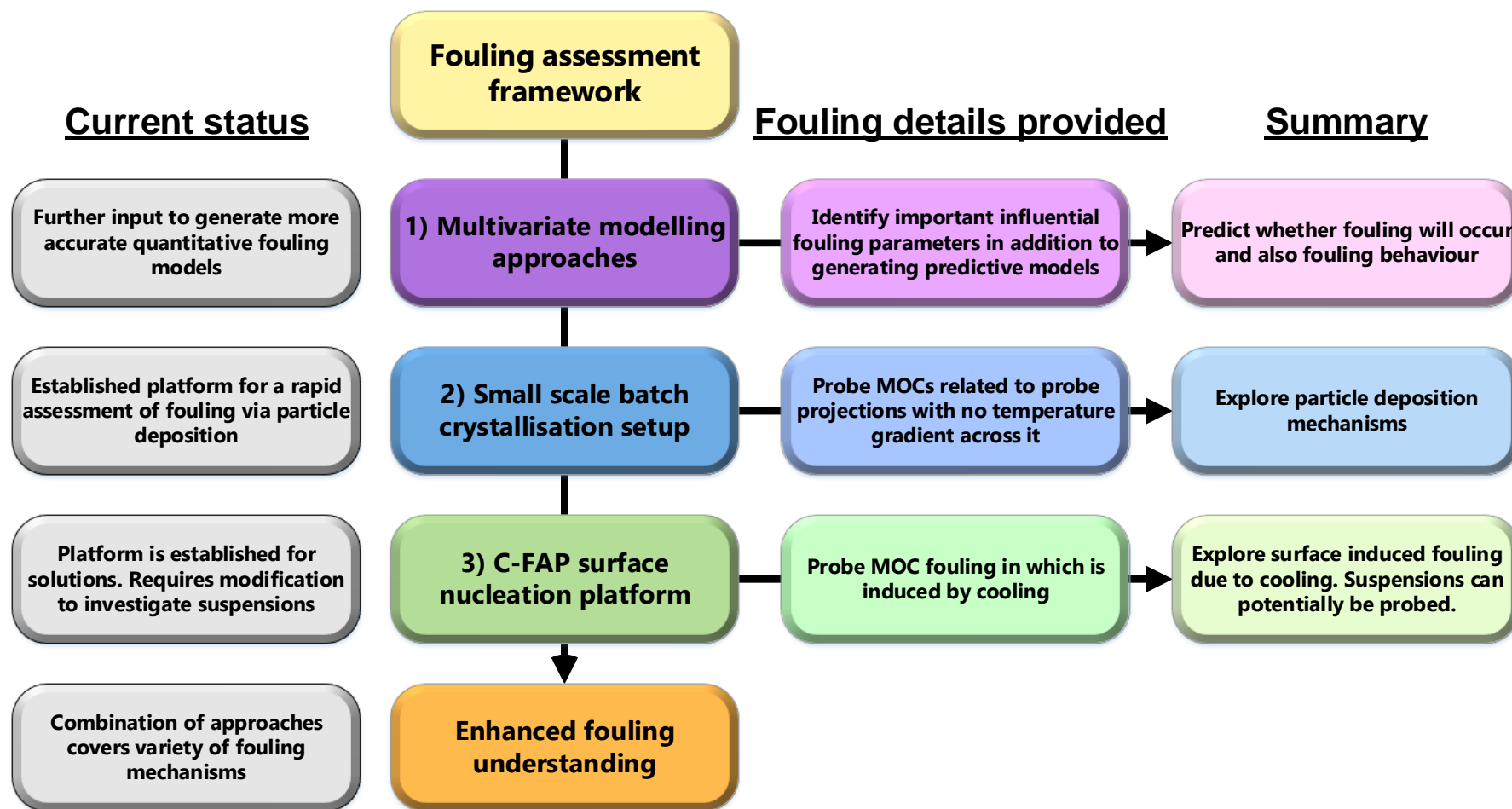


Figure 9.3: Schematic diagram highlighting the sequential approach for further fouling investigations.

The application of each fouling assessment method provides fouling information specific for each setup. The relationship between each setup and a real continuous crystallisation campaign was not established i.e. correlating assessment data to fouling within a continuous crystallisation (Figure 9.4).

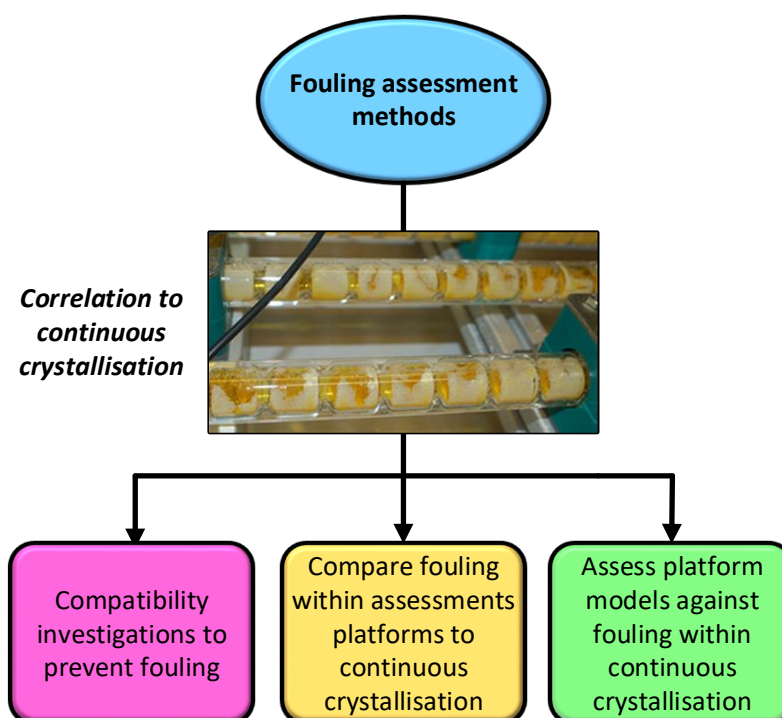


Figure 9.4: Establishing the relationship between fouling assessment methods to true results within a continuous crystallisation campaign.

Within this work, different MOCs were explored individually i.e. one MOC coupon explored at one given time. Within a crystallisation campaign, a crystallising solution is in constant contact with a number of MOCs which were performing various roles such as agitation, heat transfer or crystalliser structure. Research by Briggs experienced fouling during the continuous crystallisation of L-glutamic acid. It was found L-glutamic acid fouling was coordinated, as shown in Figure 9.5, in which fouling was present predominately on the stainless steel temperature probe with its presence yet fouling dominates upon the glass heat transfer surface in the temperature probes absence.²⁹⁷

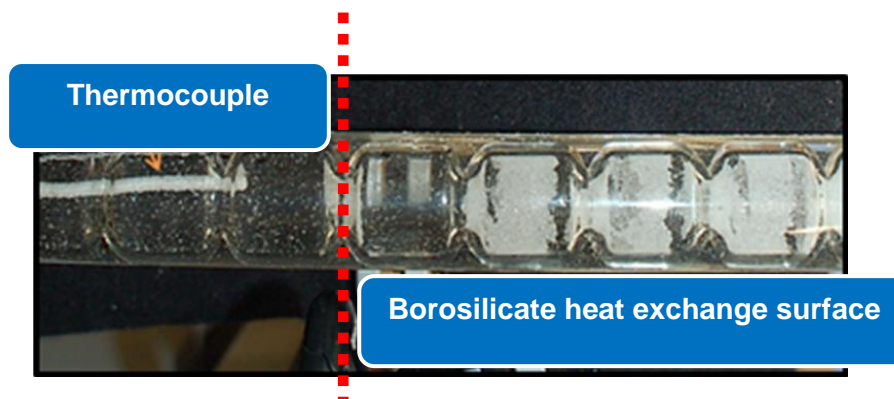


Figure 9.5: L-glutamic acid fouling encrustation along a COBC straight with flow direction left to right. Preferential fouling occurs upon the stainless steel thermocouple rather than the glass heat transfer surface whilst locations where the thermocouple is not present fouling on the vessel walls was dominant.²⁹⁷

In addition to exploring current fouling evaluation approaches detailed herein other methods would provide valuable insight into fouling and fouling mechanisms. One notable approach is the use of quartz crystal microbalance (QCM) as a tool to enhance understanding of fouling mechanisms in particular related to continuous crystallisation. The use of QCM as a tool to investigate fouling has been demonstrated by various authors in particular for surface induced crystallisation for inorganic systems.^{147,149,298} Additionally the deposition and interaction of organic molecules from solution with the QCM surface has also been confirmed by Murray and Deshares.²⁹⁹ The prospect of employing the QCM for enhancing fouling understanding and would be an excellent tool for probing mechanisms. QCM approaches can also investigate different MOCs^{149,299} and process conditions^{147,298} highlighting its potential application to study fouling in relation to previously investigated parameters. QCM is an extremely sensitive method in which can identify the first stages of fouling initiation in which enhanced insight into mechanistic processes can be obtained.^{147,300} The combination of the C-FAP and a QCM is possible in which a similar setup was employed by Lapidot using a bespoke flow cell.^{147,301}

In terms of modelling a number of additional approaches could be performed in addition to improving overall number of experiments via more robust experimental design. The application of ANN has been applied to a number of crystallisation aspects notably fouling. Biyanto demonstrated the use of ANN to predict fouling resistance using process and fluid parameters as model

terms.³⁰² Applying ANN to generated fouling result dataset may yield models with greater predictive capabilities.

A workflow approach to successfully conduct a continuous crystallisation campaign was demonstrated by Brown and co-workers (Figure 9.6). Stage 5 of this systematic approach involves evaluating a solution's crystallisation behaviour including nucleation, agglomeration and, notably, fouling. The application of fouling experimental approaches for assessment detailed within this thesis provide a useful methodology for use within this crystallisation workflow.³⁰³

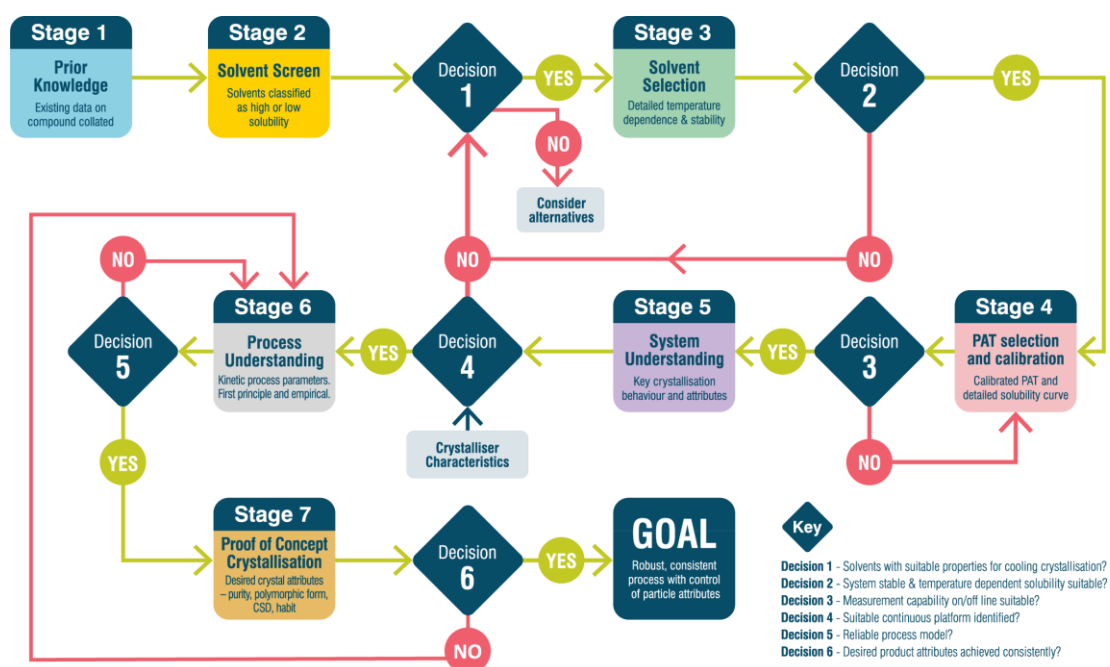


Figure 9.6: Workflow for continuous seeded crystallisation in which fouling propensity and behaviour assessments occur within stage 5.³⁰³

Chapter 10. References

1. Su, Q.; Nagy, Z. K.; Rielly, C. D., Pharmaceutical crystallisation processes from batch to continuous operation using msmpr stages: Modelling, design, and control. *Chemical Engineering and Processing: Process Intensification* **2015**, *89*, 41-53.
2. Beckmann, W., *Crystallization: Basic concepts and industrial applications*. John Wiley & Sons: Weinheim, **2013**.
3. Thirunahari, S.; Chow, P. S.; Tan, R. B., Quality by design (qbd)-based crystallization process development for the polymorphic drug tolbutamide. *Crystal Growth & Design* **2011**, *11* (7), 3027-3038.
4. Lionberger, R. A.; Lee, S. L.; Lee, L.; Raw, A.; Yu, L. X., Quality by design: Concepts for andas. *The AAPS Journal* **2008**, *10* (2), 268-276.
5. Singh, R.; Ierapetritou, M.; Ramachandran, R., An engineering study on the enhanced control and operation of continuous manufacturing of pharmaceutical tablets via roller compaction. *International Journal of Pharmaceutics* **2012**, *438* (1–2), 307-326.
6. Mullin, J. W., *Crystallization*. Elsevier Science: Oxford, **2001**.
7. Vendel, M.; Rasmuson, Å. C., Mechanisms of initiation of incrustation. *AIChE Journal* **1997**, *43* (5), 1300-1308.
8. Majumder, A.; Nagy, Z. K., Dynamic modeling of encrust formation and mitigation strategy in a continuous plug flow crystallizer. *Crystal Growth & Design* **2015**, *15* (3), 1129-1140.
9. Geddert, T.; Augustin, W.; Scholl, S., Induction time in crystallization fouling on heat transfer surfaces. *Chemical Engineering & Technology* **2011**, *34* (8), 1303-1310.
10. Kho, T.; Muller-Steinhagen, H., An experimental and numerical investigation of heat transfer fouling and fluid flow in flat plate heat exchangers. *Chemical Engineering Research & Design* **1999**, *77* (A2), 124-130.
11. Lei, C.; Peng, Z.; Day, T.; Yan, X.; Bai, X.; Yuan, C., Experimental observation of surface morphology effect on crystallization fouling in

plate heat exchangers. *International Communications in Heat and Mass Transfer* **2011**, 38 (1), 25-30.

12. Vendel, M.; Rasmuson, Å. C., Initiation of incrustation by crystal collision. *Chemical Engineering Research and Design* **2000**, 78 (5), 749-755.
13. Briarçon, S.; Colson, D.; Klein, J., Experimental study and theoretical approach of cooling surfaces fouling in industrial crystallizers. *Chemical Engineering Research and Design* **1997**, 75 (2), 147-151.
14. Narducci, O.; Jones, A. G.; Kougoulos, E., Continuous crystallization of adipic acid with ultrasound. *Chemical Engineering Science* **2011**, 66 (6), 1069-1076.
15. Nývlt, J.; Veverka, F., Scale formation on cooling surfaces in crystallizers. *Crystal Research and Technology* **1997**, 32 (6), 773-781.
16. Melo, L.; Bott, T. R.; Bernardo, C., *Fouling science and technology*. Springer Science & Business Media: Dordrecht, **2012**; Vol. 145.
17. Awad, M. M., *Fouling of heat transfer surfaces*. INTECH Open Access Publisher: **2011**.
18. Briggs, N. E. B.; Schacht, U.; Raval, V.; McGlone, T.; Sefcik, J.; Florence, A. J., Seeded crystallization of β -l-glutamic acid in a continuous oscillatory baffled crystallizer. *Organic Process Research & Development* **2015**, 19 (12), 1903-1911.
19. Bott, T. R., Aspects of crystallization fouling. *Experimental Thermal and Fluid Science* **1997**, 14 (4), 356-360.
20. Kazi, S. N.; Teng, K. H.; Zakaria, M. S.; Sadeghinezhad, E.; Bakar, M. A., Study of mineral fouling mitigation on heat exchanger surface. *Desalination* **2015**, 367, 248-254.
21. Forster, M.; Augustin, W.; Bohnet, M., Influence of the adhesion force crystal/heat exchanger surface on fouling mitigation. *Chemical Engineering and Processing* **1999**, 38 (4), 449-461.

22. Rankin, B. H.; Adamson, W. L., Scale formation as related to evaporator surface conditions. *Desalination* **1973**, *13* (1), 63-87.
23. Mitchell, C. A.; Yu, L.; Ward, M. D., Selective nucleation and discovery of organic polymorphs through epitaxy with single crystal substrates. *Journal of the American Chemical Society* **2001**, *123* (44), 10830-10839.
24. Parambil, J. V.; Poornachary, S. K.; Tan, R. B. H.; Heng, J. Y. Y., Template-induced polymorphic selectivity: The effects of surface chemistry and solute concentration on carbamazepine crystallisation. *CrystEngComm* **2014**, *16* (23), 4927-4930.
25. Ng, Y. C.; Yang, Z.; McAuley, W. J.; Qi, S., Stabilisation of amorphous drugs under high humidity using pharmaceutical thin films. *European Journal of Pharmaceutics and Biopharmaceutics* **2013**, *84* (3), 555-565.
26. Baxendale, I. R.; Braatz, R. D.; Hodnett, B. K.; Jensen, K. F.; Johnson, M. D.; Sharratt, P.; Sherlock, J.-P.; Florence, A. J., Achieving continuous manufacturing: Technologies and approaches for synthesis, workup, and isolation of drug substance. May 20–21, 2014 continuous manufacturing symposium. *Journal of Pharmaceutical Sciences* **2015**, *104* (3), 781-791.
27. Mascia, S.; Heider, P. L.; Zhang, H.; Lakerveld, R.; Benyahia, B.; Barton, P. I.; Braatz, R. D.; Cooney, C. L.; Evans, J. M. B.; Jamison, T. F.; Jensen, K. F.; Myerson, A. S.; Trout, B. L., End-to-end continuous manufacturing of pharmaceuticals: Integrated synthesis, purification, and final dosage formation. *Angewandte Chemie International Edition* **2013**, *52* (47), 12359-12363.
28. Zettler, H. U.; Weiss, M.; Zhao, Q.; Muller-Steinhagen, H., Influence of surface properties and characteristics on fouling in plate heat exchangers. *Heat Transfer Engineering* **2005**, *26* (2), 3-17.
29. Fujiwara, M.; Nagy, Z. K.; Chew, J. W.; Braatz, R. D., First-principles and direct design approaches for the control of pharmaceutical crystallization. *Journal of Process Control* **2005**, *15* (5), 493-504.
30. Arnum, P.; Whitworth, R., Continuous progress in continuous manufacturing. *Pharmaceutical Technology* **2011**, *35* (9).

31. Byrn, S.; Futran, M.; Thomas, H.; Jayjock, E.; Maron, N.; Meyer, R. F.; Myerson, A. S.; Thien, M. P.; Trout, B. L., Achieving continuous manufacturing for final dosage formation: Challenges and how to meet them may 20–21 2014 continuous manufacturing symposium. *Journal of Pharmaceutical Sciences* **2015**, *104* (3), 792-802.
32. Plumb, K., Continuous processing in the pharmaceutical industry: Changing the mind set. *Chemical Engineering Research and Design* **2005**, *83* (6), 730-738.
33. Griffin, D. W.; Mellichamp, D. A.; Doherty, M. F., Reducing the mean size of api crystals by continuous manufacturing with product classification and recycle. *Chemical Engineering Science* **2010**, *65* (21), 5770-5780.
34. Cruz, P.; Rocha, F.; Ferreira, A., Effect of operating conditions on batch and continuous paracetamol crystallization in an oscillatory flow mesoreactor. *CrystEngComm* **2016**, *18* (47), 9113-9121.
35. Boukerche, M.; Mangin, D.; Klein, J. P.; Monnier, O.; Hoff, C., Inducing the stable polymorph using heterogeneous primary nucleation. *Chemical Engineering Research and Design* **2010**, *88* (11), 1474-1478.
36. Roberge, D. M.; Zimmermann, B.; Rainone, F.; Gottsponer, M.; Eyholzer, M.; Kockmann, N., Microreactor technology and continuous processes in the fine chemical and pharmaceutical industry: Is the revolution underway? *Organic Process Research & Development* **2008**, *12* (5), 905-910.
37. Crowley, M. M.; Zhang, F.; Repka, M. A.; Thumma, S.; Upadhye, S. B.; Kumar Battu, S.; McGinity, J. W.; Martin, C., Pharmaceutical applications of hot-melt extrusion: Part i. *Drug Development and Industrial Pharmacy* **2007**, *33* (9), 909-926.
38. Houson, I., *Process understanding: For scale-up and manufacture of active ingredients*. John Wiley & Sons: Weinheim, **2011**.
39. Calabrese, G. S.; Pissavini, S., From batch to continuous flow processing in chemicals manufacturing. *AIChE Journal* **2011**, *57* (4), 828-834.

40. Anderson, N. G., Practical use of continuous processing in developing and scaling up laboratory processes. *Organic Process Research & Development* **2001**, 5 (6), 613-621.
41. Schaber, S. D.; Gerogiorgis, D. I.; Ramachandran, R.; Evans, J. M. B.; Barton, P. I.; Trout, B. L., Economic analysis of integrated continuous and batch pharmaceutical manufacturing: A case study. *Industrial & Engineering Chemistry Research* **2011**, 50 (17), 10083-10092.
42. Teoh, S. K.; Rathi, C.; Sharratt, P., Practical assessment methodology for converting fine chemicals processes from batch to continuous. *Organic Process Research & Development* **2016**, 20 (2), 414-431.
43. Zhang, H.; Lakerveld, R.; Heider, P. L.; Tao, M.; Su, M.; Testa, C. J.; D'Antonio, A. N.; Barton, P. I.; Braatz, R. D.; Trout, B. L.; Myerson, A. S.; Jensen, K. F.; Evans, J. M. B., Application of continuous crystallization in an integrated continuous pharmaceutical pilot plant. *Crystal Growth & Design* **2014**, 14 (5), 2148-2157.
44. Lee, S. L.; O'Connor, T. F.; Yang, X.; Cruz, C. N.; Chatterjee, S.; Madurawe, R. D.; Moore, C. M. V.; Yu, L. X.; Woodcock, J., Modernizing pharmaceutical manufacturing: From batch to continuous production. *Journal of Pharmaceutical Innovation* **2015**, 10 (3), 191-199.
45. Jolliffe, H. G.; Gerogiorgis, D. I., Plantwide design and economic evaluation of two continuous pharmaceutical manufacturing (cpm) cases: Ibuprofen and artemisinin. *Computers & Chemical Engineering* **2016**, 91, 269-288.
46. Food and Drug Administration <https://blogs.fda.gov/fdavoices/index.php/2016/04/continuous-manufacturing-has-a-strong-impact-on-drug-quality/> (accessed 27/3/2017).
47. Variankaval, N.; Cote, A. S.; Doherty, M. F., From form to function: Crystallization of active pharmaceutical ingredients. *AIChE Journal* **2008**, 54 (7), 1682-1688.
48. Knox, M.; Trifkovic, M.; Rohani, S., Combining anti-solvent and cooling crystallization: Effect of solvent composition on yield and meta stable zone width. *Chemical Engineering Science* **2009**, 64 (16), 3555-3563.

49. Erdemir, D.; Lee, A. Y.; Myerson, A. S., Nucleation of crystals from solution: Classical and two-step models. *Accounts of Chemical Research* **2009**, *42* (5), 621-629.
50. Davey, R.; Garside, J., *From molecule to crystallizers - an introduction to crystallization*. Oxford University Press Oxford, **2006**.
51. Chew, J. W.; Black, S. N.; Chow, P. S.; Tan, R. B., Comparison between open-loop temperature control and closed-loop supersaturation control for cooling crystallization of glycine. *Industrial & Engineering Chemistry Research* **2007**, *46* (3), 830-838.
52. Barrett, P.; Glennon, B., Characterizing the metastable zone width and solubility curve using lasentec fbrm and pvm. *Chemical Engineering Research and Design* **2002**, *80* (7), 799-805.
53. Liang, K.; White, G.; Wilkinson, D.; Ford, L. J.; Roberts, K. J.; Wood, W. M. L., An examination into the effect of stirrer material and agitation rate on the nucleation of l-glutamic acid batch crystallized from supersaturated aqueous solutions. *Crystal Growth & Design* **2004**, *4* (5), 1039-1044.
54. Lawton, S.; Steele, G.; Shering, P.; Zhao, L.; Laird, I.; Ni, X.-W., Continuous crystallization of pharmaceuticals using a continuous oscillatory baffled crystallizer. *Organic Process Research & Development* **2009**, *13* (6), 1357-1363.
55. Gebauer, D.; Kellermeier, M.; Gale, J. D.; Bergström, L.; Cölfen, H., Pre-nucleation clusters as solute precursors in crystallisation. *Chemical Society Reviews* **2014**, *43* (7), 2348-2371.
56. Rawlings, J. B.; Miller, S. M.; Witkowski, W. R., Model identification and control of solution crystallization processes: A review. *Industrial & Engineering Chemistry Research* **1993**, *32* (7), 1275-1296.
57. Ulrich, J.; Strege, C., Some aspects of the importance of metastable zone width and nucleation in industrial crystallizers. *Journal of Crystal Growth* **2002**, *237-239*, Part 3, 2130-2135.
58. Chen, J.; Sarma, B.; Evans, J. M.; Myerson, A. S., Pharmaceutical crystallization. *Crystal Growth & Design* **2011**, *11* (4), 887-895.

59. Igarashi, K.; Azuma, M.; Kato, J.; Ooshima, H., The initial stage of crystallization of lysozyme: A differential scanning calorimetric (dsc) study. *Journal of Crystal Growth* **1999**, *204* (1), 191-200.
60. Chattopadhyay, S.; Erdemir, D.; Evans, J. M.; Ilavsky, J.; Amenitsch, H.; Segre, C. U.; Myerson, A. S., Sxas study of the nucleation of glycine crystals from a supersaturated solution. *Crystal Growth & Design* **2005**, *5* (2), 523-527.
61. Volmer, M., *Kinetik der phasenbildung*. Dresden und Leipzig : Steinkopff: **1939**.
62. Daudey, P. J.; van Rosmalen, G. M.; de Jong, E. J., Secondary nucleation kinetics of ammonium sulfate in a cmsmpr crystallizer. *Journal of Crystal Growth* **1990**, *99* (1), 1076-1081.
63. Klapper, H., Generation and propagation of defects during crystal growth. In *Springer handbook of crystal growth*, Springer: Heidelberg, **2010**; 93-132.
64. Shtukenberg, A. G.; Poloni, L. N.; Zhu, Z.; An, Z.; Bhandari, M.; Song, P.; Rohl, A. L.; Kahr, B.; Ward, M. D., Dislocation-actuated growth and inhibition of hexagonal l-cystine crystallization at the molecular level. *Crystal Growth & Design* **2015**, *15* (2), 921-934.
65. Noyes, A. A.; Whitney, W. R., The rate of solution of solid substances in their own solutions. *Journal of the American Chemical Society* **1897**, *19* (12), 930-934.
66. El-Zhry El-Yafi, A. K.; El-Zein, H., Technical crystallization for application in pharmaceutical material engineering: Review article. *Asian Journal of Pharmaceutical Sciences* **2015**, *10* (4), 283-291.
67. Berthoud, A., Formation of crystal faces. *J. Chem. Phys* **1912**, *10*, 624-35.
68. Valetton, J., Kristallwachstum und chemische affinitat. *Physik. Z* **1920**, *21*, 606.

69. Luque de Castro, M. D.; Priego-Capote, F., Ultrasound-assisted crystallization (sonocrystallization). *Ultrasonics Sonochemistry* **2007**, *14* (6), 717-724.
70. Nguyen, T.; Hammond, R.; Roberts, K.; Marziano, I.; Nichols, G., Precision measurement of the growth rate and mechanism of ibuprofen {001} and {011} as a function of crystallization environment. *CrystEngComm* **2014**, *16* (21), 4568-4586.
71. Kuznetsov, Y. G.; Malkin, A.; McPherson, A., Afm studies of the nucleation and growth mechanisms of macromolecular crystals. *Journal of Crystal Growth* **1999**, *196* (2), 489-502.
72. Miyazaki, T.; Aso, Y.; Kawanishi, T., Feasibility of atomic force microscopy for determining crystal growth rates of nifedipine at the surface of amorphous solids with and without polymers. *Journal of Pharmaceutical Sciences* **2011**, *100* (10), 4413-4420.
73. Camerman, A.; Camerman, N., The stereochemical basis of anticonvulsant drug action. I. The crystal and molecular structure of diphenylhydantoin, a noncentrosymmetric structure solved by centric symbolic addition. *Acta Crystallographica Section B: Structural Crystallography and Crystal Chemistry* **1971**, *27* (11), 2205-2211.
74. Ferguson, S.; Ortner, F.; Quon, J.; Peeva, L.; Livingston, A.; Trout, B. L.; Myerson, A. S., Use of continuous msmpr crystallization with integrated nanofiltration membrane recycle for enhanced yield and purity in api crystallization. *Crystal Growth & Design* **2014**, *14* (2), 617-627.
75. Beckmann, W., Crystallization of pharmaceutical compounds polymorphs, pseudo-polymorphs and particle formation. *Engineering in life sciences* **2003**, *3* (3), 113-120.
76. Khadka, P.; Ro, J.; Kim, H.; Kim, I.; Kim, J. T.; Kim, H.; Cho, J. M.; Yun, G.; Lee, J., Pharmaceutical particle technologies: An approach to improve drug solubility, dissolution and bioavailability. *Asian Journal of Pharmaceutical Sciences* **2014**, *9* (6), 304-316.
77. Fujiwara, M.; Chow, P. S.; Ma, D. L.; Braatz, R. D., Paracetamol crystallization using laser backscattering and atr-ftir spectroscopy:

Metastability, agglomeration, and control. *Crystal Growth & Design* **2002**, 2 (5), 363-370.

78. Eder, R. J. P.; Schmitt, E. K.; Grill, J.; Radl, S.; Gruber-Woelfler, H.; Khinast, J. G., Seed loading effects on the mean crystal size of acetylsalicylic acid in a continuous-flow crystallization device. *Crystal Research and Technology* **2011**, 46 (3), 227-237.
79. Powell, K. A.; Bartolini, G.; Wittering, K. E.; Saleemi, A. N.; Wilson, C. C.; Rielly, C. D.; Nagy, Z. K., Toward continuous crystallization of urea-barbituric acid: A polymorphic co-crystal system. *Crystal Growth & Design* **2015**, 15 (10), 4821-4836.
80. Myerson, A. S.; Ginde, R., 2 - crystals, crystal growth, and nucleation. In *Handbook of industrial crystallization (second edition)*, Myerson, A. S., Ed. Butterworth-Heinemann: Woburn, **2002**; 33-65.
81. Cheong, W. C.; Gaskell, P. H.; Neville, A., Substrate effect on surface adhesion/crystallisation of calcium carbonate. *Journal of Crystal Growth* **2013**, 363, 7-21.
82. Hermanto, M. W.; Chow, P. S.; Tan, R. B. H., Implementation of focused beam reflectance measurement (fbrm) in antisolvent crystallization to achieve consistent product quality. *Crystal Growth & Design* **2010**, 10 (8), 3668-3674.
83. Borissova, A.; Khan, S.; Mahmud, T.; Roberts, K. J.; Andrews, J.; Dallin, P.; Chen, Z.-P.; Morris, J., In situ measurement of solution concentration during the batch cooling crystallization of l-glutamic acid using atr-ftir spectroscopy coupled with chemometrics. *Crystal Growth & Design* **2009**, 9 (2), 692-706.
84. Bohnet, M., Fouling of heat transfer surfaces. *Chemical Engineering & Technology* **1987**, 10 (1), 113-125.
85. Brown, C. J.; Adalakun, J. A.; Ni, X.-w., Characterization and modelling of antisolvent crystallization of salicylic acid in a continuous oscillatory baffled crystallizer. *Chemical Engineering and Processing: Process Intensification* **2015**, 97, 180-186.
86. Duncan, A.; Phillips, R., *The dependence of heat exchanger fouling on solution undercooling*. Atomic Energy Research Establishment: **1977**.

87. Shock, R. A. W., Encrustation of crystallizers. *Journal of Separation Process Technology* **1983**, 4, 1-13.
88. Ritter, R. B., Crystalline fouling studies. *Journal of Heat Transfer* **1983**, 105 (2), 374-378.
89. Förster, M.; Bohnet, M., Modification of molecular interactions at the interface crystal/heat transfer surface to minimize heat exchanger fouling. *International Journal of Thermal Sciences* **2000**, 39 (7), 697-708.
90. Crittenden, B. D.; Alderman, N. J., Negative fouling resistances: The effect of surface roughness. *Chemical Engineering Science* **1988**, 43 (4), 829-838.
91. Kern, D.; Seaton, R., A theoretical analysis of thermal surface fouling. *British Chemical Engineering* **1959**, 4 (5), 258-262.
92. Geddert, T.; Bialuch, I.; Augustin, W.; Scholl, S., Extending the induction period of crystallization fouling through surface coating. *Heat Transfer Engineering* **2009**, 30 (10-11), 868-875.
93. Wu, S., *Polymer interface and adhesion*. CRC Press: Florida, **1982**.
94. Keysar, S.; Semiat, R.; Hasson, D.; Yahalom, J., Effect of surface roughness on the morphology of calcite crystallizing on mild steel. *Journal of Colloid and Interface Science* **1994**, 162 (2), 311-319.
95. Albert, F.; Augustin, W.; Scholl, S., Roughness and constriction effects on heat transfer in crystallization fouling. *Chemical Engineering Science* **2011**, 66 (3), 499-509.
96. Watkinson, A. P., Process heat transfer: Some practical problems. *The Canadian Journal of Chemical Engineering* **1980**, 58 (5), 553-558.
97. Fleming, J. R.; Kemkes, D.; DeVoe, D. W.; Crenshaw, L.; Imbalzano, J. F., Material of construction for pharmaceutical and biotechnology processing: Moving into the 21st century. *Pharmaceutical engineering* **2001**, 1-6.

98. Kazi, S.; Duffy, G.; Chen, X. In *Fouling and fouling mitigation on different heat exchanging surfaces*, Proceedings of International Conference on Heat Exchanger Fouling and Cleaning, **2009**; 14-19.
99. Al-Janabi, A.; Malayeri, M.; Müller-Steinhagen, H.; Badran, O. In *Precipitation fouling on various austenitic alloys*, International Conference on Heat Exchanger Fouling and Cleaning, vol. 8, **2009**; 332-339.
100. De Oliveira, R.; Albuquerque, D.; Leite, F.; Yamaji, F.; Cruz, T., *Measurement of the nanoscale roughness by atomic force microscopy: Basic principles and applications*. INTECH Open Access Publisher: **2012**.
101. Rahman, M. M.; Gui, F. In *Experimental measurements of fluid flow and heat transfer in microchannel cooling passages in a chip substrate*, The ASME International Electronics Packaging Conference, Binghamton, NY, USA, 09/29-10/02/93, **1993**; 685-692.
102. Mahato, B.; Shemilt, L., Effect of surface roughness on mass transfer. *Chemical Engineering Science* **1968**, 23 (2), 183-185.
103. Al-Janabi, A.; Malayeri, M. R.; Badran, O. O., Performance of shot peened surfaces subject to crystallization fouling. *International Journal of Thermal Sciences* **2017**, 111, 379-389.
104. Herz, A.; Malayeri, M. R.; Muller-Steinhagen, H., Fouling of roughened stainless steel surfaces during convective heat transfer to aqueous solutions. *Energy Conversion and Management* **2008**, 49 (11), 3381-3386.
105. Bogacz, W.; Lemanowicz, M.; Al-Rashed, M. H.; Nakonieczny, D.; Piotrowski, T.; Wójcik, J., Impact of roughness, wettability and hydrodynamic conditions on the incrustation on stainless steel surfaces. *Applied Thermal Engineering* **2017**, 112, 352-361.
106. Zhao, Q.; Liu, Y.; Wang, C.; Wang, S.; Muller-Steinhagen, H., Effect of surface free energy on the adhesion of biofouling and crystalline fouling. *Chemical Engineering Science* **2005**, 60 (17), 4858-4865.

107. Dreiser, C.; Krätz, L. J.; Bart, H.-J., Kinetics and quantity of crystallization fouling on polymer surfaces: Impact of surface characteristics and process conditions. *Heat Transfer Engineering* **2014**, 36 (7-8), 715-720.
108. Tachtatzis, C.; Sheridan, R.; Michie, C.; Atkinson, R. C.; Cleary, A.; Dziewierz, J.; Andonovic, I.; Briggs, N. E. B.; Florence, A. J.; Sefcik, J., Image-based monitoring for early detection of fouling in crystallisation processes. *Chemical Engineering Science* **2015**, 133, 82-90.
109. Wang, L.-C.; Li, S.-F.; Wang, L.-B.; Cui, K.; Zhang, Q.-L.; Liu, H.-B.; Li, G., Relationships between the characteristics of CaCO_3 fouling and the flow velocity in smooth tube. *Experimental Thermal and Fluid Science* **2016**, 74, 143-159.
110. Chen, Y.; Quan, Z.; Ma, C. In *Investigation of fouling process for convective heat transfer in an annular duct*, International Conference on Heat Exchanger Fouling and Cleaning - Challenges and Opportunities, Portugal, Müller-Steinhagen, H.; Malayeri, M. R.; Watkinson, A. P., Eds. Portugal, **2007**.
111. Bansal, B.; Müller-Steinhagen, H., Crystallization fouling in plate heat exchangers. *Journal of Heat Transfer* **1993**, 115 (3), 584-591.
112. Quan, Z.; Chen, Y.; Ma, C., Experimental study of fouling on heat transfer surface during forced convective heat transfer. *Chinese Journal of Chemical Engineering* **2008**, 16 (4), 535-540.
113. Pääkkönen, T. M.; Riihimäki, M.; Simonson, C. J.; Muurinen, E.; Keiski, R. L., Crystallization fouling of CaCO_3 – analysis of experimental thermal resistance and its uncertainty. *International Journal of Heat and Mass Transfer* **2012**, 55 (23–24), 6927-6937.
114. Ålander, E. M.; Uusi-Penttilä, M. S.; Rasmuson, Å. C., Agglomeration of paracetamol during crystallization in pure and mixed solvents. *Industrial & Engineering Chemistry Research* **2004**, 43 (2), 629-637.
115. Khoshkhoo, S.; Anwar, J., Crystallization of polymorphs: The effect of solvent. *Journal of Physics D: Applied Physics* **1993**, 26 (8B), B90.

116. Nokhodchi, A.; Bolourtchian, N.; Dinarvand, R., Crystal modification of phenytoin using different solvents and crystallization conditions. *International Journal of Pharmaceutics* **2003**, *250* (1), 85-97.
117. Kazi, S. N.; Duffy, G. G.; Chen, X. D., Fouling and fouling mitigation on heated metal surfaces. *Desalination* **2012**, *288*, 126-134.
118. Powell, K. A.; Saleemi, A. N.; Rielly, C. D.; Nagy, Z. K., Monitoring continuous crystallization of paracetamol in the presence of an additive using an integrated pat array and multivariate methods. *Organic Process Research & Development* **2016**, *20* (3), 626-636.
119. Lapidot, T.; Heng, J. Y., Functionalized mesoporous silica for the control of crystallization fouling. *Industrial & Engineering Chemistry Research* **2016**, *55* (44), 11475-11479.
120. Diao, Y.; Myerson, A. S.; Hatton, T. A.; Trout, B. L., Surface design for controlled crystallization: The role of surface chemistry and nanoscale pores in heterogeneous nucleation. *Langmuir* **2011**, *27* (9), 5324-5334.
121. Müller-Steinhagen, H.; Malayeri, M. R.; Watkinson, A. P., Heat exchanger fouling: Mitigation and cleaning strategies. *Heat Transfer Engineering* **2011**, *32* (3-4), 189-196.
122. Müller-Steinhagen, H.; Zhao, Q., Investigation of low fouling surface alloys made by ion implantation technology. *Chemical Engineering Science* **1997**, *52* (19), 3321-3332.
123. Kota, A. K.; Kwon, G.; Tuteja, A., The design and applications of superomniphobic surfaces. *NPG Asia Materials* **2014**, *6* (7), e109.
124. Cains, P. W.; Martin, P. D.; Price, C. J., The use of ultrasound in industrial chemical synthesis and crystallization. 1. Applications to synthetic chemistry. *Organic Process Research & Development* **1998**, *2* (1), 34-48.
125. Ruecroft, G.; Hipkiss, D.; Ly, T.; Maxted, N.; Cains, P. W., Sonocrystallization: The use of ultrasound for improved industrial crystallization. *Organic Process Research & Development* **2005**, *9* (6), 923-932.

126. Siddique, H.; Brown, C. J.; Houson, I.; Florence, A. J., Establishment of a continuous sonocrystallization process for lactose in an oscillatory baffled crystallizer. *Organic Process Research & Development* **2015**, *19* (12), 1871-1881.
127. Eder, R. J. P.; Schrank, S.; Besenhard, M. O.; Roblegg, E.; Gruber-Woelfler, H.; Khinast, J. G., Continuous sonocrystallization of acetylsalicylic acid (asa): Control of crystal size. *Crystal Growth & Design* **2012**, *12* (10), 4733-4738.
128. Jamshidi, R.; Rossi, D.; Saffari, N.; Gavriilidis, A.; Mazzei, L., Investigation of the effect of ultrasound parameters on continuous sonocrystallization in a millifluidic device. *Crystal Growth & Design* **2016**, *16* (8), 4607-4619.
129. Myerson, A., *Handbook of industrial crystallization*. Butterworth-Heinemann: Woburn, **2002**.
130. McGlone, T.; Briggs, N. E.; Clark, C. A.; Brown, C. J.; Sefcik, J.; Florence, A. J., Oscillatory flow reactors (ofrs) for continuous manufacturing and crystallization. *Organic Process Research & Development* **2015**, *19* (9), 1186-1202.
131. Helalizadeh, A.; Muller-Steinhagen, H.; Jamialahmadi, M., Mixed salt crystallisation fouling. *Chemical Engineering and Processing* **2000**, *39* (1), 29-43.
132. Mayer, M.; Bucko, J.; Benzinger, W.; Dittmeyer, R.; Augustin, W.; Scholl, S., The impact of crystallization fouling on a microscale heat exchanger. *Experimental Thermal and Fluid Science* **2012**, *40*, 126-131.
133. Pääkkönen, T.; Riihimäki, M.; Puhakka, E.; Muurinen, E.; Simonson, C.; Keiski, R. In *Crystallization fouling of caco 3—effect of bulk precipitation on mass deposition on the heat transfer surface*, Proceedings of International Conference on Heat Exchanger Fouling and Cleaning VIII, **2009**.
134. Rosmaninho, R.; Santos, O.; Nylander, T.; Paulsson, M.; Beuf, M.; Benezech, T.; Yiantsios, S.; Andritsos, N.; Karabelas, A.; Rizzo, G.; Müller-Steinhagen, H.; Melo, L. F., Modified stainless steel surfaces

targeted to reduce fouling – evaluation of fouling by milk components. *Journal of Food Engineering* **2007**, 80 (4), 1176-1187.

135. Isogai, S.; Nakamura, M.; Inokuchi, H.; Kimura, H.; Koga, Y. In *Measurement and modeling for the mitigation of organic crystallization fouling*, Heat Exchanger Fouling and Cleaning: Fundamentals and Applications, Watkinson, A. P.; MüllerSteinhagen, H.; Malayeri, M. R., Eds. **2003**.
136. Geddert, T.; Kipp, S.; Augustin, W.; Scholl, S. In *Influence of different surface materials on nucleation and crystal growth in heat exchangers*, 7th International Heat Exchanger Fouling and Cleaning, Portugal, July 2007; Portugal, **2007**.
137. Bansal, B.; Chen, X. D.; Muller-Steinhagen, H., Use of non-crystallising particles to mitigate crystallisation fouling. *International Communications in Heat and Mass Transfer* **2003**, 30 (5), 695-706.
138. Mayer, M.; Bucko, J.; Benzinger, W.; Dittmeyer, R.; Augustin, W.; Scholl, S., Crystallization fouling in experimental micro heat exchangers—optical and thermal investigations. *Experimental Heat Transfer* **2013**, 26 (5), 487-502.
139. Yang, Q.; Liu, Y.; Gu, A.; Ding, J.; Shen, Z., Investigation of calcium carbonate scaling inhibition and scale morphology by afm. *Journal of Colloid and Interface Science* **2001**, 240 (2), 608-621.
140. Bansal, B.; Muller-Steinhagen, H.; Chen, X. D., Effect of suspended particles on crystallization fouling in plate heat exchangers. *Journal of Heat Transfer* **1997**, 119 (3), 568-574.
141. Goedecke, R.; Drögemüller, P.; Augustin, W.; Scholl, S., Experiments on integral and local crystallization fouling resistances in a double-pipe heat exchanger with wire matrix inserts. *Heat Transfer Engineering* **2016**, 37 (1), 24-31.
142. Kim, W. T.; Bai, C.; Cho, Y. I., A study of caco 3 fouling with a microscopic imaging technique. *International Journal of Heat and Mass Transfer* **2002**, 45 (3), 597-607.
143. Al-Janabi, A.; Malayeri, M. R.; Müller-Steinhagen, H., Experimental investigation of crystallization fouling on grooved stainless steel

surfaces during convective heat transfer. *Heat Transfer Engineering* **2009**, 30 (10-11), 832-839.

144. Heinzl, V.; Jianu, A.; Sauter, H., Strategies against particle fouling in the channels of a micro heat exchanger when performing μ piv flow pattern measurements. *Heat Transfer Engineering* **2007**, 28 (3), 222-229.
145. Al Nasser, W. N.; Al Salhi, F. H., Scaling and aggregation kinetics determination of calcium carbonate using inline technique. *Chemical Engineering Science* **2013**, 86, 70-77.
146. Boerkamp, M.; Lamb, D. W.; Lye, P. G., An intrinsic exposed core optical fiber sensor as a quantitative surface crystallization monitoring sensor. *Sensors and Actuators B: Chemical* **2013**, 177, 964-969.
147. Lapidot, T.; Campbell, K. L. S.; Heng, J. Y. Y., Model for interpreting surface crystallization using quartz crystal microbalance: Theory and experiments. *ANALYTICAL CHEMISTRY* **2016**, 88, 4886-4893.
148. Wallhäußer, E.; Hussein, W. B.; Hussein, M. A.; Hinrichs, J.; Becker, T., Detection of dairy fouling: Combining ultrasonic measurements and classification methods. *Engineering in life sciences* **2013**, 13 (3), 292-301.
149. Lin, N. H.; Shih, W.-Y.; Lyster, E.; Cohen, Y., Crystallization of calcium sulfate on polymeric surfaces. *Journal of Colloid and Interface Science* **2011**, 356 (2), 790-797.
150. Gao, Y.; Haavisto, S.; Li, W.; Tang, C. Y.; Salmela, J.; Fane, A. G., Novel approach to characterizing the growth of a fouling layer during membrane filtration via optical coherence tomography. *Environmental Science & Technology* **2014**, 48 (24), 14273-14281.
151. Sanderson, R.; Li, J.; Koen, L. J.; Lorenzen, L., Ultrasonic time-domain reflectometry as a non-destructive instrumental visualization technique to monitor inorganic fouling and cleaning on reverse osmosis membranes. *Journal of Membrane Science* **2002**, 207 (1), 105-117.
152. Peroni, C. V.; Parisi, M.; Chianese, A., Hybrid modelling and self-learning system for dextrose crystallization process. *Chemical Engineering Research and Design* **2010**, 88 (12), 1653-1658.

153. Omar, W., Effect of solvent composition on crystallization process of ascorbic acid. *Chemical Engineering & Technology* **2006**, 29 (1), 119-123.
154. Yuan, Y.; Lee, T. R., Contact angle and wetting properties. In *Surface science techniques*, Springer: Heidelberg, **2013**; 3-34.
155. Förch, R. S., H; Jenkins, TA;, Appendix c: Contact angle goniometry. In *Surface design: Applications in bioscience and nanotechnology*, Wiley-VCH Verlag GmbH & Co. KGaA: **2009**; 471-473.
156. Good, R. J.; van Oss, C. J., The modern theory of contact angles and the hydrogen bond components of surface energies. In *Modern approaches to wettability: Theory and applications*, Schrader, M. E.; Loeb, G. I., Eds. Springer US: Boston, MA, **1992**; 1-27.
157. Lamprou, D. A.; Smith, J. R.; Nevell, T. G.; Barbu, E.; Willis, C. R.; Tsibouklis, J., Towards the determination of surface energy at the nanoscale: A further assessment of the afm-based approach. *Journal of Advanced Microscopy Research* **2010**, 5 (2), 137-142.
158. Lamprou, D. A.; Smith, J. R.; Nevell, T. G.; Barbu, E.; Willis, C. R.; Tsibouklis, J., Self-assembled structures of alkanethiols on gold-coated cantilever tips and substrates for atomic force microscopy: Molecular organisation and conditions for reproducible deposition. *Applied Surface Science* **2010**, 256 (6), 1961-1968.
159. Chow, E. H. H.; Bucar, D.-K.; Jones, W., New opportunities in crystal engineering - the role of atomic force microscopy in studies of molecular crystals. *Chemical Communications* **2012**, 48 (74), 9210-9226.
160. Bowen, W. R.; Hilal, N., *Atomic force microscopy in process engineering: An introduction to afm for improved processes and products*. Butterworth-Heinemann: Oxford, **2009**.
161. Payton, O.; Champneys, A. R.; Homer, M. E.; Picco, L.; Miles, M. J., Feedback-induced instability in tapping mode atomic force microscopy: Theory and experiment. *Proceedings of the Royal Society A: Mathematical, Physical and Engineering Science* **2011**, 467 (2130), 1801-1822.

162. Hassan, A. M.; Tashtoush, G. M.; Al-Khalil, J. A., Effect of graphite and/or silicon carbide particles addition on the hardness and surface roughness of al-4 wt% mg alloy. *Journal of composite materials* **2007**, *41* (4), 453-465.
163. Calabri, L.; Pugno, N.; Menozzi, C.; Valeri, S., Afm nanoindentation: Tip shape and tip radius of curvature effect on the hardness measurement. *Journal of Physics: Condensed Matter* **2008**, *20* (47), 474208.
164. Cui, L.; Yao, M.; Ren, B.; Zhang, K.-S., Sensitive and versatile detection of the fouling process and fouling propensity of proteins on polyvinylidene fluoride membranes via surface-enhanced raman spectroscopy. *ANALYTICAL CHEMISTRY* **2011**, *83* (5), 1709-1716.
165. Rabiller-Baudry, M.; Gouttefangeas, F.; Le Lannic, J.; Rabiller, P., Coupling of sem-edx and ftir-atr to (quantitatively) investigate organic fouling on porous organic composite membranes. *Current Microscopy Contributions to Advances in Science and Technology; Mendez-Vilas A (ed.)* **2012**, 1-11.
166. Barisci, J. N.; Stella, R.; Spinks, G. M.; Wallace, G. G., Characterisation of the topography and surface potential of electrodeposited conducting polymer films using atomic force and electric force microscopies. *Electrochimica Acta* **2000**, *46* (4), 519-531.
167. De Graeve, I.; Vereecken, J.; Franquet, A.; Van Schafftinghen, T.; Terryn, H., Silane coating of metal substrates: Complementary use of electrochemical, optical and thermal analysis for the evaluation of film properties. *Progress in Organic Coatings* **2007**, *59* (3), 224-229.
168. Ringnér, M., What is principal component analysis? *Nature biotechnology* **2008**, *26* (3), 303.
169. Abdi, H.; Williams, L. J., Principal component analysis. *Wiley Interdisciplinary Reviews: Computational Statistics* **2010**, *2* (4), 433-459.
170. Bhardwaj, R. M., *Control and prediction of solid-state of pharmaceuticals: Experimental and computational approaches*. Springer: Cham, **2016**.

171. Montgomery, D. C., *Design and analysis of experiments*. John Wiley & Sons: London, **2008**.
172. Eriksson, L., *Design of experiments: Principles and applications*. Umetrics Academy: Sweden, **2000**.
173. UMetrics *Modde help*, **2015**.
174. Olsson, M.; Gottfries, J.; Wold, S., D-optimal onion designs in statistical molecular design. *Chemometrics and Intelligent Laboratory Systems* **2004**, *73* (1), 37-46.
175. Dennison, T. J.; Smith, J.; Hofmann, M. P.; Bland, C. E.; Badhan, R. K.; Al-Khattawi, A.; Mohammed, A. R., Design of experiments to study the impact of process parameters on droplet size and development of non-invasive imaging techniques in tablet coating. *Plos One* **2016**, *11* (8), e0157267.
176. Bhatia, H.; Read, E.; Agarabi, C.; Brorson, K.; Lute, S.; Yoon, S., A design space exploration for control of critical quality attributes of mab. *International Journal of Pharmaceutics* **2016**, *512* (1), 242-252.
177. Cambridge Reactor Design
<http://www.cambridgereactoranddesign.com/zebrafish/gallery.html>
 (accessed 3/3/2017).
178. Towler, G.; Sinnott, R. K., *Chemical engineering design: Principles, practice and economics of plant and process design*. Elsevier: London, **2012**.
179. Teasdale, A., Regulatory highlights. *Organic Process Research & Development* **2015**, *19* (11), 1725-1730.
180. Pham, T. N.; Day, C. J.; Edwards, A. J.; Wood, H. R.; Lynch, I. R.; Watson, S. A.; Bretonnet, A.-S. Z.; Vogt, F. G., Detection of low-level ptfе contamination: An application of solid-state nmr to structure elucidation in the pharmaceutical industry. *Journal of Pharmaceutical and Biomedical Analysis* **2011**, *54* (2), 401-405.
181. Khan, F. I.; Abbasi, S. A., *Risk assessment in chemical process industries*. Discovery Publishing House: New-Dehli, **1998**.

182. Sinnott R.K.; Towler G, *Chemical engineering design*. 5th ed.; Elsevier: Oxford, **2009**.
183. Robertson, K.; Flandrin, P.-B.; Klapwijk, A. R.; Wilson, C. C., Design and evaluation of a mesoscale segmented flow reactor (kraic). *Crystal Growth & Design* **2016**, *16* (8), 4759-4764.
184. Ni, X.; Liao, A., Effects of mixing, seeding, material of baffles and final temperature on solution crystallization of l-glutamic acid in an oscillatory baffled crystallizer. *Chemical Engineering Journal* **2010**, *156* (1), 226-233.
185. Bluma, A.; Höpfner, T.; Lindner, P.; Rehbock, C.; Beutel, S.; Riechers, D.; Hitzmann, B.; Scheper, T., In-situ imaging sensors for bioprocess monitoring: State of the art. *Analytical and Bioanalytical Chemistry* **2010**, *398* (6), 2429-2438.
186. Schaefer, C.; Lecomte, C.; Clicq, D.; Merschaert, A.; Norrant, E.; Fotiadu, F., On-line near infrared spectroscopy as a process analytical technology (pat) tool to control an industrial seeded api crystallization. *Journal of Pharmaceutical and Biomedical Analysis* **2013**, *83*, 194-201.
187. Harsanyi, A.; Conte, A.; Pichon, L.; Rabion, A.; Grenier, S.; Sandford, G., One-step continuous flow synthesis of anti-fungal who essential medicine flucytosine using fluorine. *Organic Process Research & Development* **2017**, *21* (2), 273-276.
188. Duarte, A. R. C.; Roy, C.; Vega-González, A.; Duarte, C. M.; Subra-Paternault, P., Preparation of acetazolamide composite microparticles by supercritical anti-solvent techniques. *International Journal of Pharmaceutics* **2007**, *332* (1), 132-139.
189. Abu Bakar, M. R.; Nagy, Z. K.; Saleemi, A. N.; Rielly, C. D., The impact of direct nucleation control on crystal size distribution in pharmaceutical crystallization processes. *Crystal Growth & Design* **2009**, *9* (3), 1378-1384.
190. Narváez, L.; Cano, E.; Bastidas, D. M., 3-hydroxybenzoic acid as aisi 316l stainless steel corrosion inhibitor in a h₂so₄-hf-h₂o₂ pickling solution. *Journal of Applied Electrochemistry* **2005**, *35* (5), 499-506.

191. Alconbury Weston Ltd <http://www.a-w-l.co.uk/pilot-scale-systems> (accessed 24/02/2017).
192. Barish, J. A.; Goddard, J. M., Anti-fouling surface modified stainless steel for food processing. *Food and Bioproducts Processing* **2013**, *91* (4), 352-361.
193. Zhao, X.; Chen, X. D., A critical review of basic crystallography to salt crystallization fouling in heat exchangers. *Heat Transfer Engineering* **2012**, *34* (8-9), 719-732.
194. Hasan, B. O.; Nathan, G. J.; Ashman, P. J.; Craig, R. A.; Kelso, R. M., The effects of temperature and hydrodynamics on the crystallization fouling under cross flow conditions. *Applied Thermal Engineering* **2012**, *36*, 210-218.
195. Yu, W.; Erickson, K., Chord length characterization using focused beam reflectance measurement probe - methodologies and pitfalls. *Powder Technology* **2008**, *185* (1), 24-30.
196. Haynes Hastelloy® c-276 alloy datasheet. <http://www.inkosas.cz/download/niklove-slitiny/hastelloy-c-276.pdf> (accessed 14/10/2016).
197. Hastelloy® c-276 alloy brochure <http://haynesintl.com/docs/default-source/pdfs/new-alloy-brochures/corrosion-resistant-alloys/c-276.pdf?sfvrsn=4> (accessed 14/10/2016).
198. Al-Janabi, A.; Malayeri, M. R.; Müller-Steinhagen, H.; Badran, O. O. In *Precipitation fouling on various austentic alloys*, International Conference on Heat Exchanger Fouling and Cleaning VIII, Schladming, Austria, Müller-Steinhagen, H.; Malayeri, M. R.; Watkinson, A. P., Eds. Schladming, Austria, **2009**.
199. Callahan, C. J.; Ni, X.-W., On the investigation of the effect of apparatus configurations on the nucleation mechanisms in a cooling crystallization of sodium chlorate. *The Canadian Journal of Chemical Engineering* **2014**, *92* (11), 1920-1925.
200. Mitchell, N. A.; Frawley, P. J.; Ó'Ciardhá, C. T., Nucleation kinetics of paracetamol–ethanol solutions from induction time experiments using lasentec fbrm®. *Journal of Crystal Growth* **2011**, *321* (1), 91-99.

201. Saleemi, A.; Rielly, C.; Nagy, Z. K., Automated direct nucleation control for in situ dynamic fines removal in batch cooling crystallization. *CrystEngComm* **2012**, *14* (6), 2196-2203.
202. Davim, J. P.; Reis, P., Machinability study on composite (polyetheretherketone reinforced with 30% glass fibre–peek gf 30) using polycrystalline diamond (pcd) and cemented carbide (k20) tools. *The International Journal of Advanced Manufacturing Technology* **2004**, *23* (5), 412-418.
203. Crawford, R. J.; Throne, J. L., 2 - rotational molding polymers. In *Rotational molding technology*, William Andrew Publishing: Norwich, NY, **2002**; 19-68.
204. Bansal, N. P.; Doremus, R. H., Chapter 3 - multicomponent commercial glasses. In *Handbook of glass properties*, Academic Press: San Diego, **1986**; 31-45.
205. Bansal, N. P.; Doremus, R. H., Chapter 2 - vitreous silica. In *Handbook of glass properties*, Academic Press: San Diego, **1986**; 7-30.
206. Gyepes, R.; Witte, P. T.; Horáček, M.; Císařová, I.; Mach, K., Crystal structures of titanocene 2,2'-bipyridyl complexes. Singlet versus triplet state-dependence on methyl substituents at the cyclopentadienyl ligands¹. *Journal of Organometallic Chemistry* **1998**, *551* (1–2), 207-213.
207. Ohji, T.; Singh, M., *Advanced processing and manufacturing technologies for structural and multifunctional materials v: Ceramic engineering and science proceedings*. John Wiley & Sons: **2011**; Vol. 32.
208. Newman, S. G.; Gu, L.; Lesniak, C.; Victor, G.; Meschke, F.; Abahmane, L.; Jensen, K. F., Rapid wolff-kishner reductions in a silicon carbide microreactor. *Green Chemistry* **2014**, *16* (1), 176-180.
209. Kappe, C. O., Unraveling the mysteries of microwave chemistry using silicon carbide reactor technology. *Accounts of Chemical Research* **2013**, *46* (7), 1579-1587.

210. Chemtrix <http://www.chemtrix.com/products/protrix> (accessed 24/02/2017).
211. Cverna, F., *Asm ready reference: Thermal properties of metals*. ASM International: Ohio, **2002**.
212. Sambamurthy, K., *Pharmaceutical engineering* New Age International Ltd: New Delhi, **2002**; 173-194.
213. Lima, M. M. R. A.; Monteiro, R. C. C.; Graça, M. P. F.; Ferreira da Silva, M. G., Structural, electrical and thermal properties of borosilicate glass–alumina composites. *Journal of Alloys and Compounds* **2012**, 538, 66-72.
214. Goodfellow <http://www.goodfellow.com/> (accessed 12/1/2017).
215. 3M <http://multimedia.3m.com/mws/media/993481O/3m-silicon-carbide-materials-properties.pdf> (accessed 12/1/2017).
216. Bonnet, C.; Valiorgue, F.; Rech, J.; Claudin, C.; Hamdi, H.; Bergheau, J. M.; Gilles, P., Identification of a friction model—application to the context of dry cutting of an aisi 316l austenitic stainless steel with a tin coated carbide tool. *International Journal of Machine Tools and Manufacture* **2008**, 48 (11), 1211-1223.
217. Schittich, C.; Staib, G.; Balkow, D.; Schuler, M.; Sobek, W., *Glass construction manual*. Birkhäuser GmbH: Basel, **2007**.
218. James, F. S., Properties of solids. In *The engineering handbook, second edition*, CRC Press: Florida, **2004**.
219. Askeland, D. R.; Fulay, P. P.; Wright, W. J., *The science and engineering of materials*. Wadsworth Publishing: California, **2011**.
220. Huang, R. Y. M.; Shao, P.; Burns, C. M.; Feng, X., Sulfonation of poly(ether ether ketone)(peek): Kinetic study and characterization. *Journal of Applied Polymer Science* **2001**, 82 (11), 2651-2660.

221. Morra, M.; Occhiello, E.; Garbassi, F., Surface characterization of plasma-treated ptf. *Surface and Interface Analysis* **1990**, *16* (1-12), 412-417.
222. Wenzel, R. N., Surface roughness and contact angle. *The Journal of Physical Chemistry* **1949**, *53* (9), 1466-1467.
223. Hilbert, L. R.; Bagge-Ravn, D.; Kold, J.; Gram, L., Influence of surface roughness of stainless steel on microbial adhesion and corrosion resistance. *International biodeterioration & biodegradation* **2003**, *52* (3), 175-185.
224. Allesø, M.; van den Berg, F.; Cornett, C.; Jørgensen, F. S.; Halling-Sørensen, B.; de Diego, H. L.; Hovgaard, L.; Aaltonen, J.; Rantanen, J., Solvent diversity in polymorph screening. *Journal of Pharmaceutical Sciences* **2008**, *97* (6), 2145-2159.
225. Bakar, M. R. A.; Nagy, Z. K.; Rielly, C. D., Seeded batch cooling crystallization with temperature cycling for the control of size uniformity and polymorphic purity of sulfathiazole crystals. *Organic Process Research & Development* **2009**, *13* (6), 1343-1356.
226. Mitchell, N. A.; Frawley, P. J., Nucleation kinetics of paracetamol–ethanol solutions from metastable zone widths. *Journal of Crystal Growth* **2010**, *312* (19), 2740-2746.
227. Kulkarni, S. A.; Kadam, S. S.; Meekes, H.; Stankiewicz, A. I.; ter Horst, J. H., Crystal nucleation kinetics from induction times and metastable zone widths. *Crystal Growth & Design* **2013**, *13* (6), 2435-2440.
228. Liu, J.; Rasmuson, Å. C., Influence of agitation and fluid shear on primary nucleation in solution. *Crystal Growth & Design* **2013**, *13* (10), 4385-4394.
229. Liu, J.; Svärd, M.; Rasmuson, Å. C., Influence of agitation on primary nucleation in stirred tank crystallizers. *Crystal Growth & Design* **2015**, *15* (9), 4177-4184.
230. Minnich, C. B.; Helmdach, L.; Ulrich, J.; Feth, M. P., Model-based recognition of mid-infrared sensor fouling in paracetamol crystallization. *Chemical Engineering & Technology* **2015**, *38* (8), 1303-1307.

231. Agnew, L. R.; McGlone, T.; Wheatcroft, H. P.; Robertson, A.; Parsons, A. R.; Wilson, C. C., Continuous crystallization of paracetamol (acetaminophen) form ii: Selective access to a metastable solid form. *Crystal Growth & Design* **2017**, *17* (5), 2418-2427.
232. Granberg, R. A.; Rasmuson, Å. C., Solubility of paracetamol in pure solvents. *Journal of Chemical & Engineering Data* **1999**, *44* (6), 1391-1395.
233. Kruskal, W. H.; Wallis, W. A., Use of ranks in one-criterion variance analysis. *Journal of the American statistical Association* **1952**, *47* (260), 583-621.
234. MINITAB 16 *Minitab statguide*, **2010**.
235. Kashchiev, D., *Nucleation: Basic theory with applications*. Butterworth-Heinemann: Oxford, **2000**.
236. Zhang, R.; Ma, C. Y.; Liu, J. J.; Wang, X. Z., On-line measurement of the real size and shape of crystals in stirred tank crystalliser using non-invasive stereo vision imaging. *Chemical Engineering Science* **2015**, *137*, 9-21.
237. Ilevbare, G. A.; Liu, H.; Edgar, K. J.; Taylor, L. S., Maintaining supersaturation in aqueous drug solutions: Impact of different polymers on induction times. *Crystal Growth & Design* **2012**, *13* (2), 740-751.
238. Little, L. J.; Sear, R. P.; Keddie, J. L., Does the γ polymorph of glycine nucleate faster? A quantitative study of nucleation from aqueous solution. *Crystal Growth & Design* **2015**, *15* (11), 5345-5354.
239. Jiang, S.; ter Horst, J. H., Crystal nucleation rates from probability distributions of induction times. *Crystal Growth & Design* **2011**, *11* (1), 256-261.
240. Forsyth, C.; Burns, I. S.; Mulheran, P. A.; Sefcik, J., Scaling of glycine nucleation kinetics with shear rate and glass-liquid interfacial area. *Crystal Growth & Design* **2016**, *16* (1), 136-144.

241. Kuldipkumar, A.; Kwon, G. S.; Zhang, G. G. Z., Determining the growth mechanism of tolazamide by induction time measurement. *Crystal Growth & Design* **2007**, 7 (2), 234-242.
242. Lyczko, N.; Espitalier, F.; Louisnard, O.; Schwartzenruber, J., Effect of ultrasound on the induction time and the metastable zone widths of potassium sulphate. *Chemical Engineering Journal* **2002**, 86 (3), 233-241.
243. Sharma, M. M.; Chamoun, H.; Sarma, D. S. R.; Schechter, R. S., Factors controlling the hydrodynamic detachment of particles from surfaces. *Journal of Colloid and Interface Science* **1992**, 149 (1), 121-134.
244. Ålander, E. M.; Rasmuson, Å. C., Mechanisms of crystal agglomeration of paracetamol in acetone–water mixtures. *Industrial & Engineering Chemistry Research* **2005**, 44 (15), 5788-5794.
245. Thulukkanam, K., *Heat exchanger design handbook*. CRC Press: Florida, **2013**.
246. Abohamra, E.; Ulrich, J., Untersuchung zu arteigenen kristallinen verkrustungen in einem kristallisationsprozess. *Chemie Ingenieur Technik* **2010**, 82 (7), 1081-1084.
247. Åström, K. J.; Hägglund, T., The future of pid control. *Control Engineering Practice* **2001**, 9 (11), 1163-1175.
248. Ang, K. H.; Chong, G.; Li, Y., Pid control system analysis, design, and technology. *IEEE transactions on control systems technology* **2005**, 13 (4), 559-576.
249. Jha, S.; Karthika, S.; Radhakrishnan, T., Modelling and control of crystallization process. *Resource-Efficient Technologies* **2017**, 3 (1), 94-100.
250. Jones, A. G., *Crystallization process systems*. Butterworth-Heinemann: Oxford, **2002**.
251. Selekman, J. A.; Roberts, D.; Rosso, V.; Qiu, J.; Nolfo, J.; Gao, Q.; Janey, J., Development of a highly automated workflow for investigating

polymorphism and assessing risk of forming undesired crystal forms within a crystallization design space. *Organic Process Research & Development* **2016**, 20 (1), 70-75.

252. Hilfiker, R.; Berghausen, J.; Blatter, F.; Burkhard, A.; Paul, S. D.; Freiermuth, B.; Geoffroy, A.; Hofmeier, U.; Marcolli, C.; Siebenhaar, B.; Szelagiewicz, M.; Vit, A.; Raumer, M. v., Polymorphism - integrated approach from high-throughput screening to crystallization optimization. *Journal of Thermal Analysis and Calorimetry* **2003**, 73 (2), 429-440.
253. Gani, R.; Jiménez-González, C.; ten Kate, A.; Crafts, P. A.; Jones, M.; Powell, L.; Atherton, J. H.; Cordiner, J. L., A modern approach to solvent selection. *Chemical Engineering* **2006**, 113 (3), 30-43.
254. Papadakis, E.; Tula, A. K.; Gani, R., Solvent selection methodology for pharmaceutical processes: Solvent swap. *Chemical Engineering Research and Design* **2016**, 115, 443-461.
255. Kramer, H. J. M.; Bermingham, S. K.; van Rosmalen, G. M., Design of industrial crystallisers for a given product quality. *Journal of Crystal Growth* **1999**, 198–199, Part 1, 729-737.
256. Lakerveld, R.; Benyahia, B.; Heider, P. L.; Zhang, H.; Wolfe, A.; Testa, C. J.; Ogden, S.; Hersey, D. R.; Mascia, S.; Evans, J. M. B.; Braatz, R. D.; Barton, P. I., The application of an automated control strategy for an integrated continuous pharmaceutical pilot plant. *Organic Process Research & Development* **2014**, 19 (9), 1088 - 1100.
257. Wibowo, C.; Ng, K. M., Workflow for process synthesis and development: Crystallization and solids processing. *Industrial & Engineering Chemistry Research* **2002**, 41 (16), 3839-3848.
258. Rashid, A.; White, E.; Howes, T.; Litster, J.; Marziano, I., From raw data to process: The path to a batch or a continuous crystallizer design for ibuprofen. *Organic Process Research & Development* **2017**, 21 (2), 187-194.
259. Denbigh, K. G., *The principles of chemical equilibrium: With applications in chemistry and chemical engineering*. Cambridge University Press: Cambridge, **1981**.

260. Guo, Z. Y.; Liu, X. B.; Tao, W. Q.; Shah, R. K., Effectiveness–thermal resistance method for heat exchanger design and analysis. *International Journal of Heat and Mass Transfer* **2010**, 53 (13–14), 2877-2884.
261. Amjad, Z.; Demadis, K. D., *Mineral scales and deposits: Scientific and technological approaches*. Elsevier: Oxford, **2015**.
262. Mwaba, M. G.; Rindt, C. C. M.; Van Steenhoven, A. A.; Vorstman, M. A. G., Validated numerical analysis of caso4 fouling. *Heat Transfer Engineering* **2006**, 27 (7), 50-62.
263. Shih, W.-Y.; Rahardianto, A.; Lee, R.-W.; Cohen, Y., Morphometric characterization of calcium sulfate dihydrate (gypsum) scale on reverse osmosis membranes. *Journal of Membrane Science* **2005**, 252 (1), 253-263.
264. Uchymiak, M.; Lyster, E.; Glater, J.; Cohen, Y., Kinetics of gypsum crystal growth on a reverse osmosis membrane. *Journal of Membrane Science* **2008**, 314 (1), 163-172.
265. Omar, W.; Al-Sayed, S.; Sultan, A.; Ulrich, J., Growth rate of single acetaminophen crystals in supersaturated aqueous solution under different operating conditions. *Crystal Research and Technology* **2008**, 43 (1), 22-27.
266. Ó'Ciardhá, C. T.; Mitchell, N. A.; Hutton, K. W.; Frawley, P. J., Determination of the crystal growth rate of paracetamol as a function of solvent composition. *Industrial & Engineering Chemistry Research* **2012**, 51 (12), 4731-4740.
267. Rantanen, J.; Khinast, J., The future of pharmaceutical manufacturing sciences. *Journal of Pharmaceutical Sciences* **2015**, 104 (11), 3612-3638.
268. Ketterhagen, W. R.; am Ende, M. T.; Hancock, B. C., Process modeling in the pharmaceutical industry using the discrete element method. *Journal of Pharmaceutical Sciences* **2009**, 98 (2), 442-470.
269. Agatonovic-Kustrin, S.; Beresford, R., Basic concepts of artificial neural network (ann) modeling and its application in pharmaceutical research.

270. Chen, Z.-P.; Morris, J.; Borissova, A.; Khan, S.; Mahmud, T.; Penchev, R.; Roberts, K. J., On-line monitoring of batch cooling crystallization of organic compounds using atr-ftir spectroscopy coupled with an advanced calibration method. *Chemometrics and Intelligent Laboratory Systems* **2009**, 96 (1), 49-58.
271. Wicker, J. G.; Cooper, R. I., Will it crystallise? Predicting crystallinity of molecular materials. *CrystEngComm* **2015**, 17 (9), 1927-1934.
272. Bhardwaj, R. M.; Price, L. S.; Price, S. L.; Reutzel-Edens, S. M.; Miller, G. J.; Oswald, I. D. H.; Johnston, B. F.; Florence, A. J., Exploring the experimental and computed crystal energy landscape of olanzapine. *Crystal Growth & Design* **2013**, 13 (4), 1602-1617.
273. Florence, A. J.; Johnston, A.; Price, S. L.; Nowell, H.; Kennedy, A. R.; Shankland, N., An automated parallel crystallisation search for predicted crystal structures and packing motifs of carbamazepine. *Journal of Pharmaceutical Sciences* **2006**, 95 (9), 1918-1930.
274. Gracin, S.; Brinck, T.; Rasmuson, Å. C., Prediction of solubility of solid organic compounds in solvents by unifac. *Industrial & Engineering Chemistry Research* **2002**, 41 (20), 5114-5124.
275. Koswara, A.; Nagy, Z. K., Anti-fouling control of plug-flow crystallization via heating and cooling cycle. *IFAC-PapersOnLine* **2015**, 48 (8), 193-198.
276. Mayer, M.; Bucko, J.; Benzinger, W.; Dittmeyer, R.; Augustin, W.; Scholl, S., Modeling fouling factors for microscale heat exchangers. *Experimental Heat Transfer* **2015**, 28 (3), 222-243.
277. Brahim, F.; Augustin, W.; Bohnet, M., Numerical simulation of the fouling process. *International Journal of Thermal Sciences* **2003**, 42 (3), 323-334.
278. Yang, M.; Young, A.; Niyetkaliyev, A.; Crittenden, B., Modelling fouling induction periods. *International Journal of Thermal Sciences* **2012**, 51, 175-183.

279. Zhang, F.; Xiao, J.; Chen, X. D., Towards predictive modeling of crystallization fouling: A pseudo-dynamic approach. *Food and Bioproducts Processing* **2015**, *93*, 188-196.
280. Warsinger, D. M.; Tow, E. W.; Swaminathan, J.; Lienhard V, J. H., Theoretical framework for predicting inorganic fouling in membrane distillation and experimental validation with calcium sulfate. *Journal of Membrane Science* **2017**, *528*, 381-390.
281. Wang, Y.-N.; Tang, C. Y., Protein fouling of nanofiltration, reverse osmosis, and ultrafiltration membranes—the role of hydrodynamic conditions, solution chemistry, and membrane properties. *Journal of Membrane Science* **2011**, *376* (1–2), 275-282.
282. Prat, D.; Pardigon, O.; Flemming, H.-W.; Letestu, S.; Ducandas, V.; Isnard, P.; Guntrum, E.; Senac, T.; Ruisseau, S.; Cruciani, P.; Hosek, P., Sanofi's solvent selection guide: A step toward more sustainable processes. *Organic Process Research & Development* **2013**, *17* (12), 1517-1525.
283. Tully, G.; Hou, G.; Glennon, B., Solubility of benzoic acid and aspirin in pure solvents using focused beam reflective measurement. *Journal of Chemical & Engineering Data* **2015**, *61* (1), 594-601.
284. Gaivoronskii, A. N.; Granzhan, V. A., Solubility of adipic acid in organic solvents and water. *Russian Journal of Applied Chemistry* **2005**, *78* (3), 404-408.
285. Liu, W.; Dang, L.; Black, S.; Wei, H., Solubility of carbamazepine (form iii) in different solvents from (275 to 343) k. *Journal of Chemical & Engineering Data* **2008**, *53* (9), 2204-2206.
286. Li, H.; Yu, P.; Luo, Y., Correlation between organic fouling of reverse-osmosis membranes and various interfacial interactions. *Chemical Engineering & Technology* **2015**, *38* (1), 131-138.
287. Mahlangu, T. O.; Hoek, E. M. V.; Mamba, B. B.; Verliefe, A. R. D., Influence of organic, colloidal and combined fouling on nf rejection of nacl and carbamazepine: Role of solute–foulant–membrane interactions and cake-enhanced concentration polarisation. *Journal of Membrane Science* **2014**, *471*, 35-46.

288. Bott, T. R.; Melo, L. F., Fouling of heat exchangers. *Experimental Thermal and Fluid Science* **1997**, *14* (4), 315-315.
289. Fujikawa, H.; Morozumi, S., Modeling staphylococcus aureus growth and enterotoxin production in milk. *Food Microbiology* **2006**, *23* (3), 260-267.
290. Baty, F.; Delignette-Muller, M.-L., Estimating the bacterial lag time: Which model, which precision? *International Journal of Food Microbiology* **2004**, *91* (3), 261-277.
291. Uchymiak, M.; Lyster, E.; Glater, J.; Cohen, Y., Kinetics of gypsum crystal growth on a reverse osmosis membrane. *Journal of Membrane Science* **2008**, *314* (1–2), 163-172.
292. Bohnet, M., Influence of the transport properties of the crystal/heat transfer surface interfacial on fouling behavior. *Chemical Engineering & Technology* **2003**, *26* (10), 1055-1060.
293. Al-Janabi, A.; Malayeri, M. R., A criterion for the characterization of modified surfaces during crystallization fouling based on electron donor component of surface energy. *Chemical Engineering Research and Design* **2015**, *100*, 212-227.
294. Kazi, S. N.; Duffy, G. G.; Chen, X. D., Mineral scale formation and mitigation on metals and a polymeric heat exchanger surface. *Applied Thermal Engineering* **2010**, *30* (14–15), 2236-2242.
295. Food and Drug Administration <https://blogs.fda.gov/fdavoices/index.php/2016/02/modernizing-pharmaceutical-manufacturing-to-improve-drug-quality-ensuring-a-safe-and-adequate-supply-of-drugs/> (accessed 25/4/2017).
296. Myerson, A. S.; Krumme, M.; Nasr, M.; Thomas, H.; Braatz, R. D., Control systems engineering in continuous pharmaceutical manufacturing. May 20–21, 2014 continuous manufacturing symposium. *Journal of Pharmaceutical Sciences* **2015**, *104* (3), 832-839.

297. Briggs, N. E. B. Polymorph control of pharmaceuticals within a continuous oscillatory baffled crystalliser. University of Strathclyde, **2015**.
298. Hoang, T. A.; Rohl, A. L.; Jeffrey, M. I.; Ang, H. M., A study of gypsum scale formation using quartz crystal microbalance. *Developments in Chemical Engineering and Mineral Processing* **2006**, 14 (1-2), 313-321.
299. Murray, B. S.; Deshares, C., Monitoring protein fouling of metal surfaces via a quartz crystal microbalance. *Journal of Colloid and Interface Science* **2000**, 227 (1), 32-41.
300. Kraus, P. R.; Cooper, F. L.; Emmons, D. H.; Ferguson, S.; McClain, R. D.; Spates, J. J. In *Use of quartz crystal microbalance sensors for monitoring fouling and viscoelastic phenomena in industrial process applications*, Sicon/01. Sensors for Industry Conference. Proceedings of the First ISA/IEEE. Sensors for Industry Conference (Cat. No.01EX459), 2001; **2001**; 241-245.
301. Lapidot, T. Heterogeneous crystallisation of calcium sulphate in the presence of silica particles. Imperial College London, **2015**.
302. Biyanto, T. R., Fouling resistance prediction using artificial neural network nonlinear auto-regressive with exogenous input model based on operating conditions and fluid properties correlations. *AIP Conference Proceedings* **2016**, 1737 (1), 050001.
303. Brown, C. J.; McGlone, T.; Yerdelen, S.; Srirambhatla, V.; Mabbott, F.; Gurung, R.; Briuglia, M. L.; Ahmed, B.; Polyzois, H.; McGinty, J.; Perciballi, F.; Fysikopoulos, D.; MacFhionnghaile, P.; Siddique, H.; Raval, V.; Harrington, T. S.; Vassileiou, A.; Robertson, M.; Prasad, E.; Johnston, A.; Johnston, B.; Nordon, A.; Srai, J. S.; Halbert, G.; ter Horst, J.; Price, C.; Rielly, C. D.; Sefcik, J.; Florence, A. J., Enabling precision manufacturing of active pharmaceutical ingredients: Workflow for seeded cooling continuous crystallisation. *Molecular Systems Design and Engineering* **2017**, Article under review.

